A Point-of-Care Diagnostic for Tuberculosis

By

Suzan Abdullah Alzeer

School of Pharmacy and Pharmaceutical Sciences, Cardiff University

Thesis submitted to Cardiff University as a requirement for the degree of Doctor of Philosophy (PhD)

June 2025

Declaration

This thesis is the result of my own independent work, except where otherwise stated, and the views expressed are my own. Other sources are acknowledged by explicit references. The thesis has not been edited by a third party beyond what is permitted by Cardiff University's Use of Third-Party Editors by Research Degree Students Procedure.

Suzan Alzeer ……

Acknowledgements

First and foremost, I am profoundly grateful to God for His countless blessings, guidance, and strength throughout this journey.

I wish to express my sincere gratitude to the Ministry of Education in the Kingdom of Saudi Arabia for sponsoring my studies at Cardiff University and providing me with the opportunity to undertake this research.

My deepest thanks go to my advisor, Prof. Les Baillie, whose guidance has been invaluable. His constant encouragement, motivation, and enthusiasm have been a source of inspiration throughout this research. I am also deeply grateful to Prof. Adrian Porch for his invaluable supervision, and to Dr. Evans Ahortor for his expertise and training in the microwave system, which has significantly enhanced my work.

To my beloved mother, Safa Alkazendar, I owe everything I have achieved. Your unwavering support and encouragement have been the foundation of my success; without you, none of this would have been possible.

To my husband, Eng. Saad Alrasheed, thank you for your patience, understanding, and constant support. Your unwavering belief in me has meant the world.

To my dear children, Fahad, Sarah, and Abdurahman, you have endured so much during this journey. Your smiles have been my greatest source of strength and inspiration, motivating me to persevere. Thank you for bringing so much joy and purpose to my life.

Finally, I extend my heartfelt thanks to my siblings and friends for their constant support, encouragement, and belief in me.

Publications and presentations related to the study

Publications

S. Wilson-Garner**, S. Alzeer**, L. Baillie, A. Porch; High-volume biological sample processing using microwaves. *J. Appl. Phys.* 28 January 2024; 135 (4): 044901. https://doi.org/10.1063/5.0178755

Poster presentation

Online poster: The development of a microwave-assisted magnetic nanoparticle-based DNA assay for the detection of *Mycobacterium tuberculosis*. **S. Alzeer,** L. Baillie, A. Porch .Microwaves and nanoparticles for real-time detection of human pathogens, Kiev, Ukraine. (October 2022).

A point-of-care diagnostic for tuberculosis. **S. Alzeer**, L. Baillie, A. Porch .Tuberculosis: The forgotten pandemic. Microbiology Society Annual Conference. Birmingham, UK. (April 2023).

The development of a microwave-assisted magnetic nanoparticle-based DNA assay for the detection of *Mycobacterium tuberculosis*. **S. Alzeer**, L. Baillie, A. Porch .Life Sciences Research Network Wales, Cardiff, UK.(November 2023)

Oral presentation

A point-of-care diagnostic for tuberculosis. **S. Alzeer**, L. Baillie, A. Porch .Pharmacy school postgraduate research day, School of Pharmacy and Pharmaceutical Sciences, Redwood Building, Cardiff University, Cardiff, UK (April 2023).

Abstract

Mycobacterium tuberculosis is a significant global health concern, requiring rapid and accurate detection methods for effective diagnosis and prompt treatment. This research builds on previous studies to advance the development of a point-of-care (POC) assay for the rapid identification of *M. tuberculosis*, employing the BCG strain of *M. bovis* as a surrogate model. A microwave-assisted DNA extraction technique was optimised to rapidly release DNA from *M. bovis* suspended in water and in simulated sputum containing methylcellulose to mimic the viscosity of respiratory samples.

DNA probes specific for the *IS6110* and *IS1081* gene targets were developed, attached to magnetic nanoparticles, and assessed for their ability to capture target DNA in different sample volumes. The sensitivity and specificity of the assay were optimised, resulting in a reduction in the time taken to identify *M. bovis* positively. The sensitivity of the approach was further enhanced by increasing the sample volume from 200 µL to 10,000 µL. This microwave-based method yielded faster results than conventional methods, such as culture and PCR. Our results suggest that there is potential to further increase assay sensitivity and reduce detection time, ultimately leading to the development of a rapid, sensitive assay for the detection of *M. bovis* and *M. tuberculosis*.

Table of Contents

List of Figures

List of Tables

List of abbreviations

Acquired Immune Deficiency Syndrome (AIDS)

American Type Culture Collections (ATCC) Bovine Tuberculosis (B. tb)

Colony Forming Unit (CFU)

Computer Tomography (CT)

Culture Filtrate Protein (CFP-10)

Cystic Fibrosis (CF)

Directly Observed Treatment Short-Course (DOTS)

Early secreted antigen 6 kilodaltons (ESAT-6)

Electric (E)

Electromagnetic (EM)

Enzyme Linked Oligonucleotide Hybridisation Assay (ELOSHA) Ethambutol (ETMB)

ethylenediaminetetraacetic acid (EDTA)

Extensive Drug Resistance (XDR)

Glycopeptidolipid (GPL)

High Performance Liquid Chromatography (HPLC)

Human Immune Deficiency Virus (HIV)

Insertion Sequence (IS)

Interferon Gamma (INF-γ)

Isoniazid (INH)

Lipoarabinomannan (LAM)

Loop Mediated Isothermal Amplification (LAMP)

Magnetic (H)

Microwave (MW)

Minimum Inhibition concentration (MIC)

MTBDR*plus*

MTBDRsI

Multidrug Resistant TB (MDR-TB)

Mycobacterium abscessus (*M. abscessus*)

Mycobacterium bovis (*M. bovis*)

Mycobacterium Tuberculosis Complex (MTBC).

Mycolic Acids (MA)

Non-tuberculous mycobacteria (NTM)

Phosphate Buffered Saline (PBS)

Phosphatidylinositol 3-phosphate (PIP3)

Point-of-Care (POC)

Polymerase Chain Reaction (PCR)

Purified Protein Derivative (PPD)

Pyrazinamidase (PZase)

Pyrazinamide (PZ)

Region of Difference 1 (RD1)

RIF Resistance Determining Region (RRDR) Rifampicin (RIF)

Total Drug Resistance (TDR)

Tuberculin Skin Test (TST)

Tuberculosis (TB)

Whole Genome Sequencing (WGS)

World Health Organisation (WHO) Ziehl-Neelsen (ZN)

β-subunit of the RNA polymerase (*rpoB*)

Chapter 1 Introduction, aims, and objectives

1.1 Mycobacteria

Mycobacterial species are a significant focus of biological research due to their pathogenicity in both human and animal populations (Moyo et al., 2021). The genus *Mycobacterium* was first designated in 1896 by Lehmann and Neumann, primarily based on characteristics observed in the strain *Mycobacterium tuberculosis* (*M. tuberculosis*), such as the presence of mycolic acids in the cell wall, aerobic growth, and a bacillary cell shape (Meehan et al., 2021). The genus encompasses several species, categorised into three groups that are discussed in more detail later in this chapter: *Mycobacterium tuberculosis* complex (MTBC), *Mycobacterium leprae*, and atypical or non-tuberculous mycobacteria (NTM) (Singh et al., 2020a). This diverse group includes over 200 species that express various virulence factors (Singh et al., 2020a), with *Mycobacterium tuberculosis* being the major human pathogen and the second leading cause of global mortality, surpassed only by coronavirus disease (COVID-19) (Meehan et al., 2021; Armstrong et al., 2023). It is important to note that *M. tuberculosis* causes twice as many fatalities as HIV/AIDS (WHO, 2022), highlighting the urgent need for research in this area.

Phenotypically, mycobacteria are Gram-positive, catalase-positive, non-motile, non-spore-forming, rod-shaped bacteria ranging from 0.2 to 0.6 μm in width and 1.0 to 10 μm in length (Qutob et al., 2022). Their cellular structure is characterised by a unique and significant cell wall envelope containing a high concentration of mycolic acid, primarily alkyl and extended β-hydroxy fatty acids. This unique structure, characterized by a thick, waxy cell wall rich in mycolic acids, provides structural strength and significantly contributes to mycobacteria's resistance to antibiotics. The cell wall acts as a barrier, preventing the penetration of many drugs and limiting their effectiveness. Additionally, the mycolic acids play a role in protecting the bacteria from environmental stress and antimicrobial agents. (Rahlwes et al., 2023). Due to the nature of this cell wall, mycobacteria are described as acid-fast bacilli

(AFB) (Figure 1.1), meaning they are resistant to decolourisation by acid during laboratory staining procedures—a characteristic useful for distinguishing mycobacteria from other bacterial species (Bayot et al., 2024).

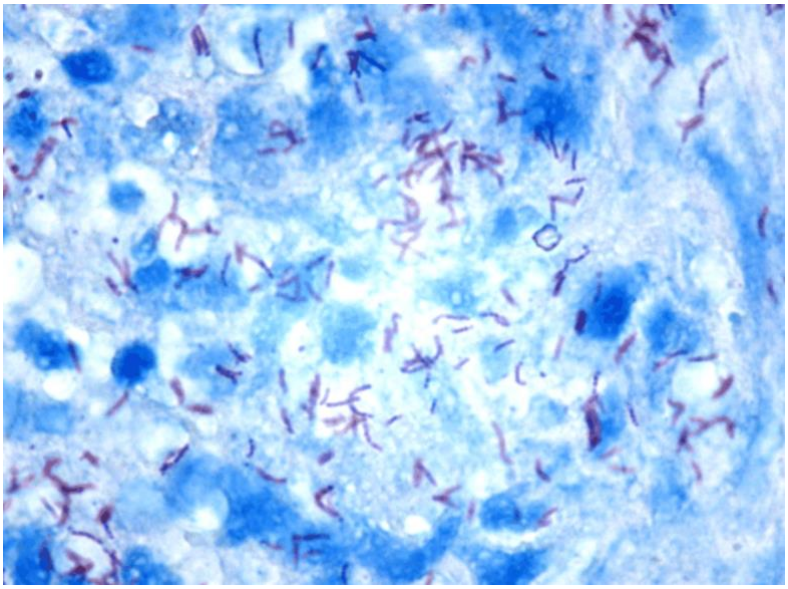

Figure 1.1 Microscopic image showing acid-fast bacilli, indicative of *Mycobacterium* species (Man et al., 2016).

The colonial morphology of mycobacteria grown on solid culture media varies between species, ranging from rough to smooth and from white to orange or pink in colour (Hedin et al., 2023). Most are aerobic organisms, although a few are microaerophilic (Pereira et al., 2020). Mycobacteria can also be classified by their growth rate (slow or rapid), pigment production (pigmented or non-pigmented), and their ability to cause disease (tuberculous or non-tuberculous). These classification criteria are significant in understanding the characteristics of mycobacteria (Lagune et al., 2023).

1.2 Mycobacterium tuberculosis complex (MTBC)

Slow-growing tuberculous mycobacteria cause tuberculosis; this group comprises six members, collectively known as the *Mycobacterium tuberculosis* complex (MTBC) (Mvubu & Jacoby, 2023). The MTBC is thus a group of six closely related variants, which are: *M. tuberculosis*, the causative agent of tuberculosis in humans; *Mycobacterium*

africanum; *Mycobacterium bovis* (*M. bovis*); *Mycobacterium canettii*; *Mycobacterium pinnipedii*; and *Mycobacterium microti*. These are all 99.99% similar at the nucleotide level, with identical 16S rRNA subunit sequences; however, they differ in their host ranges, phenotypes, and pathogenicity (Zhang et al., 2022).

Clinically, *M. tuberculosis* is the most pathogenic strain for humans, affecting the mammalian respiratory system (Pal et al., 2022). More than one-third of the global human population is estimated to be afflicted by this pathogen (Xia et al., 2023), and tuberculosis can also infect animals, which can subsequently spread the pathogen to humans (Kanabalan et al., 2021). *M. bovis*, the causative agent of bovine tuberculosis, stands out within the complex for its ability to infect a wide range of animals, including both wild and domestic species (Borham et al., 2022a). Within the MTBC, *M. tuberculosis* and *M. bovis* are the most common and problematic strains, and they are therefore discussed in further detail below.

1.3 Human tuberculosis

Tuberculosis (TB) is the second leading cause of human mortality worldwide, after coronavirus disease (COVID-19). Each year, more than 10 million people contract TB, and over 1.3 million deaths associated with the disease were reported globally in 2022 (World Health Organization, 2022). The burden of TB is concentrated in eight countries: India, China, Indonesia, the Philippines, Pakistan, Nigeria, Bangladesh, and South Africa, which collectively account for two-thirds of the world's cases (World Health Organization, 2022). *Mycobacterium tuberculosis* (*M. tuberculosis*), the causative agent of TB (Alsayed & Gunosewoyo, 2023a), primarily spreads through the inhalation of infectious aerosols generated by infected individuals (Coleman et al., 2022). These aerosols can remain airborne for 20 minutes to six hours and are typically inhaled by individuals in close proximity to the infected person (Krishnan et al., 2022). Susceptibility to TB infection is heightened in

individuals with compromised immune systems, whether due to age or underlying conditions such as HIV (Qi et al., 2023). Globally, an estimated 78,000 deaths from TB occur annually among individuals co-infected with HIV (World Health Organization, 2022).

1.4 Clinical forms of infection

TB can manifest in two forms: active and latent (Kim et al., 2023). Latent TB (LTBI) occurs when an infected individual shows no symptoms, has a negative chest X-ray, and routine cultures do not detect the pathogen (Banerjee et al., 2021). Upon entry into the lungs, the bacilli are engulfed by antigen-presenting cells, such as alveolar macrophages or dendritic cells, which form solid granulomas that keep the bacteria dormant. Reactivation of latent TB occurs only when these granulomas break down, which may happen in cases of immunosuppression; active infection then ensues. In its latent form, however, the bacterium is not transmissible to others (Boom et al., 2021; Viswanathan, 2023).

Pulmonary active TB can lead to airflow obstruction, restrictive ventilatory defects, and impaired gas exchange, reducing the lung's ability to inhale and exhale air (Allwood et al., 2020). The condition also results in lung stiffening, cavitation, excessive fibrosis, inflammation, and loss of lung function (Ivanova et al., 2023). Approximately 15 to 25% of abdominal TB cases are associated with concurrent pulmonary TB, often due to lymphatic spread (Abi et al., 2022). However, bone, joint, and skin TB are relatively rare, accounting for 2.2 to 4.7% and 8.4 to 13.7% of all TB cases, respectively (Yadav, 2022). Central nervous system (CNS) tuberculosis is even less common, occurring in approximately 1% of all TB cases (Dian et al., 2021). Tuberculous meningitis is the most common form of CNS tuberculosis, typically occurring when the bacillus spreads to the CNS via the lymphatic system or bloodstream (Katrak, 2021). It is particularly associated with immunodeficiency, HIV infection, and cancer patients (Ayele & Amogne, 2021).

1.5 Virulence factors

M. tuberculosis lacks classical virulence factors, such as the production of recognised extracellular toxins seen in pathogens like *Shigella dysenteriae* and *Vibrio cholerae* (Kanabalan et al., 2021). The organism's genome consists of approximately 4,000 genes, with only 91 of these associated with virulence. These genes are involved in various functions, including maintaining cell wall integrity, creating signal transduction pathways, synthesising regulatory proteins, lipid metabolism, and the production of cell surface proteins (Maladan et al., 2021). The cell wall of *M. tuberculosis* is distinct from that of other bacteria due to the presence of mycolic acid, a long-chain α-alkyl β-hydroxy fatty acid attached to its peptidoglycan layer. This unique structure is believed to hinder antibiotic uptake (Holzheimer et al., 2021) (Figure 1.2), while the cell wall also contains several efflux pumps that contribute to the bacterium's overall drug resistance (Remm et al., 2022).

As shown in Figure 1.2, the cell envelope also includes other glycolipids that are crucial during infection. Lipoarabinomannan, for example, stimulates the release of tumour necrosis factor (TNF-α), a significant cytokine produced during infection, whose overproduction can induce extensive tissue damage (Correia-Neves et al., 2022a). LAM also inhibits macrophage-mediated destruction by suppressing the activity of protein kinase C, thereby allowing the pathogen to evade immune surveillance more effectively (Correia-Neves et al., 2022b). The glycolipids trehalose 6,6-dimycolate (TDM), also known as cord factor, and phthiocerol dimycocerosate (PDM) function similarly, targeting phagosomal-lysosomal processes (Nguyen & Yates, 2021). TDM is the predominant lipid in the *M. tuberculosis* cell envelope, and it is responsible for inducing the granulomas that lead to the increased production of cytokines, inhibiting phagosomal-lysosomal fusion. In contrast, PDM prevents the phagosomal acidification crucial to the intracellular destruction of bacteria (Schami et al., 2023).

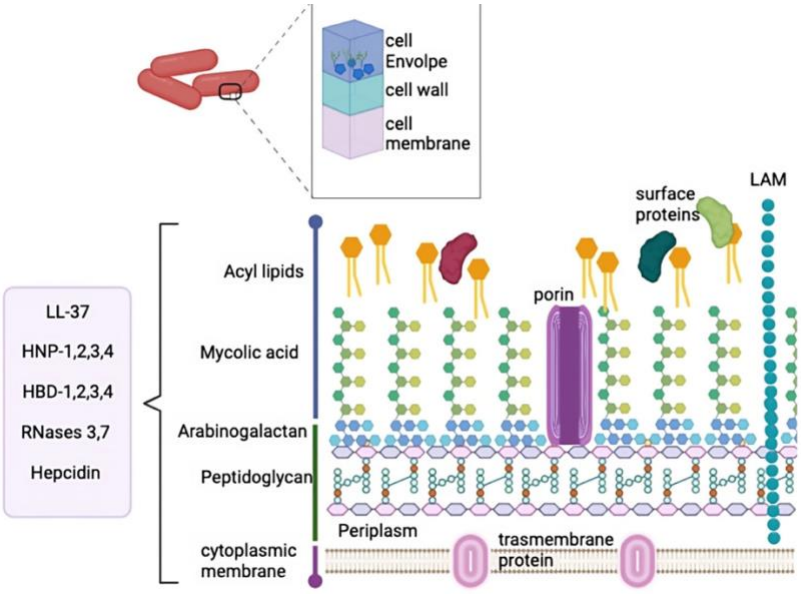

Figure 1.2 Schematic representation of the major components of the *M. tuberculosis* cell wall.

The inner layer consists of peptidoglycan covalently linked to an arabinogalactan layer, while the outer membrane contains mycolic acids, glycolipids such as mannosylated lipoarabinomannan (LAM), and mannoglycoproteins (Jacobo-Delgado et al., 2023).

1.6 Interactions with phagosome and lysosome

The bacterium is transmitted through the inhalation of air droplets containing viable bacilli (Dinkele et al., 2024). Following entry into the lungs, macrophages engulf the bacteria and transport them into the acidic compartment of the lysosomes, a process critical for initiating the immune response. Within the lysosome, the bacteria typically encounter harsh conditions, including low pH and digestive enzymes, which are intended to destroy the pathogen. However, *M.tuberculosis* has evolved mechanisms to survive and replicate in this environment. Only those bacteria that evade delivery into this lysosome can survive and cause infection (Carranza & Chavez-Galan, 2019).

As shown in the schematic in Figure 1.3, latent TB infection begins with the entry of *M. tuberculosis* bacilli into the lungs. Upon reaching the alveoli, they are commonly engulfed by macrophages via phagocytosis. If phagocytosis fails, however, *M. tuberculosis* can infect the interstitial tissues of the alveolar epithelium or the alveolar macrophages, which then migrate to the lung parenchyma. Subsequently, dendritic or inflammatory cells can transfer *M.*

tuberculosis to the pulmonary lymph nodes for T cell priming (Gong & Wu, 2021). Active TB occurs during granuloma formation: if the bacilli load becomes too large for containment within the granuloma, or if necrosis of the granuloma occurs, rupture can happen, leading to active and symptomatic TB (Cronan, 2022).

The bacterial surface glycolipid LAM helps the bacillus evade transport to the lysosome by preventing the formation of phosphatidylinositol 3-phosphate (PIP3), which is crucial for this process (Nguyen & Yates, 2021). This pathway is further inhibited by a lipid phosphatase (SapM) and protein phosphatases (PtpA and PtpB) released into the cytosol upon bacterial entry into the cell: SapM breaks down PIP3 on the phagosomal membrane, while the protein tyrosine phosphatases (A/B) interfere with trafficking processes (Margenat et al., 2023). Another mechanism employed by the pathogen to prevent phagosome and lysosome fusion involves the production of a signalling molecule that enhances the synthesis of protein kinase G (PnKG), which inhibits the fusion process (Nguyen & Yates, 2021).

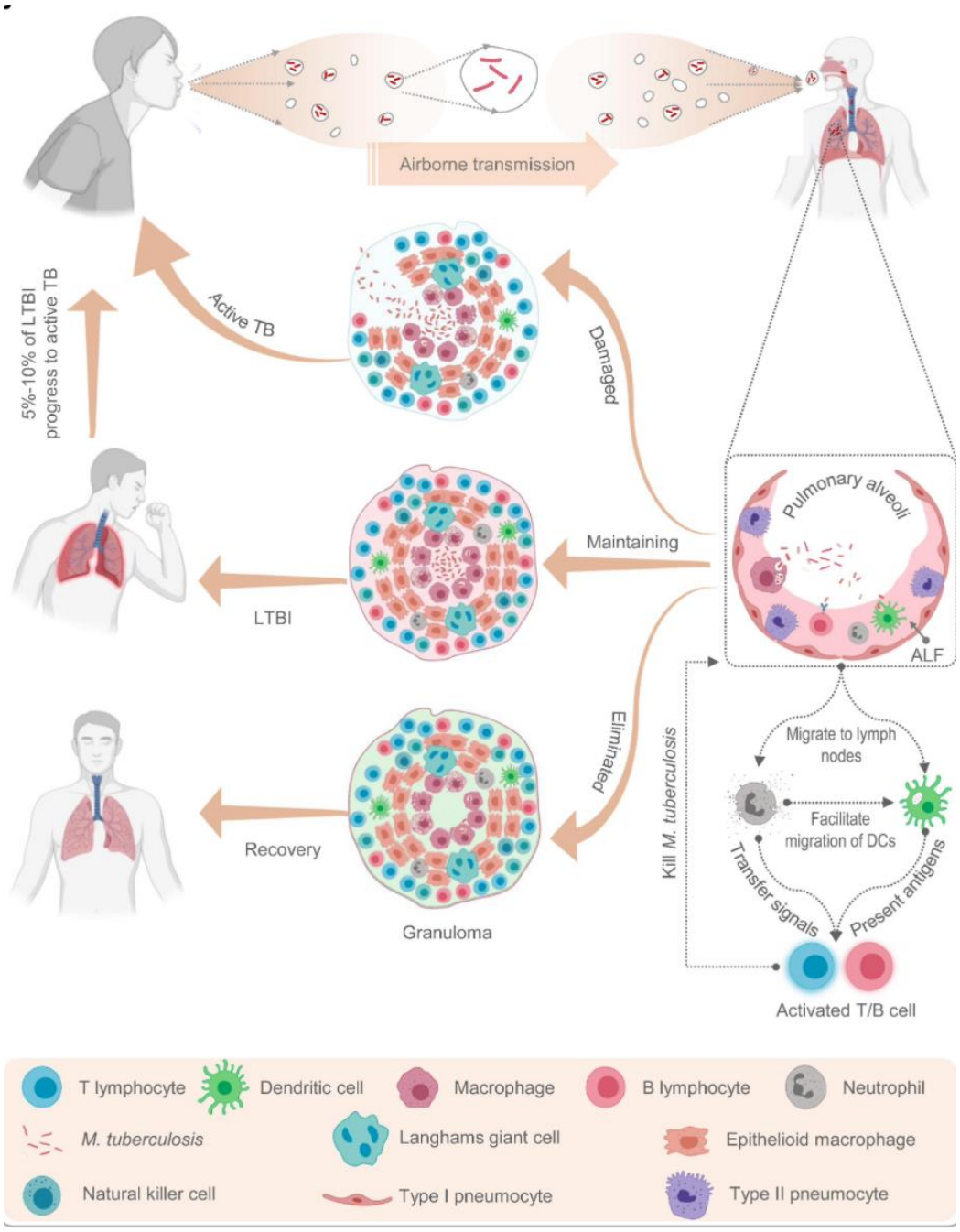

Figure 1.3 Infection stages of (a) latent and (b) active TB. (Gong and Wu 2021).

1.7 Antibiotic treatment

In recent years, antibiotic resistance has risen, prompting healthcare professionals to use a wider range of antibiotic combinations (Arrigoni et al., 2022). According to a 2019 report by the WHO, 41% of TB infections now show resistance to rifampicin, a key antibiotic that was previously used as a first-line treatment for TB (WHO, 2020). The current guidelines for antibiotic treatment recommend a combination of four primary antibiotics: rifampicin (RIF), ethambutol (ETMB), pyrazinamide (PZ), and isoniazid (INH). Where resistance develops, second-line antibiotics, such as fluoroquinolones, are available, alongside injectable antibiotics like amikacin, kanamycin, and capreomycin (Alsayed & Gunosewoyo, 2023). Nevertheless, the WHO now considers the emergence of drug-resistant tuberculosis to be its most challenging and urgent problem (World Health Organization, 2022).

1.7.1 First line antibiotic treatment

Four main drugs are employed for first-line TB treatment; these should be taken together to prevent the emergence of bacterial resistance (Alsayed & Gunosewoyo, 2023b). Their mechanisms of action and resistance are discussed below.

1.7.1.1 Rifampicin (RIF)

RIF, a lipophilic drug, inhibits mRNA elongation by binding to the beta-subunit of RNA polymerase (*rpoB*), halting bacterial protein synthesis and growth (Yang et al., 2023). Resistance arises when mutations occur in the antibiotic binding site, specifically within the 81 base pair regions of the *rpoB* gene known as the RIF resistance-determining region (RRDR); approximately 95% of RIF-resistant strains exhibit mutations in this DNA region (Zeng et al., 2021). Resistance to RIF also indicates multidrug resistance (MDR), as all strains resistant to RIF are also resistant to isoniazid (Shea et al., 2021).

1.7.1.2 Isoniazid (INH)

INH is a prodrug that requires activation by the bacterial enzyme catalase-peroxidase, encoded by the *katG* gene (Ofori-Anyinam et al., 2023). Once activated, INH forms a complex with NAD+/NADH, known as the INH-NADH adduct, which inhibits enoyl-acyl carrier protein (ACP) reductase, an enzyme crucial to mycolic acid synthesis, a critical component of cell wall biosynthesis (Falcao et al., 2022). Resistance to INH typically arises from mutations in the *katG* gene, leading to a failure in prodrug activation (Falcao et al., 2022).

1.7.1.3 Ethambutol (ETMB)

ETMB disrupts the biosynthesis of both arabinogalactan and lipoarabinomannan (LAM) within the cell wall (Zhang et al., 2020). Specifically, it targets the *embB* gene at position 306; however, studies have shown that mutations in this gene do not directly lead to drug resistance (Bwalya et al., 2022). Consequently, research is ongoing to identify other genes responsible for ETMB resistance (Wu et al., 2022), as changes in the *embB* gene alone do not provide a definitive indicator of resistance to ETMB.

1.7.1.4 Pyrazinamide (PZ)

PZ is a prodrug that undergoes activation to pyrazinoic acid through the action of pyrazinamidase (PZase) (Gopal et al., 2020). The precise mechanism by which PZ exerts its antimicrobial effect is not fully understood. However, it has been suggested that PZ inhibits fatty acid synthase type I in actively replicating bacteria (Gopal et al., 2020). It has also been suggested that PZ disrupts bacterial membrane energetics by depleting membrane potential and hindering active membrane transport (Lamont et al., 2020). The primary mechanism for resistance to PZ involves mutations in the *pncA* gene, which encodes PZase (Tunstall et al., 2021). However, resistance to PZ has also been linked to mutations in *panD*, which is

targeted by PZ and inhibits pantothenate and coenzyme A synthesis, both essential for energy production and fatty acid metabolism in bacteria (Hameed et al., 2020).

In cases where resistance is limited to a single drug other than rifampicin, the remaining three drugs may still be effective. However, in the event of rifampicin resistance, which implies broader resistance as discussed, second-line drugs are recommended, and treatment should be adjusted based on susceptibility testing results (Hameed et al., 2020).

1.7.2 Second line antibiotic treatment

1.7.2.1 Fluoroquinolones

The fluoroquinolones used in TB treatment include ciprofloxacin, moxifloxacin, levofloxacin, and ofloxacin (Rusu et al., 2023). These drugs inhibit DNA gyrase, a type II topoisomerase composed of two A and two B subunits encoded by the *gyrA* and *gyrB* genes, respectively (Collins & Osheroff, 2024). DNA gyrase is crucial for bacterial DNA synthesis (Cheng et al., 2020). The Quinolone Resistance Determining Region (QRDR) is a specific region within the *gyrA* and *gyrB* genes where mutations can lead to resistance (Shaheen et al., 2021).

1.7.2.2 Aminoglycosides

Amikacin (AK), kanamycin (KM), and capreomycin are vital injectable drugs used to treat resistant TB (Mantefardo & Sisay, 2021). These drugs function by inhibiting protein translation; resistance to them is often linked to mutations in the 16S rRNA, encoded by the *rrs* gene (Singh et al., 2020).

1.8 Current treatment

The current standard treatment for active TB consists of a six-month course of antibiotics (Alsayed & Gunosewoyo, 2023). However, the treatment duration can vary based on factors such as the site of infection, patient age, and prior treatment history (Vanino et al., 2023).

According to the WHO, TB treatment is divided into two phases: intensive and continuous (World Health Organization, 2022). During the intensive phase, which lasts for the first two months of treatment, patients must take a daily combination of isoniazid, rifampicin, pyrazinamide, and ethambutol (Bi et al., 2022). Following the completion of the intensive phase, the continuous phase commences, involving four months of treatment with isoniazid and rifampicin alone. This drug regimen may, however, be adjusted based on susceptibility testing results (Bi et al., 2022). For patients with central nervous system tuberculosis (CNS TB), pyridoxine (vitamin B6) is added to prevent the development of peripheral neuropathy, for example (Court et al., 2021).

1.9 Antibiotic resistance in *M. tuberculosis*

Drug-resistant TB strains spread in a similar manner to drug-susceptible strains, primarily through airborne transmission from person to person (Chen et al., 2022; Liebenberg et al., 2022). Two types of resistance are observed in TB: multi-drug resistance (MDR) and extensively drug-resistant (XDR). MDR refers to resistance to rifampicin and isoniazid, while XDR denotes MDR strains that are resistant to additional second-line antibiotics (Nimmo et al., 2022). Potential causes of drug resistance include non-adherence to treatment, the use of single drugs instead of combination therapy, poor drug quality, and incomplete treatment courses (Liebenberg et al., 2022). Delays in initiating appropriate treatment or the use of incorrect medications can exacerbate the spread of resistant strains (Zhang et al., 2023), making it crucial to develop assays capable of rapidly confirming the presence of the pathogen and determining its sensitivity to RIF (Malenfant & Brewer, 2021). Better access to such diagnostic tools can minimise the spread of resistance and allow for optimal patient treatment outcomes.

1.10 Policies and strategies to prevent TB infection

The WHO's “End TB” strategy, launched in 2015, aims to achieve a world free of TB by 2050. Interim goals include a 90% reduction in infections and a 95% reduction in tuberculosis-related deaths by 2035, compared to 2015 levels (World Health Organization, 2024). This strategy is built upon three main pillars: integrated patient-centred care, policy change and the development of supportive systems, and intensified research and development.

Integrated patient-centred care and prevention encompasses four key elements:

1. Early, accurate and rapid diagnosis of TB.
2. Increased treatment coverage for infected individuals, including those with drug-resistant TB.
3. The provision of preventive treatment for high-risk groups, including individuals infected with HIV.
4. Management of co-morbid diseases alongside TB.

Policy and support systems can vary; however, they must include the following four points:

1. Government commitment to adequate resourcing of TB care and prevention efforts.
2. Engagement of all communities, including government and private organisations, in TB control initiatives.
3. Addressing social determinants, such as poverty, which influence TB incidence.
4. Provision of social protection measures to support TB patients and their families.

Intensified research and innovation must have two key focuses:

1. The discovery and implementation of new tools and strategies for TB control.
2. The development of point-of-care rapid diagnostic tests and new treatment regimens for TB (World Health Organization, 2024).

These efforts must also accelerate progress towards the WHO's ambitious goal of eliminating TB as a global health threat by 2050.

1.11 Bovine tuberculosis

Bovine tuberculosis (bTB) is a severe zoonotic disease with significant economic and health impacts (Bezos et al., 2023). *Mycobacterium bovis* (*M. bovis*), the causative agent of bTB, is responsible for up to 10% of human TB cases in developing countries, according to estimates by the World Organisation for Animal Health (OIE) (Fareed et al., 2024).

Bovine tuberculosis shows the highest prevalence rates in Africa and parts of Asia, although cases have also been reported in the Americas and Europe (Bruczyńska et al., 2022; Fareed et al., 2024). Globally, agriculture suffers annual losses of $3 billion due to the slaughter of infected animals (Singhla & Boonyayatra, 2022), and in England, the number of animals slaughtered due to TB incidents increased by 5% to 21,298 animals between April 2023 and March 2024. There was a 17% increase in Wales, where 11,197 animals were slaughtered during the same period (Department for Environment, Food & Rural Affairs, 2023). Cattle, as the primary reservoir for *M. bovis*, are crucial for many human livelihoods, providing essential dairy products and clothing, particularly in developing countries (Opadoyin Tona, 2022). However, the economic burden of bTB extends beyond direct agricultural losses, affecting public health and necessitating comprehensive control measures to prevent further spread.

Transmission of *M. bovis* occurs through various routes: between animals (most commonly between cattle), from animals to humans (zoonotic transmission), from humans to animals (sporadic transmission), and among humans. However, the exact mechanisms of *M. bovis* transmission remain poorly understood (Justus et al., 2024). Known transmission routes include ingestion (through contaminated unpasteurised milk and meat), inhalation, or direct

contact with mucous membranes and skin abrasions (Collins et al., 2022). The disease progresses slowly, taking months or even years to cause death in infected animals, during which time they can spread the disease to many other susceptible parties (Borham et al., 2022).

Current monitoring of bTB in developed countries involves a combination of slaughterhouse surveillance and antemortem testing. Slaughterhouse surveillance relies on visually detecting lesions in carcasses; however, it is estimated to detect only 27 to 46% of infected cattle annually (Frankena et al., 2007; García-Díez et al., 2023). Antemortem testing relies on measuring cell-mediated immune responses, employing various tests such as the tuberculin skin test and gamma interferon (IFN-γ) release assays, further described in section 1.1.5 (Kelly et al., 2022).

1.12 Non-tuberculous mycobacteria (NTM)

Non-tuberculous mycobacteria (NTM), including *Mycobacterium abscessus* (*M. abscessus*), are an important subgroup within the genus, contributing to its diversity and clinical significance (Chin et al., 2020). NTM can infect both humans and animals, including poultry and fish (To et al., 2020). They pose risks to immunocompromised individuals, such as those with cystic fibrosis (Chin et al., 2020) or HIV/AIDS (Chiang et al., 2021). NTM can be further classified based on their growth rates, with some being rapid growers (e.g., *M. abscessus*, *M. smegmatis*, *M. chelonae*) with a growth period of 2 to 3 days, and others being slow growers (e.g., *M. kansasii*, *M. avium*), which require around seven days for growth (Sharma & Upadhyay, 2020). The WHO has highlighted the need to apply a combination of clinical, radiographic, and microbiological criteria to diagnose NTM infections (Feng et al., 2020). This includes using molecular techniques to identify the specific species of NTM and ruling out other diseases, such as TB (Centers for Disease Control and Prevention, 2024).

Treatment must be adapted to the unique species determined; however, it typically involves long-term administration of multiple drugs, subject to close monitoring of their efficacy and any potential adverse reactions (Johnson et al., 2023).

1.13 Surrogate model for TB diagnosis

Due to the challenges of working with *M. tuberculosis*, including its slow growth, which necessitates 6 to 8 weeks to confirm a diagnosis—mainly due to its slow replication rate and the requirement for specialized culturing conditions—and the need for biosafety level 3 facilities, many researchers use faster-growing and/or less virulent mycobacterial strains to optimise their work. In this study, the BCG strain of *M. bovis* was employed, as it is harmless to humans and readily available. This strain can act as a surrogate model for *M. tuberculosis*, as it shares significant genetic homology while not posing the same safety risks or requiring the same lengthy cultivation time.

1.14 Mycobacterial diagnostic methods

Accurate and timely diagnosis is crucial for effective patient treatment (Meyer et al., 2021). In TB, early and precise diagnosis, followed by the prompt initiation of appropriate treatment and comprehensive patient follow-up, are essential (Meyer et al., 2021). However, such a strategy poses challenges, particularly in resource-constrained settings, such as some African countries (Mendelsohn et al., 2022).

There is no single rapid, accurate, affordable, and straightforward diagnostic method for TB. Traditional diagnostic techniques, such as microscopy and bacterial culture, lack specificity and sensitivity and are time-consuming. Conversely, newer DNA-based technologies offer enhanced sensitivity but are associated with high costs and require specialised equipment and skilled technical personnel (Shivakumar & Sunil Shettigar, 2023).

Developing a simple, inexpensive, and rapid assay with high sensitivity and specificity, capable of quickly (within minutes) determining the antibiotic sensitivity of any identified TB pathogen, would significantly aid global efforts to control TB. The current methods utilised for diagnosing TB are discussed below in this context.

1.14.1 Microscopy

Microscopic methods are the most economical and, historically, the traditional laboratory-based approaches for detecting TB (Campelo et al., 2022). The unique cell wall composition (characterized by a high concentration of mycolic acids, which are long-chain fatty acids that form a waxy, hydrophobic layer) of *M. tuberculosis* allows it to retain the Ziehl-Neelsen (ZN) stain, which offers a rapid and practical method for visualising acid-fast bacilli (AFB) (Prakoeswa et al., 2022). However, while effective as a rapid screening tool, Ziehl-Neelsen staining lacks specificity and sensitivity, typically between 22% and 43% compared to primary culture methods. The lowest number of *tuberculosis* bacteria that a smear can typically detect is around 5,000 to 10,000 bacteria per millilitre of sputum. This number reflects the limitations of smear microscopy, which has relatively low sensitivity compared to more advanced diagnostic methods. However, this can vary based on sample quality.

Fluorescence microscopy, which is more sensitive than conventional light microscopy, also suffers from specificity issues (Rekha et al., 2021), as well as being unable to distinguish between virulent and non-virulent mycobacteria or determine antibiotic sensitivity (Abebe et al., 2020). Fluorescence microscopy is also relatively costly due to the frequent need to replace mercury vapour lamps, and its requirements for external power and a dark room limit its use in field settings (Abebe et al., 2020).

1.14.2 Mycobacterial culture

The gold standard for diagnosing TB is isolating the bacterium from a sputum sample collected from the patient (Heyckendorf et al., 2020). Before culturing, the sample must undergo a decontamination process to reduce the presence of non-tuberculous bacilli originating from the normal bacterial flora of the upper respiratory tract (URT), which could interfere with the subsequent identification of the pathogen. While this step decreases the number of URT bacilli, it can also lower the recovery rate of *mycobacteria* (Heyckendorf et al., 2020).

Culturing the bacterium traditionally takes up to 6 to 8 weeks using solid media such as Löwenstein-Jensen (LJ) agar (Figure 1.4) (Ma et al., 2020a). However, highly enriched media such as Middlebrook 7H11 can shorten the culture period to 10 days (Guallar-Garrido et al., 2020). Unfortunately, safe culturing of *M. tuberculosis* necessitates access to biosafety level 3 facilities; this, coupled with its slow growth rate, may lead to delays in initiating effective treatment.

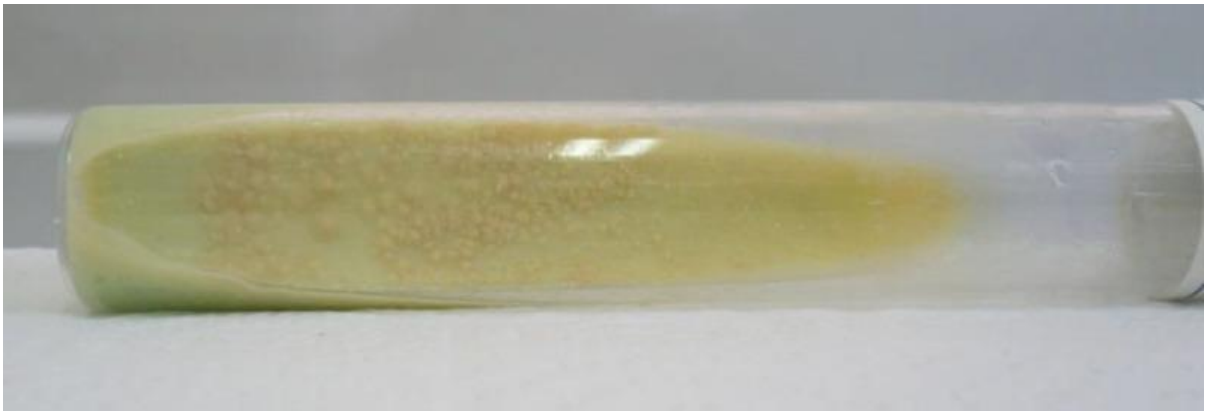

Figure 1.4 Growth of *M. tuberculosis* on Lowenstein-Jensen (LJ) agar.

(Ma et al., 2020a).

1.14.3 Chest X-ray

Historically, chest X-rays have been used as a primary tool for detecting lung abnormalities suggestive of TB (Abuzerr & Zinszer, 2023). While exhibiting high sensitivity (73 to 79%), it suffers from a relatively low specificity (31%), meaning the test is prone to false positive

results incorrectly identifying individuals without tuberculosis as being infected. However, their high sensitivity allows for effective detection of individuals with tuberculosis (Nalunjogi et al., 2021). Therefore, further investigations are often necessary to confirm a diagnosis of TB after the X-rays are examined.

More advanced and sensitive imaging tools, such as MRI and CT scanners, are available; however, while these are effective for diagnosing TB, they come at a significantly higher cost than chest X-rays (Nel et al., 2022; Abuzerr & Zinszer, 2023). Several health risks are also associated with repeated exposure to X-rays (Abuzerr & Zinszer, 2023) (Figure 1.5).

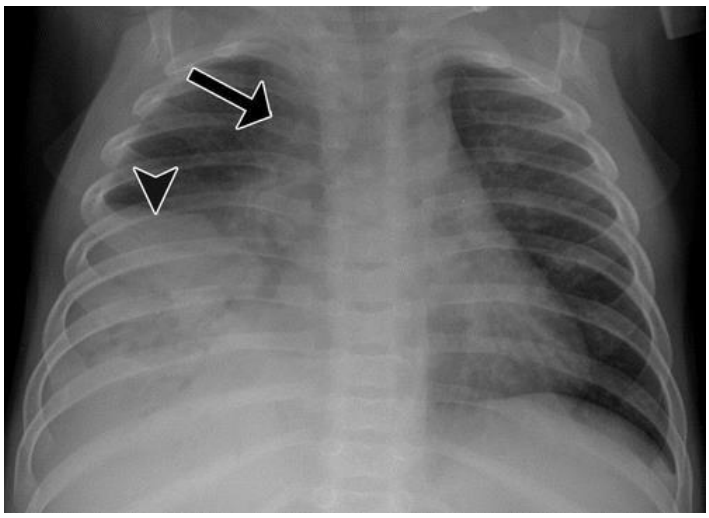

Figure 1.5 Chest X-ray of a TB patient.

Frontal chest radiograph showing thickening of the right paratracheal stripe, consistent with lymphadenopathy (arrow), and consolidation (arrowhead) in the right middle and lower lobes (Nachiappan et al., 2017).

1.14.4 Immunological methods

According to the World Health Organization (WHO), sputum is the preferred sample for tuberculosis diagnosis because it typically contains a higher bacterial load compared to other samples such as saliva. This is due to the fact that sputum originates from the lungs, which are the primary site of *M. tuberculosis* infection (WHO,2024).

While sputum remains the preferred sample for diagnosing TB, certain patient groups face challenges in producing sputum, such as children under 12 years of age and individuals with HIV (Broger et al., 2023). In these cases, serological assays are preferred (Jagannath et al., 2020). The immunological assays currently used for TB diagnosis can be categorised into two main groups: indirect and direct assays. Indirect assays detect the body's immune response to the TB pathogen, whereas direct assays target the bacterium itself.

1.14.4.1 Indirect assay

The tuberculin skin test (TST) is widely used to diagnose both active and latent TB (Prakash Babu et al., 2023). This test involves the intradermal injection of a purified protein derivative (PPD) derived from heat-killed *M. tuberculosis* cultures. If an individual has been exposed to the TB pathogen, the introduction of PPD stimulates the T cells to release interleukins, resulting in visible skin changes (Prakash Babu et al., 2023). Typically, a discrete, pale elevation of the skin (wheal), measuring between 6 to 10 mm, appears 48 to 72 hours post-administration; the size of this wheal helps determine exposure to mycobacteria (Gloria et al., 2021). However, the TST lacks specificity, as it may yield a positive result both in individuals vaccinated against TB with Bacillus Calmette-Guérin (BCG) and in those exposed to non-tuberculosis mycobacteria that share antigens with *M. tuberculosis* (Sakiyama et al., 2021). Any positive TST reaction, therefore, requires confirmation using more precise assays (Ludi et al., 2023).

Other immunological assays for TB diagnosis include the QuantiFERON-TB Gold In-Tube (QFT-GIT) assay (Qiagen Company) and the T-SPOT.TB assay (Oxford Immunotec Company). These assays measure the responses of T cells isolated from potentially infected individuals to *M. tuberculosis*-derived antigens, such as ESAT-6 and culture filtrate protein (CFP-10). In infected individuals, the T cells produce interferon-gamma (IFN-γ) in the

presence of these antigens (Moon et al., 2020; Wang et al., 2022). Unfortunately, the costs of these assays limit their widespread use in developing countries (Barker et al., 2023; Navarro & Betancur, 2024).

1.14.4.2 Direct antigen detection assays

Lipoarabinomannan (LAM), a prominent glycolipid in the mycobacterial cell wall, is a key antigenic target for TB detection (Ketema et al., 2022). Immunological tests, such as the MTB ELISA Test® marketed by Chemogen, Portland, USA, can detect LAM. While urine is the primary sample for detecting LAM, this antigen can also be detected in other sample types, such as sputum, serum, cerebrospinal fluid (CSF), and pleural fluid (Correia-Neves et al., 2019). The sensitivity and specificity of LAM assays vary depending on the sample type and the patient's immune status. In sputum samples, the sensitivity and specificity compared to smear microscopy have been reported as 55.49% and 48%, respectively (Gao et al., 2024). Along with this relatively low specificity and sensitivity, another major drawback of LAM detection is the continuous remodelling of the LAM structure, which may negatively affect antigen detection (Flores et al., 2021).

1.14.5 High performance liquid chromatography (HPLC)

High-performance liquid chromatography (HPLC) is a column chromatography technique extensively used in pharmaceutical and laboratory settings (Chew et al., 2021). This method separates components within a mixed suspension into a stationary phase (either polar or non-polar) and a mobile phase (also polar or non-polar), with the choice of phases depending on the characteristics of the sample being analysed (Sandmann, 2022). In the context of TB diagnosis, HPLC can detect the presence of mycolic acid esters, which are characteristic components of *M. tuberculosis* (Brandenburg et al., 2022). However, to achieve its high sensitivity, HPLC requires access to cultures of the pure bacterium, rendering it unsuitable as

a rapid diagnostic method (Lasch et al., 2020). Moreover, HPLC is a sophisticated method that requires trained personnel, which adds to operational costs (Thomas et al., 2022).

1.14.6 DNA-based diagnostic methods

DNA-based methods, such as the Polymerase Chain Reaction (PCR), have revolutionised TB diagnosis by significantly reducing the time required to predict antibiotic sensitivity—from the weeks required for sputum culture to just hours (Gupta et al., 2023). Despite their effectiveness, PCR methods necessitate access to advanced equipment, involve time-consuming sample processing to remove extraneous biological material, and are relatively costly compared to traditional methods such as microscopy and culturing (Liu et al., 2019; Minhas et al., 2023).

In 2010, the WHO endorsed several nucleic acid technologies for TB diagnosis, including the Cepheid Xpert MTB systems developed by the Foundation for Innovative New Diagnostics (FIND) and isothermal nucleic acid amplification tests (World Health Organization, 2010). These assays represent a significant advancement in TB diagnostics, offering rapid and accurate detection of *M. tuberculosis* and its resistance to rifampicin, a crucial first-line antibiotic. Both methods are discussed in more detail below.

1.14.6.1 Xpert MTB assays

Cepheid developed two types of systems for tuberculosis diagnosis: the Xpert MTB/RIF assay, which detects *M. tuberculosis* and rifampicin resistance, and the Xpert MTB/XDR assay, which extends the capabilities of the original test by detecting resistance to a broader range of first-line and second-line anti-tuberculosis drugs (Kay et al., 2022). The Xpert MTB/RIF assay integrates sample processing, PCR amplification, and detection within a self-contained GeneXpert cartridge, making it automated except for the initial mixing of the sample with a reagent (Kay et al., 2022; Andama et al., 2022). The test demonstrates

sensitivity ranging from 68% to 100% and specificity from 91.7% to 99.3% (Arbués & Rossetti, 2024), but it is limited to detecting rifampicin resistance and does not assess resistance to other antibiotics (Kaso & Hailu, 2021). The Xpert MTB/XDR assay provides a more comprehensive profile of drug-resistant TB by detecting resistance to multiple first-line and second-line drugs. The Xpert MTB/XDR assay demonstrates sensitivity ranging from 94% to 100% and specificity of 100% for all drugs except ethionamide, when compared to sequencing results (Cao et al., 2021). However, both tests share significant drawbacks: they are expensive (Xpert MTB/RIF costs around $12.90 per test), require reliable infrastructure (computer access, power, and maintenance), and may show reduced sensitivity in cases with low bacterial loads or extra-pulmonary TB. Furthermore, the Xpert MTB/XDR test is more costly and complex due to its broader resistance testing capabilities, limiting its implementation, particularly in resource-limited settings (Mvelase & Mlisana, 2022)

1.14.6.2 Isothermal nucleic acid amplification tests

Unlike traditional PCR, which involves repeated heating and cooling cycles to amplify the DNA templates, isothermal amplification is performed at a constant temperature, utilising a specific DNA polymerase (Kaur & Toley, 2023). Its key distinction lies in its speed: isothermal amplification produces amplicons rapidly, to the extent that these are often detectable by a visible change in assay colour (Neshani et al., 2023).

One notable isothermal method is Loop-Mediated Isothermal Amplification (LAMP), which targets genes such as *rrs*, *IS6110*, and *gyrB* in *M. tuberculosis* (Yang et al., 2021). LAMP has reported sensitivity and specificity of 92.75% and 91.67%, respectively, for detecting the *IS6110* gene (AĞEL et al., 2020). However, its performance varies across gene targets. TB-LAMP *IS6110* demonstrated 89.8% sensitivity, while TB-LAMP *mpb64* showed a higher sensitivity of 94.9% compared to MGIT culture. Both TB-LAMP targets showed

significantly higher levels of MTB detection compare to AFB microscopy and MGIT culture, with TB-LAMP *mpb64* also outperforming CB-NAAT. The agreement between TB-LAMP (*mpb64* and *IS6110*) and CB-NAAT was moderate to high (Dayal et al., 2021).

Despite their many advantages, LAMP and other isothermal assays also have several limitations: in particular, they require highly purified DNA, are relatively costly, and rely on refrigerated reagents (Neshani et al., 2023). These factors significantly influence their applicability in resource-limited settings and highlight the ongoing need to develop affordable, robust diagnostic solutions for TB detection.

1.14.6.3 Whole-genome sequencing

Whole-genome sequencing (WGS) refers to the analysis of the entire genomic DNA sequence at the same time (Souche et al., 2022), which can be used as a diagnostic method for both bacteria and viruses (Brlek et al., 2024). However, WGS requires expert knowledge to interpret the resulting genomic data, and it is thus relatively costly (Delahaye & Nicolas, 2021a). The Oxford Nanopore is an advanced third-generation sequencing device for sequencing viral and bacterial pathogens. During the Ebola outbreak in Africa, it was employed to sequence the virus (Athanasopoulou et al., 2021) by passing an electric current through a membrane with embedded nanopores. When any DNA molecule passes through such a nanopore, it creates a distinctive disturbance in the ion current, which the system can detect and interpret (Wang et al., 2021b).

The main disadvantages of the Oxford Nanopore MinION system include its high sensitivity, which makes it susceptible to environmental factors, and the requirement for an experienced laboratory technician to operate and interpret its results. Sequencing with the MinION takes

approximately 24 hours, not including sample pretreatment, host depletion, and the necessary DNA isolation. Additionally, it has a high error rate of around 11% and requires reagents that must be refrigerated (Delahaye & Nicolas, 2021). The cost per sample is around $100, making it prohibitively expensive for use in low-income countries (van der Reis et al., 2023).

1.15 Point-of-care (POC) diagnostics

Rapid and precise identification of TB infection and antibiotic sensitivity at the point of care (POC) is essential to effectively halt the transmission of the illness (Elrobaa et al., 2024). Unlike standard laboratory-based tests, POC TB diagnostic assays offer accessible, accurate, and economical TB diagnosis by enabling prompt testing at patient care sites, even in resource-constrained settings, thus facilitating the rapid initiation of treatment to potentially interrupt ongoing transmission (Hong et al., 2022). However, numerous challenges exist in providing Point-of-Care Tests (POCTs) that can fulfil the ASSURED criteria specified by the WHO, which require tests to be Affordable, Sensitive, Specific, User-friendly, Rapid and Robust, Equipment-free, and Deliverable to end-users (Otoo & Schlappi, 2022). An optimal POC test should also include the ability to detect specific biological indicators in clinical samples, accurately forecasting disease occurrence (Khan et al., 2024).

Additionally, the relevant biomarker must exhibit specificity towards the pathogen responsible for the illness without demonstrating cross-reactivity with other pathogens. However, the latter is a common issue with serological-based assays (Bohn et al., 2020). Molecular detection technologies offer significant advantages over serological tests and promise to advance point-of-care testing. Determining the precise nucleic acid sequences in *M. tuberculosis* and *M. bovis* could lead to the development of significant biological indicators for accurate and sensitive identification and tracking of therapies. Developing a rapid test that can be miniaturised into a portable device at the POC could also mitigate the

impact of mycobacteria-related diseases and other significant public health threats. A major bottleneck in developing a DNA diagnostic tool is obtaining high DNA yields of sufficient quality from the relevant pathogen, especially when dealing with bacteria such as *M. tuberculosis* with complex cell walls.

1.16 Techniques for bacteria cell wall lysis

Three considerations are crucial for developing DNA-based diagnostic techniques for point-of-care (POC) applications. First, the quantity of DNA is important; a sufficient yield is required to enhance the assay's sensitivity (Song et al., 2024). Second, the quality of the DNA is vital, as many extraction techniques can compromise its integrity, leading to fragmentation or an increase in contaminants that affect the outcome (Jansson et al., 2024). Furthermore, the time needed to isolate the DNA is also essential; POC testing, where prompt results are critical, requires rapid extraction (Song & Gyarmati, 2022). Various methods have been employed to extract DNA from bacterial cells, including boiling, sonication, microwave treatment, and chemical-mechanical techniques.

Physical disruption methods for extracting DNA, such as heating, bead beating, or sonication, are typically straightforward to implement. However, they often lead to fragmented DNA due to heating or DNA shearing (Bello et al., 2020).

Fragmented DNA may lead to reduced hybridization efficiency, as shorter DNA fragments have fewer complementary regions available for probe binding, resulting in incomplete or weak signals. Additionally, the fragmentation can cause partial or inconsistent target sequence recognition, decreasing assay sensitivity and increasing the likelihood of false negatives or inaccurate quantification (Ekram et al., 2024).

Furthermore, contaminants like proteins and carbohydrates can diminish the DNA's purity, affecting the reliability of the results (de Bruin et al., 2019).

On the other hand, chemical methods for releasing DNA can take more than 20 hours, which is impractical for point-of-care diagnostics where speed is crucial (Ma et al., 2020). There is an urgent need for novel, easier-to-use instruments that can effectively carry out cell lysis in small quantities in environments with limited resources. The use of microwave energy is one intriguing strategy being investigated, as it has the potential to extract DNA more quickly and efficiently (Taglia et al., 2022).

1.17 Microwave (MW) mediated cell lysis

Bollet et al. initially described the technique of microwave-assisted cell lysis in 1991. Their study employed a regular microwave oven to extract chromosomal DNA from Gram-positive and acid-fast bacteria. Further studies have explored the use of microwave irradiation for DNA extraction from various eukaryotic organisms, including fungi, plants, and animals. Computer-controlled microwave systems have been assessed for their efficacy in DNA production, considering varied power levels, durations of exposure, and diverse types and amounts of biological samples.

In this research, a specialised microwave cavity applicator was developed, designed, and constructed in collaboration with the School of Engineering at Cardiff university. The DNA extraction process has been optimised using a specially designed device paired with modified microwave electronics, which were adapted to enhance efficiency and control the irradiation parameters. The following sections provide a clear and detailed explanation of the microwave-assisted DNA extraction method and describe the components of the microwave device and its cavity.

1.17.1 Microwave radiation

Microwaves (MWs) are a form of non-ionising radiation that is part of the electromagnetic spectrum, ranging from 1 to 30 cm (frequencies of 30 GHz down to 1 GHz, respectively) (Wang et al., 2022). They have multiple applications in the health, food, and communications industries. Microwaves are composed of alternating electric (E) and magnetic (H) fields and can be absorbed by various materials, including biological tissues (Baghdasaryan et al., 2022). One of the most widely used frequency bands for Industrial, Scientific, and Medical (ISM) applications is from 2.4 to 2.5 GHz for MW heating ('thermal') and excitation ('non-thermal') (Ahortor et al., 2020).

Water is an excellent absorber of microwave radiation, owing to the friction between water molecules (as a result of their hydrogen bonding network) when excited by electric fields oscillating at GHz frequencies (Mohorič & Bren, 2020). Within most aqueous materials, including biological tissues, MWs at a frequency of around 2.45 GHz penetrate to a depth of a few centimetres. MW effect is due to the generation of heat (thermal effects), while the contribution, if any, of non-thermal effects has yet to be established (Martusevich et al., 2022).

Biological membranes contain electrically excitable molecules, such as proteins and lipids, which change their behaviour in the presence of an E field (Ahortor et al., 2020). For example, the phospholipid membrane forms transient gaps (pores) when an E field greater than the membrane potential is applied, leading to a voltage drop, and the lipid will reorient to the E field (Martusevich et al., 2022). The size and duration of these pores are modulated by MW parameters such as frequency, pulse length, amplitude, and duration of MW exposure (Zhao et al., 2021). Although similar effects have been observed using direct current (DC) and low-frequency fields, the demonstration of such pore formation specifically at microwave

frequencies remains limited and warrants further study. The effective transmembrane potential required to induce membrane poration is 0.2–1.0 V (Navickaite et al., 2020). However, the inevitable heating of the bacterial cell following microwave exposure may drive DNA release, but at the same time, it may also denature the DNA structure, resulting in a loss of the target one is trying to detect. For this reason, the work presented here will involve pulsed microwaves to ensure bulk temperatures do not exceed 60°C (Taglia et al., 2022). Nevertheless, the use of bulk temperature as an indicator can overlook the possibility of localised heating, which may still contribute to thermal DNA damage (Gu et al., 2023). This highlights the need to distinguish thermal from potential non-thermal effects of microwave irradiation. Short, high-amplitude microwave pulses have been proposed to induce membrane effects without significant bulk heating, though further investigation is required to validate this in biological systems (Rougier et al., 2014).

A microwave cavity applicator has been developed, designed, and constructed in the School of Engineering, along with bespoke microwave electronics for its excitation. The components of this cavity and microwave device will be discussed in the following section.

1.17.2 Microwave cavity

The cavity is cylindrical in geometry, machined from aluminium, with an internal diameter of 92 mm and an internal height of 40 mm; these dimensions were chosen to match the microwave frequency (2.45 GHz) and ensure proper energy distribution, making them important for consistent and effective sample heating. It operates in its TM010 mode, resonant at 2.45 GHz when the cavity is empty, and reduces to around 2.3–2.4 GHz when loaded with an aqueous sample, depending on the volume. In this mode, there is a high (and approximately uniform) electric field along its axis, within which the sample is bathed.

Samples are held within a standard 1.5 ml Microcentrifuge tube (Figure 1.6) and inserted into a hole drilled along the cavity's axis. Microwaves are coupled into the cavity via a coaxial cable terminating in a loop, which couples to the high magnetic field around the cavity's perimeter. By rotating this loop, the input impedance of the cavity can be adjusted in a controlled manner (with any sample). When critically coupled, the loop is fixed at a unique position, absorbing all incident microwave power without reflection. Critical coupling occurs when the microwave cavity and the load (sample) are perfectly matched in terms of impedance, ensuring that the maximum amount of energy is transferred to the sample, with no power being reflected back into the system.

When empty, the cavity is designed to have a high-quality (Q) factor, which is a dimensionless parameter indicating how efficiently the system stores energy relative to how much it loses—higher Q means less energy loss and a narrower resonance peak. When a sample is inserted, approximately 98% of the incident microwave power (when critically coupled) is absorbed by the sample, and only 2% by the cavity. Critical coupling occurs when the impedance of the cavity matches that of the sample, enabling nearly all the input power to be transferred with minimal reflection—this is monitored by measuring reflected power and adjusting the coupling loop accordingly.

Assuming a 200 μL aqueous sample (mass ≈ 0.2 g), and a typical input power of 12 W, the initial heating rate is:

12 W ÷ (4.2 J/°C × 0.2 g) ≈ 14°C/s

This would cause the sample to reach boiling temperature within approximately 6 seconds. This has been confirmed experimentally. Therefore, in practical applications, the microwaves are pulsed to maintain the high electric field amplitude while reducing the bulk temperature rise. Pulsing preserves non-thermal effects and minimises thermal damage to DNA. A typical

duty cycle is 1%, meaning the microwaves are switched on only 1% of the time in each cycle. As a result, the effective heating rate is approximately 100 times lower than that observed under continuous wave (CW) operation.

The low-power microwave source can be adjusted to any frequency between 2–4 GHz and has an output power of 0 dBm (1 mW). This signal is pulsed and then amplified by approximately 45 dB using a power amplifier, reaching a maximum output of 45 dBm (~30 W). However, due to power losses in the circuit components—such as cables, connectors, and the circulator—only around 12 W is available for sample excitation. These losses, estimated at ~3 dB, are inherent in the system and were minimised through careful impedance matching and component selection.

A circulator and two power meters are used to monitor the power entering and reflected from the cavity. For each sample, critical coupling is achieved by adjusting the position and rotation of the coupling loop, and this is verified by ensuring that the reflected power is approximately zero at the resonant frequency.(Figure1.7).

In practice, the power reflection coefficient |S11|2|S11|2 is reduced to below −20 dB, indicating that less than 1% of the power is reflected and over 99% is absorbed by the cavity.

A bespoke LabVIEW program, running on a laptop computer, controls the microwave exposure experiment. The only manual operation required is the precise adjustment—by rotation and insertion—of the coupling loop to ensure critical coupling for each sample. On running the control program, the user inputs the resonant frequency, the duty cycle, the pulse width, and the time for exposure (Figure 1.8).

The testing of microwave systems against several DNA isolation methods will be discussed in Chapter Three, considering factors such as DNA quantity, DNA quality, and the time required for extraction.

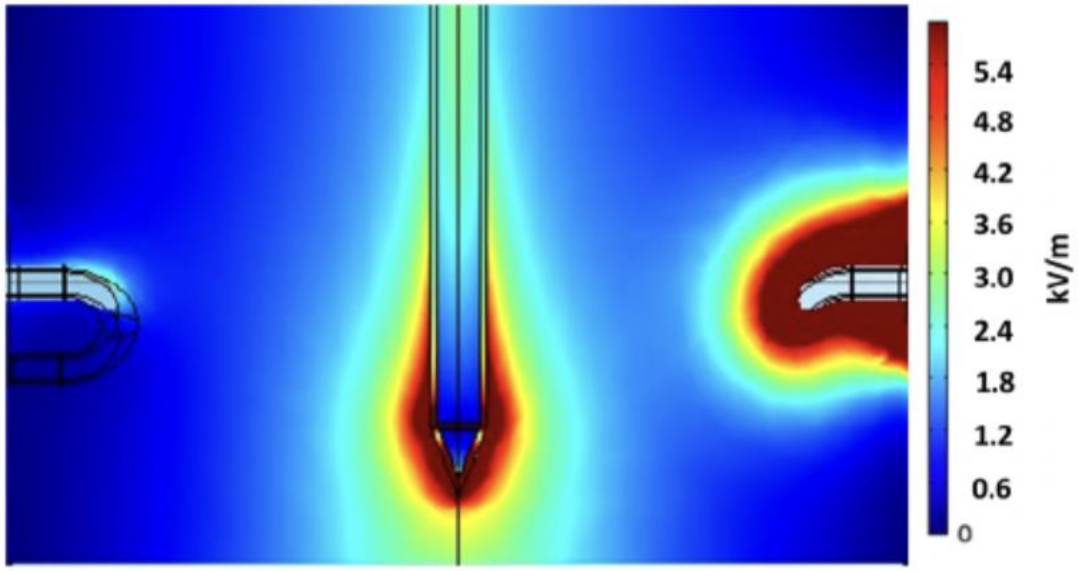

Figure 1.6 (A) COMputational SOLutions modelling of the electric field (E) and magnetic field (H) distribution at the centre of the one-hole TM010 cavity.

COMSOL Multiphysics® simulation of the electric field (E) distribution within a TM010 cylindrical cavity containing an Eppendorf tube along the central axis. The cavity is excited using a 12 W power input via a coupling loop on the right-hand side, which interacts with the magnetic field at the cavity perimeter. The colour gradient represents the E-field strength (in kV/m), with peak intensity observed around the sample.

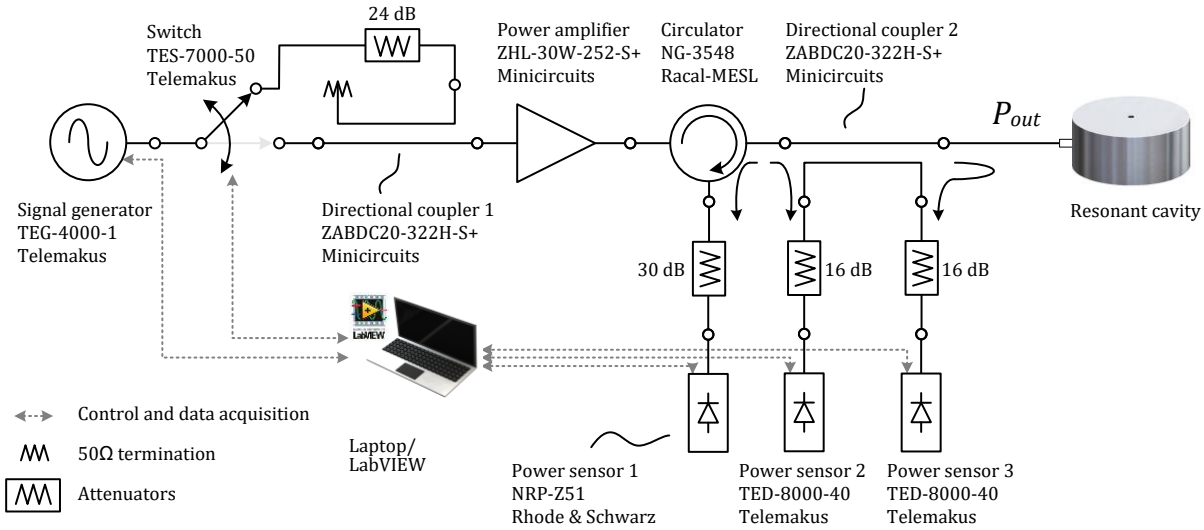

Figure 1.7 Schematic diagram of the bench-top microwave application system.
Reproduced and modified with permission from (Williams et al. 2016).

1.18 Cell wall and membrane differences in microorganisms

The bacterial cell wall is a complex, mesh-like structure that is crucial for maintaining the shape and structural stability of the cell. Moreover, bacterial cell wall fragments exhibit various immunostimulatory and cytotoxic characteristics, which are essential in the development of diseases and the progression of pathogenesis (Dörr et al., 2019). As shown in Figure 1.9, bacteria can be classified into three groups based on their cell wall properties: Gram-positive, Gram-negative, and acid-fast (Kang et al., 2023). These groups can be distinguished by the thickness of their peptidoglycan (PG) layer (Egan et al., 2020). Mycobacteria are acid-fast organisms due to their ability to resist acid decolourisation during staining techniques (Morel et al., 2020). Their cell walls exhibit a distinctive composition that incorporates characteristics of both Gram-positive and Gram-negative bacteria. Mycobacteria display a peptidoglycan (PG) layer almost as thick as that found in Gram-positive bacteria (Maitra et al., 2019). Additionally, they have an outermost waxy layer, resembling the outer membrane of Gram-negative bacteria (Ma et al., 2024). The complex composition of this structure poses challenges to the extraction of DNA from mycobacteria (Paul et al., 2020;

Mahardika et al., 2023). As obtaining high-quality, pure DNA is essential for accurate testing, this must be considered when developing DNA diagnostic tools for tuberculosis.

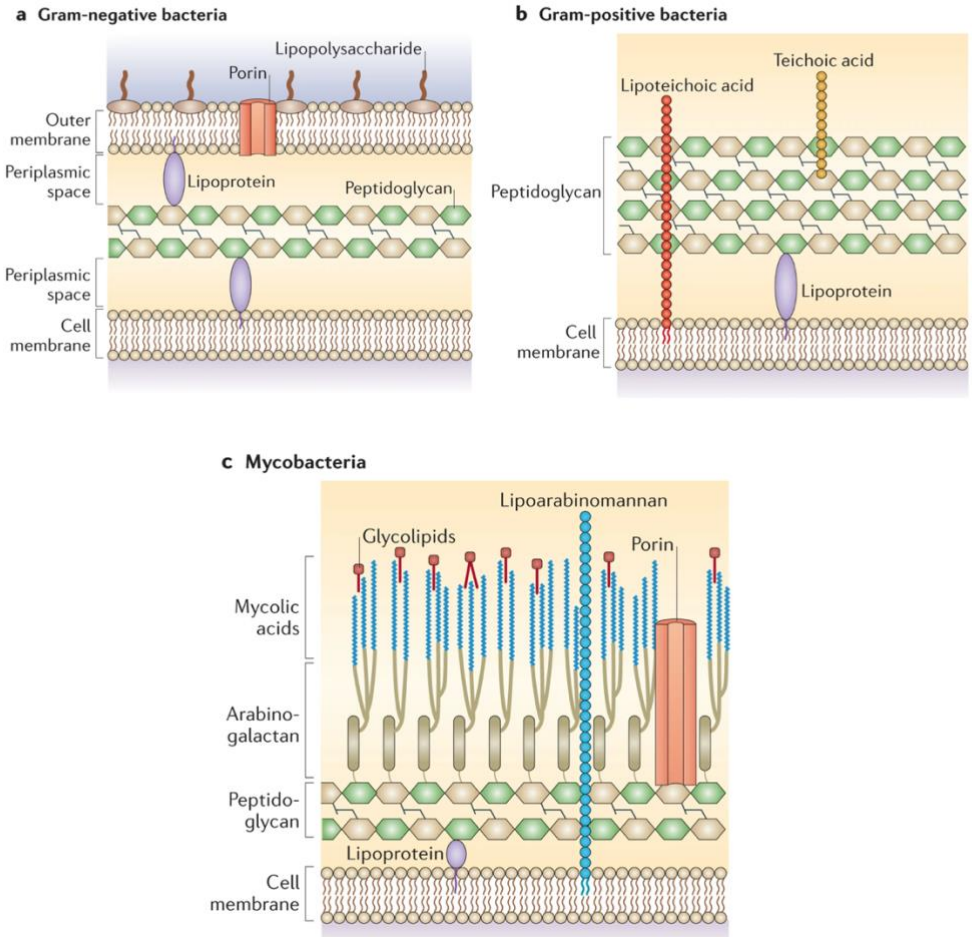

Figure 1.8 Cell wall composition of microorganisms showing structural diversity.
Gram-negative (A), Gram-positive (B) and Mycobacteria (C). Picture adapted from Brown et al., (2015).

1.19 Aims and objectives of the project

1.19.1 Aim

The overall aim of this project is to advance the development of a point-of-care (POC) assay capable of detecting the presence of *M. tuberculosis* in clinical samples. It builds on previous research undertaken between the Cardiff Schools of Engineering and Pharmacy to develop a microwave-based POC assay for the detection of pathogenic microorganisms in clinical samples.

The current project employs the BCG strain of *M. bovis*, a harmless relative of *M. tuberculosis* that shares considerable genetic homology with the latter, to develop a system capable of detecting such organisms in real time.

1.19.2 Objectives

1. To evaluate and compare different DNA extraction methods from bacteria suspended in water and simulated sputum, with a focus on yield, extraction time, and quality.
2. To develop gene targets with high sensitivity and specificity for *M. bovis* as a model for *M. tuberculosis*.
3. To optimise DNA capture methods in small sample samples (200 µL) of bacteria suspended in water and simulated sputum samples.
4. To increase the sample volume (10,000 µL) to more closely model real world, clinical samples

Chapter 2 Materials and methods

2.1 Materials

The following culture media were purchased: Löwenstein–Jensen medium (LJ), Luria-Bertani (LB) broth, and LB agar (Thermo Fisher Scientific, UK), 7H9 broth media, and 7H10 agar (Becton Dickinson, USA). Biological media were prepared according to the manufacturer's protocols and sterilised for 15 minutes at 121°C and 100 kPa using a bench-top autoclave (CertoClav EL steriliser, Austria). Deionised water was obtained from an ELGA Purelab Option BP15 dispenser (ELGA LabWater, UK).

2.2 Instruments

Nanodrop ND-1000 spectrophotometer (LabTech), Orbital incubator shaker MaxQ™ 440 (Thermo Fisher Scientific), Eppendorf AG Centrifuge 5417R (Hamburg, Germany), Heat Block DRI-Block® DB.3D (Techne), UV/Vis spectrophotometer Ultrospec 2100 Pro (Biochrom, USA), MSE Soniprep 150 (Gemini Lab Equipment), and T100 Thermocycler (Bio-Rad, UK).

2.3 Bacterial isolates

2.3.1 *Mycobacterium tuberculosis* H37Ra

Mycobacterium tuberculosis H37Ra is an attenuated variant of M. tuberculosis. It was purchased from the American Type Culture Collection (ATCC), UK, and can be handled under biosafety level 2 conditions.

2.3.2 *M. bovis BCG* str. Pasteur 1173P2 expressing GFP

The Bacillus Calmette-Guérin (BCG) strain of *Mycobacterium bovis* is an attenuated variant of *M. bovis*, a human vaccine designed to protect against infection by pathogenic variants, including *M. tuberculosis*. Its attenuated nature allows it to be handled safely under biosafety level 2 conditions. This strain was purchased from the Health Protection Agency (HPA) Culture Collections Service (Public Health England, UK) and has been modified to express

green fluorescent protein (GFP). The BCG-GFP strain was kindly provided by Dr Brigitte Gicquel, Pasteur Institute, France (Vázquez et al., 2014).

2.3.3 *M. bovis* BCG NCTC 5692

The Bacillus Calmette-Guérin (BCG) strain of *Mycobacterium bovis* is an attenuated variant specifically developed as a vaccine to protect against infections caused by pathogenic strains, including *M. tuberculosis*. Its attenuated properties enable safe handling under biosafety level 2 conditions. This strain was obtained from the HPA Culture Collections Service (Public Health England, Porton Down, UK).

2.3.4 *M. smegmatis* Mc2155 S2 expressing GFP

M. smegmatis was purchased from the HPA Culture Collections Service (Public Health England, Porton Down, UK). Similar to the BCG strain, this isolate has been modified to express GFP and can be safely managed under biosafety level 2 conditions. Dr James Blaxland kindly provided the *M. smegmatis* GFP (Blaxland, 2015).

2.3.5 *M. abscessus* ATCC 19977

This strain was purchased from the American Type Culture Collection (ATCC), UK. This isolate does not express GFP and can be safely handled under biosafety level 2 conditions.

2.3.6 *E.coli* NCTC 1093

E. coli is a Gram-negative bacterium, which means it appears pink under a microscope due to its thin peptidoglycan layer and outer membrane. It has a rod-shaped (bacilli) morphology and is a fast-growing organism, typically taking 16 to 24 hours to grow aerobically. This strain was purchased from the American Type Culture Collection (ATCC), UK, and can be safely handled under biosafety level 2 conditions.

2.4 Bacterial culture

2.4.1 Preparing bacterial culture

All the microorganisms were cultured in their respective media. For *M. bovis* BCG and *M. tuberculosis*, 10 mL of 7H9 broth was used, with *M. bovis* BCG incubated for two weeks at 37°C in a shaking incubator (MaxQ™ 440, Thermo Fisher Scientific) at 200 rpm. *M. tuberculosis* required 4 to 6 weeks to grow under the same conditions. *M. smegmatis*, *E. coli*, and *M. abscessus* were cultured in 10 mL of LB broth and incubated at 37°C. *M. smegmatis* and *M. abscessus* cells were cultured for 48 to 72 hours, while *E. coli* was cultured overnight. All cultures were agitated continuously in an orbital incubator shaker at 200 rpm. The cells were harvested by centrifugation at 4,000 rpm for 10 minutes and then resuspended in phosphate-buffered saline (PBS).

2.4.2 Determining the purity of cell cultures

To determine purity and ensure that the samples were not contaminated with other bacteria or fungi, they were subjected to the following analyses.

2.4.2.1 Determination of the purity of individual cultures using the streaking method

Cell suspensions were streaked onto their respective agar plates to isolate single colonies with uniform colonial morphology (indicating pure bacterial cultures) or mixed morphologies (suggesting bacterial contamination). Using a sterile inoculating loop, 10 µL of cell suspension was transferred onto the appropriate agar type, as previously mentioned. The plates were incubated for the relevant durations. After incubation, single colonies were observed for uniformity and strain-specific colonial morphology. To further characterise individual isolates, colonies were stained using the Gram and Ziehl-Neelsen methods and examined under oil immersion with a 100x objective lens using a light microscope (Leica DM750). All resulting figures are presented in Appendix 1.

2.4.2.2 Bacterial staining methods to determine bacterial purity

2.4.2.2.1 Acid fast staining - Ziehl Neelsen stain

A specific technique was developed by Franz Ziehl and Friedrich Neelsen to identify mycobacterial species (Figure 2.1). A single colony of bacteria growing on agar was suspended in PBS. Ten microlitres of the stock suspension were diluted (1/100) in fresh PBS, and 10 µL was spotted and smeared on a microscope slide. The slide was then dried in a biosafety cabinet and heat-fixed for staining.

The staining procedure was as follows: The slide was flooded with 0.3% carbol fuchsin and heated over a flame for 5 minutes to allow the carbol fuchsin to penetrate the robust cell wall of the mycobacteria. The slide was then washed with tap water to remove any excess stain. Decolourisation was performed by adding 95% ethanol containing 5% HCl for 5 minutes, after which the slide was rinsed with water to remove excess decolouriser. Finally, the slide was counterstained with 1% methylene blue for 1 minute and cleaned with tap water. The slide was dried in the biosafety cabinet at room temperature and examined under oil immersion with a 100x objective lens using a light microscope.

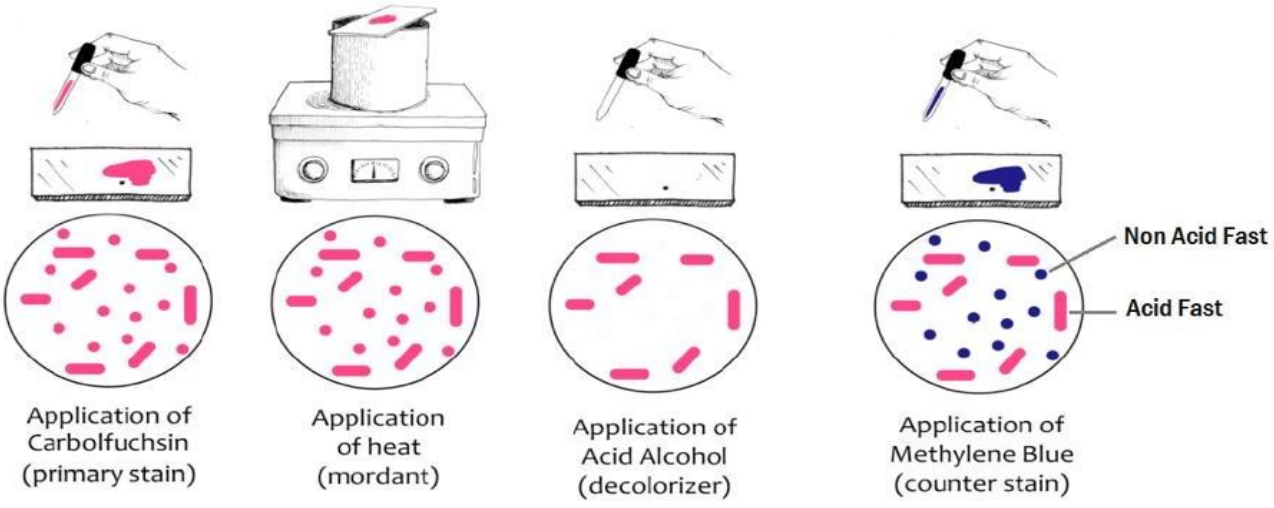

Figure 2.1 Ziehl-Neelsen Stain (ZN-Stain): Principle, procedure, reporting and modifications. (Laboratory Info, 2018).

2.4.2.2.2 Gram staining

This method, developed by Hans Christian Gram, was employed to distinguish between distinct types of bacteria based on their cell wall composition. It relies on the thickness of the peptidoglycan layer in the bacterial cell wall, which can be either thick (Gram-positive) or thin (Gram-negative). The method consists of acquiring a single colony from a fresh bacterial culture and diluting it in 5000 µL of distilled water. Ten microlitres of this suspension are then spotted onto a microscope slide and fixed using heat. After fixation, cover the slide with 2% crystal violet solution and allow it to sit for 1 minute before rinsing gently with tap water. Next, add iodine to the slide for 1 minute, then rinse with water to remove any excess iodine. Decolourise with 95% ethanol dropwise for 5 seconds, then wash gently with tap water. Following this, add Safranin to the slide, leave it for 1 minute, and rinse with water to remove any excess Safranin. Finally, allow the slides to dry at room temperature before observing them under a light microscope (LEICA Microscope Company) using a 100x objective lens with oil immersion (Figure 2.2).

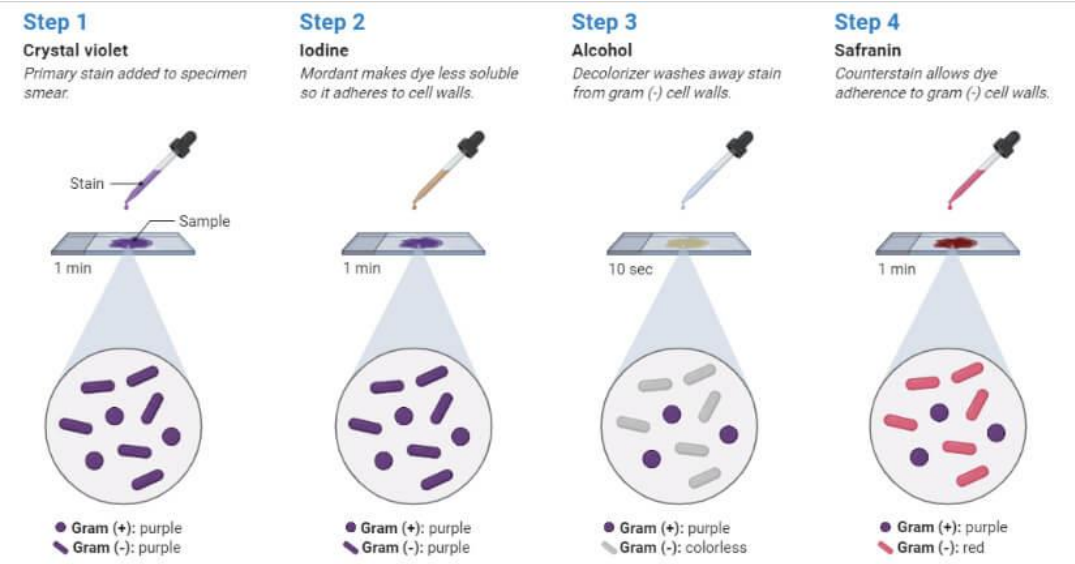

Figure 2.2 Gram stain. Principle, procedure, reporting and modifications. (Micropnote.2022).

2.5 Production of bacterial stock cultures

2.5.1 Preparation of cryo-protective bead stocks

Bacterial cultures were prepared using either LB agar (for *M. abscessus*, *E. coli*, and *M. smegmatis*) or 7H10 agar (for *M. bovis* and *M. tuberculosis*), as described previously.

Three colonies were aseptically transferred to a Microbank™ cryo-protective bead tube (Pro-Lab Diagnostics Ltd, UK) using a 10 µL sterile loop and stored at -80°C.

2.5.2 Glycerol storage

A 500 µL aliquot of a 48-hour bacterial culture in its respective broth was mixed with 150 µL glycerol and transferred to a 1.5 ml cryogenic storage vial (Fisher Scientific Limited, UK). The mixture was vortexed and stored at -80°C.

2.6 Standardisation of cell concentration

2.6.1 Preparation of bacterial cell suspensions

Bacterial clumping, particularly common in *Mycobacterium* species due to their waxy cell walls, poses significant challenges for experiments requiring precise and reproducible bacterial concentrations. While adding low concentrations of detergents to culture media can reduce clumping, it does not eliminate the issue; therefore, additional techniques are required to obtain single-cell bacterial suspensions.

One effective method involves using a five-µm polyethersulfone (PES) filter. To prepare a single-cell suspension, 10 mL of bacterial culture was loaded into a 10 mL syringe. The suspension was then passed through the five-µm PES filter (PALL Life Sciences; cat. 4650) by gently applying pressure to the syringe plunger. This filtration process effectively separates bacterial cells, resulting in a suspension composed predominantly of single bacterial cells.

2.6.2 Standardization of cell concentration - Miles and Misra method

A suspension of *M. avium* with an optical density (OD) of 1.0 at 600 nm corresponds to approximately 2×10^8 CFU/mL (Radomski et al., 2013). Cell density, which indirectly measures the turbidity of the cell solution, depends on a range of factors, including cell number, size, and nutritional requirements (Neurohr & Amon, 2020). Since these parameters can vary, the cells employed in this study were standardised to determine their concentration for use in subsequent assays.

To standardise the bacterial concentrations, a calibration curve was generated by correlating cell concentration with varying optical densities (OD). Initially, *M. bovis*, *M. abscessus*, *E. coli*, *M. smegmatis*, and *M. tuberculosis* cells were cultured and pelleted by centrifugation at 4000 × g for 10 minutes. The bacterial pellets were washed twice with sterile 1X PBS solution to prepare the stock bacterial concentration. This stock concentration was serially diluted (1/10) in PBS to create bacterial suspensions with OD values ranging from 0.05 to 1.2 (measured at 600 nm). These suspensions were further diluted (1/10) in eight sequential steps. Following the methodology of Miles and Misra (1938), 20 µL from each dilution was plated in triplicate on the appropriate agar media, as previously described. The plates were then incubated under the required conditions for each organism.

The lowest dilution that yielded between 30 and 100 countable colonies on the agar plate was used to determine the cell concentration of each sample (expressed as colony-forming units /mL). This process was repeated twice to ensure accuracy, and the mean colony-forming units were calculated using the following formula:

Colony-forming units per millilitre (CFU/mL) = Mean colony count × dilution factor / Volume inoculated (mL)

The mean number of colony-forming units per millilitre (y-axis) was plotted against the optical densities on the x-axis, and a line of best fit was generated. The estimated concentration of cells was calculated from the graph equation with known optical density values. While initial calculations were performed using bacterial concentrations (CFU/mL), all results are expressed as total bacterial quantities (CFU) to simplify data interpretation and emphasise the total bacterial load within the sample volume.

2.7 NanoDrop for DNA measurements

The NanoDrop assay was used to evaluate the purity and concentration of the extracted DNA. This technique holds 2 µL droplets of nucleic acids between two optical pedestals, using a novel sample retention system that relies on surface tension (García-Alegría et al., 2020a).

First, 2 µL of the DNA sample was pipetted directly onto the sensor surface of the NanoDrop device. The surface tension formed a vertical optical channel for light transmission and created a liquid column between the optical fibres (Bruijns et al., 2022). A xenon flash lamp was then used as the light source, and a spectrometer utilising a linear CCD array was employed to analyse the light that passed through the sample (Bruijns et al., 2022).

At 260 nm, the wavelength at which nucleotides, RNA, single-stranded DNA (ssDNA), and double-stranded DNA (dsDNA) absorb, the sample's absorbance was determined (Bunu et al., 2020). The purity of the DNA was then assessed using the 260/280 and 260/230 absorbance ratios. Regarding the 260/280 ratio, it is generally accepted that "pure" DNA has a ratio of approximately 1.8, whereas "pure" RNA has a ratio of approximately 2.0 (Viljoen et al., 2022). Proteins, phenols, or other materials that absorb close to 280 nm may cause contamination if the ratio is significantly lower than these values (García-Alegría et al., 2020b). In addition, the A260/A230 ratio can be used to detect contamination by phenolic compounds and other substances that absorb at 230 nm, with a ratio typically around 2.0 for

pure nucleic acids. This methodical approach facilitated the successful evaluation of the extracted DNA's concentration and purity, ensuring its suitability for use in subsequent processes.

2.9 Preparation of simulated sputum

Simulated sputum was prepared by dissolving 1% (w/v) aqueous methylcellulose (Thermo Scientific Chemicals) in one litre of sterile water (Demers et al., 2010). The resulting solution was sterilised by autoclaving, and 25 mL aliquots were aseptically dispensed into single-use sterile centrifuge tubes, which were stored at 4°C before use.

2.9.1 Preparation of bacterial suspension in simulated sputum

A known concentration of bacteria was centrifuged (6000 × g, 10 min, 4°C). The supernatant was discarded, and the pellets were resuspended in 200 µL or 10,000 µL of simulated sputum. To ensure uniform distribution of bacteria, the samples underwent vortexing for 30 seconds before being added to the synthetic sputum.

2.10 Statistics

All experiments were performed at least twice under independent conditions. Statistical analysis of the data was performed using GraphPad Prism. An independent samples t-test was conducted to determine the statistical significance between the two groups. Data were considered significant when the p value was < 0.05. Analysis of variance (ANOVA) was performed to determine the difference among group means. To determine the differences within groups, post-hoc analysis was performed using the Bonferroni and Tukey tests. p values less than 0.05 were considered significant.

Chapter 3 Assessing the efficiency of microwave DNA extraction in comparison to standard methods

3.1 Introduction

The sensitivity of any DNA-based detection analysis depends on its ability to extract sufficient quantities of high-quality target DNA from the sample (Mahardika et al., 2023). Effective lysis of the bacteria is essential for bacterial detection, as it releases the target DNA (Ma et al., 2020). In the case of mycobacteria, where DNA extraction is particularly challenging due to the bacterium's complex and waxy cell wall, disruptive methods are required for successful DNA release (Prajwal et al., 2023). This chapter will explore the advantages and limitations of current DNA release methods for mycobacteria and subsequently compare these to the results obtained using our customised microwave approach, focusing on time, yield, and DNA purity.

3.2 Physical disruption methods

In physical disruption methods such as boiling, sonication, microwave treatment, and bead-beating, the cell membrane is physically broken by high temperatures, sound waves, electromagnetic waves, shear forces, or external forces to release cellular components.

3.2.1 Boiling and sonication

Boiling and sonication are techniques widely employed to extract genetic material, such as DNA, from microorganisms (Shin et al., 2021; Basapathi Raghavendra et al., 2023). They are characterised by their speed, simplicity, and cost-effectiveness (Shin et al., 2021); however, as no purification stage is included in the process, they generate low-quality DNA (Lesiani et al., 2023). The boiling method involves boiling the bacterial suspension, which could pose a health risk to the operator without suitable protective measures (Sophian et al., 2022). Furthermore, boiling will cause DNA fragmentation, potentially affecting the integrity of the resulting DNA.

Sonication subjects the bacterial suspension to sound waves produced by an oscillating transducer (Saputra et al., 2024). This process induces agitation in the bacterial cells, resulting in lysis. However, although sonication effectively breaks down cells, it also has the potential to cause DNA shearing, which may impact the quality of the extracted DNA (Sun et al., 2022). Moreover, excessive sonication can generate heat, which may further degrade DNA. Therefore, meticulous process optimisation is essential to prevent damage (Pilo et al., 2022).

3.2.2 Bead-beating

Bead-beating is a highly effective method to employ for thick-walled bacteria, such as mycobacteria, which typically require mechanical damage for effective cell disruption. However, there are several associated challenges. Firstly, there is no consensus on the optimal duration for bead-beating required to achieve complete lysis, leading to variability in extraction results depending on the specific microbial community being analysed. Secondly, longer bead-beating durations can increase the probability of damaging the integrity of the released DNA, thereby negatively impacting its quality (Cullen et al. 2022). Additionally, bead-beating can be expensive due to ongoing costs for consumables, such as beads and sample tubes, which contribute to the overall expense (Scharf et al. 2020). It also requires specialized equipment and may pose potential biohazard concerns (Zhang et al., 2021). While this method is relatively rapid, it does not effectively remove cellular debris (Scharf et al., 2020).

3.2.3 Microwave method

The microwave method, which aids with cell lysis, was introduced by Bollet et al. (1991). In their study, a standard microwave oven was used to extract chromosomal DNA from Gram-positive and acid-fast bacteria. More recent studies have expanded the use of microwave irradiation for DNA extraction from eukaryotic organisms, including fungi, plants, protists, and

animals (Taglia et al., 2022). However, a major limitation of using a conventional microwave oven is the lack of precise control over temperature distribution and energy delivery. This can lead to uneven or excessive heating, which may fragment the DNA. The uncontrolled conditions also contribute to inconsistent yields and incomplete cell lysis.

Work conducted in the Baillie laboratory has demonstrated the feasibility of using microwaves to release DNA from *Mycobacterium* (Ahortor, 2019). As with the other methods described, the DNA is present in a suspension of cellular debris.

3.2.4 Chemical disruption methods

Chemical and mechanical methods for DNA isolation from bacteria can be used separately or combined (de Bruin et al., 2019). Chemical procedures include enzymatic methods, such as lysozyme and proteinase K, and chemical materials that employ organic and inorganic solutions (Gupta, 2019). However, these methods can encounter difficulties when attempting to recover DNA from certain strains of bacteria. For example, while lysozyme works well against Gram-positive bacteria, its effectiveness significantly declines against Gram-negative bacteria because of the outer membrane's protection, which prevents access to the peptidoglycan layer (Baron et al., 2016).

A combination of enzymatic and chemical treatments is more effective; however, this tends to be a time-consuming approach that may not result in the complete lysis of thick-walled bacteria (Wang et al., 2021). As for mechanical disruption, these approaches do not remove cellular debris, meaning that a DNA purification step may be necessary before the sample can be further characterised.

Evidence shows that the combination of bead-beating and chemical lysis techniques improves the release of DNA from microorganisms (de Bruin et al., 2019; Ma et al., 2020). However, it remains difficult to implement on a wide scale (Li et al., 2020). Although the combination of

bead-beating with chemical methods can increase DNA yield, the shear forces involved may result in lower-quality DNA (Ma et al., 2020b).

3.2.5 Commercial kits for DNA isolation

Commercial DNA extraction kits, such as the DNeasy Blood & Tissue Kit (Qiagen), work through chemical methods and a purification process that yields high-quality DNA (Pankoke et al., 2021). These kits utilise various DNA purification principles, including solution-based and solid-phase protocols. Solid-phase methods involve using DNA-binding materials, such as silica membranes, silica-coated magnetic beads, or anion-exchange columns, which specifically bind to DNA before releasing it into an appropriate buffer. Conversely, solution-based protocols, like salting out, rely on DNA precipitation for purification (Pankoke et al., 2021).

In summary, physical methods for DNA extraction are more straightforward and cost-effective but often yield low quantities and quality of DNA, making them impractical, especially when working with complex bacteria such as mycobacteria. Chemical methods, while potentially more effective, typically require more time, rendering them unsuitable for point-of-care (POC) settings. Additionally, these methods can be expensive and inaccessible in low-income countries. In contrast, microwave procedures are easy to use and faster than alternative techniques. They can be optimised to improve their efficacy in isolating DNA from complex bacteria, such as mycobacteria, for which they have shown beneficial results. Nonetheless, the resultant DNA may lack sufficient purity and can be degraded by direct microwave exposure.

3.3 Aims and objectives

This chapter aimed to compare the efficacy of the current microwave-based DNA release approach in this study with other, more traditional methods in terms of extraction time, yield, and purity. It will determine these factors for bacteria suspended in two different media: water and simulated sputum.

The chapter objectives are as follows:

1. To compare the effectiveness of different DNA extraction methods across three species of mycobacteria and *E. coli* as a Gram-negative model in the two different media: water and simulated sputum.
2. To evaluate each method's DNA yield, extraction time, and quality in the context of different bacterial species.
3. To optimise the microwave-based technique for DNA isolation, specifically targeting both single-stranded DNA (ssDNA) and double-stranded DNA (dsDNA) in mycobacteria across the two different media: water and simulated sputum.

3.4 Materials

3.4.1 Chemicals

Urea, Tris-HCl, 1% Triton X-100, Tween-20, proteinase, acid-washed diatomaceous earth, and TE buffer were purchased from Fisher Scientific, UK. The DNeasy Blood & Tissue Kit was obtained from Qiagen, UK. Zirconia beads (0.1 mm) were purchased from BioSpec, USA. All reagents were of molecular biology grade.

3.4.2 Preparation of diatomaceous earth solution

Diatomaceous earth powder (10 g) was mixed with 50 mL of sterile Milli-Q water and 500 µL of 37% HCl. The mixture was stirred and stored at 4 °C for further use.

3.4.3 Instruments

Nanodrop (ND-1000 spectrophotometer, LabTech), Ultrospec 2100 Pro spectrophotometer (USA), Digital Dry Bath (Benchmark Scientific), MSE Soniprep 150 (Gemini Lab Equipment), and the MW system.

3.5 Methods

3.5.1 Sample processing

The initial conditions for culturing the bacterial isolates and preparing the suspensions were informed by methods developed in the Baillie lab (Ahortor et al., 2019). Specifically, the choice to standardize the bacterial suspensions to contain 10^8 bacteria was based on Evans' methodology, which established this concentration as optimal for ensuring consistent DNA extraction and comparative analysis across different bacterial species. Furthermore, the use of water and simulated sputum as media for suspending the bacteria was chosen based on the standard protocols outlined in Evans' research, which demonstrated their efficacy in simulating clinical conditions for DNA extraction. These conditions were carefully selected to replicate the processes and ensure comparability with established methods in the field.

3.5.2 Physical disruption; boiling and sonication methods

To begin, 200 µL of each bacterial suspension in nuclease-free water, containing 10^8 bacteria, was added to separate Microcentrifuge tubes. The bacterial suspension was heated to 100 °C and boiled for 15 minutes using a Digital Dry Bath (Benchmark Scientific) for the boiling extraction method. After boiling, the solution was centrifuged at 10,000 × g for 1 minute (Shin et al., 2021).

Bacteria suspended in nuclease-free water were subjected to pulse sonication, with 10-15 seconds on cycles followed by 10-15 seconds off cycles. Applying the sonication technique, the bacterial suspension was sonicated at 40 kHz and 120 W (MSE Soniprep 150, Gemini Lab Equipment) while placed in an ice bath to maintain a low temperature. Sonication was conducted for 5 minutes to prevent excessive heat generation, which could damage the DNA.

Following sonication, the samples were centrifuged at 10,000 × g for 1 minute at room temperature (Chen & Yuan, 2023). The supernatant containing the released DNA was carefully collected (Chen & Yuan, 2023).

For both methods, the ssDNA concentrations were determined using a NanoDrop spectrophotometer, as mentioned in Chapter 2, Section 2.8. All tests were performed three times to ensure the accuracy and consistency of the results.

3.5.3 Chemical-mechanical method

Samples consisting of 200 µL of bacteria suspended in nuclease-free water, containing 10^8 bacteria, were prepared and lysed with 250 µL of lysis buffer (consisting of 8 M urea, 60 mM Tris-HCl, 1% Triton X-100, 10% Tween-20, and 3 mg/mL proteinase) and 500 µL of zirconia beads. The cells were subjected to lysis via overnight incubation at 60 °C while undergoing continual agitation at 200 rpm. A solution of diatomaceous earth was added to each lysed sample to collect the released DNA. The mixture was then held at 37 °C for 60 minutes before the DNA attached to the diatomaceous earth was separated via centrifugation at 10,000 × g for 60 seconds, and the supernatant was removed. Bound DNA was washed twice with 900 µL of ice-cold 70% alcohol and 900 µL of absolute acetone. After washing, the DNA attached to the diatomaceous earth was dried at 50 °C for 20 minutes using a heat block to eliminate any remaining acetone. To extract the DNA from the diatomaceous earth, 100 µL of 1x TE buffer was introduced, and the sample was incubated at 55 °C for 20 minutes while being continuously stirred. Subsequently, the mixture was centrifuged at 10,000 × g for 1 minutes, and the supernatant containing the DNA was aliquoted into a new Microcentrifuge tube to be quantified using a NanoDrop, as mentioned in Chapter 2, Section 2.8.

3.5.4 Commercial method: DNeasy blood & tissue kit (Qiagen)

The DNeasy Blood & Tissue Kit (Qiagen) was utilised to extract DNA following the manufacturer's instructions (Diawara et al., 2009). The entire process took approximately 120 minutes.

First, bacterial samples were collected and suspended in nuclease-free water containing 10^8 bacteria. Proteinase K, an enzyme that breaks down proteins and aids in lysing bacterial cells, was then added to the solution. To ensure complete lysis, the mixture was incubated for one hour at 56°C. The lysate was subsequently transferred to a DNeasy Mini Spin Column, facilitating DNA binding to a silica membrane within the column.

Centrifugation was performed at 6,000 × g for one minute. During this step, the DNA adhered to the membrane of the spin column while contaminants and impurities flowed through and were discarded. Two washing stages were carried out to ensure the removal of any remaining contaminants. Buffer AW1 was added to the column in the first wash and centrifuged at 6,000 × g for one minute. The second wash utilised Buffer AW2, and the column was centrifuged at 20,000 × g for three minutes, essential for eliminating any residual impurities that could inhibit downstream applications.

Following the washing steps, 200 µL of nuclease-free water was added directly to the membrane of the spin column to elute the DNA. The column was incubated at room temperature for one minute before final centrifugation at 6,000 × g for an additional minute to collect the purified DNA.

The purity and yield of the extracted DNA obtained using the Qiagen procedure were then measured using a NanoDrop, as mentioned in Chapter 2, Section 2.8.

3.5.5 MW mediated release of nucleic acids

To establish the optimum microwave (MW) conditions for the release of dsDNA and ssDNA, 200 µL samples of *M. bovis* suspension in water or simulated sputum (10^8 bacteria) were

irradiated with MWs pulsed at varying duty cycles (30%, 40%, and 50%) for 20 seconds. MW pulsing was maintained at a width of 1,000 ms, while the ON period was varied at 300 ms, 400 ms, and 500 ms. *M. bovis* without MW treatment was included as a negative control. These initial MW parameters were selected based on the optimisation framework established by Ahortor et al., which provided a validated starting point for evaluating DNA release efficiency under different pulsing conditions.

Next, MW-treated samples were centrifuged at 10,000 × g for 1 minutes, and the supernatant containing the DNA was aliquoted into a new Microcentrifuge tube to be quantified using a NanoDrop, as mentioned in Chapter 2, Section 2.8. All tests were repeated three times to confirm the accuracy and replicability of the results.

3.6 Statistics

All experiments were performed at least twice under independent conditions. Statistical analysis of the data was performed using GraphPad Prism. An independent samples t-test was conducted to determine the statistical significance between the two groups. Data were considered significant when the (probability value) p value was < 0.05. Analysis of variance (ANOVA) was performed to assess the differences among group means. To evaluate differences within groups, post-hoc analysis was carried out using the Bonferroni and Tukey tests. p values less than 0.05 were considered significant.

3.7 Results

3.7.1 Determining the optimum MW treatment conditions for the release of nucleic acids

The concentrations of ssDNA and dsDNA released in water or simulated sputum samples following MW treatment at varying duty cycles were quantified using the NanoDrop. Following 20 seconds of irradiation, the bacteria suspended in water exhibited their highest detectable levels of ssDNA release at the 30% and 40% duty cycles, with no significant difference between them (p value > 0.05) (Figure 3.1). When the bacteria were suspended in simulated sputum, peak ssDNA concentration was achieved at the 40% duty cycle, with levels comparable to those observed for bacteria suspended in water (Figure 3.1).

However, the amount of ssDNA released from bacteria suspended in the simulated sputum following exposure to the 30% duty cycle was lower than that following exposure to the 40% duty cycle, suggesting that the simulated sputum may inhibit the microwaves' ability to mediate DNA release.

There was a significant drop in ssDNA levels at the 50% duty cycle for both sample types. This indicates that overexposure to microwaves could be detrimental to DNA recovery, possibly due to localised heating.

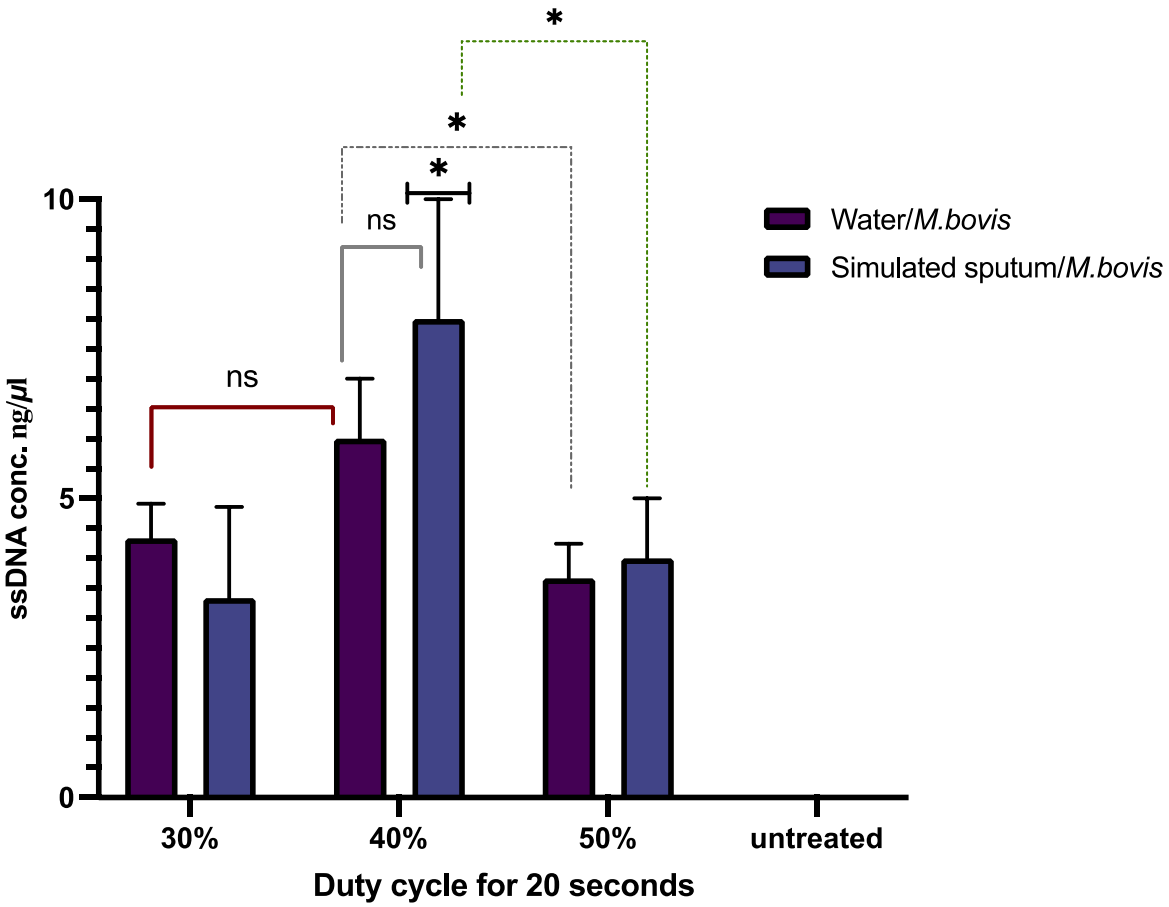

Figure 3.1 MW induced release of ssDNA from *M. bovis*1173P suspended in water and simulated sputum.

M. bovis 1173P2, with a bacterial quantity of 10^8 , was treated with 12 W microwave energy pulsed at 30%, 40%, and 50% duty cycles for 20 seconds. The concentration of ssDNA released was determined using the NanoDrop. The data represents the means of triplicate experiments ± standard deviation.* represents a *p* value <0.05.

The release of dsDNA was highest at the 40% duty cycle for *M. bovis* 1173P2 suspended in water and significantly decreased at the 50% duty cycle (Figure 3.2). Conversely, bacteria suspended in the simulated sputum exhibited maximal release of dsDNA during the 40% and 50% duty cycles, with no significant distinction between these. Also in Figure 3.1 There was no significant difference between the bacteria suspended in water or simulated sputum samples when treated at the 40% duty cycle (*p* value < 0.05).

The quantity of dsDNA released was lower than that of ssDNA under the same exposure conditions, which implies that dsDNA is being degraded. Microwaves can separate dsDNA into its distinct DNA strands, which may occur in our test system (Huang et al., 2022). The

significant difference (p value < 0.05) between the dsDNA levels for bacterial samples suspended in water and simulated sputum at the 50% duty cycle suggests a possible protective role for simulated sputum. Further analysis is needed to understand the behaviour of microwave radiation with sputum. In conclusion, a 40% duty cycle for 20 seconds appears to be the most effective protocol for releasing both ssDNA and dsDNA from *M. bovis* suspended in water and simulated sputum.

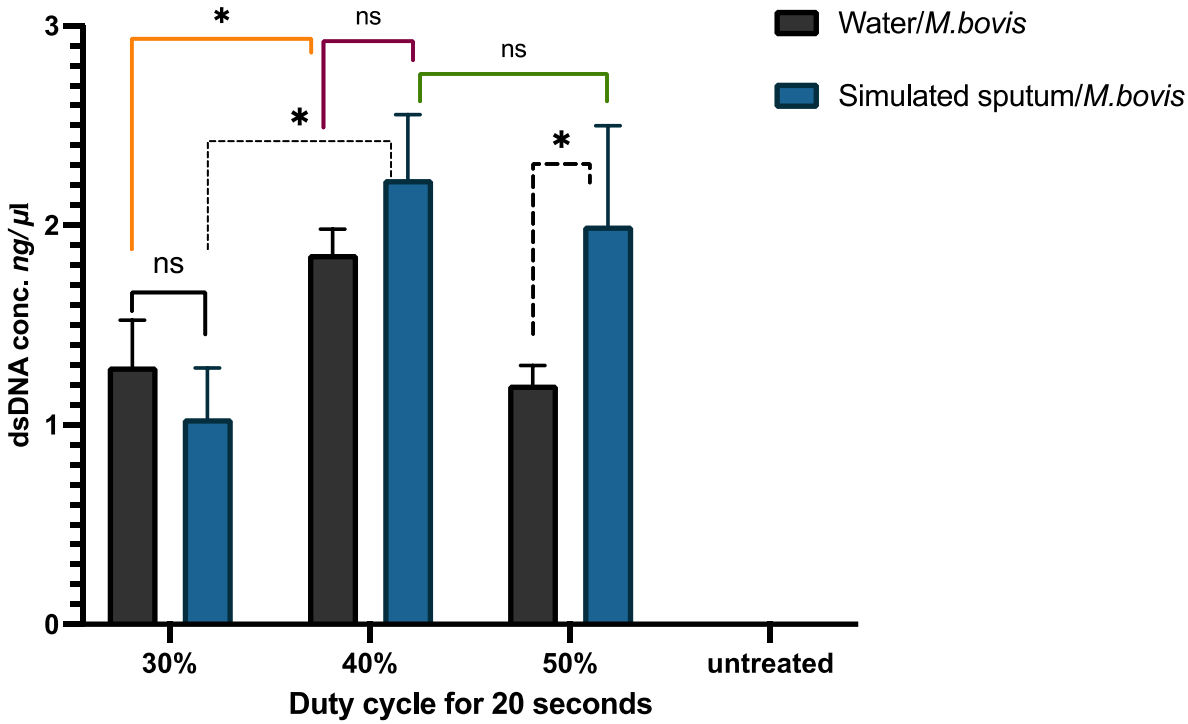

Figure 3.2 MW induced release of dsDNA from *M. bovis* 1173P2 suspended in water and simulated sputum.
M. bovis 1173P2, with a bacterial quantity of 10^8, was treated with 12 W microwave energy pulsed at 30%, 40%, and 50% duty cycles for 20 seconds. The concentration of dsDNA released were determined using the NanoDrop. The data represents the mean of the triplicate experiment ± standard deviation. * represents a p value <0.05.

3.7.2 Comparing the efficiency of the microwave extraction method for ssDNA to other extraction methods

The point-of-care assay being developed detects ssDNA. Therefore, this study compared the efficiency of the microwave approach with that of other mainstream DNA extraction methods

in terms of ssDNA yield, purity, and the time required for extraction. Of all the ssDNA extraction methods evaluated, the chemical-mechanical method produced the highest ssDNA yields (ng/µL) for all bacterial types when the organism was suspended in water (Figure 3.3). This outcome met expectations, as the chemical-mechanical method integrates enzymatic, chemical, and mechanical techniques and has been optimised for the extraction of DNA from mycobacteria (Ahortor, 2019). Other DNA extraction methods yielded ssDNA quantities within a similar range, with no significant differences. There were also no significant differences in ssDNA release among the tested *Mycobacterium* species. However, *E. coli*, the Gram-negative model, exhibited the highest ssDNA release across all methods except for the microwave radiation approach.

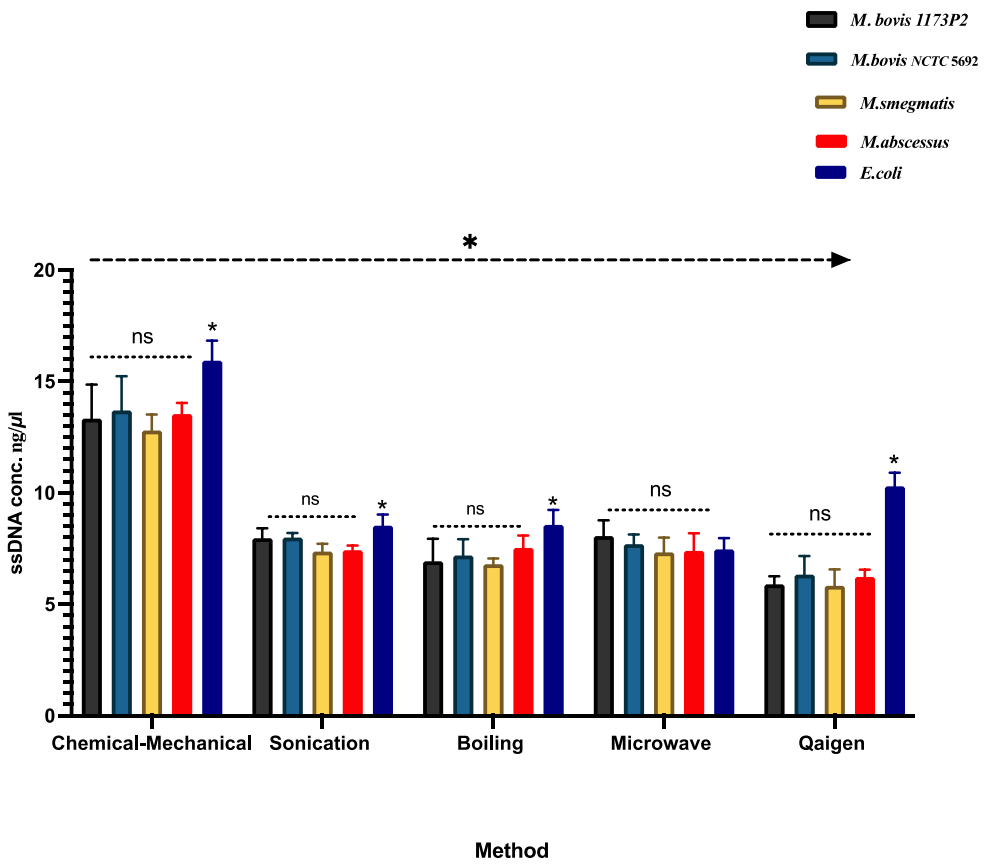

Figure 3.3 Comparison of single stranded DNA yields from bacteria suspended in water using different extraction methods.
ssDNA extraction was performed on suspensions of the following bacteria in water: *M. bovis* (M. bovis 1173P2 and M. bovis 5692) and non-*bovis* isolates, including *M. smegmatis* Mc2155 S2, *M. abscessus* ATCC 19977, and *E. coli* NCTC 1093, at a quantity of 10^8 bacteria. The extraction methods used included chemical-mechanical, boiling, sonication, microwave, and a commercial kit (Qiagen). The data represent the mean of two replicates ± standard error (SE). *p value*represents a value < 0.005, and 'ns' indicates no significance.

To establish the degree of contamination of the resulting DNA extracts with cell-derived material, the A260/A280 ratios for each extract were compared. Not surprisingly, the Qiagen method demonstrated superior DNA purity due to the incorporation of a purification system (Figure 3.4). Unexpectedly, the microwave disruption method achieved relatively high levels of purity, with A260/A280 ratios ranging from 1.77 to 1.85. Sonication and boiling produced the lowest purity levels, with ratios ranging from 1.2 to 1.3. This result was surprising, as, like microwave treatment, they rely on physical disruption to release the DNA, and there is no optimal purification step.

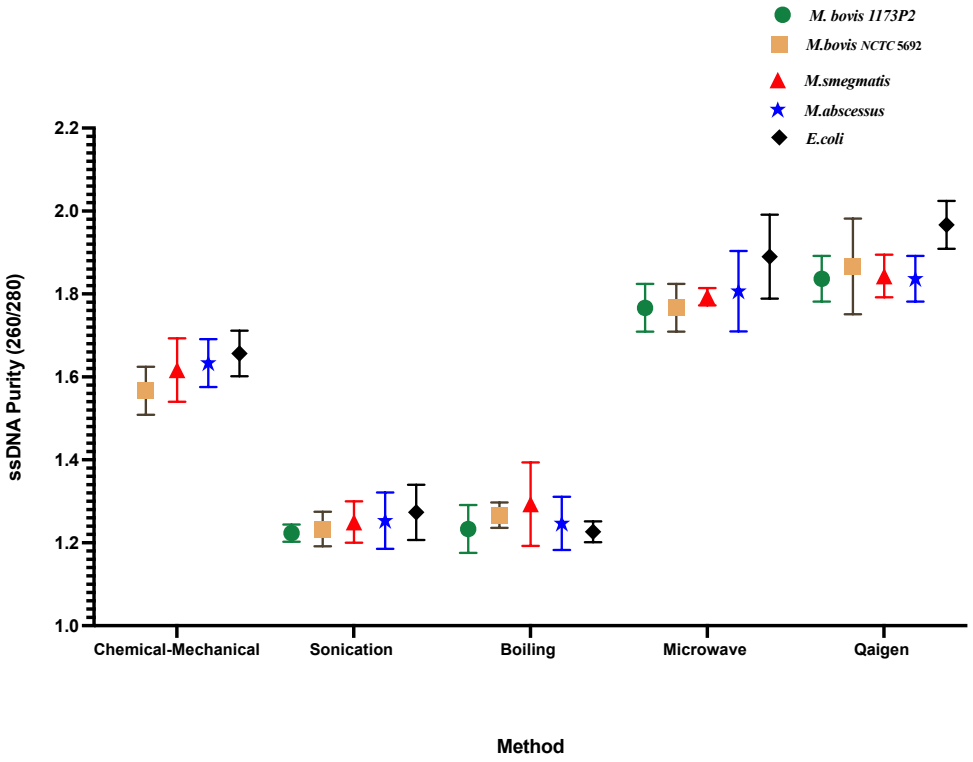

Figure 3.4 Comparison of DNA purity using different extraction methods.
ssDNA extraction was performed on suspensions of the following bacteria in water: *M. bovis* (M. bovis 1173P2 and M. bovis 5692) and non-*bovis* isolates, including *M. smegmatis* Mc2155 S2, *M. abscessus* ATCC 19977, and *E. coli* NCTC 1093, at a quantity of 10^8 bacteria. The extraction methods used included chemical-mechanical, boiling, sonication, microwave, and a commercial kit (Qiagen). The data represent the mean of two replicates ± standard error (SE). *p value* < 0.005 indicates statistical significance, and 'ns' denotes no significance.

Regarding the time required to release ssDNA from samples suspended in water, microwave treatment was the fastest method, requiring approximately 10 minutes in total—comprising 20

seconds of microwave irradiation and around 9 minutes for sample handling (Table 3.1). This makes it a promising approach for the development of rapid point-of-care diagnostic assays.

Table 3.1 Time required to extract ssDNA from bacterial suspensions in water using different methods.

This table summarizes the time required to extract single-stranded DNA (ssDNA) from bacterial suspensions in water using various methods. The times represent the mean values derived from three independent repeats for each method, ensuring reproducibility. The methods compared include the Microwave Method, which demonstrated the fastest extraction time, followed by the Boiling Method, Qiagen Method, and Chemical-Mechanical Method, which required significantly longer durations.

Method	**Time**
Microwave Method	10 Minutes
Boiling method	15 Minutes
Qiagen Method	120 Minutes
Chemical-Mechanical	20 Hours

While the chemical-mechanical method offered the highest DNA yield, its lower purity and lengthy extraction time render it unsuitable for integration into a rapid point-of-care assay. Although practical, the Qiagen method, with its moderate extraction time and highest purity, takes considerably longer than the microwave method and requires the incorporation of several steps. Methods such as sonication and boiling were relatively fast but not as efficient as microwave extraction in terms of time and purity.

3.8 Discussion

This chapter compares the effectiveness of different DNA extraction methods for bacteria suspended in water. As expected, the chemical-mechanical method yielded the highest quantity of ssDNA for all species of bacteria (Lim et al., 2018; Ahortor, 2019). This is likely a reflection of the more efficient disruption of the bacterial cell. It was also noted that the DNA yield from *E. coli* was the highest for all methods except the microwave-based approach. This observation might be expected, as *E. coli*, a Gram-negative bacterium, possesses a comparatively uncomplicated cell wall structure in contrast to the complex and lipid-rich cell wall of mycobacteria (Marco & Roberta, 2003). The finding may suggest that microwaves are better suited to handle a broader range of microorganisms than the other approaches.

Somewhat surprisingly, the microwave method, although less efficient than the chemical-mechanical method in terms of DNA yield, was almost as effective as the Qiagen method in terms of DNA purity. One possibility is that microwave exposure leads to the creation of temporary membrane pores through which DNA can be released, while the majority of the bacteria remains intact, thereby reducing contamination (Ahortor et al., 2020).

While the yield from the microwave system was lower than that from the chemical-mechanical method, the time required to liberate DNA was considerably shorter—just 10 minutes compared to 20 hours—making it more suitable for inclusion in a rapid point-of-care assay. Furthermore, by optimising the microwave exposure conditions, it may be possible to increase DNA yield (Copty et al., 2006).

Indeed, exposure of *M. bovis* to microwaves at a power setting of 12 W with a 40% duty cycle for 20 seconds resulted in the highest yield levels of both ssDNA and dsDNA from samples suspended in water. This exposure duration (20 seconds) was based on earlier work undertaken in the Baillie laboratory (Ahortor et al., 2020b).

The quantity of dsDNA released was lower than that of ssDNA under the same exposure conditions for samples suspended in water, suggesting that dsDNA is being broken down into its composite single strands. Researchers have found that DNA can break down into single strands upon exposure to radiation or chemicals, resulting in double-strand breaks that require cellular repair mechanisms to preserve genomic integrity (Ranjha et al., 2018).

A decrease in ssDNA concentrations was also observed at a 50% duty cycle, suggesting that DNA degradation may occur at higher microwave power settings, likely due to increased thermal effects associated with elevated temperatures.

While the ability to release DNA from bacteria in water is of interest, the efficiency of microwaves using real-world samples needs to be determined. Previous studies have reported that, for real-world samples such as saliva, blood, and semen, a 40-second exposure at a power level of 300 W is required to achieve effective DNA release (Taglia et al., 2022). To model the conditions encountered in a sputum sample, a synthetic material designed to mimic the physical properties of real-world sputum was used.

It was found that, in the presence of simulated sputum, greater energy was required to significantly increase detectable dsDNA levels. No significant reduction in dsDNA was observed at the 50% power levels. These results suggest that the simulated sputum matrix may be inhibiting the action of the microwaves, although the underlying mechanism remains to be determined.

These results need to be interpreted with caution. While simulated sputum is designed to mimic the physical properties of real-world sputum, it does not replicate its biological composition. As the main component of the simulated sputum used in this study is methylcellulose, however, real clinical sputum contains a complex mixture of proteins, mucins, blood, cellular debris, immune modulators, and other biological materials that may physically and chemically influence the microwave-assisted DNA extraction process.

In conclusion, a 40% microwave duty cycle for 20 seconds was the most effective protocol for releasing ssDNA and dsDNA from *M. bovis* suspended in water and simulated sputum. It will form the basis for future optimisation work.

Chapter 4 The design of DNA probes for the detection of *mycobacterium tuberculosis*.

4.1 Introduction

Identifying pathogen-specific DNA targets is a key requirement of any relevant detection system (Ha et al., 2018; Nehra et al., 2022). This can be achieved by designing probes specific to various conserved regions within the bacterial genome (Curk et al., 2020), which are less likely to be influenced by evolution or environmental factors (Guerrero et al., 2010). Multiple gene target sequences have been utilised for *M. tuberculosis* detection by PCR over time (Huang et al., 2021), including *IS6110*, *mpb64*, *IS1081*, *devR*, *hsp65*, *esat6*, *cfp10*, the *16S rDNA* gene (*rrs*), and *rpoB* (Park et al., 2020; Gcebe et al., 2024).

The *IS6110* gene target is most commonly used for the detection of *M. tuberculosis*: it belongs to the IS3 group of insertion sequences (Salazar et al., 2024) and offers the advantage of being highly conserved and unique to the *M. tuberculosis* complex (MTBC) (Krishnakumariamma et al., 2023). Multiple copies of *IS6110*, up to 25 per genome, are commonly found in most *M. tuberculosis* strains (Krishnakumariamma et al., 2023); however, several uncommon strains discovered in Brazil, Vietnam, and Southern India lack this target (Le Hang et al., 2021). A resolution to this problem is the use of multiplex gene targets, as seen with multiplex PCR (Lodha et al., 2022). This approach is widely employed in nucleic acid diagnostics for gene deletion analysis, mutation and polymorphism analysis, quantitative analysis, and RNA detection (Owusu et al., 2023).

Analysis of the literature suggests that genes such as *IS1081* and *mpb64*, which are both stable and exist in numerous copies within the target genome of *M. tuberculosis*, could be combined with the *IS6110* gene in a detection assay to increase sensitivity and specificity (Yang et al., 2021).

Unlike *IS6110*, *IS1081* is considered present in all MTBC species at a more stable copy number of five to seven repeats per genome (Chang et al., 2022). It has been reported that

the *IS1081* gene is a reliable marker for identifying members of the MTBC (Lin et al., 2021; Sharma et al., 2022; Zeineldin et al., 2023; Li et al., 2024). Regarding the *mpb64* gene, numerous studies have demonstrated that it exhibits the highest sensitivity among various gene targets, including *IS6110* (Raj et al., 2016a; Angmo et al., 2023). Thus, by combining these three gene targets, developing a highly sensitive and specific assay may be possible.

4.2 Gene target probe design

A bioinformatics-based approach was used to identify unique target DNA sequences. Bioinformatics employs computational methods to analyse biological data, such as protein or DNA sequences, to gather evidence about their function, find homologs, detect sequence trends, and determine evolutionary relationships (Asai et al., 2024). The National Centre for Biotechnology Information (NCBI) and other open-source databases provide the sequencing data necessary to access the full potential of this approach (Sayers et al., 2023a). In addition to providing access to genetic data, the NCBI database also enables researchers to determine the identity of new nucleotide or protein sequences by assessing their similarity to the many known sequences retained in its repository (Dash et al., 2021). The process of finding homologs is made easier by a specific software tool known as the Basic Local Alignment Search Tool (BLAST), which can be employed to determine the specificity of small segments of DNA probes (Lemmon & Gardner, 2008; Dash et al., 2021; Sayers et al., 2023).

4.3 Predicting secondary DNA structure

The secondary structure refers to the interactions between nucleotide bases that create bonds between different nucleic acids regions (Tieng et al., 2023) . It has a major effect on the efficiency of oligonucleotide probe hybridisation (Tieng et al., 2023), and can potentially prevent a probe binding to its complimentary target sequence (Gu et al., 2022) . Efforts to predict and avoid such structures are commonly employed in probe design schemes (Phan et

al., 2023). Proper evaluation of both probe and target site secondary structures together is thus required to improve hybridization prediction and design effectiveness (Canady et al., 2020). Numerous secondary structure prediction software applications are available, including RDN Analyzer, an innovative computer-based tool optimised for DNA secondary structure prediction and sequence analysis. This tool predicts base pairings and secondary structures in DNA (S. & E.R., 2023). In contrast, the RNA Structure Webserver, focuses on RNA and DNA secondary structures (Bellaousov et al., 2013; Arias-Carrasco et al., 2018). Other algorithms that can predict the secondary structure of a given molecule, offering the ability to estimate the possibility of base pairings (Bellaousov et al., 2013; Arias-Carrasco et al., 2018).

This work used previously identified diagnostic targets and validated PCR probe sequences for *Mycobacterium tuberculosis* to design DNA probes compatible with the microwave-based detection platform.

4.4 Aims and objectives

This chapter aims to design DNA probes capable of distinguishing *Mycobacterium tuberculosis* from other mycobacteria and compatible with the requirements of our POC assay platform.

The chapter objectives are as follow :

1. To identify gene targets unique to *M. tuberculosis*.
2. To employ a bioinformatics approach to identify nucleotide sequences within each target gene that, when combined, can detect the target sequence.
3. To confirm the ability of the nucleotide sequences to bind to the target DNA.

4.5 Materials

4.5.1 Chemicals

The QIAGEN DNeasy Blood & Tissue Kit was purchased from QIAGEN. The Low Molecular Weight DNA Ladder was obtained from Biolab (UK), all probes from Fisher Scientific (Invitrogen, UK), DNA loading buffer (BIOLINE, H4P-112I), and SafeView Nucleic Acid Stain from NBS Biologicals Ltd.

4.5.2 Instruments

Nanodrop (ND 1000 spectrophotometer, LabTech), spectrophotometer (Ultrospec 2100 pro, USA), Thermal cycler (T100, Bio-Rad).

4.5.3 Bioinformatic tools used to identify target sequences.

Several online and open-source-resources were used to assist in the identification of target sequences:

- National Centre for Bioinformatic Information (NCBI). https://www.ncbi.nlm.nih.gov/. (Accessed November 2020)
- NCBI-BLAST. (https://blast.ncbi.nlm.nih.gov/Blast.cgi?PROGRAM=blastn&PAGE_TYPE=BlastSearch&LINK_LOC=blasthome). (Accessed December 2020)
- RNA Structure Webserver.(https://rna.urmc.rochester.edu/RNAstructureWeb/Servers/Predict1/Predict1.html (Accessed December 2020).

4.6 Methodology

4.6.1 Probe synthesis and modification

Following a comprehensive literature review, PCR primers targeting the *IS6110*, *mpb64*, and *IS1081* gene regions were utilised as a foundation for designing DNA probes compatible with the selected platform technology.

The complete nucleotide sequences for the *IS6110*, *mpb64*, and *IS1081* genes of *Mycobacterium tuberculosis* were downloaded in FASTA format from NCBI in November 2020. The reference number (RefSeq) for *Mycobacterium tuberculosis* is NC_000962.3, and the selected gene RefSeqs are as follows: *IS6110* (AJ242907.1), *mpb64* (CP007027.1), and *IS1081* (PP001721.1).

Using the BLAST tool, a similarity search was conducted against the NCBI nucleotide database to retrieve any sequences that matched the published PCR detection target sequences. Ten targets within the *IS6110*, *mpb64*, and *IS1081* gene sequences were identified, exhibiting 100% homology with *M. tuberculosis*. Utilising these PCR primer sequences, a series of probe pair combinations were designed to meet the requirements of the microwave-based detection method.

The anchor and detector probes were explicitly designed to consist of 17 and 22 nucleotide sequences, with 5'-biotin (anchor probe) and 3'-HRP (detector probe) modifications. The sequence included five thymine residues between the biotin and the 17-nucleotide sequence to enhance the anchor probe's flexibility, as shown in Figure 4.1 (Ahortor, 2019).

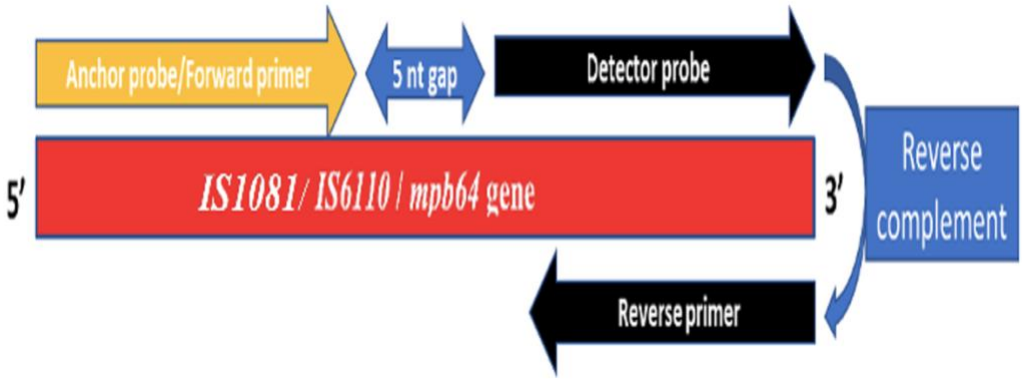

Figure 4.1 Schematic representation of the DNA probe design.

The anchor (17 nucleotides) and detector (22 nucleotides) probes were designed to target the same nucleotide strand of the bacterial gene target. A 5-nucleotide gap was maintained between the anchor and detector probes (Ahortor, 2019).

4.7 Predicting the secondary structure of potential probe binding regions

The DNA sequences within the region to which probe pair combinations bound in the *IS6110*, *mpb64*, and *IS1081* gene sequences were retrieved from NCBI and imported into the RNA Structure Webserver (https://rna.urmc.rochester.edu/RNAstructureWeb/Servers/Predict1/Predict1.html) to screen for possible secondary structures.

4.8 Confirmation of probe specificity using PCR method

PCR confirmed that the anchor and detector probe combinations could bind to their gene targets. The anchor probe was used as the forward primer, while the reverse complement of the detector probe was employed as the reverse primer.

All primers were commercially synthesised by Invitrogen and received in lyophilised powder form from the manufacturer. Before use, they were stored at -20 °C and reconstituted appropriately.

The primers were reconstituted with sterile water to achieve a final concentration of 100 µmol/L. Each reconstituted primer was held at 4 °C for 30 minutes to allow complete dissolution. For each PCR run, 20 µL of the stock primer was used; the

solution was then further diluted in 80 µL of sterile water to give a final working concentration of 20 µmol/L.

The primers were screened against DNA extracts of *M. bovis* 1173P2, *M. smegmatis* Mc2155 (S2), and *M. abscessus*(ATCC 19977). DNA was extracted using the QIAGEN DNeasy Blood & Tissue Kit (QIAGEN, UK) and standardised to a concentration of 10 ng/µL. PCR was performed as described in Chapter 3, Section 3.7.5, using a T100 Thermal Cycler (BIO-RAD) and HotStarTaq DNA Polymerase (QIAGEN 203205). The primary mix for the PCR reaction was formulated, as shown in Table 4.1. Before the reaction, the contents of each vial were mixed by vortexing, and the reagents were stored on ice.

Table 4.1 Volume of reagent used in each PCR reaction (Qiagen Quick-Start Protocol).

Master Mix preparation	Volume (ul)
10 X PCR Buffer	2.5
5 X Q solution	5
dNTP	0.5
Primer F (20 umol/L)	0.25
Primer R (20 umol/L)	0.25
HotStar Taq DNA poly	0.125
Deionised Water H_2O	11.375
DNA template	5
Total reaction volume	**25**

The optimal PCR conditions for amplifying the *IS6110*, *mpb64*, and *IS1081* gene targets were as follows: denaturation at 95 °C for 5 minutes, followed by 35 cycles of denaturation at 95 °C for 30 seconds, annealing at temperatures ranging from 70 °C to 60.7 °C for 30 seconds, and extension at 72 °C for 45 seconds, with a final extension step at 72 °C lasting 5 minutes (Kabir et al., 2018).

The resulting PCR products were visualised on a 2.5% agarose gel stained with SafeView Nucleic Acid Stain (NBS Biologicals Ltd) and viewed under UV light. To prepare the gel, 2.5 grams of agarose powder (TopVision Agarose, Thermo Scientific) were added to 100 mL of 1X TBE electrophoresis buffer in a 500 mL glass Duran bottle. After mixing the liquid and powder, the bottle was placed in a microwave and irradiated at full power for 3 minutes until the agar had fully dissolved. Once the mixture cooled, 4 µL of SafeView Nucleic Acid Stain (NBS Biologicals Ltd) was added and mixed gently before being poured into a gel tray with a casting dam and comb. After solidification, the comb and casting dam were removed.
For gel loading, 10 µL of each PCR product was mixed with 1 µL of DNA loading buffer (BIOLINE, H4P-112I); the samples were then loaded into the wells of the agarose gel. A positive control containing a molecular weight ladder ranging from 25 to 766 bp (Low Molecular Weight DNA Ladder, New England Biolabs) was loaded into the first well. The gel was placed in an electrophoretic tank (Bio-Rad) and covered with TBE buffer. Electrophoresis was performed at 80 V for 90 minutes, followed by visualisation under ultraviolet illumination using a Gel Image Analysis System (Bio-Rad Universal Hood II Gel Doc System), with images captured electronically for further analysis. The PCR reaction was repeated three times for each primer combination.

4.9 Targeting *IS6110 and IS1081* gene sequences in *M. bovis* NCTC 5692 and *M. tuberculosis* H37Ra

DNA was isolated from *M. bovis* NCTC 5692 and an attenuated strain of *M. tuberculosis* H37Ra using the QIAGEN DNeasy Blood & Tissue Kit (QIAGEN, UK) extraction method, before being standardised to a concentration of 10 ng/µL, as described previously. The PCR method described above was utilised to validate the sensitivity of the selected DNA probes. Each assay was repeated three times.

4.10 Results

4.10.1 Sequence alignment of published *M. tuberculosis* specific diagnostic PCR primer probes to their gene targets

The nucleotide sequences of the genes encoding *IS6110*, *mpb64*, and *IS1081* of *M. tuberculosis* were downloaded from NCBI and used to identify regions of homology with published diagnostic PCR primer probes. The reverse complement sequence of the 3' primer pair was used to identify the downstream binding region on the forward DNA strand. The same colour represents each primer pair in Figures 4.2, 4.3, and 4.4.

Figure 4.2 Nucleotide sequence of the *IS6110* gene.

Homology with PCR primer probe recognition sequences is highlighted in different colours. Each colour represents the primers used in a different study: red sequences (Chakravorty et al., 2017a), blue sequences (Nghiem et al., 2015), green sequences (Raj et al., 2016), and purple sequences (Sekar et al., 2008a).

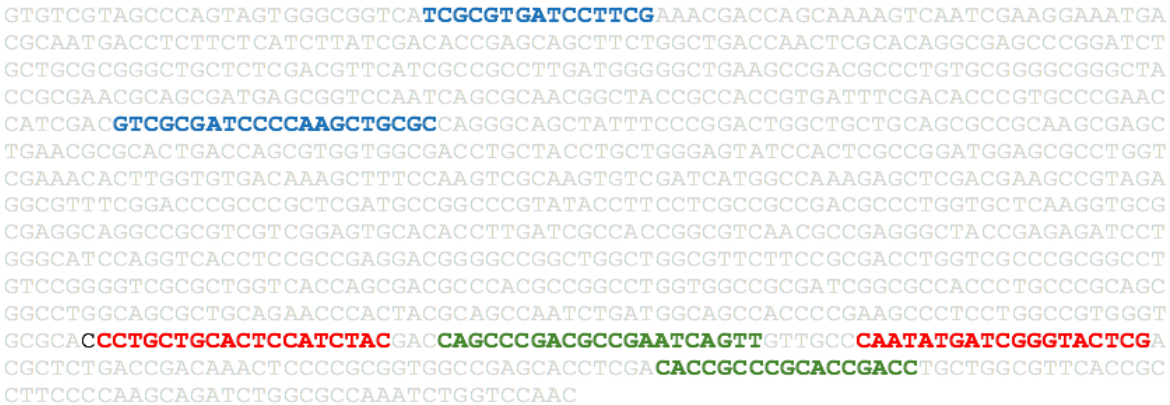

Figure 4.3 Nucleotide sequence of the *mpb46* gene.

The selected PCR primer probe is highlighted in a different colour. Each colour represents primers used in a different study: blue sequences (Raj et al., 2016), red sequences (Khosravi et al., 2017), and green sequences (Nghiem et al., 2015).

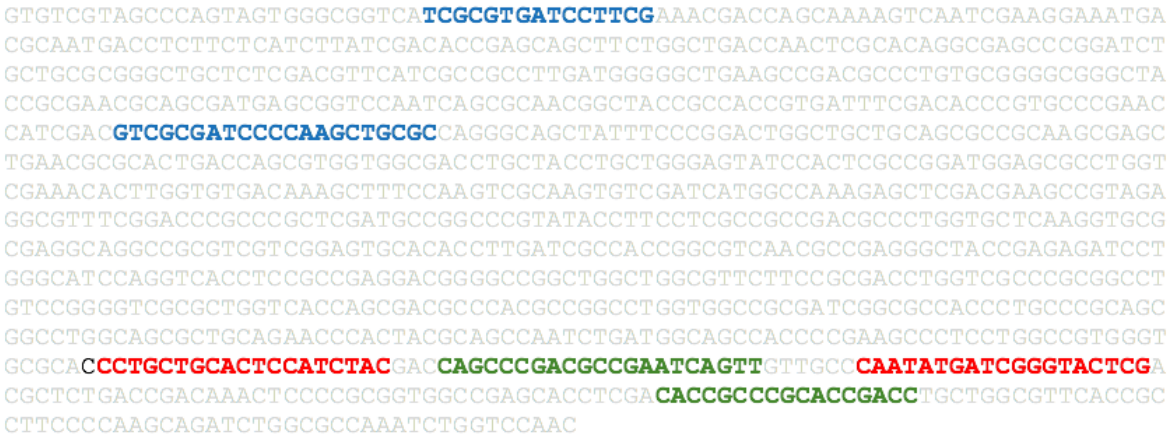

Figure 4.4 Nucleotide sequence of the *IS1081* gene.

PCR primer probes are highlighted in different colours, with each colour representing primers used in a different study: blue sequences (Chakravorty et al., 2017), red sequences (Lyu et al., 2020), and green sequences (Soolingen et al., 1992).

DNA probes were designed to conform to the structural constraints of the microwave detection system—specifically, they had to maintain defined lengths, spacing (e.g. 5-nt gap), and orientation to ensure optimal hybridisation and signal detection within the assay format. These sequences are shown in Tables 4.2, 4.3, and 4.4 below.

Table 4.2 DNA probe sequences for the detection of *IS6110* gene targets.

Each sequence includes a 17-nucleotide anchor probe (highlighted in purple) and a 22-nucleotide detector probe (highlighted in yellow), separated by a 5-nucleotide gap. These colour-coded regions illustrate the structural layout required for the microwave detection system.

5″ CGTCCAGCGCCGCTTCGGACCACCAGCACCTAACCGGCTGTGGG 3″
3″ CAGGGTTCGCCTACGTGGCCTTTGTCACCGACGCCTACGCTCGC 5″
5″ CGAAGAATCCGCTGAGCTGAAGCGCTTAGCGGCGGGACAACGCC 3″
3″ CTCGTCCAGCGCCGCTTCGGACCACCAGCACCTAACCGGCTG 5″
3″ CCTACTACGACCACATCAACCGGGAGCCCAGCCGCCGCGAGCT 5″

Table 4.3 DNA probe sequences for the detection of *mpb64* gene targets.

Each sequence includes a 17-nucleotide anchor probe (highlighted in purple) and a 22-nucleotide detector probe (highlighted in yellow), separated by a 5-nucleotide gap. These colour-coded regions illustrate the structural layout required for the microwave detection system.

5″ TCCGCTGCCAGTCGTCTTCCCCATTGTGCAAGGTGAACTGAGCA 3″
3″ CACGCTGTGGCAGGCTGACACCGATCCGCTGCCAGTCGTCTTCC 5″
5″ TGGCCTAGACTCGCGAGGACCGCGCGGTGGTCACTGCGCGGATT 3″
5″ CGTTCCGCGATCGACTCGATGCTGGCCTAGACTCGCGAGGACCG 3″
5″ GTGAACTGAGCAAGCAGACCGGACAACAGGTATCGATAGCGCCG 3″
3″ AGTCGTCTTCCCCATTGTGCAAGGTGAACTGAGCAAGCAGACCG 5″
5″ GGACCCGGTGAATTATCAGAACTTCGCAGTCACGAACGACGGGG 3″
3″ GATAGCGCCGAATGCCGGCTTGGACCCGGTGAATTATCAGAACT 5″

Table 4.4 DNA probe sequences for the detection of *IS1081* gene targets

Each sequence includes a 17-nucleotide anchor probe (highlighted in purple) and a 22-nucleotide detector probe (highlighted in yellow), separated by a 5-nucleotide gap. These colour-coded regions illustrate the structural layout required for the microwave detection system.

5″ TCGCGTGATCCTTCGAAACGACCAGCAAAAGTCAATCGAAGGAA 3″
3″ GCGTGTCGTAGCCCAGTAGTGGGCGGTCATCGCGTGATCCTTCG 5″
5″ CCTGCTGCACTCCATCTACGACCAGCCCGACGCCGAATCAGTTG 3″
3″ GCCCGACGCCGAATCAGTTGTTGCCCAATATGATCGGGTACTCG 5″
3″ CCCTGCTGCACTCCATCTACGACCAGCCCGACGCCGAATCAGTT 5″
5″ CAGCCCGACGCCGAATCAGTTGTTGCCCAATATGATCGGGTACT 3″
5″ CACCGCCCGCACCGACCTGCTGGCGTTCACCGCCTTCCCCAAGC 3″
3″ ACTCCCCGCGGTGGCCGAGCACCTCGACACCGCCCGCACCGACC 5″
3″ CTCCATCTACGACCAGCCCGACGCCGAATCAGTTGTTGCCCAAT 5″

4.11 Screening of probe combinations for secondary structures

To identify the probe combinations with the highest chance of specifically binding to the target, all sequences that included more than four of the same nucleotides and were predicted using the RNA Structure software package to form secondary structures were excluded. The remaining sequences are shown in Tables 4.5, 4.6, and 4.7. Results figures are shown in Appendix 1.

Table 4.5 Optimised *IS6110*-specific probe combinations.

The 5-nucleotide spacer separating the anchor and detector regions is shown in **red**.

CGTCCAGCGCCGCTTCG GACCA CCAGCACCTAACCGGCTGTGGG
CTCGTCCAGCGCCGCTTCGG ACCAC CAGCACCTAACCGGCTG
CCTACTACGACCACATCAACC GGGAG CCCAGCCGCCGCGAGCT

Table 4.6 Optimised *mpb64*-specific probe combinations.

The 5-nucleotide spacer separating the anchor and detector regions is shown in **red**.

GTGAACTGAGCAAGCAG ACCGG ACAACAGGTATCGATAGCGCCG
AGTCGTCTTCCCCATTGTGCAA GGTGA ACTGAGCAAGCAGACCG
GATAGCGCCGAATGCCGGCTTG GACCC GGTGAATTATCAGAACT

Table 4.7 Optimised *IS1081*-specific probe combinations.

The 5-nucleotide spacer separating the anchor and detector regions is shown in **red**.

CAGCCCGACGCCGAATC AGTTG TTGCCCAATATGATCGGGTACT
CCCTGCTGCACTCCATCTACGA CCAGC CCGACGCCGAATCAGTT
CTCCATCTACGACCAGCCCGAC GCCGA ATCAGTTGTTGCCCAAT

4.12 Confirming the ability of optimised probes to bind to target DNA

A PCR was performed to confirm that the probes retained their ability to bind to the target DNA. Table 4.8 details the different primers for each gene target. Each primer set consists of a forward primer that matches the DNA sequence and a reverse primer with a sequence complementary to the original DNA sequence.

Table 4.8 Probe combinations for PCR screening.

Name of probe	Target gene	Sequence
IS6 1	***IS6110***	Forward primer 5″ CGTCCAGCGCCGCTTCG 3″ Reverse primer 3″ CCCACAGCCGGTTAGGTGCTGG 5″
IS6 2		5″CCTACTACGACCACATCAACC 3″ 3″ AGCTCGCGGCGGCTGGG 5″
IS6 3		5″ CTCGTCCAGCGCCGCTTCGG 3″ 3″ CAGCCGGTTAGGTGCTG 5″
MP 1	***Mpb64***	5″ GTGAACTGAGCAAGCAG 3″ 3″ CGGCGCTATCGATACCTGTTGT 5″
MP 2		5″AGTCGTCTTCCCCATTGTGCAA 3″ 3″ CGGTCTGCTTGCTCAGT 5″
IS8 1	***IS1081***	5″ CAGCCCGACGCCGAATC 3″ 3″ AGTACCCGATCATATTGGGCAACAACT 5″
IS8 2		5″ CCCTGCTGCACTCCATCTACGACCAGC 3″ 3″ AACTGATTCGGCGTCGG 5″
IS8 3		5″ CTCCATCTACGACCAGCCCGACGCCGA 3″ 3″ ATTGGGCAACAACTGAT 5″

4.13 Determination of the ability of candidate probes to detect *M. bovis 1173P2* DNA

The anchor and detector probe-based PCR primers were designed to amplify a 50 bp region. The results for the probes targeting the *IS6110* gene are shown in Figure 4.5. Primer pairs IS6 1 and IS6 3 produced bands of varying molecular sizes across a range of annealing

temperatures, including a band of the predicted size. However, the IS6 2 primers failed to generate a PCR product of the expected size.

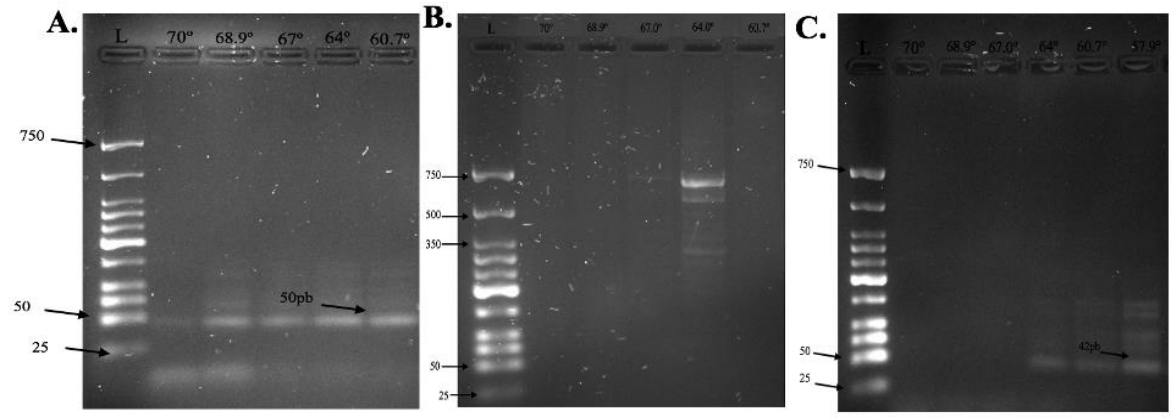

Figure 4.5 PCR products obtained at different annealing temperatures using IS6 1 primer (A), IS6 2 primer (B), and IS6 3 primer (C), all targeting the *IS6110* gene.

Template DNA was extracted from *M. bovis* 1173P2 using the Qiagen method and standardised to a final concentration of 10 ng/µL. The following annealing temperatures were assessed: 70.0, 68.9, 67.0, 64.0, and 60.7 °C. PCR amplicons (5 µL) were electrophoresed in a 2.5% agarose gel stained with Safeview™ in a 1X TBE electrophoresis buffer. A molecular weight ladder was used in lane 1 for reference. These reactions were repeated in triplicate, with consistent results as shown above.

To assess the feasibility of eliminating the additional DNA bands generated by primer pairs one and three, amplification cycles were reduced from 35 to 30 (Bovo et al., 1999). As shown in Figure 4.6, this modification eliminated the additional bands. The optimum annealing temperature for the IS6 1 primer set was 60.7 °C, while for IS6 3, it was 64.0 °C.

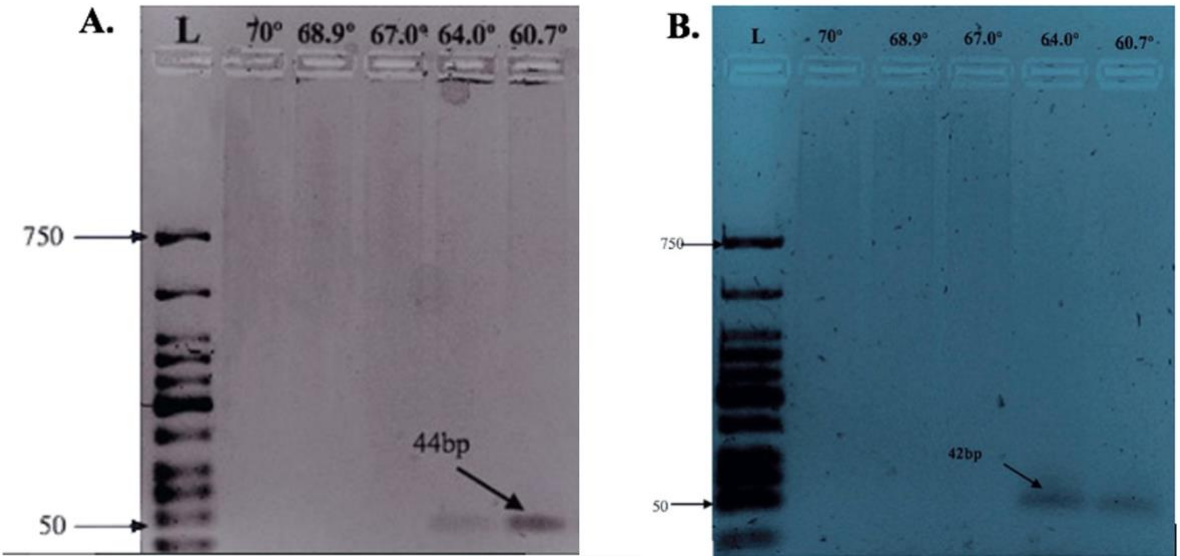

Figure 4.6 PCR products obtained at different annealing temperatures using IS6 1 primer (A) and IS6 3 primer (B), both targeting the *IS6110* gene sequence.

Template DNA was extracted from *M. bovis* 1173P2 using the Qiagen method and standardised to a final DNA concentration of 10 ng/µL. The following annealing temperatures were assessed: 70.0, 68.9, 67.0, 64.0, and 60.7 °C. PCR amplicons (5 µL) were electrophoresed in a 2.5% agarose gel stained with Safeview™ in 1X TBE electrophoresis buffer. A molecular weight ladder is shown in lane 1 for reference. These reactions were repeated in triplicate, with consistent results as shown above.

Concerning probes designed to target *IS1081*, the IS8 1 primers failed to generate a PCR product across any annealing temperatures. The IS8 3 primers generated multiple bands, one of which was of the expected size (Figure 4.7B). The IS8 2 primers were the only primers to produce a single band of the expected size against *M. bovis* 1173P2 DNA at 60.7 °C.

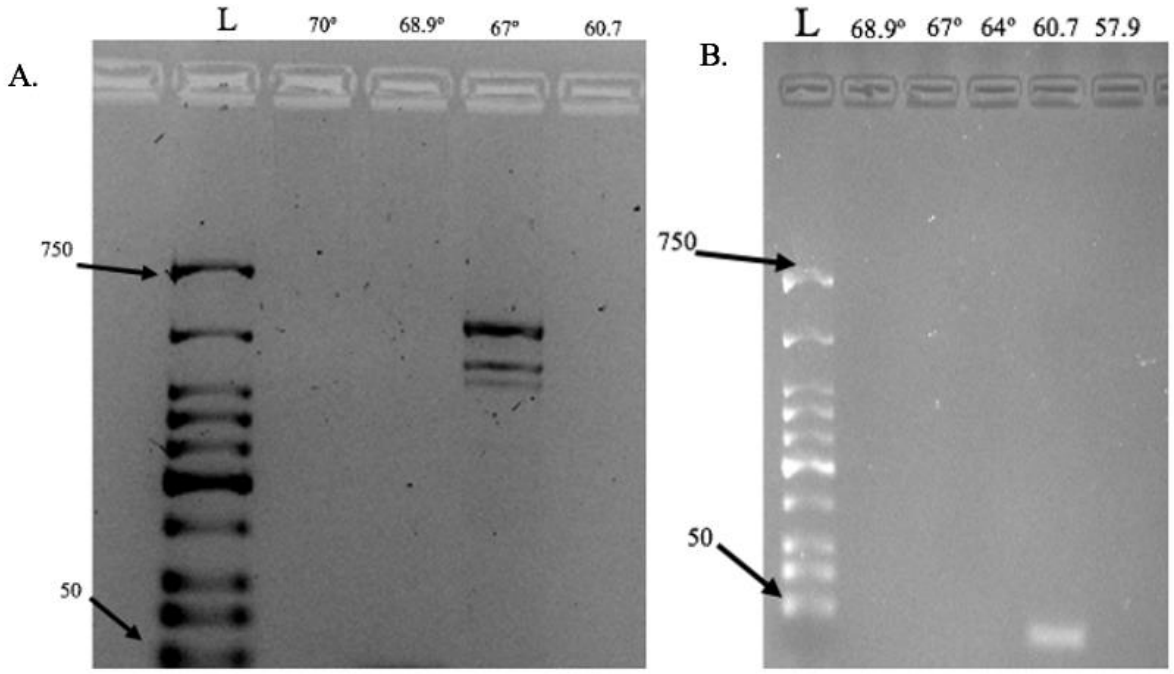

Figure 4.7 PCR products obtained at different annealing temperatures using IS8 2 primer (A) and primer IS8 3 (B) targeting the *IS1081* gene sequence.

Template DNA was extracted from *M. bovis* 1173P2 using the Qiagen method and standardised to a final DNA concentration of 10 ng/µL. The following annealing temperatures were assessed: 70.0, 68.9, 67.0, 64.0, and 60.7°C. PCR amplicons (5 µL) were electrophoresed in a 2.5% agarose gel stained with Safeview™ in 1X TBE electrophoresis buffer. A molecular weight ladder is shown in lane 1 for reference. These reactions were repeated in triplicate, with consistent results.

Both primers designed to target the *mpb64* gene failed to generate detectable PCR products across a range of annealing temperatures when DNA from *M. bovis* 1173P2 was used as the target. To determine whether this was due to an issue with the target strain, the PCR was repeated using DNA extracted from a second isolate, *M. bovis* NCTC 5692. Once again, no PCR signal was generated using these primers.

To determine if the primers' design was flawed, the PCR was repeated using DNA extracted from *M. tuberculosis* H37Ra. As illustrated in Figure 4.8, a single band of the expected size was produced by the MP 1 primers, while no amplicon was generated by the MP 2 primers.

To determine if the gene target was missing from the *M. bovis* isolates, the genome sequences of both isolates were screened in the NCBI database, and no homolog to the *mpb64* gene was found. These results suggest that, unlike *M. tuberculosis*, the *mpb64* gene target is missing from these isolates.

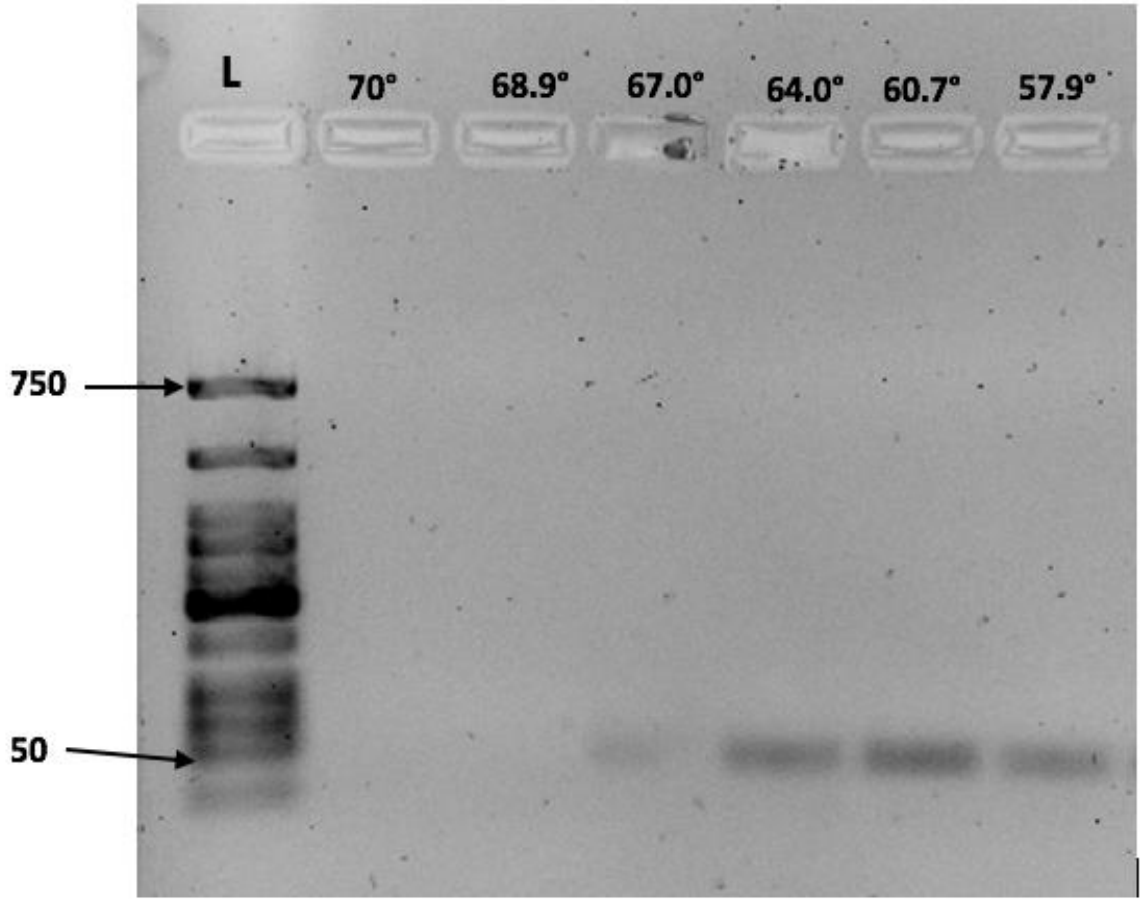

Figure 4.8 PCR products obtained at different annealing temperatures using MP 1 primer targeting the *mpb64* gene sequence.

Template DNA was extracted from *M. tuberculosis* H37Ra using the Qiagen method and standardised to a final DNA concentration of 10 ng/µL. The following annealing temperatures were assessed: 70.0, 68.9, 67.0, 64.0, 60.7, and 57.9°C. PCR amplicons (5 µL) were electrophoresed in a 2.5% agarose gel stained with Safeview™ in 1X TBE electrophoresis buffer. A molecular weight ladder is shown in lane 1 for reference. These reactions were repeated in triplicate, with consistent results.

Based on the results to date the sequences based on *IS6110* and *IS1081* should be further explored as diagnostic targets for *M. tuberculosis* .

4.14 Determination of the specificity of the *IS6110* and *IS1081* candidate probes

The specificity of the IS6 1, IS6 3, and IS8 2 primers was evaluated using genomic DNA extracted from two closely related mycobacterial species, *M. smegmatis* Mc2155 (S2) and *M. abscessus* (ATCC 19977). The IS6 1 and IS8 2 probes failed to produce amplicons when tested with DNA from *M. smegmatis* Mc2155 (S2) and *M. abscessus* ATCC 19977, suggesting they may be specific to *M. bovis*. Unfortunately,

the IS6 3 primers generated amplicons when tested against genomic DNA from *M. abscessus*, suggesting a lack of specificity (Figure 4.9).

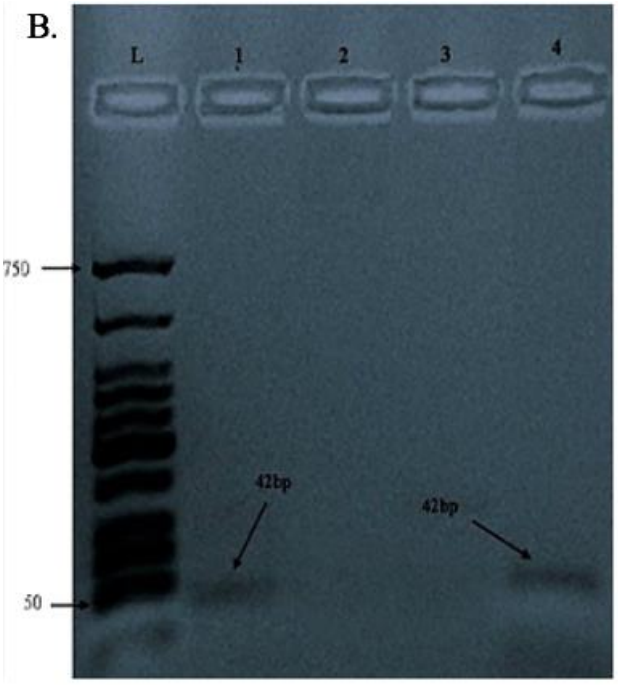

Figure 4.9 The specificity of IS6 3 primer.

PCR was performed using the designed IS6 3 probes, amplified at their respective annealing temperatures, as described in Section 4. DNA was extracted from all bacterial isolates using the Qiagen method and standardised to a final DNA concentration of 10 ng/µL. The anchor and detector probes (reverse complements) were used as forward and reverse primers, respectively, against *M. bovis* 1173P2 and non-*M. bovis* DNA extracts. PCR amplicons (5 µL) were electrophoresed in a 2.5% agarose gel stained with Safeview™ in 1X TBE electrophoresis buffer. L = 44 bp molecular weight marker; lane 1 = *M. abscessus*; lane 2 = *M. smegmatis*; lane 3 = PCR primary mix control; lane 4 = *M. bovis*1173P2.

4.15 Determination of the ability of the IS6 1 and IS8 2 primers to recognise DNA from *M. bovis* NCTC 5692 and *M. tuberculosis* H37Ra

To confirm the specificity of the selected probes for *M. bovis* and *M. tuberculosis*, the ability of the IS6 1 and IS8 2 primers to recognise genomic DNA from *M. bovis* isolate NCTC 5692 and *M. tuberculosis* H37Ra was assessed. As shown in Figure 4.10, amplicons of the expected size were generated by both primers.

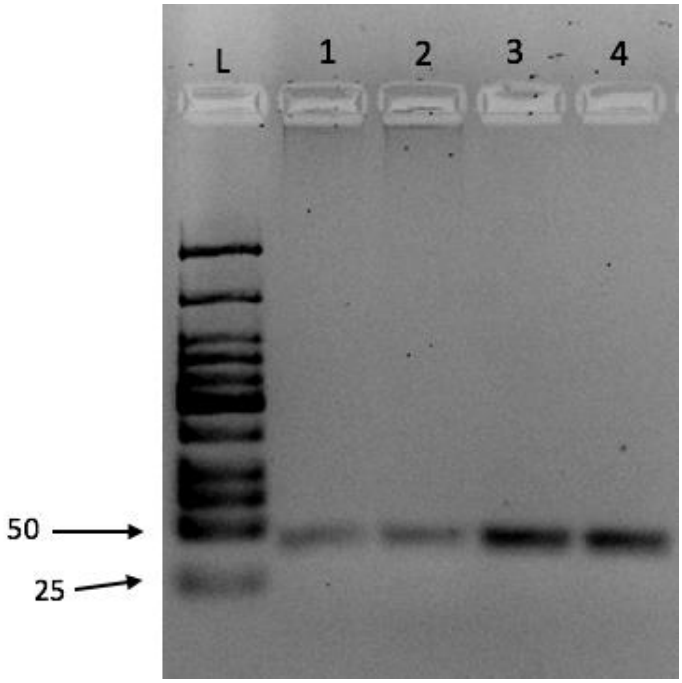

Figure 4.10 Targeting the *IS6110* and *IS1081* genes of *M. bovis* NCTC 5692 and *M. tuberculosis* H37Ra.

DNA was extracted from all bacterial isolates using the Qiagen method and standardised to a final DNA concentration of 10 ng/µL. PCR amplicons (5 µL) were electrophoresed in a 2.5% agarose gel stained with Safeview™ in 1X TBE electrophoresis buffer. Lane 1 = IS6 1 probe against *M. bovis* NCTC 5692 genomic DNA; lane 2 = IS8 2 probe against *M. bovis* NCTC 5692 genomic DNA; lane 3 = IS6 1 gene probe against *M. tuberculosis* H37Ra genomic DNA; lane 4 = IS8 2 gene probe against *M. tuberculosis* H37Ra genomic DNA.

4.16 Discussion

A bioinformatics-based approach was employed to design probes specific to *M. bovis* and *M. tuberculosis*, optimized for our point-of-care assay to detect single-stranded DNA sequences. These probes were based on DNA sequences from PCR primers with known specificity for the target organisms and were screened for their ability to bind to conserved regions of the *IS6110* and *IS1081* genes of *M. bovis* and *M. tuberculosis*.

The *IS6110* gene has been widely used in numerous studies to confirm the presence of *M. tuberculosis* complex (MTBC) (McEvoy et al., 2007; Comín et al., 2022). However, some MTBC isolates lack this target. To address this limitation, the potential inclusion of the *IS1081* and *mpb64* gene targets was explored in this project (Huyen et al., 2013; Kanabalan et al., 2021).

Although primer probes that recognised *IS1081* with the required level of specificity were identified, this was not the case for the *mpb64* gene target. This gene was selected because it is reported to have high specificity for MTBC, with sensitivity rates ranging from 75% to 90% and specificity rates of up to 100% (Sunil et al., 2016). While the probes designed in this study recognised *M. tuberculosis* H37Ra, they failed to generate an amplicon when tested against *M. bovis* 1173P2 and NCTC 5692. A subsequent review of the literature revealed that not all isolates of *M. bovis* carry the *mpb64* gene target (Liu et al., 1993). The absence of this gene target from our test isolates was confirmed by a review of genome sequences deposited in the NCBI database.

In conclusion, DNA sequences specific to *IS6110* and *IS1081* were identified and could be employed in the point-of-care assay.

Chapter 5 A Rapid method for detecting members of the mycobacterium tuberculosis complex using a microwave assisted enzyme linked oligonucleotide sandwiched hybridisation assay (ELOSHA)

4.17 Introduction

Accurately diagnosing bacterial infections is crucial for controlling the spread of illness and improving patient care (Peri et al., 2021). Effective disease management minimises side effects and inhibits the development and spread of antibiotic resistance (Muteeb et al., 2023). Over the past few decades, most bacterial infections have been diagnosed via clinical indicators and standard laboratory-based culture methods (Rentschler et al., 2021). However, some microorganisms, such as *M. tuberculosis*, are challenging to isolate using routine methods owing to their specialised nutritional requirements and slow growth rate, highlighting the necessity for testing methods independent of bacterial culture (Heidary et al., 2022).

Several methods have been employed to rapidly detect microorganisms and molecules, such as bacteria, proteins, and metabolites, including gas chromatography-mass spectrometry (GC-MS), ultra-high-performance liquid chromatography-tandem mass spectrometry (LC-MS/MS), high-performance liquid chromatography (HPLC), enzyme-linked immunosorbent assay (ELISA), and biosensors - analytical devices have the ability to convert biological information into detectable signals, such as optical, electrochemical, magnetic, or thermal signals (Lee & Kim, 2022). While most of these methods are specific and sensitive, they often require significant time, expensive equipment, and specialist operators (Doğan, 2024). Another universally recognised approach involves DNA-based diagnostic tools, which are renowned for their sensitivity and specificity in clinical settings (Choe et al., 2015).

DNA-based diagnostic tools are widely used for infection diagnosis (Prabhakar & Lakhanpal, 2020). Despite their high sensitivity and specificity, current techniques (such as PCR) can take several hours to generate results due to the need for sample processing before analysis.

Coupled with the cost of the system and the need for specialist training, these methods may be inappropriate for bedside operations (Minhas et al., 2023).

These limitations have driven the development of alternative detection technologies, such as lateral flow assays (LFAs). LFAs are primarily based on the principle of enzyme-linked immunosorbent assays (ELISA). They detect proteins and DNA in clinical samples (with proteins being the most common detection target) (Tsurusawa et al., 2021). The detection of DNA is extremely sensitive and advantageous in disease diagnosis because it is more biochemically stable than RNA, proteins, and cells (Klumpp-Thomas et al., 2021).

While LFAs exhibit great promise, their sensitivity and signal strength depend on the quantity of DNA present in the sample, particularly when a DNA amplification step is not part of the method. To overcome this limitation, magnetic particles (MPs) enhance targeted DNA recovery from samples (Pankhurst et al., 2003; Chen et al., 2017; Modh et al., 2018). The characteristic properties of MPs and their applications in diagnostic assays are discussed below.

4.18 Magnetic particles (MPs) and applications in biosensing

One of the primary challenges regarding a DNA-based approach is extracting a sufficient concentration and quality of DNA from a sample to support subsequent analysis. To address this limitation, magnetic particles (MPs) are commonly utilised to capture and retrieve DNA from samples (Kim et al., 2020). These MPs are typically constructed from magnetite (Fe_3O_4) or maghemite (γ-Fe_2O_3) and range in size from sub-nanometres to micrometres (Kim et al., 2020). MPs are widely used in biosensing due to their high density, hydrophilicity, homogeneous dispersion in suspension, colloidal stability, and superparamagnetism (Joudeh & Linke, 2022). These properties make it possible to control the movement of these components within a sample via shaking or a magnetic field, which facilitates the

concentration and transport of the desired analyte to one location for practical analysis (Joudeh & Linke, 2022).

4.19 Attachment of target specific DNA probes to magnetic particles

Preparing high-quality DNA/magnetic particle (MP) conjugates presents a significant challenge. Ideally, the resulting conjugate should demonstrate colloidal stability, efficient DNA probe labelling, and presentation to maximise hybridisation with the target DNA while minimising non-specific DNA binding (Ahortor, 2019). Using this approach, DNA targets can be concentrated from diverse samples and hybridised to their complementary probes (Farinha et al., 2021). DNA probes can be affixed to MPs using various chemistries (Ivanov et al., 2023). For instance, thiol groups can be attached to the terminals of the DNA probe, enabling the DNA to bind to metal surfaces via a metal-thiolate bond, which is a chemical bond formed between a wide range of metals and a thiolate (or thiol) group under suitable conditions, as shown in Figure 5.1 (Ma et al., 2022). Thiolate groups are represented by the general formula $R\text{-}S^-$ (where R is an organic group), and they contain a sulphur atom bonded to a hydrogen atom. The metal–thiolate bond typically involves the interaction of the sulphur atom from the thiolate group with a metal atom (Chen, 2021). The sulphur atom donates an electron pair to form a coordinate covalent bond with the metal atom, which, in turn, accepts the electron pair (Azcárate et al., 2013).

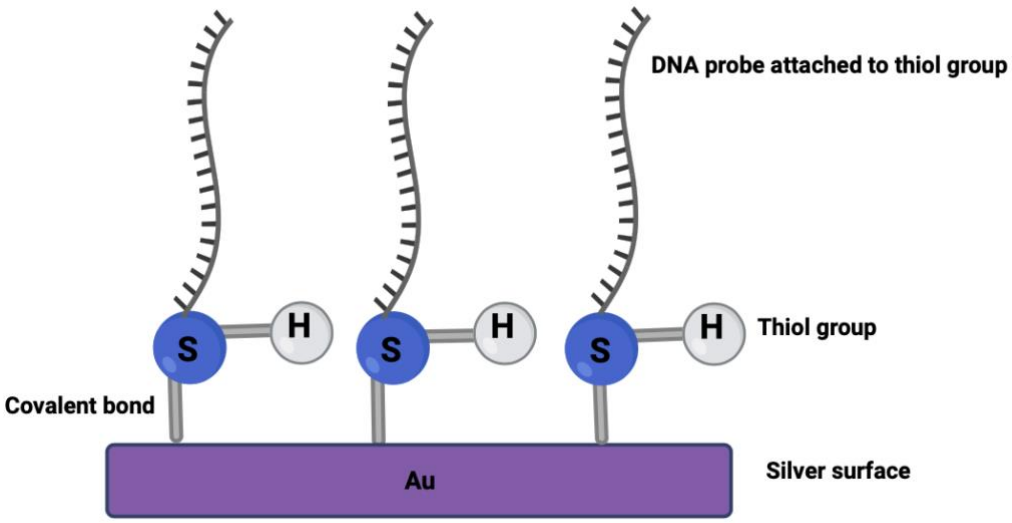

Figure 0.1 A Metal–thiolate bond.

The thiolated probe is attached to a silver surface via the formation of a bond between the metal component of the silver and the thiolate group (a sulphur atom bonded to a hydrogen atom) of the probe. (Created by BioRender.com).

As an illustrative example, Aslan et al. (2008) utilised a thiolated DNA probe attached to silver to develop a system capable of detecting *B. anthracis* in under 30 seconds. Supplementary methods for attaching DNA sequences to MPs have been developed, including chemical modification of the MPs' surface to incorporate functional groups such as carboxylate (-COOH) or amine ($-NH_2$) (Wieszczycka et al., 2021). Additionally, proteins such as streptavidin (Figure 5.2) can be employed. Streptavidin is a tetrameric bacterial protein isolated from *Streptomyces avidinii*, providing high-affinity biotin binding (Lu et al., 2011). The streptavidin-biotin complex is a potent, naturally occurring binding partner exhibiting significantly greater binding strengths than typical protein-ligand pairs (Luong & Vashist, 2020). It has been extensively employed in biochemical sensing applications and has played a prominent role in the discovery of potentially novel drug targets (Wang et al., 2020). Biotin is confined in the active site of streptavidin by eight hydrogen bonds and van der Waals interactions among non-polar groups (Luong & Vashist, 2020; Ayan et al., 2022).

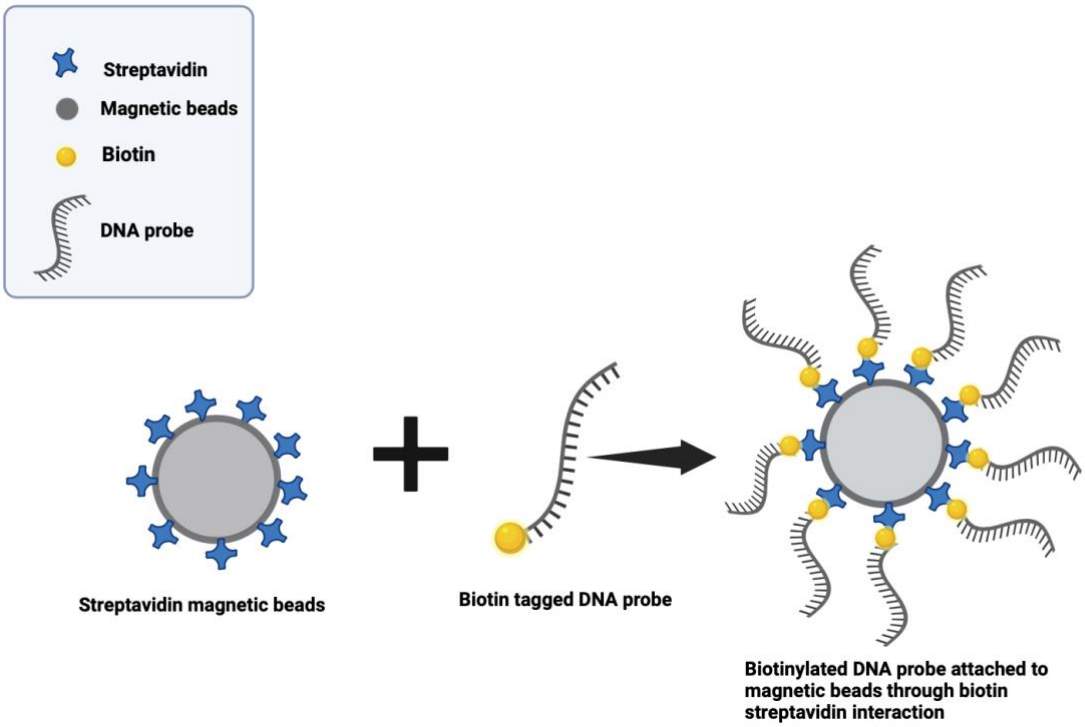

Figure 0.2 - Principle of DNA probe binding to magnetic particles (MP).

The DNA probe is tagged with biotin, which exhibits a high affinity for binding to streptavidin attached to the magnetic particles. (Created by BioRender.com).

Previous studies have demonstrated that commercially available streptavidin-coated MPs (Dynabeads MyOne streptavidin-coated beads C1), labelled with biotin-tagged DNA probes in combination with microwaves, can be used to detect *M. abscessus* and *M. smegmatis* (Ahortor, 2019). Building on these results, an approach will be developed capable of detecting *M. bovis*, a member of the *M. tuberculosis* complex that serves as a surrogate model for *M. tuberculosis*.

4.20 Detection of pathogen specific DNA sequences using an enzyme linked oligonucleotide sandwich hybridisation assay

The enzyme-linked oligonucleotide sandwich hybridisation assay (ELOSHA) provides a higher level of sensitivity than culture and smear microscopy methods (Bahadır & Sezgintürk, 2016; Lorenson et al., 2019a). It involves capturing a ssDNA target sequence between two complementary probes (capture and detector) to form a three-strand DNA complex. The capture probe has biotin attached at the 5' end, anchoring the ssDNA to an MP's surface, while the reporter probe is labelled with an enzymatic signal (Figure 5.3). Preceding the anchor probe at the 5' end is a sequence of five thymidine residues to enable probe flexibility when bound to the MP via a biotin-streptavidin interaction. The robustness and reproducibility of ELOSHA assays depend on several factors, including the flexibility and length of the capture probe (Parham et al., 2007; Patel et al., 2011; Lorenson et al., 2019a). Probe sequences longer than 20 base pairs provide stability for target-probe binding (Wang, 2011). The presence of the target gene is indirectly determined via a signal generated from the horseradish peroxidase (HRP)-labelled detector probe upon reaction with substrates such as 3,3,5,5-tetramethylbenzidine (TMB) (Harpaz et al., 2020). TMB reacts with HRP to create a blue colour with maximum absorbance at 370 and 652 nm. This enzyme-substrate reaction is terminated by adding 0.1 M hydrochloric acid or 0.1 M sulphuric acid, which creates a yellow colour with absorption maxima at 450 nm (Zhu et al., 2021).

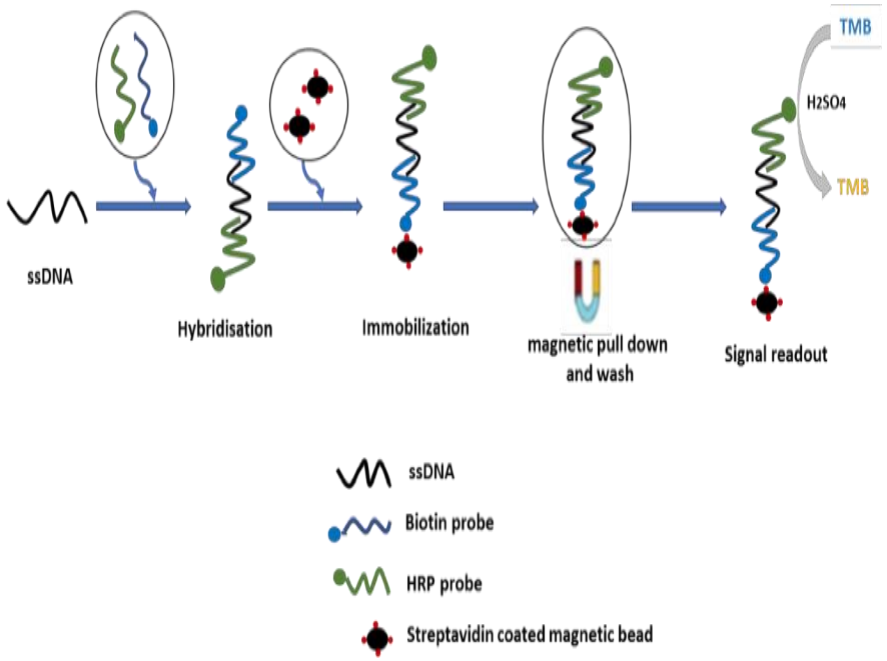

Figure 0.3 Principles of sandwich hybridisation assay.

The three-strand hybrid complex (anchor probe-target ssDNA-detector probe) is immobilised on the surface of the magnetic particles (MPs) and separated via the application of a magnetic field. The presence of target DNA is indirectly detected by the signal intensity generated by the HRP attached to the detector probe. The enzyme-substrate reaction is then terminated by the addition of H_2SO_4 (Ahortor, 2019).

4.21 Evaluating the sensitivity and specificity of the ELOSHA assay using simulated sputum

To date, research has been conducted using microorganisms and DNA suspended in simple solutions such as water or PBS to facilitate the standardisation of test results. Real-world clinical samples (particularly sputum) comprise a complex mixture of microorganisms and host-derived cellular and extracellular material, which has the potential to inhibit microwave-mediated DNA release and subsequent capture by MPs. Using patient-derived sputum samples to support the preliminary stages of assay development is challenging for ethical reasons and the potential risk of infection. The World Health Organization (WHO) recommends using simulated sputum-derived specimens for quality control evaluation in laboratory testing procedures (WHO, 2022). Simulated sputum provides a practical substitute for evaluating the effectiveness of the ELOSHA assay; however, it is crucial to note that the synthetic sample is designed to mimic the physical characteristics of real sputum rather than its biological and electrical features.

4.22 Aim

The primary aim of this chapter is the development of a version of the ELOSHA capable of detecting *M. bovis* (a surrogate model for *M. tuberculosis*) using the DNA probes designed in Chapter 4.

The chapter objectives are as follows:

1. To optimise assay parameters to detect *M. bovis* in water and simulated sputum samples.
2. To evaluate the specificity and sensitivity of the assay in detecting *M. bovis* in water and simulated sputum.
3. To develop and implement optimisation strategies aimed at reducing assay time and enhancing sensitivity.

4.23 Materials

Three different commercially available magnetic beads (MPs) were used: Dynabeads™ M-270 Streptavidin, Dynabeads MyOne streptavidin-coated beads, and C-1 and Hydrophilic Streptavidin Magnetic Beads (Invitrogen, Thermo Fisher). Tween 20, Triton X-100, Bovine Serum Albumin (BSA), H_2SO_4, and 1-Step™ Ultra TMB-ELISA solution were purchased from Thermo Fisher Scientific. A MagRack 6 for separating magnetic beads was acquired from Sigma-Aldrich. *IS6110* and *IS1081* specific DNA probes were obtained from Fisher Scientific Invitrogen.

4.24 Methodology

4.24.1 Determination of the binding capacity of streptavidin coated magnetic beads c1 for biotin labelled dna probes

Initially, 100 µL (4 mg/mL) of streptavidin-coated beads C-1 (Dynabeads MyOne) were washed three times with PBS to remove all traces of the azide-containing storage buffer, which could potentially inhibit the hybridisation assay. To attach biotin-labelled probes (*IS6110* and *IS1081* DNA anchor probes) to the MPs, 10 µL of 20 µM biotin-labelled probes were incubated with 100 µL of MPs at room temperature for one hour using an orbital shaker (200 rpm). Unbound probes were removed from the MPs by applying a magnet (MagRack 6, GE Healthcare) and rinsing with 1X PBS. To determine whether the biotin probes had bound to the MPs, the concentration of probes before and after addition to MPs was determined, and the proportion of bound probes was calculated by subtracting the probe concentration remaining in the suspension from the original probe concentration (before the addition of MPs). The concentration of free probe DNA before and after binding to MPs was determined using a NanoDrop (as detailed in Chapter 2, Section 2.8).

4.24.2 Preventing non-specific binding of DNA to MPs using chemical blocking agents

The magnitude of the non-specific background signal can be minimised by preventing the binding of non-target DNA and the HRP-labelled DNA reporter probe to the MPs. To identify the most appropriate blocking agent, MPs (streptavidin-coated beads C1) labelled with DNA probes were prepared (see Section 5.8.1) and incubated with 200 µL of one of the following solutions: 1% Tween 20, 1% (BSA + Triton X-100 + Tween 20), 1% (BSA + Triton X-100 + Tween 80), and 1% BSA in a PBS solution. Each mixture was agitated for one hour at 200 rpm at room temperature. The magnetic particles (MPs) were then separated from the blocking solution using a magnetic rack. The tubes were placed in the rack, allowing the MPs to be attracted to the tube wall by the magnetic field. This enabled easy removal of

the supernatant without the need for specialised equipment. The MPs were subsequently washed with hybridisation buffer (Saline Sodium Citrate Solution, Sigma-Aldrich).

To determine the blocking efficiency, the treated MPs were incubated with 5 µL of HRP-labelled DNA reporter probe, in the absence of target DNA, in 150 µL of hybridisation buffer for one hour at room temperature. Following this, the MPs were washed three times with hybridisation buffer, added to 100 µL of TMB, and incubated for six minutes at 37 ºC to allow for the detection of any HRP-mediated colour change. This reaction was terminated by adding 50 µL of 1M H_2SO_4, after which the mean absorbance at 450 nm was determined using a plate reader (Infinite M Plex - Tecan). This sequence was repeated three times.

4.24.3 Detection of *M. bovis* ssDNA using ELOSHA

The standard ELOSHA method, as outlined by Ahortor (2019), was used to confirm the functionality of *M. bovis*-specific *IS6110* and *IS1081* gene target probes. ssDNA was extracted from 200 µL of *M. bovis* 1173P2 using two methods: the Qiagen method (Lauro et al., 2007) and the microwave excitation method (Ahortor, 2019) as detailed in Chapter 3, Section (3.7.2). For the microwave treatment method, the bacterial suspension was adjusted to 10^8 bacteria in 200 µL suspension (Chapter 2, Section 2.7.2) and subjected to microwave exposure at 40% DC for 20 seconds based on the optimised conditions established in Chapter 3 (Section 3.5.1) without any additional purification. Pure DNA was also extracted from the bacteria using the Qiagen method to evaluate the impact of comparatively crude DNA preparations on the magnitude of the ELOSHA signal. To ensure a valid comparison, the ssDNA concentration was standardised to correspond with the concentration level of the microwaved ssDNA. Both suspensions (microwaved bacterial and pure DNA suspension) were incubated separately with 10 µL of magnetic particles (MPs) functionalised with a biotin anchor probe, 5 µL of HRP reporter probe (10 µM), and 150 µL of SSC hybridisation buffer (Saline Sodium Citrate buffer). The mixture was incubated in a Microcentrifuge tube

and agitated at 200 rpm in an orbital incubator at 50 °C for one hour. A magnet was used to separate the MP/DNA hybrid complex from the solution, and the supernatant containing unbound probes was discarded.

The MP/DNA hybrid complex was washed three times with hybridisation buffer, and the presence of the target gene was indirectly determined by adding 100 µL of TMB substrate, followed by a 6-minute incubation period at 37 ºC. Subsequently, 100 µL of 1M H_2SO_4 was added, and the optical density was measured using a plate reader at 450 nm. For each gene target, a positive result was determined as a reading greater than the mean optical density (OD) plus three times the standard deviation of the respective negative controls (Classen et al., 1987; Lardeux et al., 2016). A coloured line in the presented assay results represents the cut-off value for each gene target.

To confirm the assay's specificity, genomic DNA from non-*bovis* isolates *M. smegmatis* Mc2155 (S2), *M. abscessus*ATCC 19977, and *E. coli* NCTC 1093 were used as controls. To facilitate a valid comparison, the ssDNA concentrations of these control samples were adjusted to correspond with the same ssDNA amount isolated from *M. bovis* 1173P2. This step ensured that any differences observed between the assay results were not attributed to variations in DNA concentration but instead reflected the assay's specificity in accurately detecting and distinguishing *M. bovis* DNA from other mycobacterial species. The assay also included a no-template control (NTC) to assess the non-specific binding of the HRP-labelled DNA probe to the MPs. Each assay was repeated three times.

4.24.4 Determining the limit of detection (LOD) and specificity of the ELOSHA assay

This study evaluated the sensitivity of *IS6110* and *IS1081*-specific DNA probes for detecting target DNA sequences in chemically extracted DNA (Qiagen method) and microwaved bacterial suspensions. Assay sensitivity was evaluated using microwaved *M. bovis* 1173P2

suspended in 200 µL of water. A series of bacterial quantities were tested: 10^8, 10^7, 10^6, 10^5, 10^4, 10^3, 10^2, and 10^1, to determine the limit of detection. Each bacterial concentration was prepared before microwave treatment and then microwaved separately.

Subsequently, serial dilutions of purely extracted DNA were prepared, starting with a concentration equivalent to that released from microwaving a suspension of 10^8 *M. bovis* 1173P2 bacteria. These suspensions were analysed using the process detailed in Section 5.8.3. It is important to highlight that all serial dilutions were performed before the microwave treatment for the microwave method.

The specificity of the probes was assessed via a positive and a negative mix. The positive mix included microwave-extracted ssDNA from *M. bovis* 1173P2 and non-*bovis* isolates, including *M. smegmatis* Mc2155 S2, *M. abscessus* ATCC 19977, and *E. coli* NCTC 1093. The negative mix consisted of a cocktail of ssDNA from non-*bovis* isolates only.

For each non-*bovis* isolate, the ssDNA concentration was adjusted to correlate with the microwave-extracted *M. bovis*1173P2 ssDNA. A no-template control (NTC) was used as the negative control. Two hundred microlitres of these mixtures were tested (as detailed in Section 5.8.3), and sensitivity and specificity assays were repeated three times.

4.24.5 Optimisation of the conventional method to enhance the sensitivity of the ELOSHA assay

To date, evaluations of the ELOSHA assay have been limited to samples suspended in water and using a specific type of magnetic beads (C-1) (Ahortor, 2019). Further optimisation is required to assess the potential improvements that may result from these modifications, including using different-sized MPs, modifying the anchor probe spacer, reducing the binding period, and adjusting the hybridisation incubation temperature.

4.24.5.1 Assessing the impact of different-sized magnetic beads

To determine the impact of different sizes and types of MPs (Figure 5.4), this research implemented a comparison regarding the performance of commercially available MPs (Table 5.1) by evaluating their ability to bind to the *IS6110* DNA anchor probe at a concentration of 948.5 ng/µL (following the method outlined in Section 5.8.1). Subsequently, the impact of particle characteristics on the efficiency of DNA probe binding was determined, as described in Section 5.8.3.

Table 0.1 Features of magnetic beads employed for enhanced DNA binding.

Type of magnetic beads	**Size (diameter)**	**Binding ability to ss oligonucleotide**	**Concentration**	**Amount used in the experiment**	**Ligand**
Hydrophilic Streptavidin Magnetic Beads (H)	2-3 µm	> 400 pmol ss oligonucleotides	4 mg/mL	250 µL	Hydrophilic Streptavidin
Dynabeads™ M-270 Streptavidin	2.8 µm	~200 pmol ss oligonucleotides	10 mg/mL	100 µL	Hydrophobic Streptavidin
Dynabeads™MyOne™ Streptavidin C1	1 µm	~500 pmol ss-oligonucleotides	10 mg/mL	100 µL	Hydrophobic Streptavidin

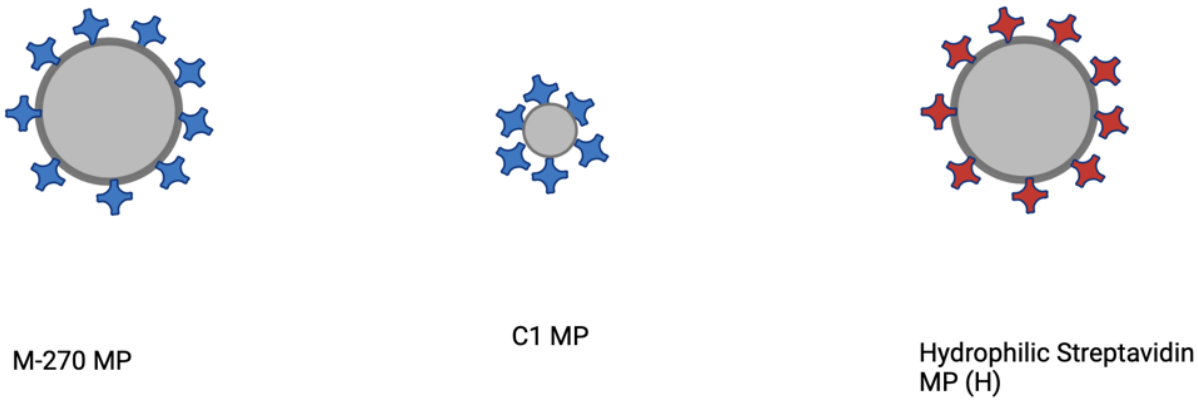

Figure 0.4 Illustration of the magnetic beads.

M-270 magnetic particles (MPs) and hydrophilic streptavidin MPs share the characteristic of being larger, while the C1 beads are the smallest of the tested particles. When considering the streptavidin type, MPs with hydrophilic streptavidin (red star) exhibit an elevated level of purity, whereas C1 and M-270 beads are associated with hydrophobic streptavidin (blue star). (Created by BioRender.com).

Although all three magnetic beads share similar streptavidin functionality, they differ in size, ligand properties, and binding capacities (table 5.1). These differences may affect probe coupling efficiency and should be considered when selecting the optimal bead type for assay development.

4.24.5.2 Assessing the impact of altering the number of thymidine bases incorporated into the thiol terminus of DNA capture probes

Studies have reported that incorporating a string of thymidine (T) nucleotides between the thiol group and the DNA binding region can increase target DNA binding by enhancing the flexibility of the capture probes on the MP surface (Li, 2002). To evaluate the impact of increasing the number of thymidine bases incorporated into the capture probes, this research synthesised a version of the *IS6110* and *IS1081* capture probes in which the number of Ts was increased from 5 to 10 and 15 (Table 5.2). The ability of these variants to capture target DNA was assessed using ELOSHA (Section 5.8.3), and this assay was performed in triplicate.

Table 0.2 DNA anchor probe spacer length modification.

Gene	5Ts anchored probe	10Ts anchored probe	15Ts anchored probe
IS6110	**TTTTT**CGTCCAGCGCCGCTTCG	**TTTTTTTTTT**CGTCCAGCGCCGCTTCG	**TTTTTTTTTTTTTTT**CGTCCAGCGCCGCTTCG
IS1081	**TTTTT**CCCTGCTGCACTCCATCTACGACCAGC	**TTTTTTTTTT**CCCTGCTGCACTCCATCTACGACCAGC	**TTTTTTTTTTTTTTT**CCCTGCTGCACTCCATCTACGACCAGC

4.24.5.3 Assessing the impact of reducing the target DNA binding period

In the current version of the assay, the MPs functionalised with a DNA capture probe are incubated with the target DNA for 60 minuts at 50 °C. To determine the feasibility of reducing

the incubation period, this study examined the impact of employing the following incubation periods: 10, 20, 30, 40, 50, and 60 minutes. Each assay was repeated three times.

4.24.5.4 Assessing the impact of altering the incubation temperature and incubation period on target DNA capture

DNA hybridisation depends on the DNA probe's capacity to recognise and bind to a specific target DNA sequence; for this to occur, both DNA strands must be single-stranded. The melting point, sometimes called the denaturation temperature, is the temperature at which complementary DNA strands begin to separate into single strands, releasing them to hybridise with complementary sequences (DNA hybridisation) (Hertel et al., 2022). This process results in stable duplex structures between the complementary strands. It is beneficial to modify the hybridisation temperature to coincide with the melting temperature (Khandelwal & Bhyravabhotla, 2010).

The melting temperature of the *IS6110* and *IS1081* probe sequence duplex ranges from 60 °C to 65 °C; therefore, this study examined the impact of increasing the incubation temperature of the ELOSHA from 50 °C to 60 °C. It also evaluated the impact of reducing the incubation period at 60 °C by conducting the assay over the following periods: 10, 20, 30, 40, 50, and 60 minutes. This experiment was replicated three times to ensure consistency and reliability of the results.

4.24.5.5 Assessing the impact of modifying shaker speed on assay performance

Agitating the sample increases the opportunities for the DNA probe-functionalised MPs to disperse throughout the entire sample and capture target DNA, particularly for viscous samples such as sputum. To determine the ideal shaking speed, samples were shaken at 100 and 200 rpm over two different time intervals of 30 and 60 minutes. This experiment was conducted three times to ensure reliability and consistency.

4.24.6 Preparation of target DNA suspensions in simulated sputum

Initially, simulated sputum was prepared as described in Chapter 2, Section 2.9. Subsequently, 10^8 *M. bovis* 1173P2 bacteria were suspended in 200 µL of simulated sputum, following the method outlined in Chapter 2, Section 2.9.1, and then subjected to microwave treatment at a 30% duty cycle for 20 seconds, as detailed in Chapter 3, Section 3.5.1. The ssDNA concentration was measured using a NanoDrop spectrophotometer.

4.24.7 Detection of *M. bovis* suspended in simulated sputum using ELOSHA.

Given the critical role of sputum in diagnosing pulmonary tuberculosis, it was essential to evaluate the probes' sensitivity, specificity, and ability to distinguish *M. bovis* from other strains in sputum using the ELOSHA method. Bacterial isolates, including *M. smegmatis* Mc2155 (S2), *M. abscessus* (ATCC 19977), and *E. coli* NCTC (1093), were prepared in 200 µL of simulated sputum following an identical methodology to *M. bovis* 1173P2 (as described in Section 5.8.3). The ssDNA from these non-*bovis* isolates was isolated using the microwave method and quantified using NanoDrop. To ensure valid comparisons, the amount of ssDNA extracted from non-*bovis* isolates was adjusted to match the DNA level obtained from microwaving *M. bovis* 1173P2 (10^8). This standardisation process was crucial for attaining an accurate comparison and analysis. The experiment was repeated three times to ensure quality and consistency.

The assay's sensitivity was evaluated using microwaved *M. bovis* 1173P2 suspended in 200 µL of simulated sputum. To determine the limit of detection, a range of bacterial quantities was tested: 10^8, 10^7, 10^6, 10^5, 10^4, 10^3, 10^2, and 10^1. As with bacterial suspensions in water, bacteria suspended in simulated sputum were serially diluted and then treated with microwave radiation. Following the protocol outlined in Section 5.8.4, the specificity of *M. bovis* 1173P2 suspended in simulated sputum was also determined.

4.24.8 Evaluating the optimized procedure with simulated sputum samples

4.24.8.1 Assessing the impact of attaching DNA capture probes to different sizes of magnetic beads

Previously, the impact of employing different commercial magnetic beads in the ELOSHA assay was assessed by detecting bacteria suspended in water (Section 5.8.5.1). To ensure a similar level of sensitivity, the bacteria were suspended in simulated sputum. As described in Section 5.8.8, the *M. bovis* 1173P2 strain was first suspended in simulated sputum, and the DNA concentration was standardised across various samples to ensure the accuracy of the comparison. Subsequently, two varieties of magnetic beads (Hydrophilic Streptavidin Magnetic Beads *(H) and* Dynabeads™ MyOne™ Streptavidin C1*)* were utilised to compare their capability to capture target DNA. This comparison was conducted following the protocol outlined in Section 5.8.5.1.

4.24.8.2 Assessing the effect of a modified incubation period on the capture of MPs and DNA in simulated sputum samples

The *M. bovis* 1173P2 strain was suspended in simulated sputum as per the procedure outlined in Section 5.8.6. Subsequently, DNA extraction was performed using the microwave system (Ahortor, 2019). The examination involved testing several incubation periods (precisely 10, 20, 30, 40, 50, and 60 minutes) at 60 °C, according to the protocol outlined in Section 5.8.5.3.

4.25 Statistics

All experiments were performed at least twice under independent conditions. Statistical analysis of the data was performed using GraphPad Prism. An independent samples t-test was conducted to determine the statistical significance between the two groups. Data were considered significant when the p value was < 0.05. Analysis of variance (ANOVA) was performed to determine the difference among group means. To determine the differences within groups, post-hoc analysis was performed using the Bonferroni and Tukey tests. p values less than 0.05 were considered significant.

4.26 Results

4.26.1 Determining the binding capacity of streptavidin coated magnetic beads (C1) for biotin labelled DNA probes

To confirm the ability of the biotin-labelled *IS6110* and *IS1081* DNA anchor probes to bind to streptavidin-coated MPs, they were mixed and incubated. As illustrated in Figure 5.5, there was a highly significant reduction (p value < 0.001) in the concentration of biotin-labelled DNA probe remaining in the solution after removing MPs with a magnet. Additionally, the binding capacity of the MPs for the *IS6110* and *IS1081* DNA anchor probes was determined to be 98% and 98.6%, respectively (based on the ratio of bound and free biotin probes in solution). There were no significant differences in the binding efficiency of the different anchor probes.

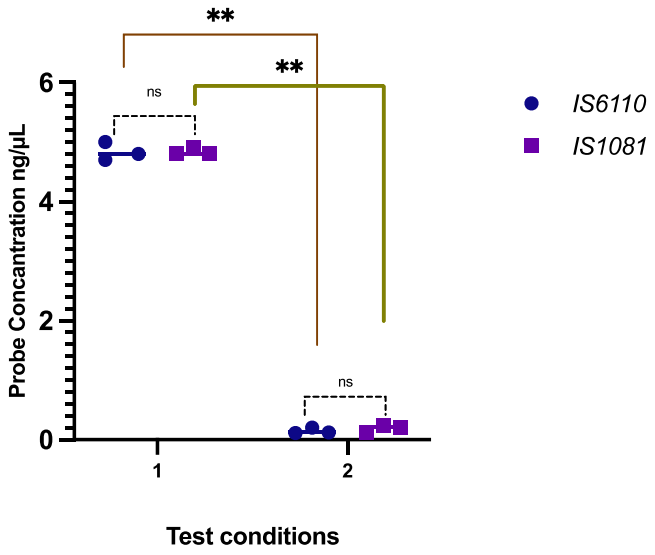

Figure 0.5 Binding characterisations of biotin-labelled probes for Magnetic particles.

IS6110 and *IS1081* biotin-labelled probes (10 µL, 20 µM) were added to C1 MPs (4 mg/mL) and incubated at room temperature for one hour. In this figure, 1 represents the probes in solution before the addition of MPs, and 2 represents the probes following the addition and removal of MPs. The concentration of biotin probes before and after the addition to MPs was quantified using Nanodrop. The data represent the mean of triplicate experiments. ** denotes p value <0.001, and 'ns' indicates no significance.

The complexes underwent three washes with hybridisation buffer to release non-specifically bound biotin-labelled anchor probes from the MPs and anchor probe complexes. As depicted in Figure 5.6, the initial wash resulted in the release of most of the unbound material (p value < 0.001). The binding capacity of the magnetic particles (MPs) was determined to be 91.5% and 91.5% for the *IS6110* and *IS1081* gene probes, respectively, based on the ratio of bound and free biotin probes in the solution. The binding efficiencies of the two anchor probes did not exhibit significant differences.

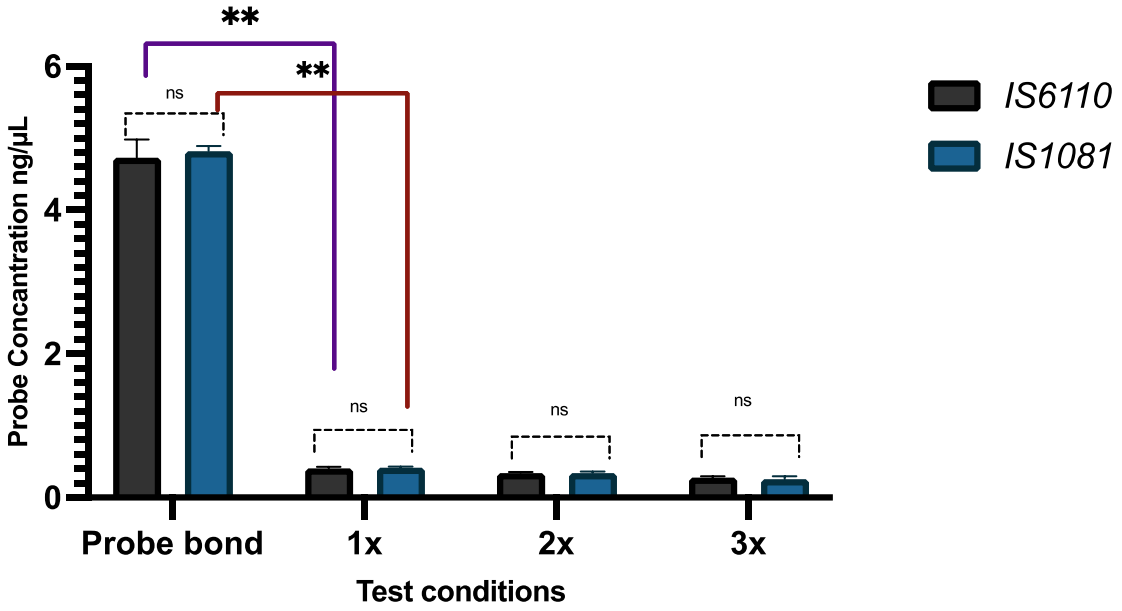

Figure 0.6 Determination of the ability of biotin labelled anchor probes to leech from MPs following repeated washing.

Biotin probes bound to MPs (probe bound) were washed three times (1x, 2x, and 3x) with hybridisation buffer, and the concentration of free probes was determined using Nanodrop. The data represent the mean of triplicate experiments. ** denotes p value <0.001, and 'ns' indicates no significance.

4.26.2 Preventing the binding of non-specific DNA to MPs by using chemical blocking agents

To determine the ability of non-specific DNA to bind to streptavidin-coated C1 MPs, nanoparticles were mixed with HRP-labelled DNA probes that lacked biotin labels. Following incubation, the MPs were washed three times and resuspended in TMB solution (an enzymatic substrate for HRP), which exhibits a colour change in the presence of the

enzyme. A resulting colour change confirmed the presence of non-specific DNA binding (Figure 5.7).

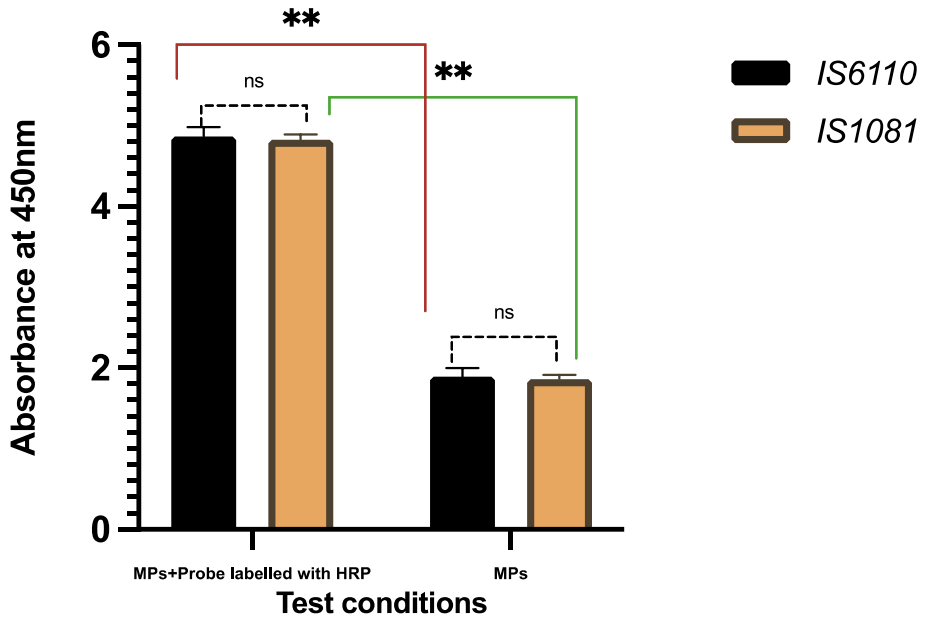

Figure 0.7 Detection of non-specific binding of HRP labelled DNA probes to Dynabeads™MyOne™ Streptavidin C1 MPs.

HRP-labelled *IS6110* and *IS1081* DNA probe binding to magnetic particles (MPs). MPs (4 mg/mL) were incubated with *IS6110* and *IS1081* specific DNA probes, separately labelled with HRP (5 µL, 10 µM), and washed three times with hybridisation buffer. TMB substrate was then added, and incubation occurred for 7 minutes before the addition of the stopping agent H_2SO_4. The background signal was determined in the absence of the DNA probe. The data represent the mean of triplicate experiments. ** denotes *p* value <0.001, and 'ns' indicates no significance.

To minimise non-specific DNA binding to MPs functionalised with biotin-labelled DNA anchor probes, several blocking solutions were evaluated for their ability to prevent the binding of HRP-labelled reporter probes. As illustrated in Figure 5.8, all the buffer solutions reduced non-specific DNA binding to the MPs to some degree. Of these formulations, 1% BSA + 1% Triton X-100 + 1% Tween 20 proved the most effective at blocking DNA binding (*p* value < 0.001). Notably, even in the presence of this highly effective blocking agent, a detectable background signal can still be observed, which emphasises the importance of including negative controls to identify non-specific binding.

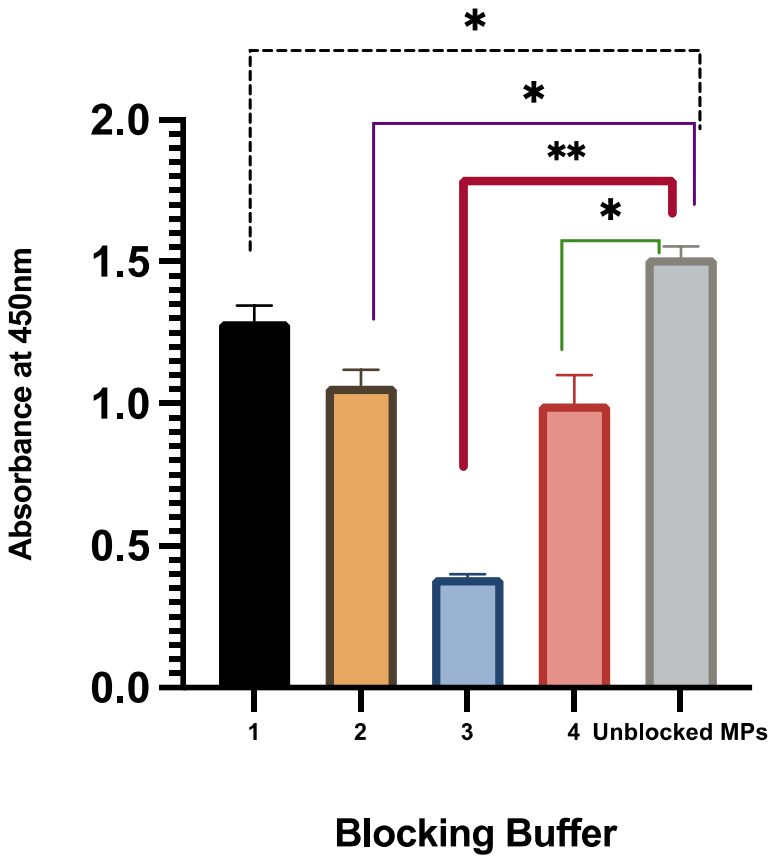

Figure 0.8 The Ability of different blocking buffers to reduce the non-specific binding of DNA to MPs.

The ability of the following blocking agents to reduce the binding of an HRP-labelled IS6110 DNA probe to MPs functionalised with biotin-labelled IS6110 anchor probes was assessed: (1) 1% Tween 20, (2) 1% BSA + Triton X-100 + Tween 80, (3) 1% BSA + Triton X-100 + Tween 20, and (4) 1% BSA. The IS6110 HRP probe (5 µL, 10 µM) was added to the blocked MPs and incubated for 1 hour. The presence of HRP probes was determined by adding TMB. The data represent the mean of triplicate experiments. * denotes *p* value <0.05 and ** denotes p value <0.001.

4.26.3 Detection of *M. bovis* suspended in water using ELOSHA

The ability of the *IS6110* and *IS1081* specific DNA probes to distinguish between two strains of *M. bovis*—*M. bovis*1173P2 and *M. bovis* 5692—and other non-*bovis* isolates, including *M. smegmatis* Mc2155 (S2), *M. abscessus* ATCC 19977, and *E. coli* NCTC 1093, was evaluated. A bacterial suspension of *M. bovis* 1173P2 containing 10^8 bacteria was microwaved at 30% DC for 20 seconds (as detailed in Chapter 3, Section 3.5.1), which resulted in an ssDNA concentration of 6 ng/µL and a 260/280 ratio of 1.4. Subsequently, all bacterial isolate samples were standardised to the same ssDNA level.

Pure ssDNA was also extracted chemically using the Qiagen method and standardised to match the concentration obtained from the microwave excitation method to facilitate a direct comparison. Additionally, the 260/280 ratio for ssDNA was measured using NanoDrop, and a reading of 1.9 was registered, which indicates that the chemical method generated a purer sample. As shown in Figure 5.9, when using the Qiagen method, the *M. bovis* strains generated a significantly stronger signal than the other isolates (p value < 0.001). However, no significant differences were observed between the two sets of probes. Correspondingly, the variances between individual *M. bovis* isolates were not statistically significant (p value > 0.05), which signifies that both gene targets offered a similar level of sensitivity.

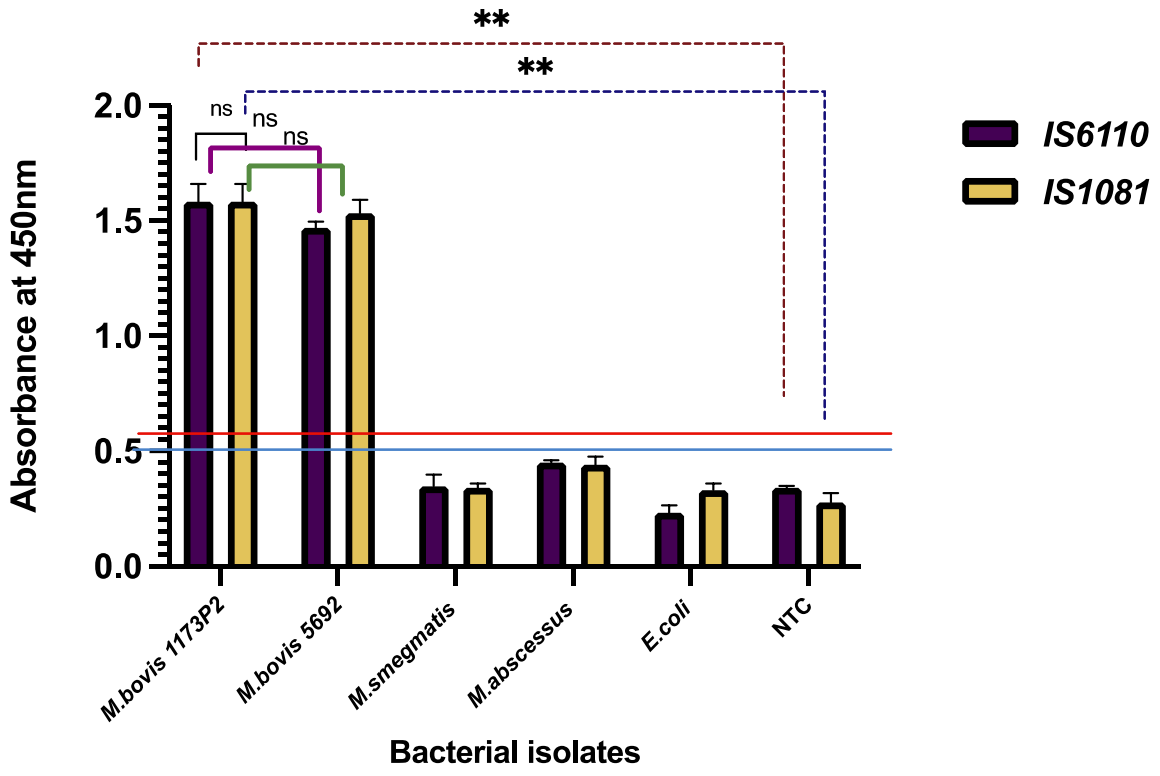

Figure 0.9 Detection of chemically extracted (Qiagen method) *M. bovis* ssDNA using *IS6110* and *IS1081* specific DNA probes.

ssDNA was extracted from test organisms using the Qiagen method and standardised to attain a final ssDNA concentration of 6 ng/µL. The ability to distinguish between *M. bovis* and non-*bovis* isolates was based on the magnitude of the HRP-generated colour change, as determined by measuring the mean absorbance. The cutoff value for a positive test was an absorbance value of 0.53 and 0.50, represented as red (*IS6110* probe) and blue (*IS1081* probe) lines on the figure (using *M. abscessus* as the negative control). A no-template control (NTC) was

also included. The data represent the mean of triplicate experiments. ** denotes *p* value <0.001 and ns denotes no significance.

The chemically extracted ssDNA samples, DNA released by the action of microwaves on *M. bovis* generated a significantly stronger signal (*p* value < 0.001) than the non-*bovis* isolates, and there were no significant differences between the responses observed using the different gene targets (Figure 5.10). The overall magnitude of the signals was lower than those observed using chemically purified ssDNA, which can be attributed to the absence of purification steps in the microwave treatment process. This result was anticipated, given that the microwave DNA extraction procedure does not include any purification steps; therefore, these contaminants have a negative impact on the magnitude of the ELOSHA signal. However, despite the contaminants, the assay successfully differentiated between *M. bovis* and non-*bovis* isolates, supporting its procedural robustness.

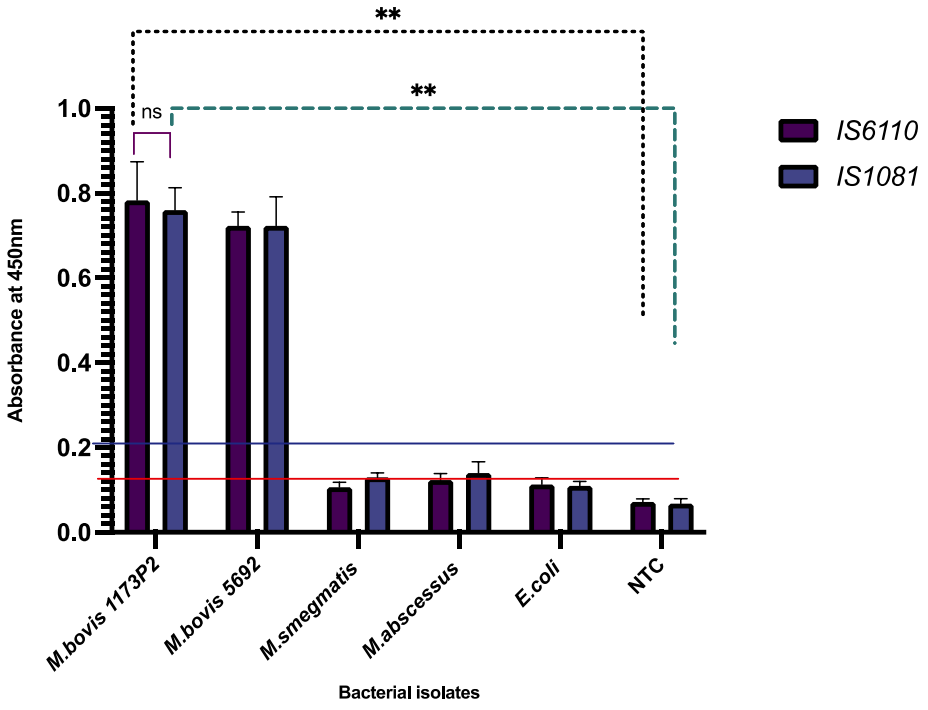

Figure 0.10 Detection of microwaved *M. bovis* Suspension using *IS6110* and *IS1081* specific DNA probes.

Genomic material was released from *M. bovis* 1173P2 (10^8 bacteria) suspended in water. A concentration of 6 ng/µL was achieved via exposure to microwave radiation at 30% DC for 20 seconds. The ssDNA from the alternate *M. bovis* isolate and non-*bovis* isolates was also isolated using the microwave method and standardised to 6 ng/µL. The ability to distinguish between *M. bovis* and non-*bovis* isolates relied on the magnitude of the HRP-generated colour change, as determined by measuring the mean absorbance. The cut-off concentrations for a negative sample (DNA from microwaved *M. abscessus*) were calculated as 0.13 and 0.22, respectively, and are

represented by red (*IS6110*) and blue (*IS1081*) lines. A no-template control (NTC) was also included. The data represent the mean of triplicate experiments. ** denotes *p* value <0.001, and ns denotes no significance.

4.26.4 Determination of the limit of detection of an ELOSHA assay

The sensitivity of the assay for chemically purified ssDNA and microwaved bacterial culture was determined for both gene targets. A serial dilution of chemically extracted ssDNA, starting at 6.4 ng/µL, was tested to determine the limit of detection for chemically extracted DNA (Qiagen method). The concentrations tested included 6.4 ng/µL, 301.9 pg/µL, 30.5 pg/µL, 3 pg/µL, 0.6 pg/µL, 30.5 fg/µL, and 3 fg/µL.

The lower limit of detection (LOD) for both target genes using chemically purified ssDNA was 0.6 pg/µL, and cutoff values were established as 0.45 for the *IS6110* probe and 0.54 for the *IS1081* gene target (Figures 5.11 and 5.12).

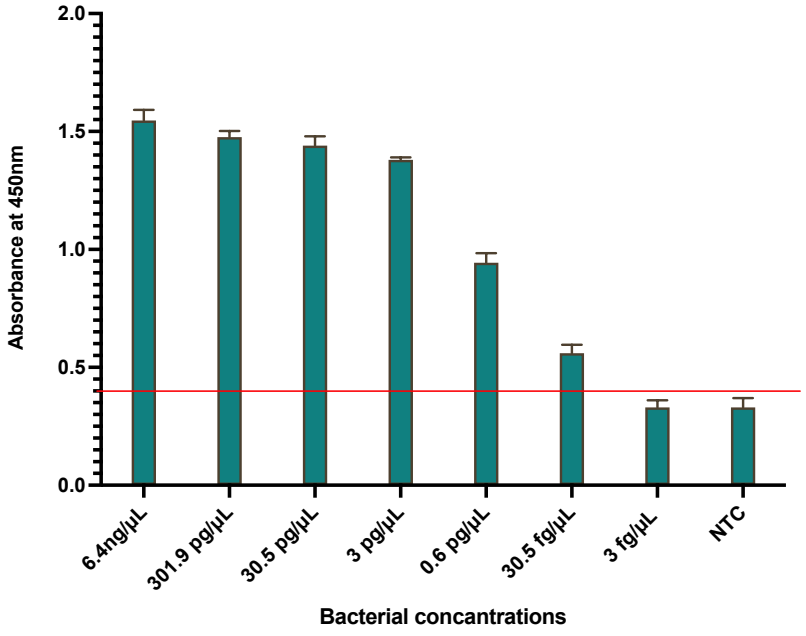

Figure 0.11 Assay sensitivity of *IS6110* DNA probes for chemically purified ssDNA (Qiagen method) extracted from *M. bovis* 1173p2 ssDNA.

The limit of detection for purified extracted DNA was 0.6 pg/µL (when measured against a cut-off value of 0.45) and is represented by the orange horizontal line. The no template control (NTC) was used as the negative to determine the cut-off value. This data represents the mean of a triplicated experiment.

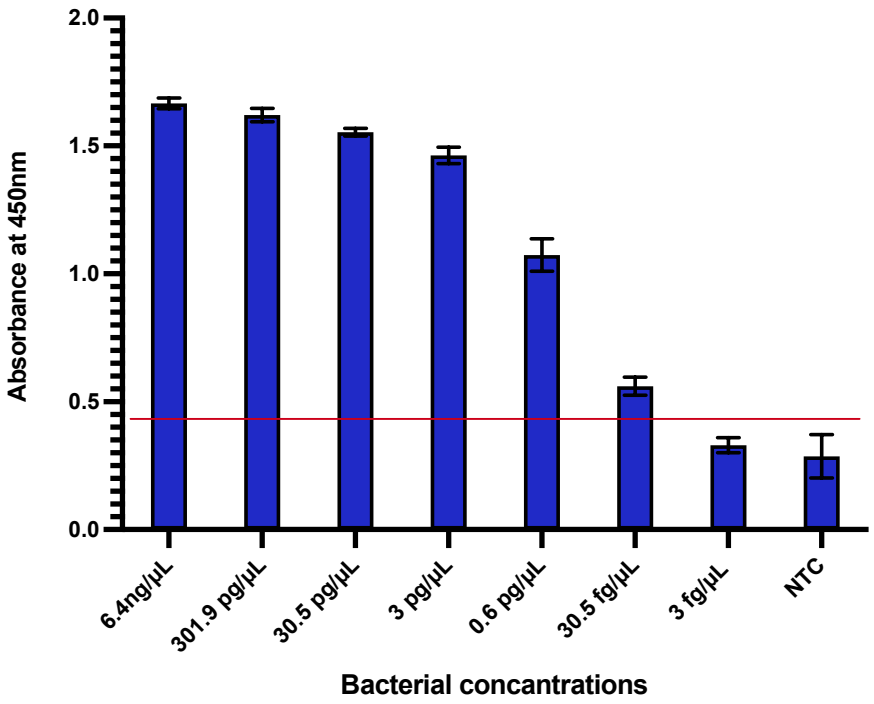

Figure 0.12 Assay sensitivity of *IS1081* DNA probes for chemically purified ssDNA (Qiagen method) extracted from *M. bovis* 1173P2 ssDNA.

The limit of detection for purified extracted DNA was determined to be 0.6 pg/µL when measured against a cut-off value of 0.54 and is represented by the horizontal orange line. The no template control (NTC) was used as the negative to determine the cut-off value. This data represents the mean of a triplicated experiment.

M. bovis 1173P2 was suspended in water and diluted to produce the following range of bacterial quantities: 10^8, 10^7, 10^6, 10^5, 10^4, 10^3, 10^2, and 10^1. Each bacterial quantity was microwaved separately, and the resulting extract was tested for the presence of ssDNA. The LOD for both genes was 10^3, with cutoff values of 0.077 for the *IS6110* probe and 0.075 for the *IS1081* gene target (Figures 5.13 and 5.14). A no-template control (NTC) was utilised as the negative control for both targets to ensure the precision and reliability of the detection limits.

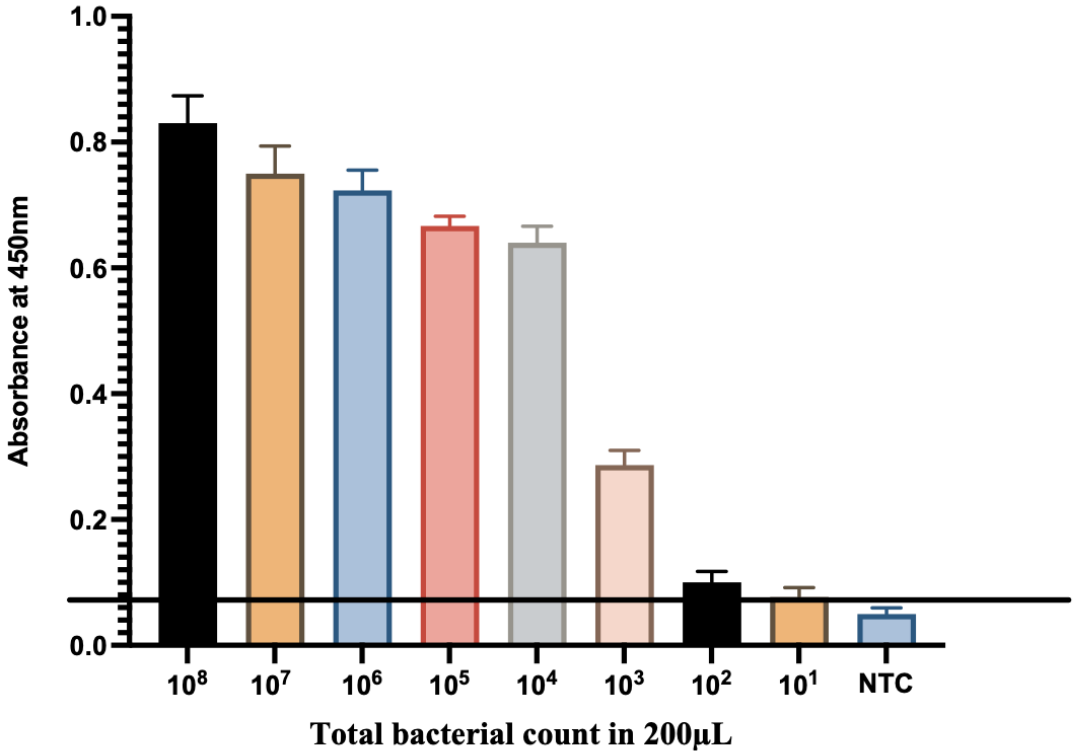

Figure 0.13 Assay sensitivity of *IS6110* DNA probes for microwaved *M. bovis* 1173P2 suspensions.

The limit of detection for microwaved *M. bovis* 1173P2 suspensions was determined to be 10^3, when measured against a cut-off value of 0.077 and is represented by the horizontal black line. The no template control (NTC) was used as the negative to determine the cut-off value. This data represents the mean of a triplicated experiment.

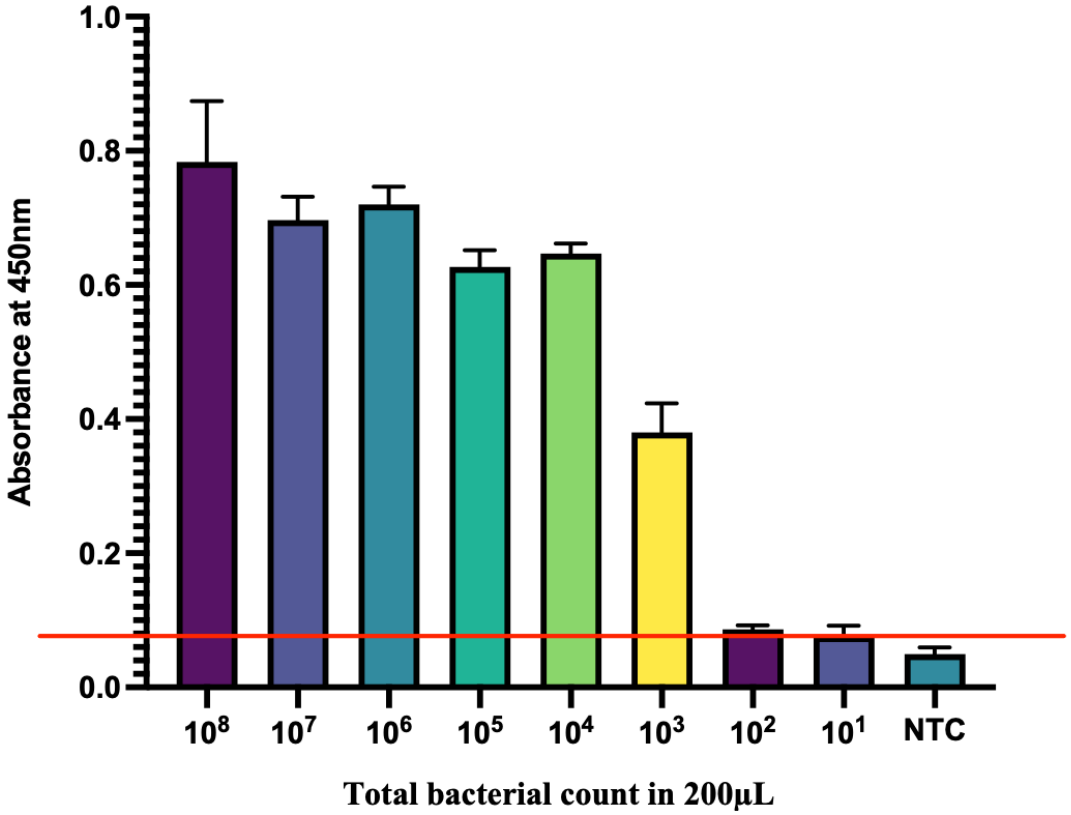

Figure 0.14 Assay sensitivity of *IS1081* DNA probes for microwaved *M. bovis* 1173P2 suspensions.

The limit of detection for microwaved *M. bovis* 1173P2 suspension was determined to be 10^3 , when measured against a cut-off value of 0.075 and is represented by the horizontal red line. The no template control (NTC) was used as the negative to determine the cut-off value. This data represents the mean of a triplicated experiment.

4.26.5 Determining the specificity of the ELOSHA assay

While the DNA probes demonstrated their capability to differentiate between *M. bovis* 1173P2 and other bacterial isolates, evaluating their specificity in the presence of DNA from other bacterial isolates was imperative. To determine specificity, DNA from a microwaved culture of *M. bovis* 1173P2 (10^8) was mixed with DNA from *M. smegmatis* Mc2155 S2, *M. abscessus* ATCC 19977, and *E. coli* NCTC 1093. All of the ssDNA was mixed at a concentration of 6.3 ng/µL. As illustrated in Figure 5.15, the assay successfully identified *M. bovis* 1173P2 DNA in the presence of DNA from other bacterial isolates.

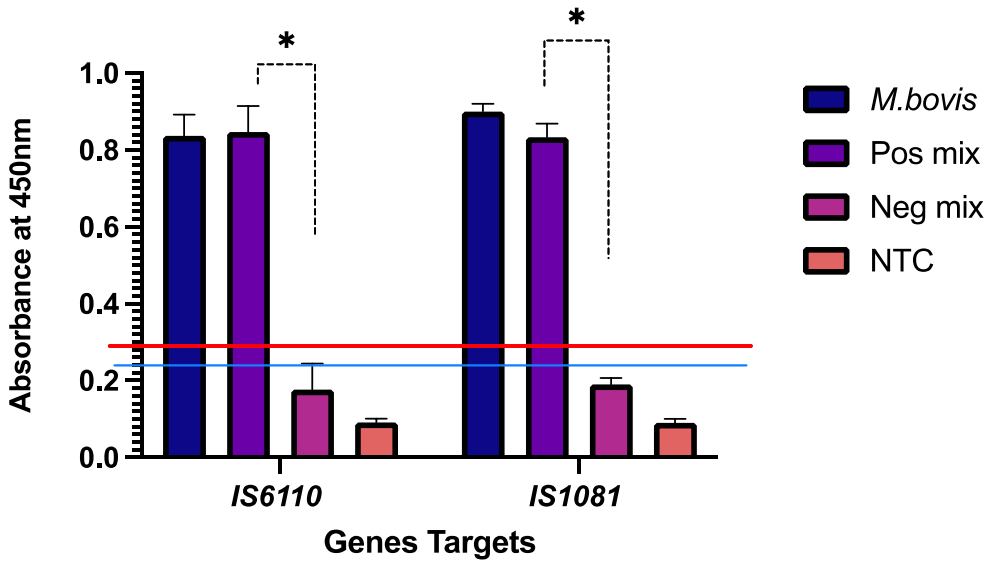

Figure 0.15 Specificity of the *IS6110* and *IS1081* DNA probes for *M. bovis* 1173P2 in the presence of DNA extracted from other bacterial species.

The signal generated by microwaved *M. bovis* 1173P2 suspension and the positive mix consisting of microwaved *M. bovis* 1173P2 suspension and non-M. bovis isolates (*M. smegmatis* Mc2155 S2, *M. abscessus* ATCC 19977 and *E.coli* NCTC 1093) was significantly higher than that of the negative mix (microwaved non-bovis isolates suspension). The no-template control (NTC) has a *p value* < 0.001 for both genes. The cut-off value for a positive test was determined as an absorbance value of 0.38 and 0.24 (using the negative mix as the control for cut-off determination) and is represented by the horizontal red and blue lines for the *IS6110* and *IS1081* genes, respectively. This data represents the mean of triplicated experiments ± standard deviation. * represents a significant *p* value <0.001.

4.26.6 Assessing the impact of altering the size of the magnetic beads (MPs) on the ability to capture target DNA

All the optimisation studies previously described were performed using Dynabeads™ MyOne™ Streptavidin C1 MPs, measuring 1 µm in diameter. The impact of using different-sized, commercially available magnetic particles (MPs) on the ability to capture target DNA was then assessed. Details of the MPs used in this study are summarised in Table 5.1 and Figure 5.4, with the results presented in Table 5.3.

Table 0.3 Binding of *IS6110* specific biotin labelled DNA anchor probe to commercially available magnetic beads.

Type of MPs	Concentration of DNA remaining in suspension following binding to MPs (n=3)	% of DNA probe binding to MPs (n=3)
Hydrophilic Streptavidin Magnetic Beads (H)	10 ng/µL	98.94%
Dynabeads™ M-270 Streptavidin	12 ng/µL	98.74%
Dynabeads™ MyOne™ Streptavidin C1	0.7 ng/µL	99.92%

The C1 MPs exhibited the highest binding capacity for the *IS6110*-specific DNA probe, and this difference was statistically significant (p value < 0.001) compared to the other beads. This could be attributed to differences in the sizes of the MPs: smaller magnetic beads provide a greater surface area for the anchored probe, which may explain the strong affinity observed with the smallest MPs, such as C1. Notably, all the MPs captured over 98% of the available DNA.

The ability of different MPs functionalised with the *IS6110*-specific DNA probe to capture 10 ng/µL of Qiagen-purified *M. bovis* 1173P2 DNA suspended in water was then assessed. The hydrophilic magnetic beads (H) produced a significantly higher signal (p value < 0.05), as shown in Figure 5.16; however, there was no statistically significant difference between the results achieved using C1 and M-270 beads (p value > 0.05).

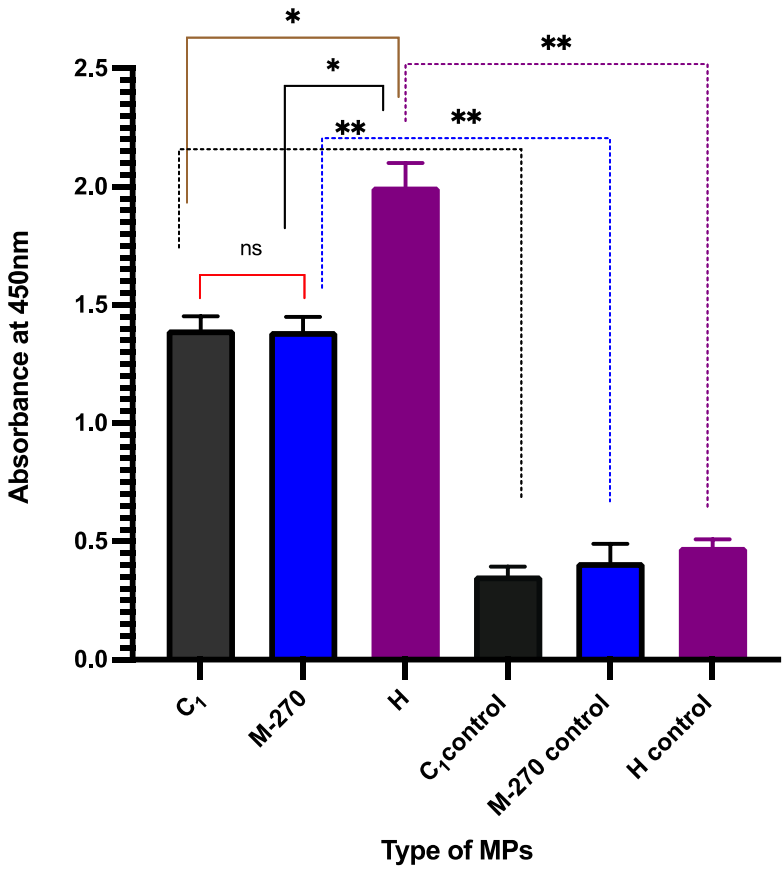

Figure 0.16 Comparison of the ability of different magnetic particles functionalised with the *IS6110* specific DNA probe to detect *M. bovis* 1173p2 DNA.

The magnetic beads (Dynabeads™ MyOne™ Streptavidin C1 (C1) Dynabeads™ M-270 Streptavidin (M-270), and Hydrophilic Streptavidin Magnetic Beads (H)) were tested against DNA chemically isolated from *M. bovis* 1173P2, standardised to a concentration of 10 ng/µL, and suspended in water. The differentiation between the categories of MPs was based on the magnitude of the HRP-generated colour change (as determined by measuring mean absorbance). A no-template control (NTC) was included. This data represents the mean of triplicated experiments ± standard error. indicate statistical results. * represents significant p value <0.05, ** represents significant p value <0.001, and ns indicates no significance.

The ability of the assay to detect microwaved *M. bovis* 1173P2 at a total quantity of 10^3 bacteria in the suspension was then assessed. This quantity, identified in earlier studies (Section 5.11), represents the minimum detectable bacterial concentration. As illustrated in Figure 5.17, hydrophilic MPs functionalised with the *IS6110* probes produced statistically higher positive signals (p value < 0.05) than the other types of MPs.

The reason for the enhanced DNA capture by the hydrophilic magnetic beads is unclear, particularly considering that the sole difference lies in the type of streptavidin. Therefore,

additional physical-chemical experimentation is required to account for these results.

Hydrophilic Streptavidin Magnetic Beads (H) were used in subsequent studies.

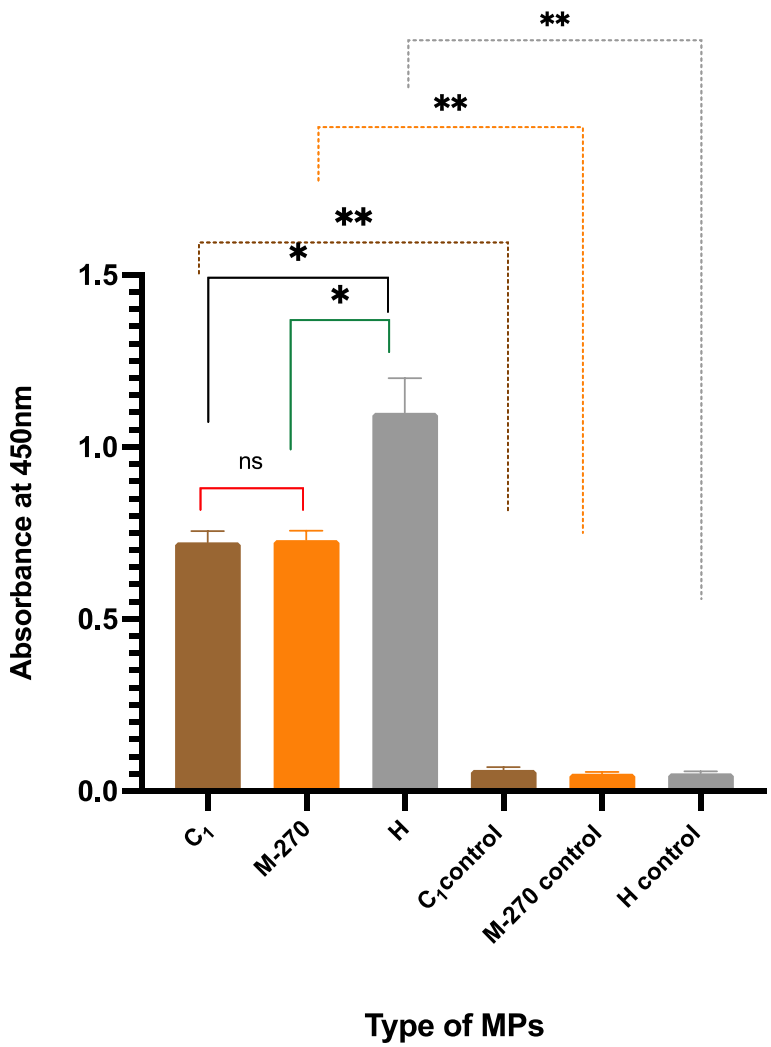

Figure 0.17 Comparison of the ability of different magnetic particles functionalised with the *IS6110* specific DNA probe to detect a microwaved *M. bovis* 1173p2 bacterial suspension.

The magnetic beads (Dynabeads™ MyOne™ Streptavidin C1 (C1) Dynabeads™ M-270 Streptavidin (M-270), and Hydrophilic Streptavidin Magnetic Beads (H)) were tested against microwaved *M. bovis* 1173P2 suspension**.** The differentiation between several types of MPs was based on the magnitude of the HRP-generated colour change (as determined by measuring mean absorbance). A no-template control (NTC) was included. The data represents the mean of triplicated experiments ± standard error. indicate statistical results. * represents significant *p* value <0.05. **= represents significant *p* value <0.001. ns indicates no significance.

4.26.7 The Impact of altering the number of thymine nucleotides in the 5-prime region of the DNA anchored probe on its ability to capture target DNA

While some studies suggest that increasing the number of thymine bases in the DNA-anchored probe's 5'-prime region enhances target DNA capture (Day et al., 1991), other research indicates the reverse (Peterson, 2001; Barchanski et al., 2012). These divergent findings highlight the need for additional research regarding the impact of modifying the T content on the capture of target DNA.

The impact of incorporating 5, 10, and 15 T nucleotides into the DNA probes was determined. Additionally, the effect of the type of MPs employed on DNA capture was assessed. As illustrated in Figures 5.18 and 5.19, increasing the number of Ts to 15 had an adverse effect on the ability to bind target DNA to both types of MPs. This effect was most pronounced for the H (hydrophilic) MPs. The T x 5 probes attached to the H-MPs bound significantly more DNA (p value < 0.05) than those attached to C1 MPs.

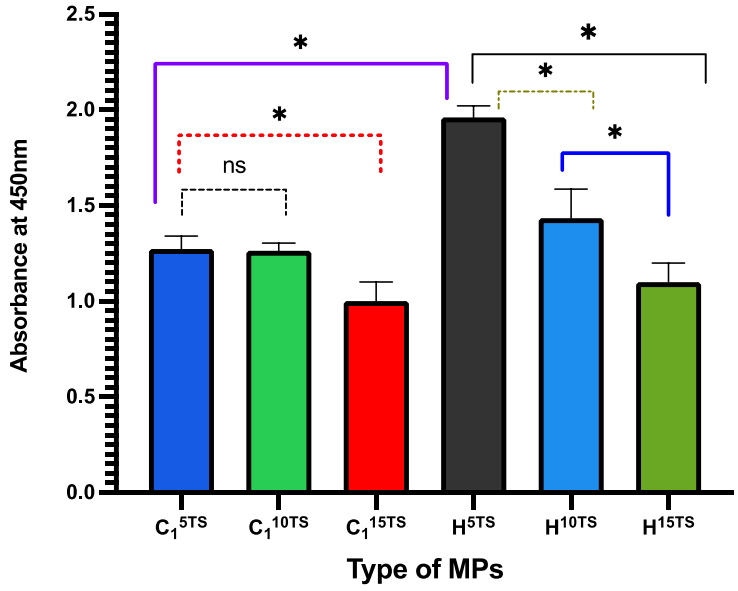

Figure 0.18 The impact of increasing the number of thymine bases (Ts) in the 5' region of the DNA capture *IS6110* probe on its ability to capture target DNA.

IS6110-specific probes containing 5Ts, 10Ts, and 15Ts were bound to C1 and H (hydrophilic) magnetic beads and assessed regarding their ability to capture DNA. Genomic material was chemically isolated (via the Qiagen method) from *M. bovis* 1173P2 and standardised to a concentration of 10 ng/µL. The difference in the number

of Ts was determined by the magnitude of colour change generated by HRP (as measured by mean absorbance). This data represents the mean of triplicated experiments ± standard error. * represents a significant *p* value <0.05 and ns indicates no significance.

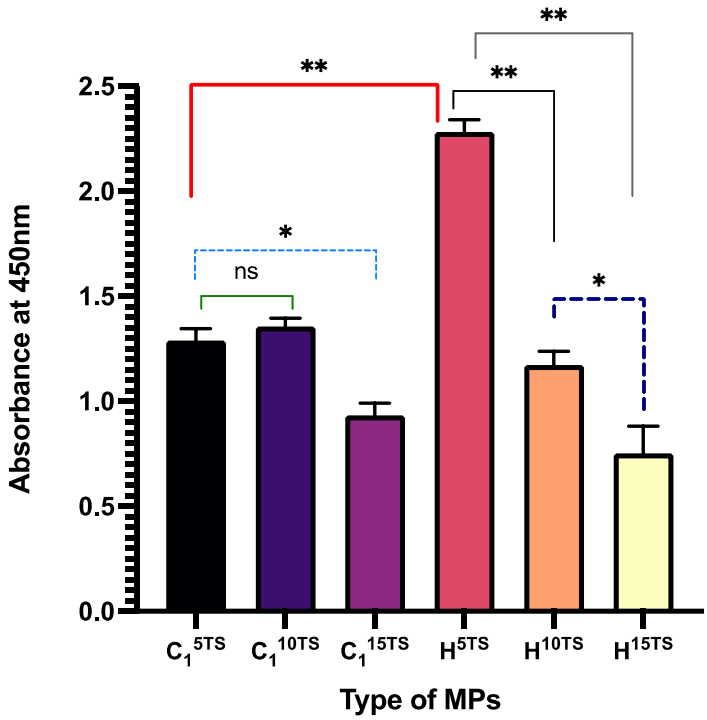

Figure 0.19 The impact of increasing the number of thymine bases (Ts) in the 5' region of the DNA capture *IS1801* probe on its ability to capture target DNA.

IS1801-specific probes containing 5Ts, 10Ts, and 15Ts were bound to C1 and H (hydrophilic) magnetic beads and assessed regarding their ability to capture DNA. Genomic material was chemically isolated (via the Qiagen method) from *M. bovis* 1173P2 and standardised to a concentration of 10 ng/µL. The difference in the number of Ts was determined based on the magnitude of the colour change generated by HRP (as measured by mean absorbance). This data represents the mean of triplicated experiments ± standard error. * represents significant *p* value <0.05, **represent significant *p* value <0.001, and ns indicates no significance.

The two factors can explain these results. Firstly, the longer the length of the oligonucleotide probes on the MP surface, the greater the chance of them becoming entangled, thus reducing their ability to capture the target DNA. Secondly, electrostatic repulsion between densely packed oligonucleotides (Xu & Craig, 2005): DNA probes carry a net negative charge, and an increase in the negative charge around the magnetic beads can induce electrostatic repulsion, thereby reducing the rate of DNA hybridisation (Xu & Craig, 2005; Fritz et al., 2002). In conclusion, hydrophilic (H) magnetic beads functionalised with DNA probes containing five thymine nucleotides exhibited superior performance compared to C1 MPs.

4.26.8 Assessing the impact of modifying the incubation period on the MPs' targeted DNA capture

In the current configuration of the assay, DNA probe-functionalised C1 MPs are incubated with target DNA for 60 minutes at 50°C to promote target DNA capture. The impact of reducing the incubation period on the magnitude of the resulting signal was assessed to reduce the time required for signal generation. Using *IS6110* and *IS1081* probes alongside chemically purified ssDNA, the first significant signal (p value < 0.05) was generated at 30 minutes for both probes (Figures 5.20 and 5.21).

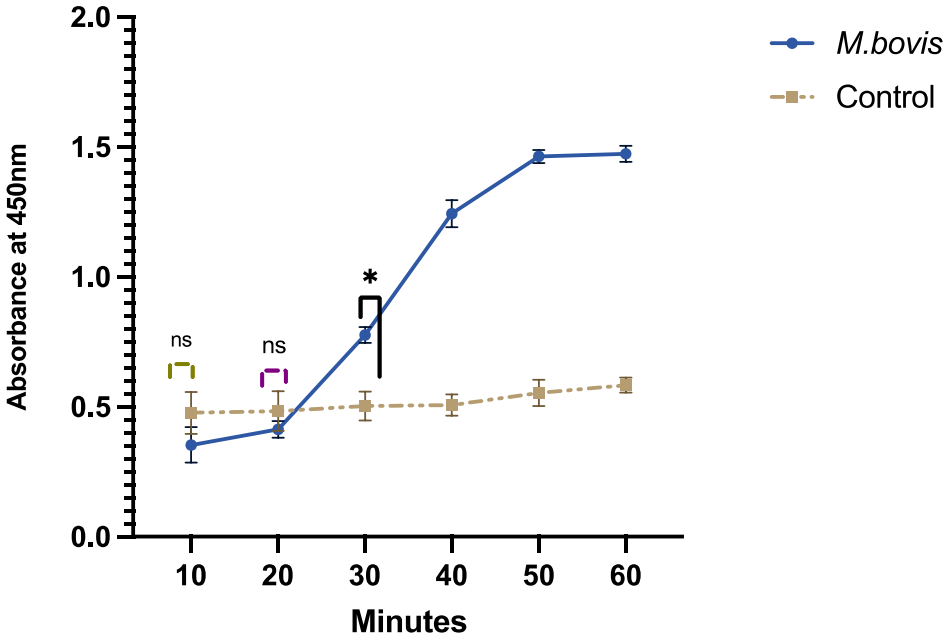

Figure 0.20 The Impact of decreasing the incubation period on the ability of Dynabeads MyOne streptavidin C1 MPs (functionalised with the *IS6110* DNA probe) to capture target DNA.

The MPs/*IS6110* DNA complex was incubated at 50ºC for 10, 20, 30, 40, 50, and 60 minutes with 10 ng/µL of target DNA which had been chemically isolated (Qiagen method) from *M. bovis* 1173P2. The results at each incubation time were compared against a no-template control. This data represents the mean of triplicated experiments ± standard error. * represents a significant p value <0.05 and ns indicates no significance.

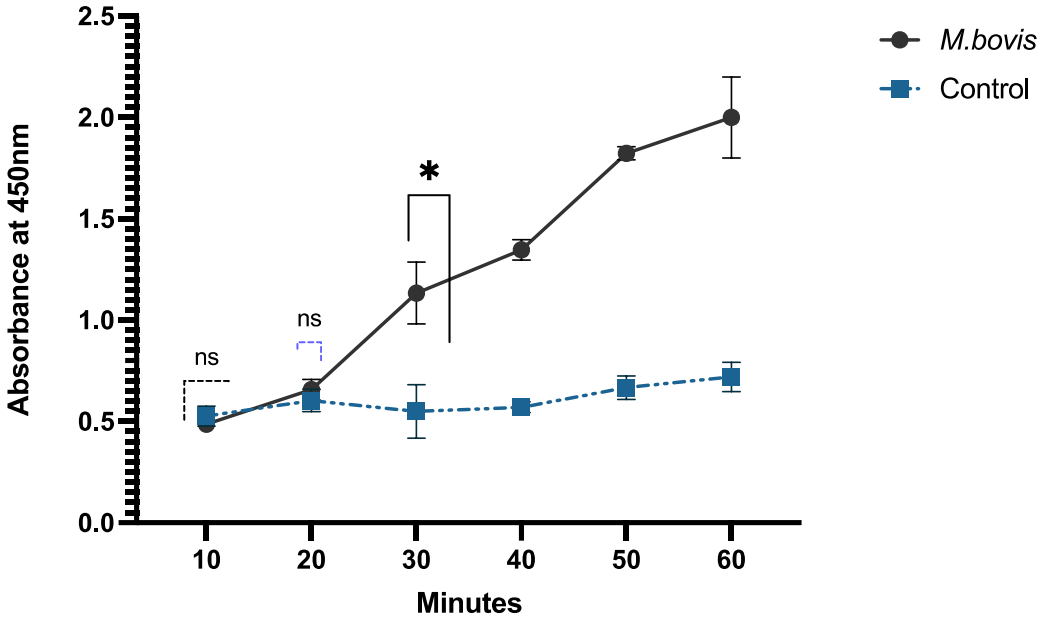

Figure 0.21 The impact of a decreased incubation period on the ability of Dynabeads MyOne streptavidin C1 MPS (functionalised with the *IS1801* DNA probe) to capture target DNA.

The MPs/*IS1801* DNA complex was incubated at 50ºC for 10, 20, 30, 40, 50, and 60 minutes with 10 ng/µL of target DNA chemically isolated from *M. bovis* 1173P2. The results at each incubation time were compared against a no-template control. This data represents the mean of a triplicated experiment ± standard error. * represents a significant *p* value <0.05 and *ns* indicates no significance.

To assess the impact of using microwaved bacterial suspensions of *M. bovis* 1173P2 at the lower limit of detection, the assay was repeated using a quantity of 10^3 bacteria. Figures 5.22 and 5.23 illustrate that the *IS6110* and *IS1081*-functionalised MPs produced statistically significant positive signals (p value < 0.05) following a 30-minute incubation. In conclusion, these results corroborate the feasibility of reducing the incubation period from 60 to 30 minutes.

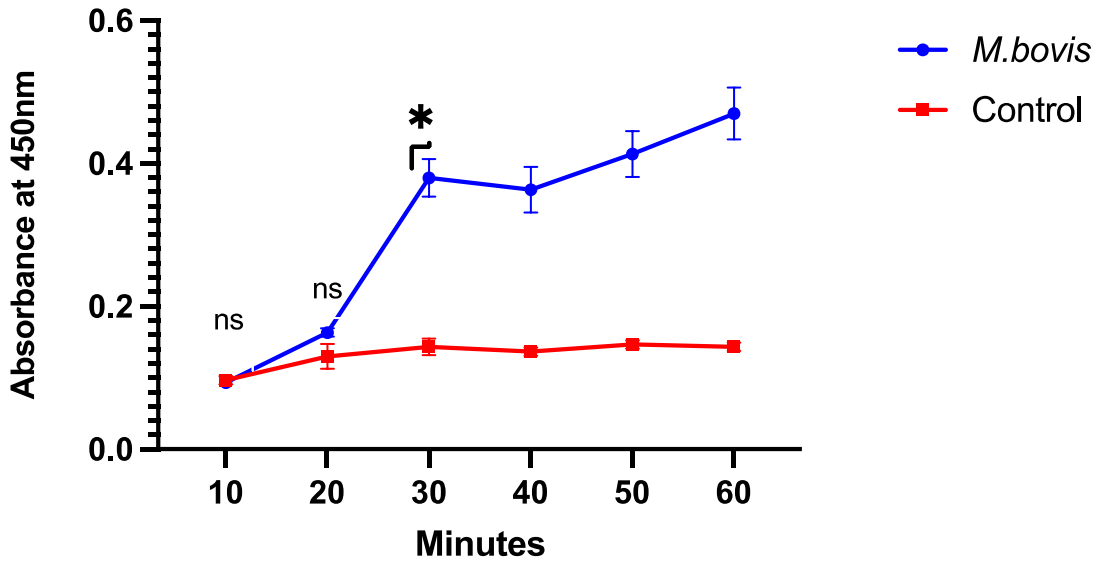

Figure 0.22 The Impact of decreasing the incubation period and target DNA concentration on the efficiency of MPs functionalised with an *IS6110*-specific DNA probe.

The MPs/*IS6110* DNA complex was incubated at 50°C for 10, 20, 30, 40, 50, and 60 minutes with a quantity of 10^3 bacteria from microwaved *M. bovis* 1173P2 suspension. The results at each incubation time were compared against a no-template control. This data represents the mean of triplicate experiments ± standard error. * represents a significant *p* value <0.05 and ns indicates no significance.

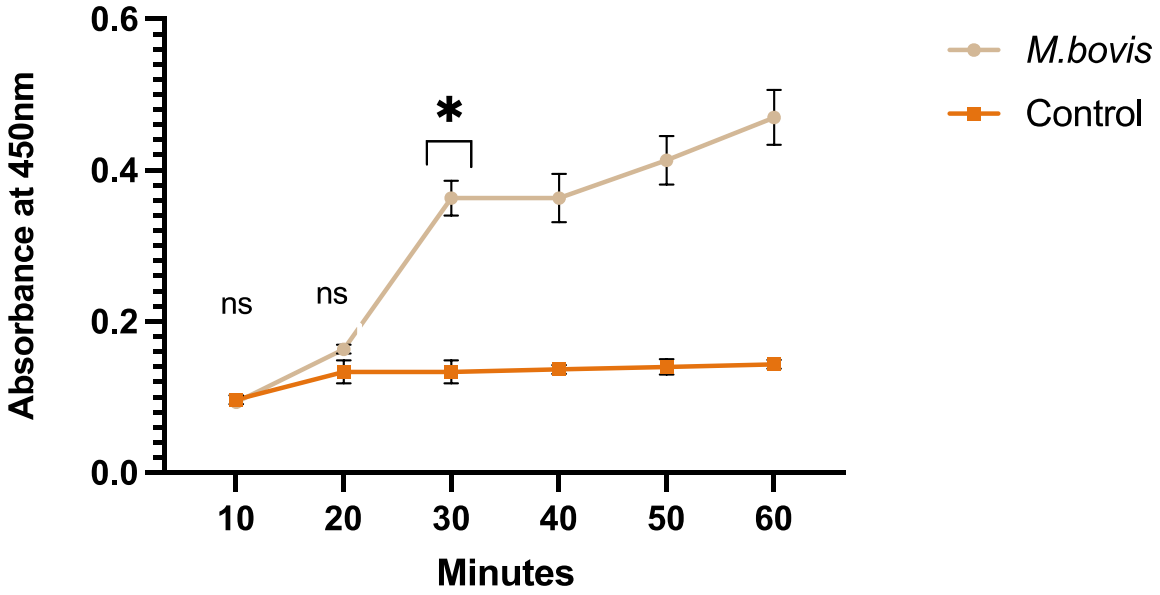

Figure 0.23 The Impact of decreasing the incubation period and target DNA concentration on the efficiency of MPs functionalised with an *IS1081*-specific DNA probe.

The MPs/*IS1081* DNA complex was incubated at 50°C for 10, 20, 30, 40, 50, and 60 minutes with a quantity of 10^3 bacteria from microwaved *M. bovis* 1173P2 suspension. The results at each incubation time were compared against a no-template control. This data represents the mean of triplicated experiments ± standard error. * represents a significant *p* value <0.05 and ns indicates no significance.

4.26.9 The Impact of modifying the incubation temperature on the ability of *IS6110* and *IS1081* specific DNA probes to capture and detect target DNA.

The temperature at which homologous strands of DNA separate can be estimated by determining the melting point (Tm). In the case of the *IS6110* and *IS1081* probes, their calculated Tm values were within the range of 60-65°C. In the current version of the assay, probe-target hybridisation occurred at 50°C; therefore, this research assessed the impact of increasing the incubation temperature to 60°C. Additionally, this study evaluated the effect of varying the incubation periods and utilised the original method as a control for comparison.

As illustrated by Figures 5.24 and 5.25, a temperature increase from 50°C to 60°C resulted in increased signal generation by the no-template control, to a point whereby it was impossible to distinguish between the no-template control and the test signals (p value > 0.05). However, the initial method, conducted at 50°C for one hour and used as a control for this study, yielded results that allowed clear differentiation between *M. bovis* and the no-template control.

One potential explanation for this observation is that the increased temperature (60°C) compromised the activity of the blocking agent, which increased the probability of non-specific DNA binding. BSA begins to unfold and denature as a protein at temperatures above 60°C, forming a gel and irreversibly aggregating, which minimises its blocking activity (Borzova et al., 2016). Considering the concurrent rise in non-specific binding, elevating the incubation temperature is impractical.

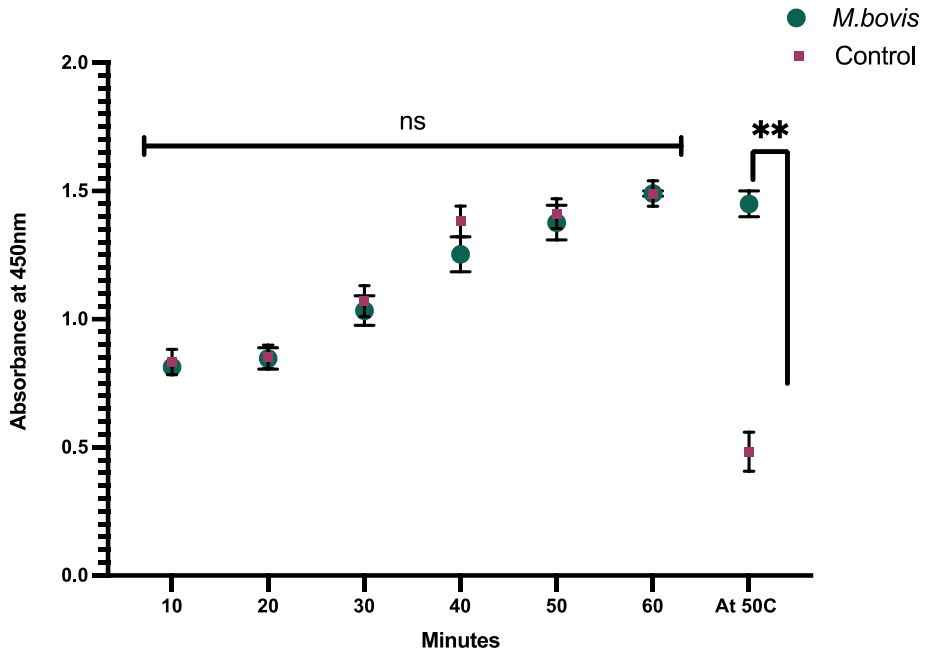

Figure 0.24 The impact of increasing the incubation temperature from 50 to 60 °C on target DNA capture by *IS6110* probe functionalised MPs.

The MPs/DNA complex was incubated at 60°C for 10, 20, 30, 40, 50, and 60 minutes. DNA was chemically isolated (Qiagen method) from the *M. bovis* 1173P2 isolate and standardised to a concentration of 10 ng/µL. DNA was detected by targeting the *IS6110* gene. Differentiation between *M. bovis* 1173P2 and the no-template control (NTC) was based on the magnitude of the HRP-generated colour change (determined by measuring the mean absorbance). This data represents the mean of triplicated experiments ± standard error. ** represents significant *p* value <0.001 and *ns* indicates no significance.

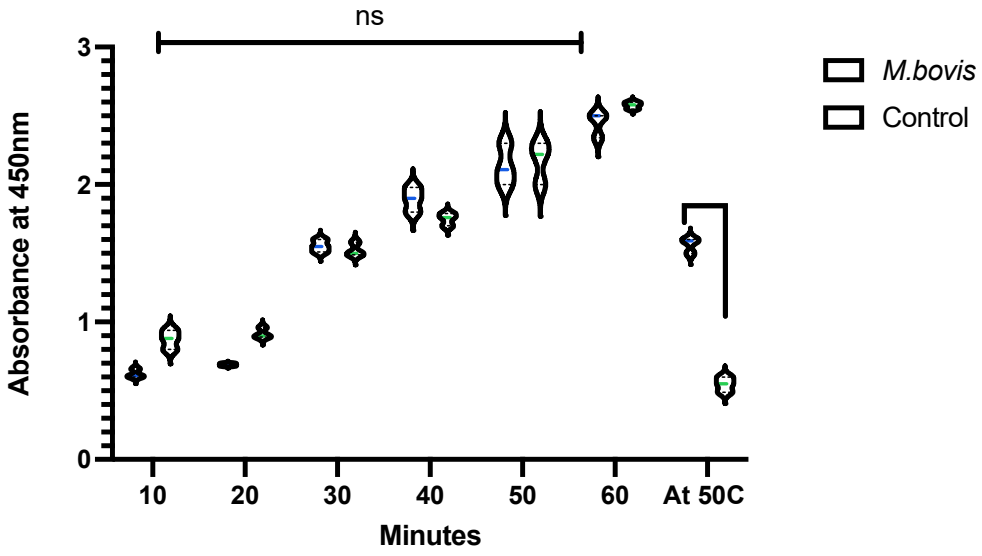

Figure 0.25 The impact of increasing the incubation temperature from 50 to 60 °C on target DNA capture by *IS1081* probe functionalised MPs.

The MPs/DNA complex was incubated at 60 °C for 10, 20, 30, 40, 50, and 60 minutes. DNA was chemically isolated (Qiagen method) from the *M. bovis* 1173P2 isolate and standardised to a concentration of 10 ng/µL. DNA was detected by targeting the *IS1081* gene. Differentiation between *M. bovis* 1173P2 and the no-template control (NTC) was based on the magnitude of the HRP-generated colour change (determined by measuring the mean absorbance). This data represents the mean of triplicated experiments ± standard error. ** represents significant p value <0.001 and ns indicates no significance.

4.26.10 The impact of modifying shaker speed on the ability of *IS6110* and *IS1081* DNA probe functionalised MPs to capture target DNA suspended in water

As illustrated in Figures 5.26 and 5.27, reducing the shaker speed from 200 rpm to 100 rpm during both time intervals resulted in a statistically significant difference, with the control samples exhibiting higher values than the test samples. This finding suggests that the DNA probes were unable to effectively capture the target DNA sequence under these optimised conditions Conversely, a shaker speed of 200 rpm resulted in a statistically significant difference between the test and control samples across both time intervals. This trend was consistent for both anchor probes and suggests that the hybridisation step requires higher energy to facilitate the interaction between the probes and target DNA.

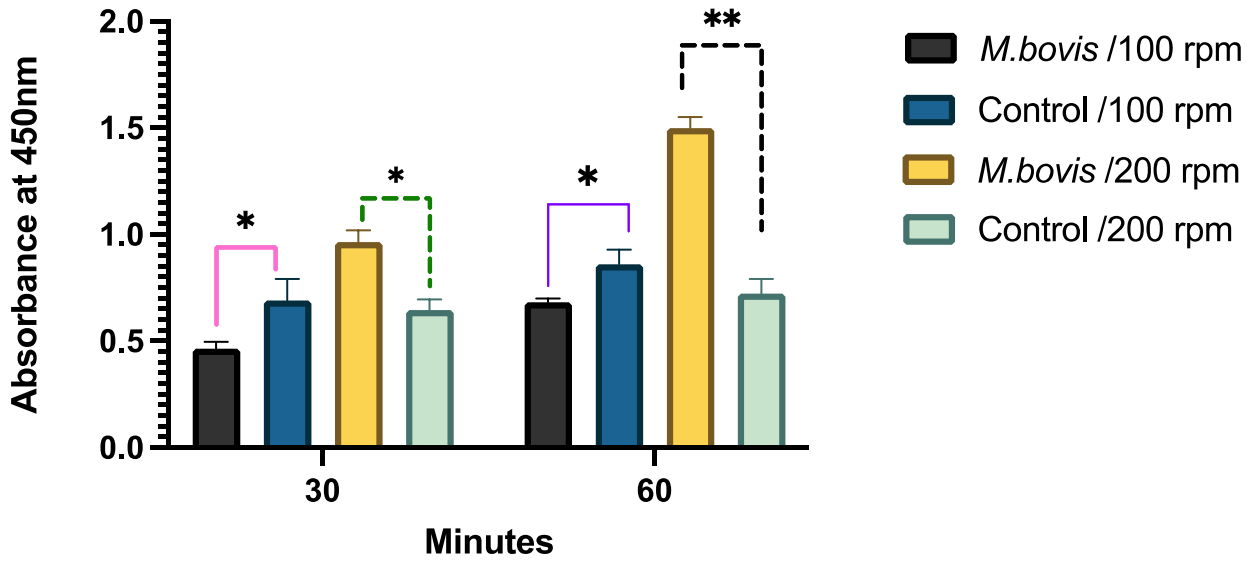

Figure 0.26 The impact of shaker speed on the capture of target DNA by *IS6110* DNA probes functionalised C1 MPs (at 30- and 60-minute time intervals).

Chemically extracted (Qiagen method) *M. bovis* 1173P2 DNA at a concentration of 10 ng/µL was incubated with C1 MPs functionalised with the *IS6110* DNA probe at 100 and 200rpm for 30 and 60 minutes. The negative control used was the no-template control (NTC). This data represents the mean of triplicated experiments ± standard error. * represents significant value *p* value <0.05, **= represents significant *p* value <0.001, and ns indicates no significance.

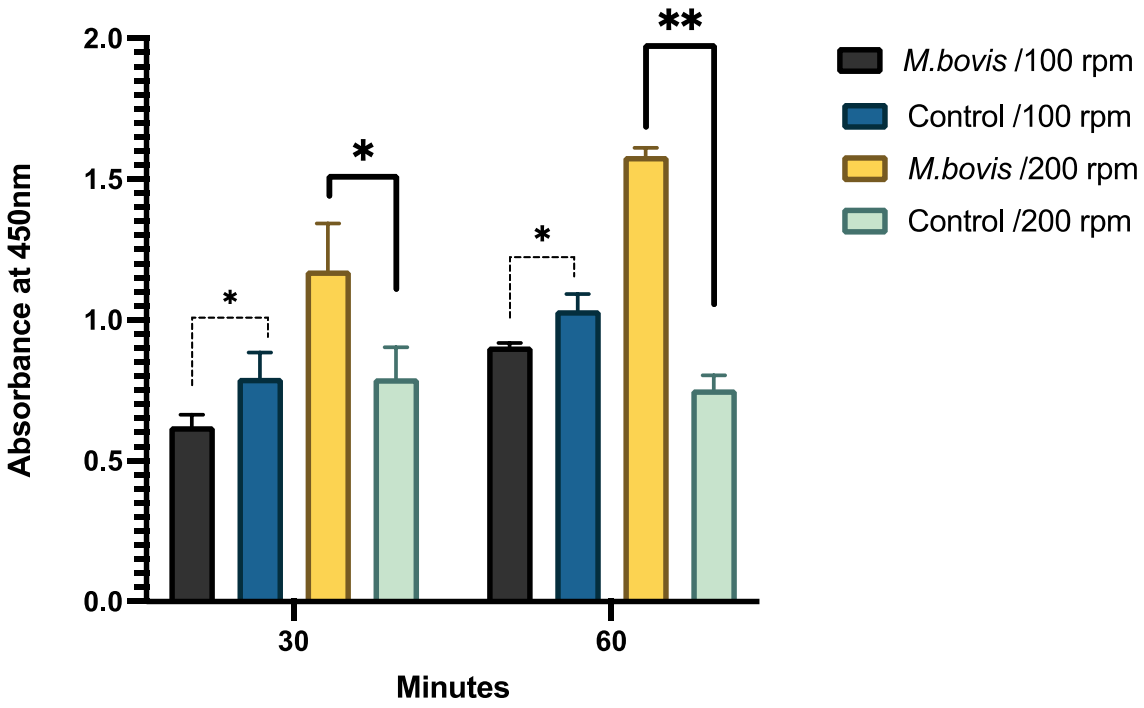

Figure 0.27 The impact of different shaker speeds on the capture of target DNA by *IS1081* DNA probe functionalised C1 MPs (at 30- and 60-minute time intervals).

Chemically extracted (Qiagen method) *M. bovis* 1173P2 DNA at a concentration of 10 ng/µL was incubated with C1 MPs functionalised with the *IS1081* DNA probe at 100 and 200rpm and for 30 and 60 minutes. The negative control used was the no-template control (NTC). This data represents the mean of triplicate experiments ± standard error. * represents significant value *p* value <0.05, ** represents significant *p* value <0.001, and ns indicates no significance.

4.26.11 Conclusions

Target DNA was detected using the *IS6110* and *IS1081* DNA probes in combination with magnetic particles (MPs), demonstrating a similar degree of sensitivity and specificity. However, increasing the number of thymine bases from 5 at the 5' end of the DNA probes adversely impacted the capture of the DNA target. Among the three commercially available magnetic beads examined in this study, the hydrophilic Streptavidin Magnetic Beads exhibited significantly superior performance in the enzyme-linked oligonucleotide sandwich hybridisation (ELOSHA) compared to the other beads.

Reducing the incubation period (from 60 to 30 minutes) did not adversely affect the assay's ability to detect target DNA. However, increasing the incubation temperature (from 50°C to

60°C) and reducing the shaker speed (from 200 rpm to 100 rpm) negatively impacted the signal strength. The assays conducted thus far utilised test analytes suspended in water. In the following section, the impact of suspending test samples in synthetic sputum to model real-world conditions will be assessed.

4.26.12 Detection of *M. bovis* 1173P2 suspended in synthetic sputum using ELOSHA.

In simulated sputum samples, the ability of the *IS6110* and *IS1081*-specific gene probes to identify DNA released from bacterial suspensions of *M. bovis* 1173P2 and *M. bovis* 5692 was evaluated. Additionally, the probes' ability to distinguish the *M. bovis* isolates from *M. smegmatis* Mc2155 (S2), *M. abscessus* ATCC 19977, and *E. coli* NCTC 1093 was determined. Upon microwave irradiation, a suspension of 10^8 *M. bovis* 1173P2 bacteria yielded 8 ng/μL of ssDNA. The DNA extracted from other isolates was adjusted to the same concentration using a NanoDrop. The signals generated by the two *M. bovis* isolates were significantly higher (p value < 0.001) than those generated by the non-*bovis* isolates (Figure 5.28). There was no significant difference in the magnitude of the responses observed against both *M. bovis* isolates using either gene target probe, which is consistent with the results obtained when the bacteria were suspended in water.

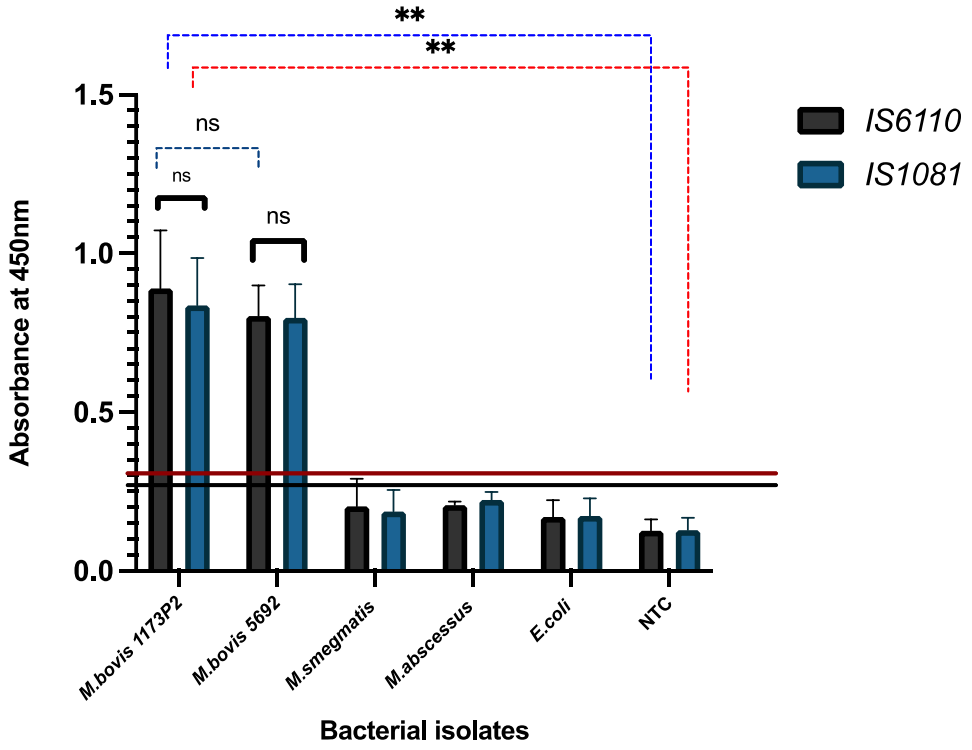

Figure 0.28 Detection of microwaved *M. bovis* 1173P2 and *M. bovis* 5692 suspended in synthetic sputum using *IS6110* and *IS1081* specific DNA probes.

Genomic material was released from test organisms suspended in synthetic sputum using microwave radiation at 30% DC for 20 seconds and was standardise to a concentration of 8 ng/µL. The ability to distinguish *M. bovis* from *M. smegmatis*, *M. abscessus* and *E.coli* is dependent on the magnitude of the HRP-generated colour change (determined by measuring the mean absorbance). The cut-off concentrations for a negative sample (DNA from microwaved *M. abscessus*) for the *IS6110* and *IS1081* probes were calculated as 0.29 and 0.27, respectively, and are represented by red (*IS6110*) and black (*IS1081*) lines. A no-template control (NTC) was also included. This data represents the mean of a triplicate experiment, ** represents a *p* value<0.001, and ns indicates no significance.

4.26.13 Determination of assay detection limit for samples suspended in simulated sputum

The sensitivity of the assay for microwaved *M. bovis* 1173P2 suspended in simulated sputum was evaluated across the following bacterial quantities: 10^8, 10^7, 10^6, 10^5, 10^4, 10^3, 10^2, and 10^1. The lower limit of detection for both gene targets, *IS6110* and *IS1081*, was 10^3, which was consistent with the level observed for bacteria suspended in water (Figures 5.29 and 5.30).

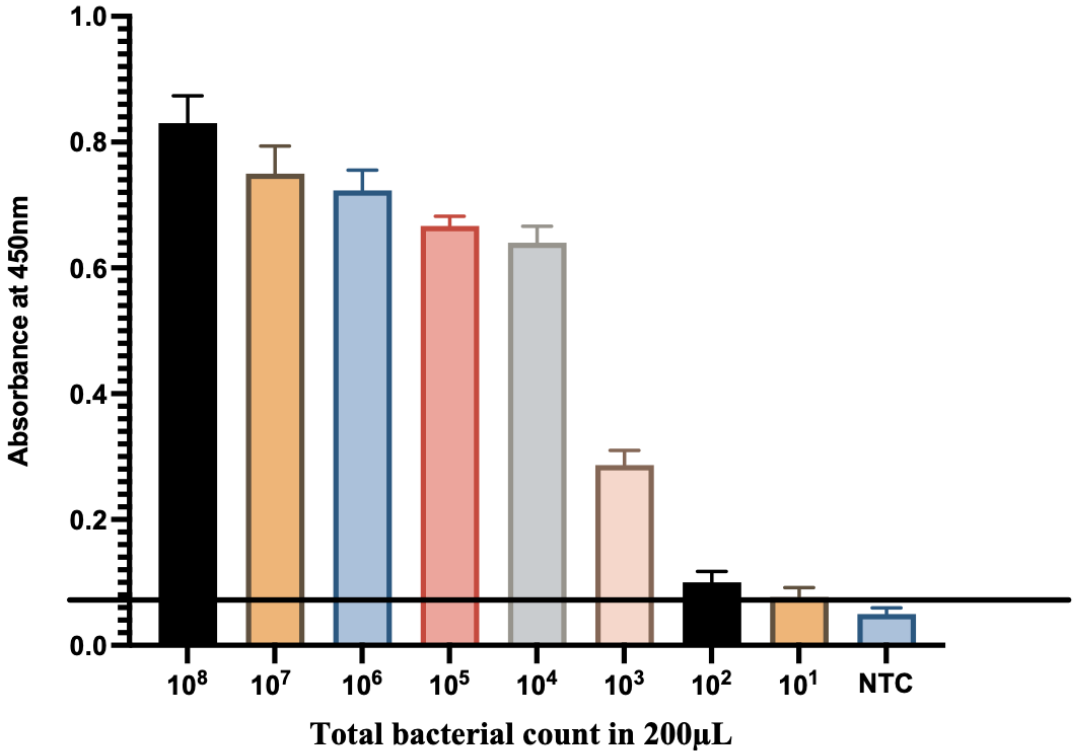

Figure 0.29 Sensitivity of ELOSHA assay using the *IS6110* DNA probes for microwaved extracted ssDNA from *M. bovis* 1173P2 suspended in simulated sputum .

The limit of detection for microwaved *M. bovis* 1173P2 suspension was determined to be 10^3 when measured against a cut-off value of 0.09nm (represented by the black horizontal line). The no template control (NTC) was used as the negative to determine the cut-off value. This data represents the mean of a triplicated experiment.

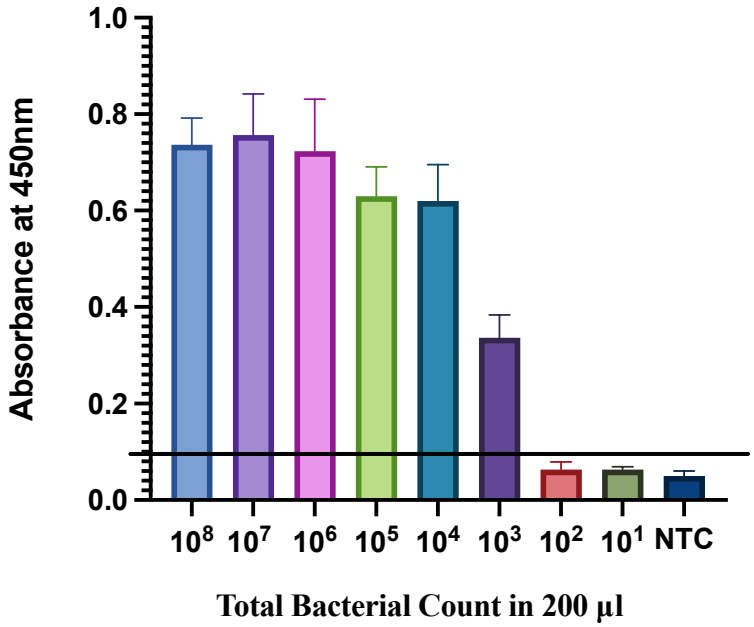

Figure 0.30 Sensitivity of ELOSHA assay using the *IS1081* DNA probes for microwaved ssDNA (extracted from *M. bovis* 1173P2) and suspended in simulated sputum.

The limit of detection for microwaved *M. bovis* 1173P2 suspension was determined to be 10^3 when measured against a cut-off value of 0.08 as represented by the black horizontal line. The no template control (NTC) was used as the negative to determine the cut-off value. This data represents the mean of a triplicated experiment.

To assess the specificity of the assay for *M. bovis* 1173P2 suspended in synthetic sputum, an aliquot of microwaved *M. bovis* 1173P2 was combined with microwaved *M. abscessus*, *M. smegmatis*, and *E. coli* (positive mix). The results were compared to those of microwaved *M. bovis* 1173P2 alone and a mixture of microwaved bacterial suspensions lacking *M. bovis* 1173P2 (negative control). All the microwaved extracted DNA was mixed at a DNA concentration of 9.1 ng/µL, the concentration produced after microwaving the *M. bovis* 1173P2 suspension alone. As depicted in Figure 5.31, the assay could detect microwaved *M. bovis* in the presence of competing bacterial isolates. There was no significant difference between the sensitivity and specificity of the assay for microwaved bacteria suspended in water and simulated sputum.

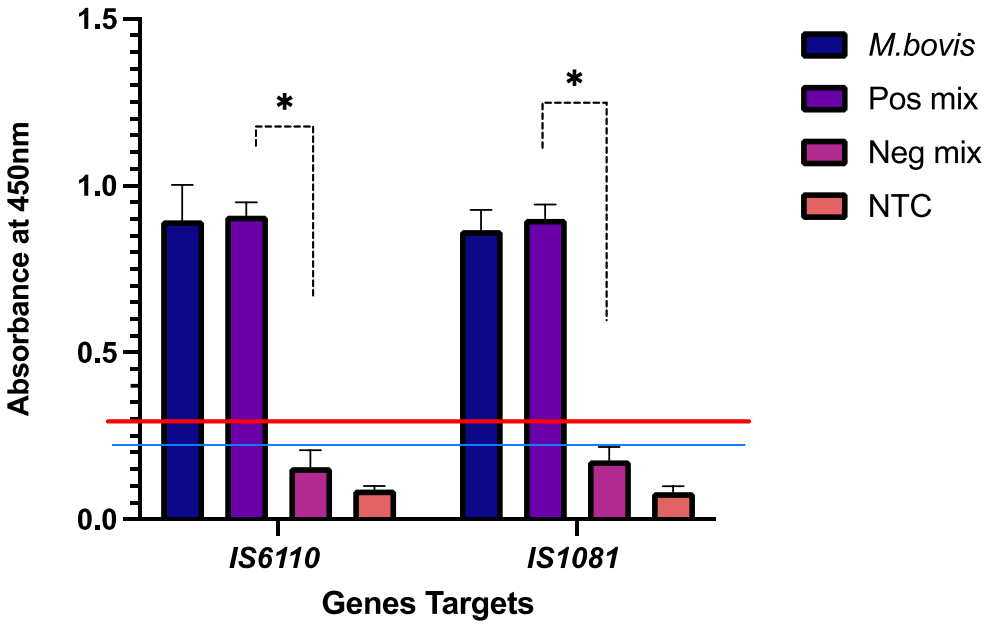

Figure 0.31 Specificity of the *IS6110* and *IS1081* DNA probes for *M. bovis* in the presence of other bacterial species in synthetic sputum.
The signal generated by *M. bovis* 1173P2 ssDNA and the positive mix (microwaved *M. bovis*, and non-bovis isolates including *M.abacessus*, *M. smegmatis* and *E.coli*) was significantly higher than that of the negative mix microwaved non-bovis isolates and the no-template control (NTC) (*p value* < 0.05) for both genes. The cut-off value for a positive test was determined at an absorbance value of 0.31 and 0.29 (using the negative mix as the control for cut-off determination) and is represented by the horizontal green and black lines for the *IS6110* (red line) and *IS1081* (blue line) genes, respectively. This data represents the mean of triplicated experiments ± standard deviation, * represents a significant *p value* <0.05.

4.26.14 Assessing how magnetic bead (MP) properties impacts on targeted DNA capture in simulated sputum

In earlier experiments, hydrophilic Streptavidin Magnetic Beads (H) functionalised with DNA probes produced the strongest signals for microwaved bacteria suspended in water. This experiment was repeated with the samples suspended in simulated sputum to determine if this remained the case in another medium.

As illustrated in Figures 5.32 and 5.33, the hydrophilic MPs, in the presence and absence of test samples, exhibited the strongest absorbance signals following 60 minutes of incubation. This included visible aggregation of hydrophilic MPs, which was not observed with the other two MPs. This phenomenon could be due to a chemical interaction between hydrophilic streptavidin and methyl cellulose (the primary component of simulated sputum). It is

conceivable that this interaction may not occur with naturally occurring sputum samples. In contrast to the hydrophilic MPs, the C1 and M-270 beads showed a clear difference (p value < 0.001) between the test and control samples, although there was no statistically significant difference in the magnitude of the C1 and M-270 bead responses (p value > 0.05). These responses paralleled those observed in samples suspended in water.

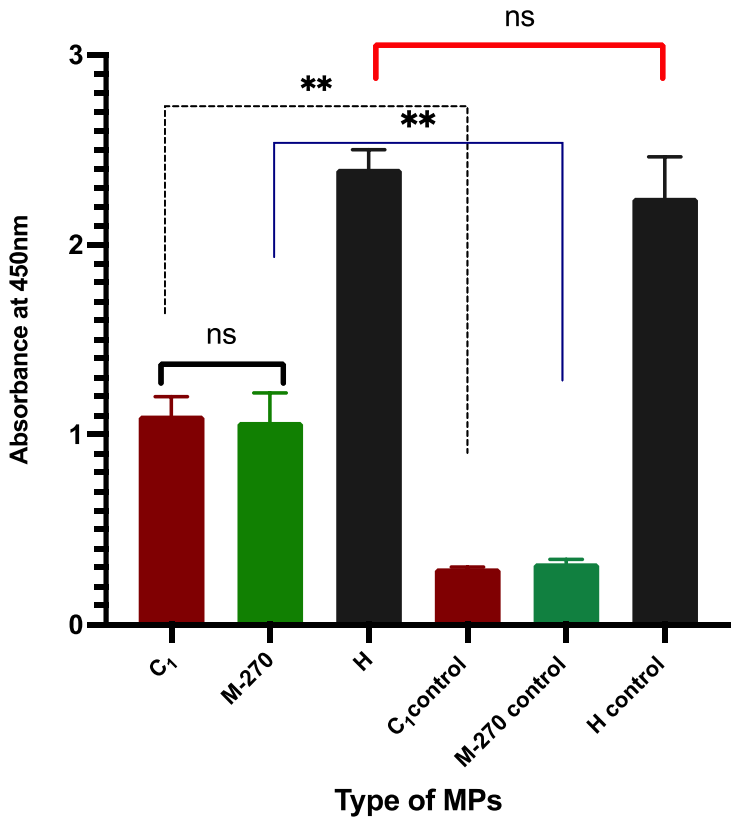

Figure 0.32 Comparison of the ability of different magnetic particles functionalised with the *IS6110* specific DNA probe to detect *M. bovis* suspended in simulated sputum.

These magnetic beads (Dynabeads™ MyOne™ Streptavidin C1 (C1), Dynabeads™ M-270 Streptavidin (M-270) and Hydrophilic Streptavidin Magnetic Beads (H)) functionalised with the *IS6110* probe were tested against *M. bovis* 1173P2. The bacteria were suspended in simulated sputum, following exposure to microwave radiation at 30% duty cycle for 20 seconds, to isolate DNA, samples where standardised to a DNA concentration of 10 ng/µL. The differentiation between distinct types of MPs was based on the magnitude of the HRP-generated colour change (as determined by measuring mean absorbance). A no-template control (NTC) was included. The data represents the mean of triplicate experiments ± standard error. This data represents the mean of triplicated experiments ± standard error. ** represents significant p value <0.001 and ns indicates no significance.

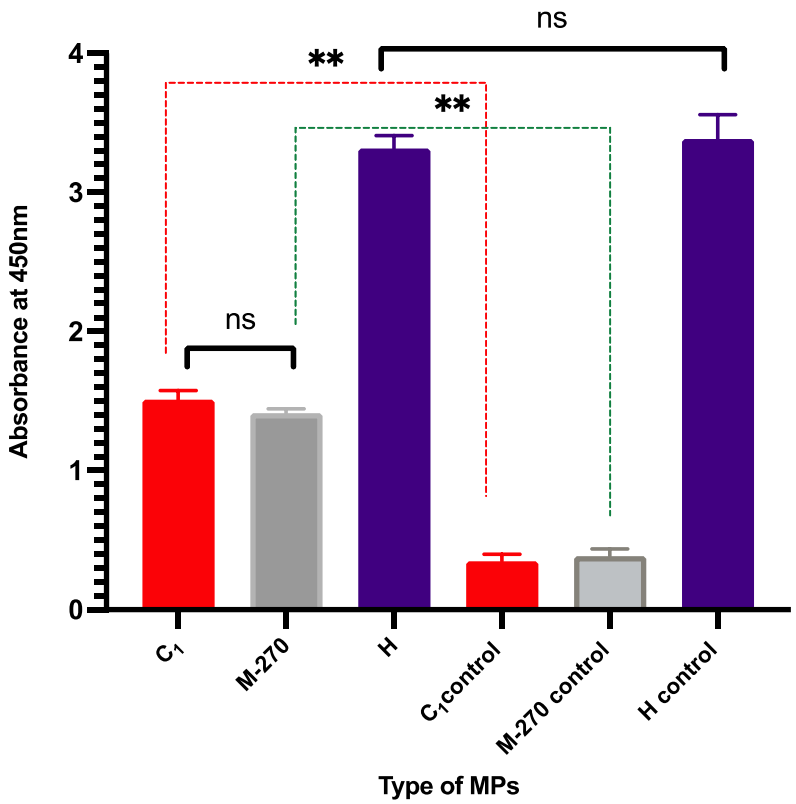

Figure 0.33 Comparison of the ability of different magnetic particles functionalised with the *IS1081* specific DNA probe to detect *M. bovis* suspended in simulated sputum.

These magnetic beads (Dynabeads™ MyOne™ Streptavidin C1 (C1), Dynabeads™ M-270 Streptavidin (M-270) and Hydrophilic Streptavidin Magnetic Beads (H)) functionalised with the *IS1081* probe were tested against *M. bovis* 1173P2. The bacteria were suspended in simulated sputum following exposure to microwave radiation at a 30% duty cycle for 20 seconds to isolate DNA, samples were then standardised to a concentration of 10 ng/µL. Differentiation between the various MPs was based on the magnitude of the HRP-generated colour change (as determined by measuring mean absorbance). A no-template control (NTC) was included. This data represents the mean of triplicated experiments ± standard error. ** represents significant *p* value <0.001 and ns indicates no significance.

In conclusion, while the hydrophilic MPs provided the strongest signal, the strong non-specific interaction with methyl cellulose made it impossible to distinguish between the test and control samples. Whether such an interaction would occur with genuine sputum is unclear. However, due to time constraints, it was agreed that future research should focus on C1 beads, as most earlier optimisation studies were conducted with these beads.

4.26.15 The impact of modifying the MP/DNA incubation period on the capture of DNA released from bacteria suspended in simulated sputum following microwave exposure

The identical protocol (Section 5.11.8) employed to evaluate the impact of modifying the incubation period in water was applied to microwaved bacteria suspended in simulated sputum. Forty minutes of incubation was the first time point at which a significant difference (p value < 0.001) could be detected between the test and control samples (Figures 5.34 and 5.35). This was ten minutes longer than for microwaved samples suspended in water, which implies that the viscosity of simulated sputum may inhibit the capture of targeted DNA.

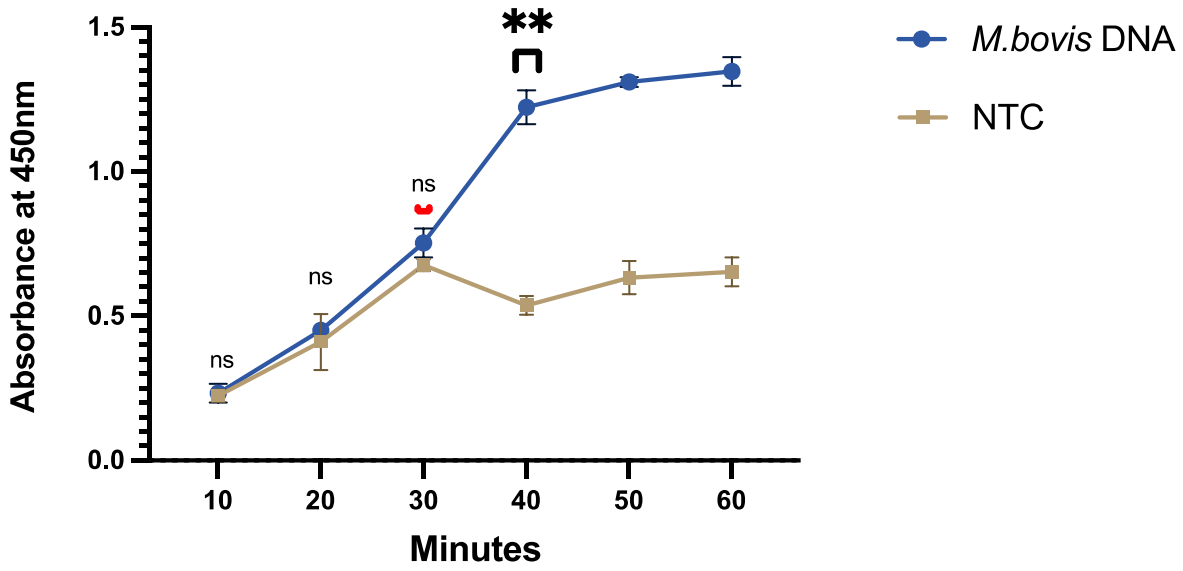

Figure 0.34 The impact of modifying the MP/DNA incubation period on the capture of DNA released from bacteria suspended in simulated sputum following microwave exposure.

The MPs/DNA complex was incubated at 50°C for 30, 40, 50, and 60 minutes. Microwaved *M. bovis* 1173P2 detection was based on targeting the *IS6110* gene. Genomic material (10 ng/µL) was released from *M. bovis* 1173P2 suspended in simulated sputum via exposure to microwave radiation at a 30% duty cycle for 20 seconds. This data represents the mean of triplicated experiments ± standard error. ** represents significant p value <0.001 and ns indicates no significance.

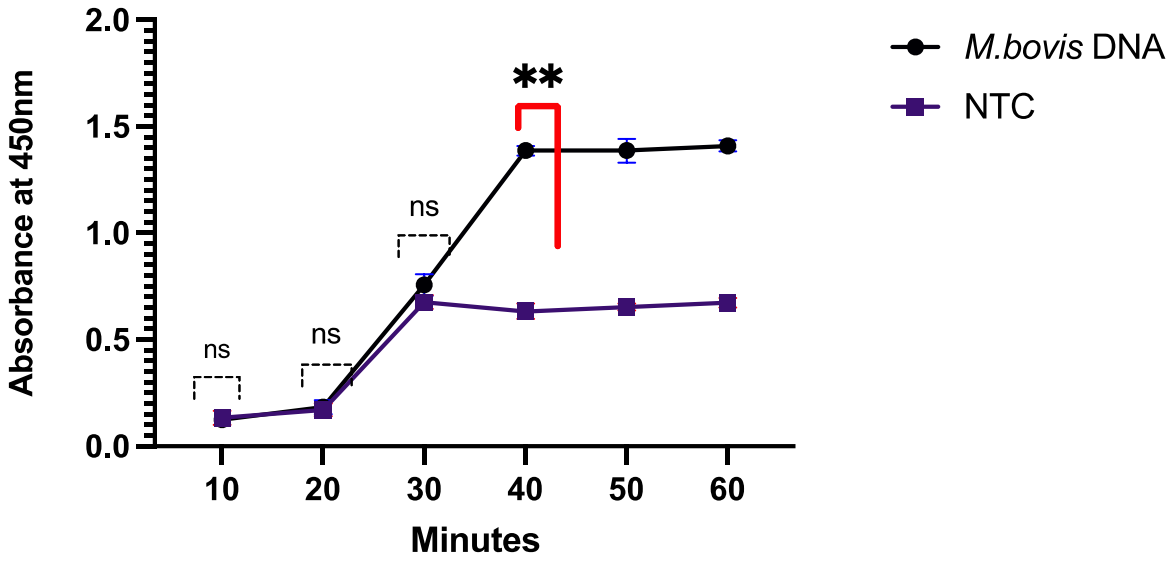

Figure 0.35 The impact of modifying the MP/DNA incubation period on the capture of DNA released from bacteria suspended in simulated sputum following microwave exposure .

The MP/DNA complex was incubated at 50 °C for 30, 40, 50, and 60 minutes. Microwaved *M. bovis* 1173P2 detection was based on targeting the *IS1081* gene. Genomic material (10 ng/µL) was released from *M. bovis* 1173P2 suspended in simulated sputum via exposure to microwave radiation at a 30% duty cycle for 20 seconds. This data represents the mean of triplicated experiments ± standard error. ** represents significant *p* value <0.001 and ns indicates no significance.

As previously described, the experiment was repeated using microwaved bacterial suspensions of *M. bovis* 1173P2 containing 10^3 bacteria in synthetic sputum. A statistically significant difference in the magnitude of the positive responses compared to the controls was observed (Figures 5.36 and 5.37). These findings confirm the feasibility of reducing the incubation period from 60 to 40 minutes in the presence of simulated sputum.

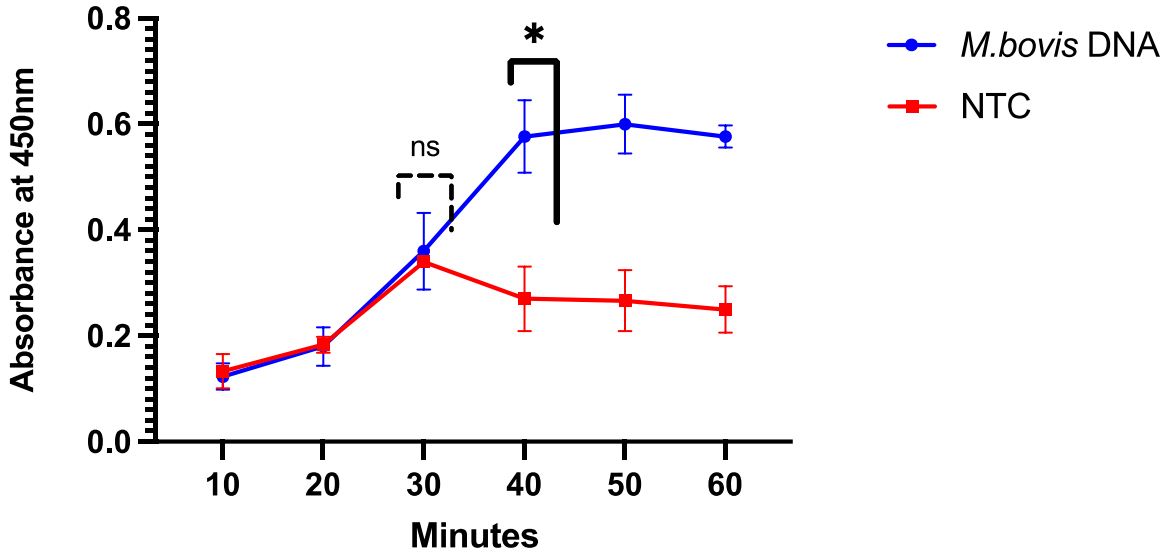

Figure 0.36 The impact of a reduced incubation period on the capture of *M. bovis* 1173P2 suspended in simulated sputum (using C1 MPs functionalised with *IS6110* specific DNA probes).

The MP/DNA complex was incubated at 50 °C for 30, 40, 50, and 60 minutes. The presence of *M. bovis* 1173P2 was detected by targeting the *IS6110* gene. Genomic material was released from a quantity of 10^3 bacteria suspended in simulated sputum via exposure to microwave radiation at a 30% duty cycle for 20 seconds. All tested suspensions were standardised to the same ssDNA level. This data represents the mean of triplicated experiments ± standard error. * represents a significant *p* value <0.005 and ns indicates no significance.

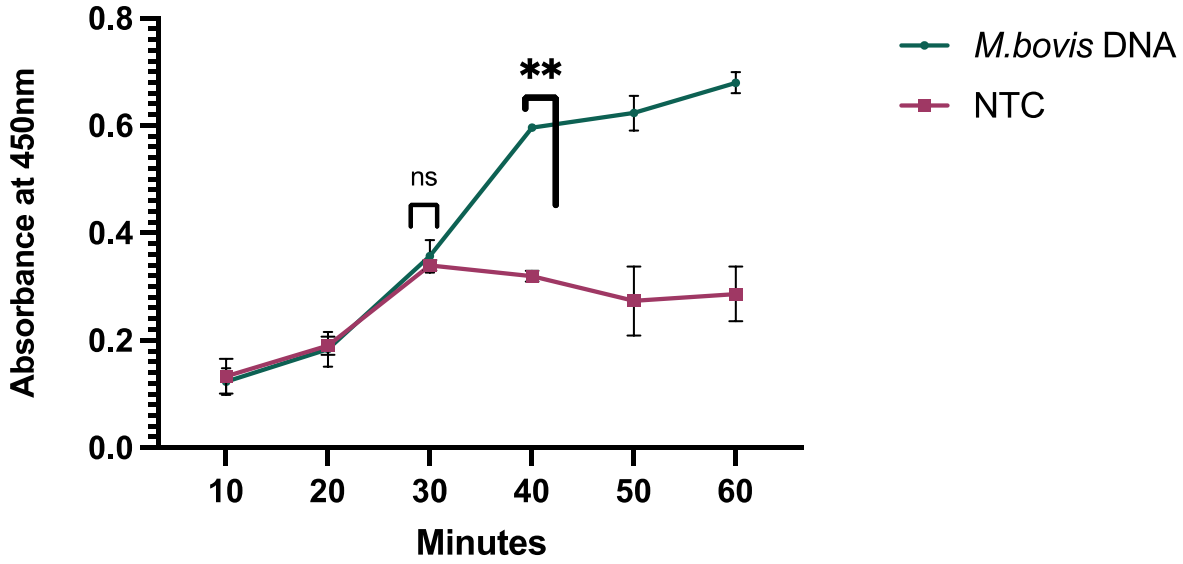

Figure 0.37 The impact of a reduced incubation period on the capture of *M. bovis* 1173P2 suspended in simulated sputum (using C1 MPs functionalised with *IS1081* specific DNA probes).

The MP/DNA complex was incubated at 50 C for 30, 40, 50, and 60 minutes. The presence of *M. bovis* 1173P2 was detected by targeting the *IS1081* gene. Genomic material was released a quantity of 10^3 bacteria suspended in simulated sputum via exposure to microwave radiation at a 30% duty cycle for 20 seconds. The tested suspensions were standardised to the same ssDNA level. This data represents the mean of triplicated experiments ± standard error. ** represents significant value *p* value <0.001 and ns indicates no significance.

In conclusion, when using simulated sputum and C1-functionalised magnetic particles, it was possible to reduce the incubation period (from sixty minutes to forty minutes) and still generate a positive signal, significantly different from the negative control.

4.27 Discussion

In this chapter, the ability of the ELOSHA approach to detect *M. bovis* in a small volume (200 µL) of water or simulated sputum was enhanced. The specificity and sensitivity of the detection probes, designed in the previous chapter, were confirmed.

Both gene targets, *IS6110* and *IS1081*, were selected because wildtype strains of *M. tuberculosis* and *M. bovis* have been reported to vary in the presence of each target sequence (Howard et al., 1998; Huyen et al., 2013). Tuberculosis detection rates have been reported to increase from 77.1% to 89.2% when multiple gene targets are employed (Kulkarni et al., 2012).

In its existing configuration, the test detected *M. bovis* in the presence of DNA from other non-bovis isolates. However, further studies are required to assess the assay's specificity against a broader panel of mycobacterial isolates and other upper respiratory tract bacterial flora representatives.

Regarding sensitivity, the assay detected 0.6 pg/µL of chemically purified DNA target and 10^3 microwaved *M. bovis* bacilli suspended in either water or simulated sputum. This makes the current version of the assay more sensitive than smear microscopy (LOD 10^5), which is the current paradigm for tuberculosis diagnoses. However, it is less sensitive than PCR, which typically achieves ranges of 10^1 to 10^2 bacilli (Wakode et al., 2022).

Further work is needed to optimise the assay system's sensitivity. This chapter explores the impact of varying parameters, including incubation period, temperature, sample agitation (shaker speed), MP selection, and DNA probe design. The results suggest the potential to increase assay sensitivity by further optimising these parameters. For example, the use of commercially available MPs imposed some limitations, and it may be possible to enhance sensitivity by employing MPs with different characteristics.

Additionally, the hybridisation time for bacteria suspended in water was successfully reduced to 30 minutes. However, the viscosity of the simulated sputum inhibited the capture of target DNA within the same time frame, necessitating an additional 10 minutes to generate a positive signal. This resulted in a total hybridisation time of 40 minutes.

As Flavell et al. (1974) noted, as the solvent's viscosity increases, the initial rate of hybridisation decreases. It is important to mention that during wet lab work, the sample's viscosity posed additional challenges when retrieving magnetic beads from the sample: some beads were lost during the transfer to the enzymic stage of the assay, which potentially reduced its sensitivity.

Given these concerns, examining the assay's effectiveness when used with real sputum samples is crucial. If viscosity continues to have a negative impact, the introduction of mucolytic substances (which reduce viscosity) should be considered (Satish et al., 2023). Unfortunately, such agents could not be tested on simulated sputum samples due to differences in composition compared to real-world samples. Further research and experimentation with real sputum will be key to developing this assay.

Incorporating the optimisation steps into the ELOSHA method resulted in an assay that required approximately 90 minutes to generate a result. While this timeframe is relatively rapid compared with PCR-based detection assays such as GeneXpert (which requires two hours to generate a result), it would benefit from further reduction (Wakode et al., 2022).

To further reduce the time needed to generate a positive signal, the HRP enzyme reporter could be substituted with an alternative system, such as a fluorescence probe (the feasibility of which has previously been reported by Aslan et al. (2008) and Joshi et al. (2014)). The advantage of such an approach is that it eliminates the need for the time-consuming sample washing steps required by ELOSHA.

Chapter 6 Detection of *Mycobacterium tuberculosis* complex in large-sample volumes using microwave-assisted (ELOSHA)

5.1 Introduction

The primary sample used to diagnose tuberculosis is sputum. However, the quality of the sample is the main factor affecting the assay's outcome (Yoon et al., 2012; Ho et al., 2015; Zimba et al., 2019a). Good-quality sputum samples, with more than 40% viable immune system cells and less than 25% epithelial cells, are ideal for testing (da Silva et al., 2010). Detecting the pathogen's presence in low volumes is particularly challenging, especially when the bacteria are unevenly distributed across a clinical sample and are primarily associated with immune cells. According to the WHO, the minimum volume of good-quality sputum required to diagnose tuberculosis reliably is 3–5 ml (Zimba et al., 2019b).

In Chapter 5, the prototype assay's ability to detect *M. bovis* 1173P2 suspended in a 200 µL water sample or simulated sputum in an Microcentrifuge tube was demonstrated. To increase the assay's sensitivity, and as part of a linked PhD project, a sample cartridge capable of processing up to 10,000 µL (referred to as the large cartridge) was designed. This cartridge was compatible with our diagnostic assay and could be microwaved (Wilson-Garner et al., 2024).

DNA probe-functionalised magnetic nanoparticles were used in this research due to their ability to bind target DNA and move throughout the sample volume. While these particles exhibited good performance in smaller quantities (200 µL), their magnetic characteristics provided a substantial advantage when increasing to higher sample volumes (10,000 µL). Incorporating shaking during hybridisation enhanced the mobility of the nanoparticles within the fluid, promoting interaction between the nanoparticles and the entire sample volume. This enhancement increased the likelihood of the nanoparticles detecting and binding to target DNA, effectively overcoming diffusion limitations in larger samples. Figure 6.1 illustrates how examining only a small portion of a larger sample risks missing bacteria that are present at low concentrations, potentially leading to false-negative results. Therefore, enhancing the

dispersion of magnetic nanoparticles within the sample promotes contact with bacteria, even at low concentrations. After capturing the DNA, magnets concentrate the magnetic beads in one place, simplifying the detection of the target DNA.

This method highlights an additional advantage of using magnetic nanoparticles: their mobility within the sample fluid significantly improves the assay's sensitivity.

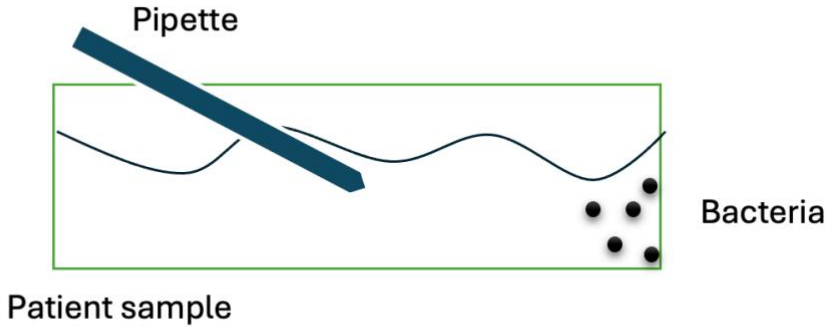

Figure 5.1 Schematic illustration of the problem of analysing a small portion of a sample.

Assays of samples with low concentrations of bacteria might miss bacteria; therefore, to obtain the most precise diagnosis, the entire sample should be assayed.

5.2 Design of a 10,000 µL cartridge: a cylindrical microwave cavity

A PhD student in the Schools of Engineering and Pharmacy at Cardiff University developed a 10,000 µL sample cartridge, which facilitates the isolation and capture of bacterial DNA using a combination of microwave irradiation and magnetic nanoparticles (Wilson-Garner et al., 2024).

The cartridge was created using a “stack” technique, in which the total volume (10,000 µL) is divided into multiple horizontally partitioned layers. This approach was chosen instead of increasing the single-chamber volume to ensure more uniform microwave energy distribution throughout the sample. By reducing the vertical depth of each partition, the risk of uneven heating, thermal gradients, and inefficient DNA release is minimised, while maintaining scalability and processing safety.

The sample is placed in the body of the cartridge, and the lid is fitted to create horizontal partitions. A seal is then applied to the top of the lid, which is secured with a clamp and four nylon screws, making the cartridge waterproof. This feature is crucial to prevent cross-contamination of samples and ensure user safety. Figures 6.2 and 6.3 display the complete simulated model.

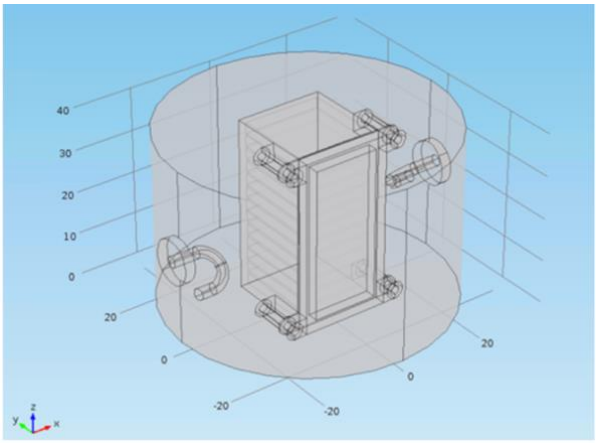

Figure 6.5.2 Model of 10,000 µL stack cartridge inside *TM*010 cylindrical cavity

(Wilson-Garner et al., 2024).

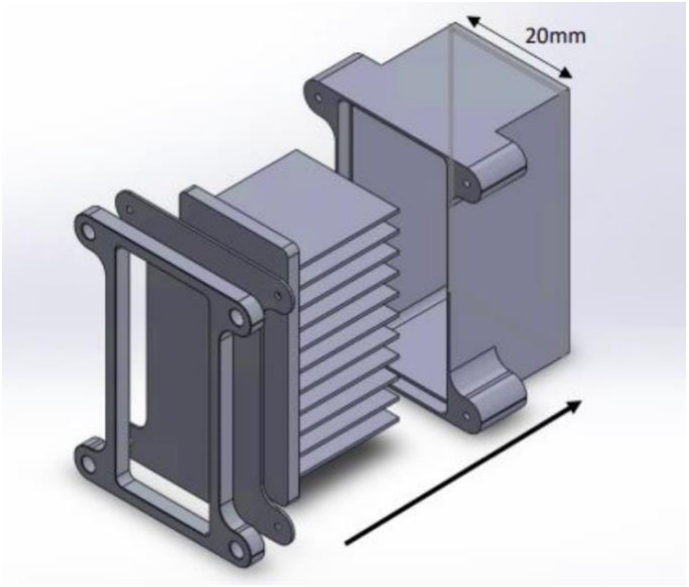

Figure 5.3 Illustration of the structure of the 10,000 µL stack cartridge modelled in solid works.

Parts from left to right: clamp, seal, lid and body. The height of the cartridge is 40-mm(Wilson-Garner et al., 2024).

Since the validity of the 200 µL Microcentrifuge tube method for detecting *M. bovis* 1173P2 has already been demonstrated (Chapter 5), it was used as a benchmark to evaluate the performance of the larger cartridge design.

5.3 Aim

This chapter aims to determine whether the assay's sensitivity can be increased by using larger sample volumes.

The chapter objectives are as follows:

1. Optimise the isolation of ssDNA from bacterial cultures suspended in 10,000 µL of water or simulated sputum using the newly designed sample cartridge.
2. Optimise the ELOSHA assay to detect the presence of *M. bovis* 1173P2 in water or simulated sputum.
3. Compare the sensitivity of the small and large volume detection approaches.

5.4 Methods

5.4.1 Identification of the microwave power levels that maximise the release of ssDNA from bacteria suspended in 10,000 µL volumes of water or simulated sputum.

To prepare the bacterial suspensions in water or simulated sputum, *M. bovis* 1173P2, *M. smegmatis* Mc2155 (S2), and *M. abscessus* ATCC 19977 were cultured on their respective agar media, as detailed in Chapter 2-Section 2.4.1. The bacterial strains were then prepared as single-cell suspensions, each containing 1×10^8 bacteria in 10,000 µL of water, following the procedures outlined in Chapter 2, Section 2.7.1. Similarly, bacterial suspensions were prepared in simulated sputum, as described in Chapter 2, Section 2.9.1.

The large-volume microwave cartridge was filled with 10,000 µL of each bacterial suspension for DNA isolation. The samples were exposed to microwave radiation (12W power level) for varying periods. The amount of ssDNA released was quantified using a NanoDrop, as described in Chapter 2, Section 2.8. Each experiment was conducted three times.

5.4.2 Detection of *M. bovis* 1173P2 DNA in 10,000 µL cartridges using the ELOSHA assay

Following the microwave-mediated DNA release from *M. bovis* 1173P2, a total of 10^8 bacteria were suspended in a 10,000 µL cartridge, and the presence of target bacterial DNA was detected using *IS6110* and *IS1081* gene-specific DNA probes. A 150 µL aliquot of hybridisation buffer (SSC buffer), 10 µL of DNA probe-functionalised

magnetic particles (Dynabeads™ MyOne™ Streptavidin C1), and 5 µL of HRP reporter probe (10 µM) were added to the sample and incubated for one hour at 50°C using an orbital incubator. A magnet was then employed to separate the MP/DNA hybrid complex from the solution, and the supernatant was discarded.

The MP/DNA hybrid complex was washed three times with hybridisation buffer. The presence of the bacterial target gene sequence was indirectly confirmed by adding 5,000 µL of TMB substrate to the cartridge, followed by a 6-minute incubation period at 37°C. Subsequently, 5,000 µL of a 1 M solution of H_2SO_4 was added, and the optical density was determined using a plate reader (Infinite M Plex -TECAN) at a wavelength of 450 nm. To distinguish a positive result from a negative one, a cut-off value was determined for each experiment by calculating the mean optical density of the negative control plus three times the standard deviation (Classen et al., 1987; Lardeux et al., 2016).

Genomic DNA extracted from non-bovis isolates, *M. smegmatis* Mc2155 (S2) and *M. abscessus* ATCC 19977, were used as control samples to determine the assay's specificity. To facilitate a valid comparison, the ssDNA concentrations of these control samples were adjusted to match that of a microwaved *M. bovis* 1173P2 culture containing 10^8 bacteria in 10,000 µL. The assay also included a no-template control (NTC) to assess the non-specific binding of the HRP-labelled DNA probe to the MPs. Each assay was repeated three times.

5.4.3 Determining the sensitivity of the assay for bacterial samples suspended in 10,000 µL of water or simulated sputum.

After determining the limit of detection (LOD) at the 200 µL Microcentrifuge tube level (Chapter 5, Section 5.10.4), the assay's sensitivity for intact bacteria at the 10,000 µL (large cartridge) level was assessed. To determine the sensitivity for *M. bovis* 1173P2, serial dilutions of the bacteria in water or simulated sputum were prepared. In the first tube, bacteria were

added to achieve a 10^8 bacterial suspension in 10,000 µL, and then serial 10-fold dilutions were made across the remaining tubes. After preparing the dilutions, each sample was added to the cartridge for microwaving. This dilution method ensured that the total number of bacteria in the cartridge was consistent with the desired concentrations, allowing for accurate sensitivity determination of the assay.

These dilutions were then exposed to microwaves at a 12W power level for 480 seconds, after which the presence of target DNA was detected using ELOSHA.

5.4.4 Determining the of impact of reducing the sample volume upon detecting target DNA

To assess the effect of decreasing the sample volume on the detection of the target DNA, 10,000 µL and 5,000 µL samples, each containing 10 ng of *M. bovis* 1173P2 ssDNA, isolated using the Qiagen DNA extraction method, as detailed in Chapter 3, Section 3.3.4, were used. ELOSHA was employed to detect the target DNA, with the original sample volume determining the amount of TMB substrate added to the cartridge. This followed a 2:1 ratio: for the 10,000 µL sample, 5 mL of TMB substrate was used, while for the 5,000 µL sample, 2.5 mL of TMB substrate was added.

5.5 Statistics

All experiments were performed at least twice under independent conditions. Statistical analysis of the data was performed using GraphPad Prism. An independent samples t-test was conducted to determine the statistical significance between the two groups. Data were considered significant when the p value was < 0.05. Analysis of variance (ANOVA) was performed to determine the difference among group means. To determine the differences within groups, post-hoc analysis was performed using the Bonferroni and Tukey tests. p values less than 0.05 were considered significant.

5.6 Results

5.6.1 Identification of the optimum microwave power levels required to release ssDNA from bacteria suspended in 10,000 µL volumes of water or simulated sputum sample.

Initially, 10,000 µL samples of water or simulated sputum containing bacterial suspensions of either *M. bovis* 1173P2, *M. smegmatis* Mc2155 (S2), or *M. abscessus* ATCC 19977, each at a concentration of 10^8 bacteria, were loaded into a custom 10,000 µL microwave cartridge. The samples were exposed to 12 W of microwave energy for durations ranging from 120 to 960 seconds, in 120-second increments. Following irradiation, the concentration of released ssDNA was quantified using NanoDrop spectrophotometry and compared to untreated controls. Data were normalised by subtracting the baseline values at time zero.

As shown in Figure 6.4, ssDNA concentration increased progressively with exposure time for all isolates, peaking at 480 seconds. Beyond this point, a marked decline in ssDNA yield was observed. Notably, *M. bovis* 1173P2 produced significantly higher ssDNA concentrations than *M. abscessus* and *M. smegmatis* ($p < 0.05$), suggesting that *M. bovis* is more susceptible to microwave-induced disruption. This observation may be attributed to differences in cell wall composition and structure, as electron microscopy (EM) revealed more extensive membrane damage in *M. bovis* cells compared to the other isolates (Wilson-Garner et al., 2024).

The peak at 480 seconds likely represents the optimal point of DNA release before thermal degradation begins. Using the specific heat capacity equation:

$$\Delta T = (P \times t) / (c \times m)$$

where:

- P = 12 W (power input)
- t = 480 s (irradiation time)
- c = 4.2 J/g·°C (specific heat capacity of water)
- m = 10 g (sample mass)

$\Delta T = (12 \times 480) / (4.2 \times 10) = 5760 / 42 \approx 137$ °C

This theoretical estimate suggests that the sample could reach temperatures well above 100 °C under confined conditions. The decline in ssDNA concentration after 480 seconds is therefore likely due to thermal denaturation or fragmentation of DNA, rather than reduced bacterial lysis. Further confirmation could be obtained through temperature-controlled bulk heating experiments or by monitoring real-time sample temperature and reflected microwave power.

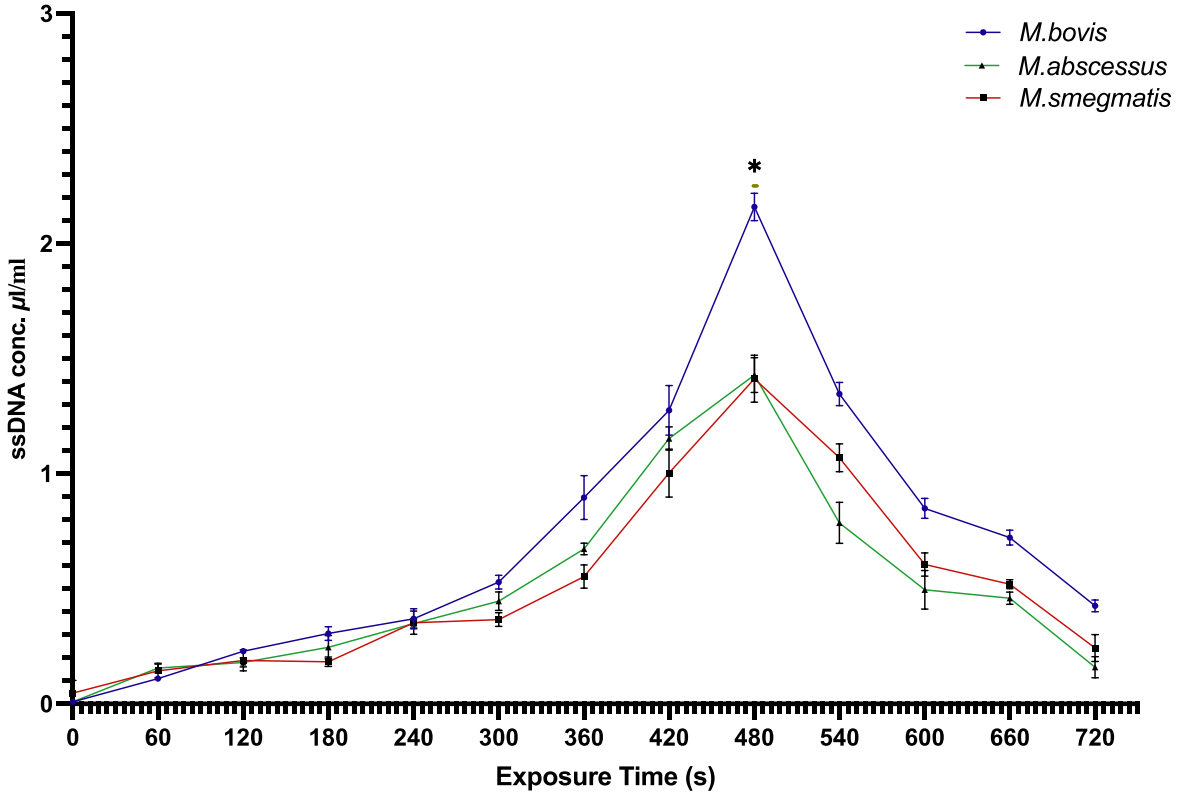

Figure 5.4 Microwave-mediated ssDNA release from bacterial isolates suspended in 10,000 µL volumes of water.

Microwaves induced the release of ssDNA from *M. bovis* 1173P2, *M. smegmatis* Mc2155 (S2), and *M. abscessus* (ATCC 19977) in water, each containing a total of 10^8 bacteria. Bacterial isolates were treated with 12W power level input for various lengths of time. The concentrations of the ssDNA were measured after an excitation period of 120 to 960 seconds (at 120-second intervals) using NanoDrop. The data were corrected by subtracting each respective t = 0s value. * denotes a significant p value < 0.05. Data represent mean of triplicate experiment ± standard deviation.

Figure 6.5 shows the results for *M. bovis*, *M. smegmatis*, and *M. abscessus* suspended in simulated sputum. As can be seen, there was a far more significant variation in free ssDNA levels than observed for the same bacteria suspended in water. The increased variability may result from the presence of methylcellulose in the simulated sputum, which, due to its viscosity properties, might interfere with the uniform dispersion of bacteria and hinder consistent DNA release after microwave treatment.

It is also more likely that this variation in results is due to problems with the NanoDrop measurement device, as it has been reported to yield inaccurate results using viscous materials (NanoDrop Microvolume Spectrophotometer - Thermo Fisher Scientific).

Additionally, Figure 6.5 illustrates that *M. bovis* and *M. smegmatis*, suspended in simulated sputum, produced their highest DNA yield at 480 seconds. However, at 360 seconds, ssDNA isolated from *M. abscessus* ATCC 19977 was higher than that from the other isolates, although this difference was not statistically significant (p value > 0.05). These results suggest that a 480-second excitation period for a 10,000 µL sample size might be sufficient for maximising DNA release from mycobacterial isolates.

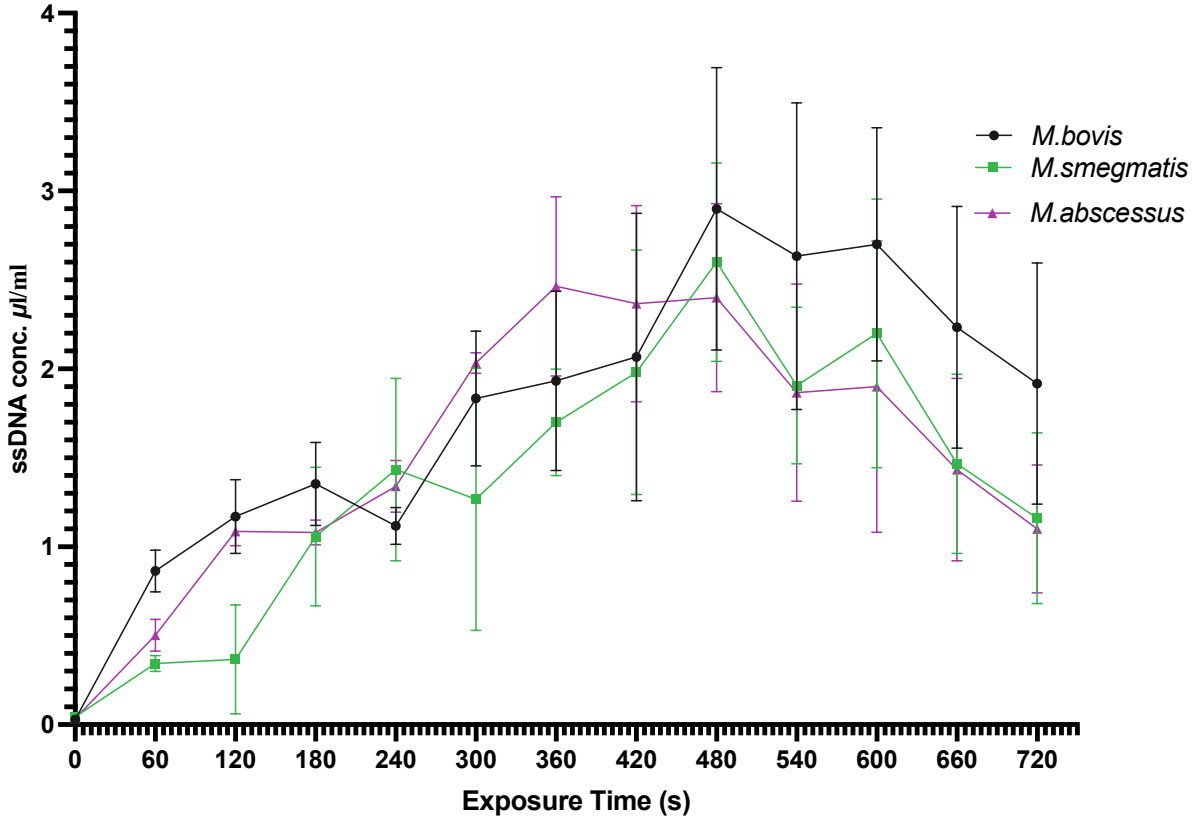

Figure 5.5 Microwave-mediated ssDNA released from bacterial isolates suspended in 10,000 µL volumes of simulated sputum.

Microwave-induced release of ssDNA from *M. bovis* 1173P2, *M. smegmatis* Mc2155 (S2), and *M. abscessus* ATCC 19977 was performed in 10,000 µL of simulated sputum, each containing a total of 10^8 bacteria. Bacterial isolates were treated with a 12 W power level input for various durations. The concentrations of ssDNA were measured after an excitation period of 120 to 960 seconds (at 120-second intervals) using a NanoDrop. The data were corrected by subtracting the respective t = 0 s values. Data represent mean of triplicate experiment ± standard deviation.

5.6.2 Detection of *M. bovis* ssDNA using the 10,000 µL cartridge in combination with the ELOSHA assay

To assess the specificity of the ELOSHA assay for *M. bovis* 1173P2, the bacterium, as well as *M. smegmatis* Mc2155 (S2) and *M. abscessus* ATCC 19977, were suspended in either 10,000 µL of water or simulated sputum, each containing a total of 10^8 bacteria. They were then microwaved at a 12W power level for 480 seconds. The presence of target DNA was detected using *IS6110*- and *IS1081*-specific DNA probes in the ELOSHA assay.

The results in Figures 6.6 and 6.7 demonstrate that the assay effectively distinguished *M. bovis* 1173P2 suspended in water and simulated sputum from the other microorganisms. However, after normalising the data with the no-template control (NTC), the signal was more potent when *M. bovis* 1173P2 was suspended in water compared to simulated sputum. This difference in signal intensity was statistically significant for both gene targets (p value < 0.05). The observed disparity may be attributed to the higher viscosity of simulated sputum, which could impact the efficiency of the ELOSHA washing steps and the recovery of specific anchored magnetic beads.

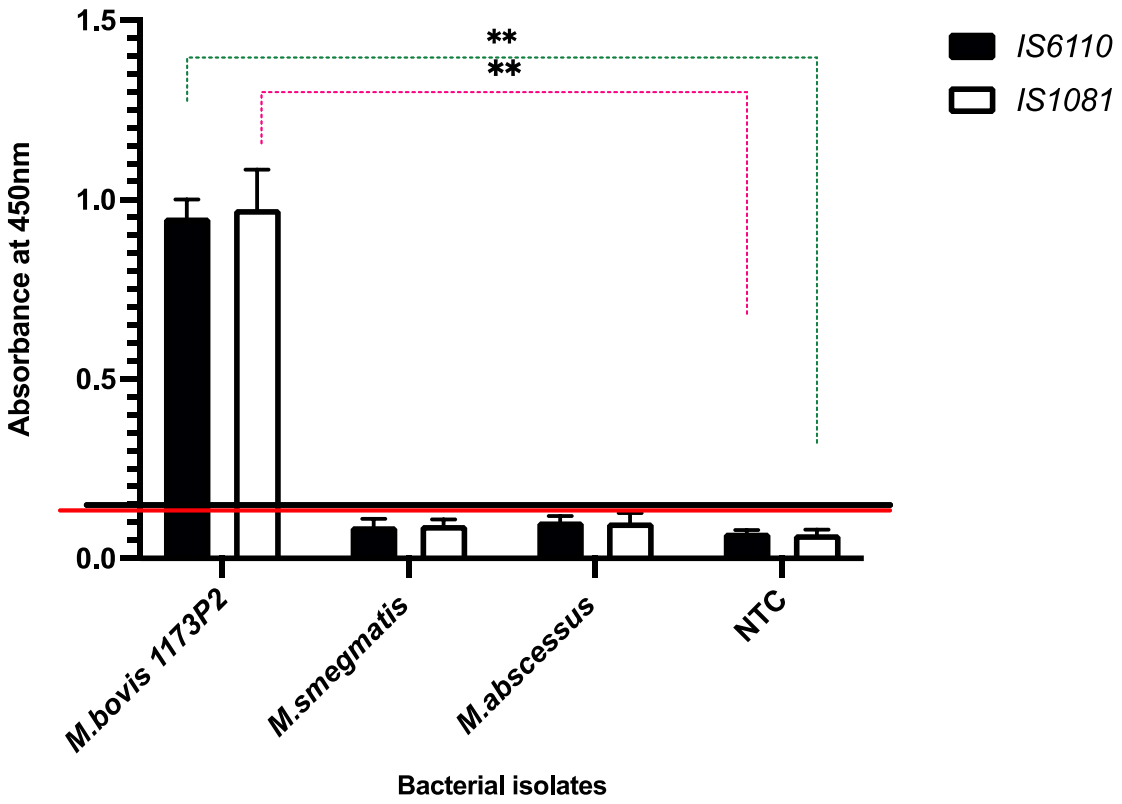

Figure 5.6 Distinguishing *M. bovis* 1173P2 from other mycobacteria suspended in 10,000 µL volumes of water using *IS6110*- and *IS1081*-specific DNA probes.

Genomic material was released from *M. bovis* 1173P2 (suspended in water at a final concentration of 10^8 bacteria in 10,000 µL). The bacterial suspensions were exposed to microwave radiation at 12 W for 480 seconds. The ability to distinguish between *M. bovis* and non-bovis isolates relied on the magnitude of the HRP-generated colour change, determined by measuring the mean absorbance. The cut-off concentrations for a negative sample (*M. abscessus*) for both probes were calculated as 0.15 and 0.14, respectively. These values are depicted as black (*IS6110*) and red (*IS1081*) lines. An NTC was included. Data represent mean of triplicate experiment ± standard deviation.. **Represents a p value < 0.001.

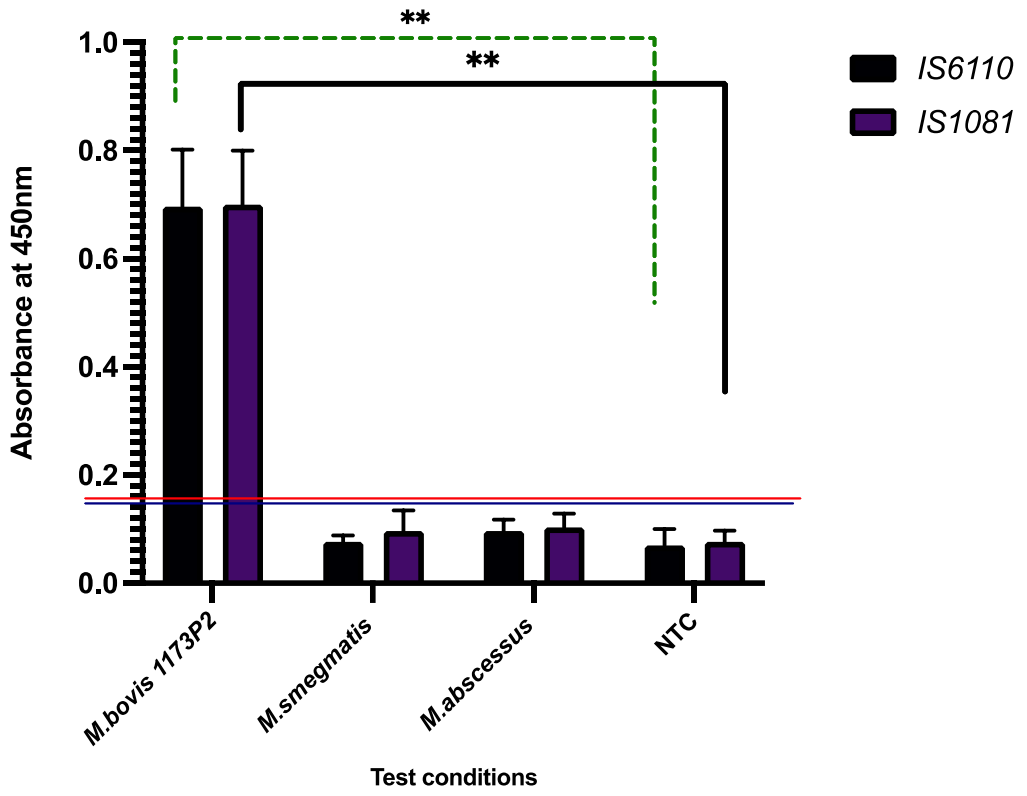

Figure 5.7 Distinguishing *M. bovis* 1173P2 from other mycobacteria suspended in 10,000 µL volumes of simulated sputum using *IS6110*- and *IS1081*-specific DNA probes.

Genomic material was released from *M. bovis* 1173P2 (suspended in simulated sputum at a final concentration of 10^8 bacteria in 10,000 µL). The bacterial suspensions were exposed to microwave radiation at 12 W for 480 seconds. The ability to distinguish between *M. bovis* and non-bovis isolates relied on the magnitude of the HRP-generated colour change, determined by measuring the mean absorbance. The cut-off concentrations for a negative sample (*M. abscessus*) for both probes were calculated as 0.16 and 0.17, respectively. These values are depicted as blue (*IS6110*) and red (*IS1081*) lines. An NTC was included. Data represent mean of triplicate experiment ± standard deviation.**Represents a p value < 0.001.

5.6.3 Establishing the limit of detection of the *IS6110* and *IS1801* DNA probes for bacteria suspended in 10,000 µL volumes of water or simulated sputum

The sensitivity of the combined assay (microwave and ELOSHA) for microwaved *M. bovis* 1173P2 ssDNA suspended in water was assessed across a range of bacterial quantities: 10^8, 10^7, 10^6, 10^5, 10^4, 10^3, 10^2, and 10^1 bacteria per 10,000 µL sample. The lowest detectable bacterial quantity for both gene targets was 10^3 in the 10,000 µL sample (Figures 6.8, 6.9, 6.10, and 6.11).

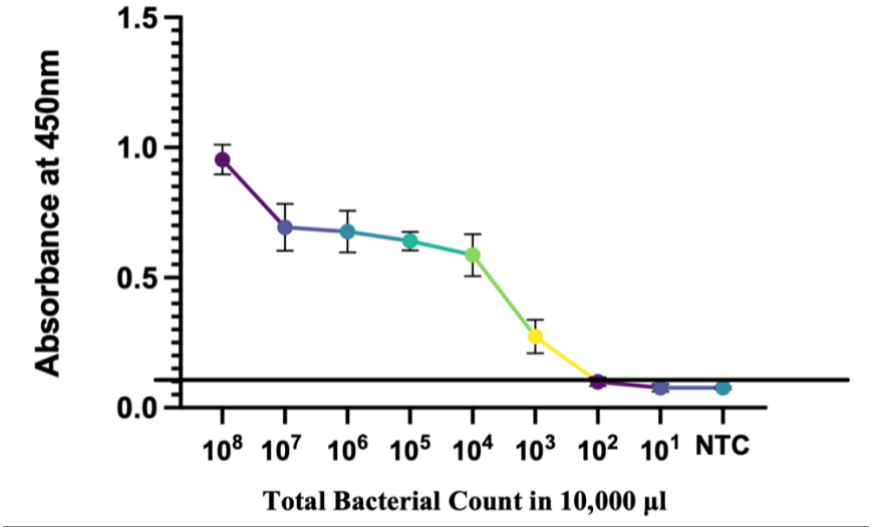

Figure 5.8 The lower limit of detect of the combined microwave/ELOSHA assay of bacteria suspended 10,000 µL of water using the *IS6110* gene probe.

A range of concentration of *M. bovis* 1173P2 bacteria suspended in 10,000 µL volume of water were microwaved in the large cartridge at 12W for 8 minutes. The resulting released ssDNA was detected using the *IS6110* gene probe and the ELOSHA assay. The cut-off value of 0.09 nm (black line). The no template control (NTC) was used as the negative to determine the cut-off value. The data is presented as the mean of triplicate experiments ± standard error.

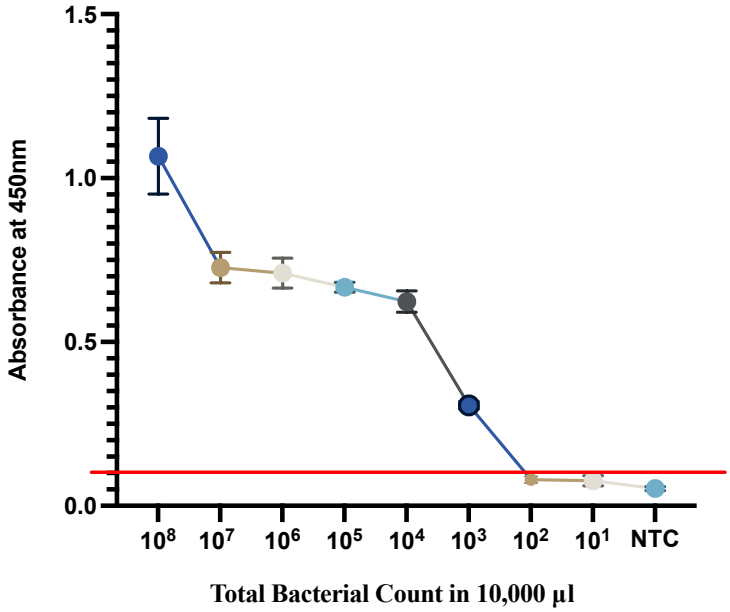

Figure 5.9 The lower limit of detect of the combined microwave/ELOSHA assay of bacteria suspended 10,000 µL of water using the *IS1081* gene probe.

A range of concentration of *M. bovis* 1173P2 bacteria suspended in 10,000 µL volume of water were microwaved in the large cartridge at 12W for 8 minutes. The resulting released ssDNA was detected using the *IS1081* gene probe and the ELOSHA assay. The cut-off value of 0.10 nm (rad line) .The no template control (NTC) was used as the negative to determine the cut-off value. The data is presented as the mean of triplicate experiments ± standard error.

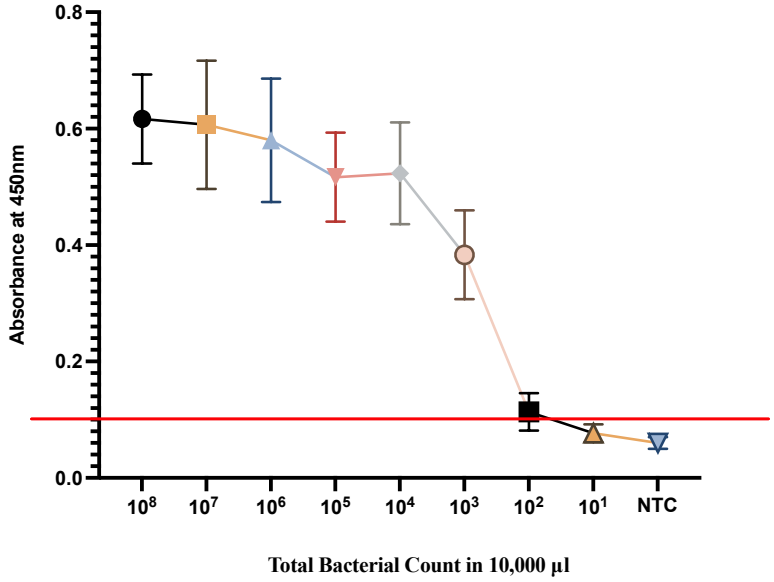

Figure 5.10 The lower limit of detect of the combined microwave/ELOSHA assay of bacteria suspended 10,000 µL of simulated sputum using the *IS6110* gene probe.

A range of concentration of *M. bovis* 1173P2 bacteria suspended in 10,000 µL volume of simulated sputum were microwaved in the large cartridge at 12W for 8 minutes. The resulting released ssDNA was detected using the *IS6110* gene probe and the ELOSHA assay. The cut-off value of 0.12 nm (rad line) . The no template control (NTC) was used as the negative to determine the cut-off value. The data is presented as the mean of triplicate experiments ± standard error.

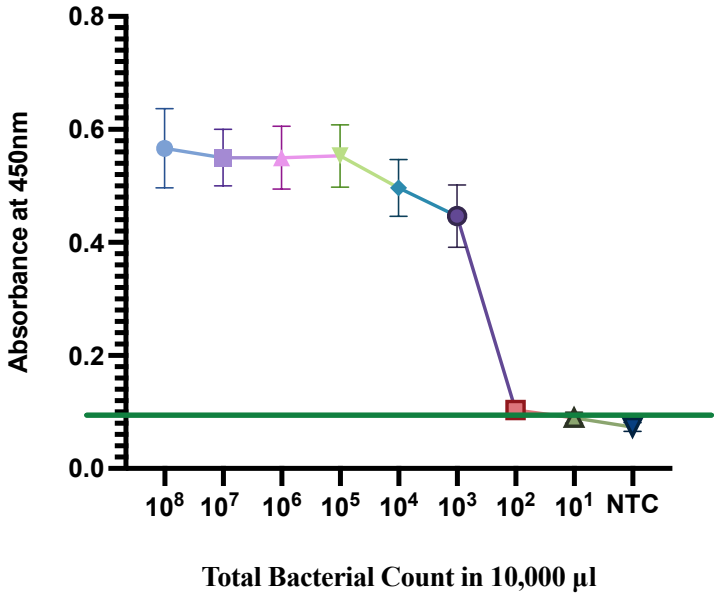

Figure 5.11 The lower limit of detect of the combined microwave/ELOSHA assay of bacteria suspended 10,000 µL of simulated sputum using the *IS1081* gene probe.

A range of concentration of *M. bovis* 1173P2 bacteria suspended in 10,000 µL volume of simulated sputum were microwaved in the large cartridge at 12W for 8 minutes. The resulting released ssDNA was detected using the *IS1081* gene probe and the ELOSHA assay. The cut-off value of 0.1 nm (green line) The no template control (NTC) was used as the negative to determine the cut-off value. The data is presented as the mean of triplicate experiments ± standard error.

5.6.4 Determining the specificity of the ELOSHA assay in the presence of competing bacteria in 10,000 µL volumes of water or simulated sputum

To assess the specificity of the assay, aliquots of *M. bovis* 1173P2 DNA were combined with a cocktail of DNA isolated from *M. smegmatis* Mc2155(S2) and *M. abscessus* ATCC 19977 (positive mix) in 10,000 µL volumes of water or simulated sputum. The results were compared to those obtained for *M. bovis* 1173P2 ssDNA and the negative control (DNA cocktail minus *M. bovis* 1173P2 DNA). The concentration of all the microwave-extracted DNA was adjusted to be equivalent to that of the microwave-extracted *M. bovis* 1173P2 ssDNA (5.4 ng/µL) without any purification step. As depicted in Figures 6.12 and 6.13, the assay detected *M. bovis* 1173P2 DNA in the presence of the competing DNA.

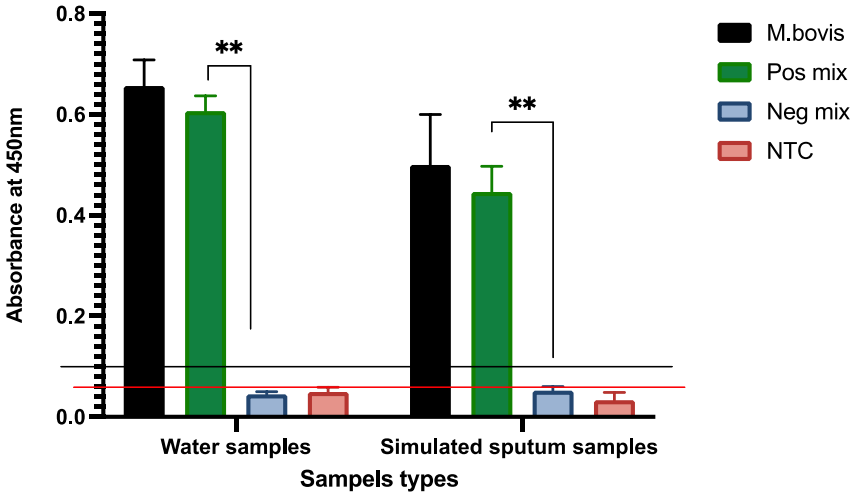

Figure 5.12 Specificity of the *IS6110* DNA probe for *M. bovis* 1173P2 in the presence of DNA extracted from other bacterial species suspended in 10,000 µL volumes of water or simulated sputum.

In both samples, the signal generated from *M. bovis* 1173P2 ssDNA and the positive mix (microwaved DNA from *M. bovis1173P2, M. abscessus* ATCC 1997 and *M. smegmatis* Mc2155 S2) was significantly higher than that of the negative mix microwaved DNA from the non-bovis isolates (*M. abscessus* ATCC 19977 and *M. smegmatis* Mc2155S2) and the NTC. The cut-off value for a positive test was determined at an absorbance value of 0.08 and 0.10 using the negative mix as the control for cut-off determination, as represented by the orange and black horizontal lines for the water samples (orange line) and simulated sputum (black line) genes, respectively. Data represent mean of triplicate experiment ± standard deviation., where. ** represents p value < 0.001.

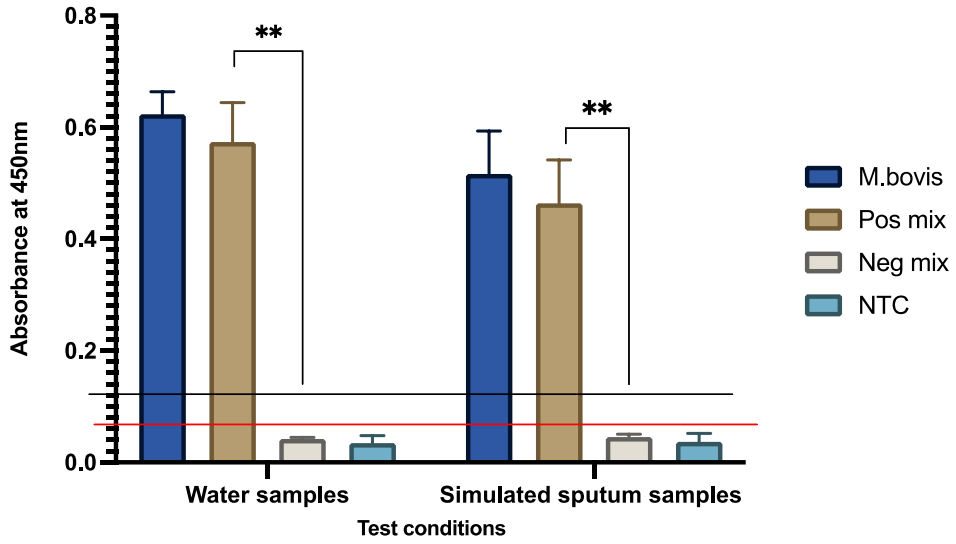

Figure 5.13 Specificity of the *IS1081* DNA probe for *M. bovis* 1173P2 in the presence of DNA extracted from other bacterial species suspended in 10,000 µL volumes of water or simulated sputum.

In both samples, the signal generated from *M. bovis* 1173P2 ssDNA and the positive mix (microwaved DNA from *M.bovis1173P2, M. abscessus* ATCC 19977 and *M. smegmatis* Mc2155 S2) was significantly higher than that of the negative mix microwaved DNA from non-bovis isolates (*M. abscessus* ATCC 19977 and *M. smegmatis* Mc2155 S2)) and the NTC. The cut-off value for a positive test was determined at an absorbance value of 0.11 and 0.08 using the negative mix as the control for cut-off determination, as represented by the orange and black horizontal lines for the water samples (orange line) and simulated sputum (black line) genes, respectively .Data represent mean of triplicate experiment ± standard deviation. **Represents *p* value < 0.001.

5.6.5 Examining the impact of reducing the sample volume upon the detection of target DNA in 5,000 µL and 10,000 µL samples

To study the effect of the sample volume on the capture of bacterial DNA, 10 ng of ssDNA chemically (Qiagen) extracted from *M. bovis* 1173P2 was suspended in 5,000 µL and 10,000 µL of water. As shown in Figure 6.14, the signal generated by the sample suspended in 5,000 µL was significantly higher (*p* value < 0.001) than that of the 10,000 µL suspension. This result demonstrates the need to optimise the ELOSHA method further to ensure the capture of all target DNA by the magnetic nanoparticles when the target is present at low concentrations.

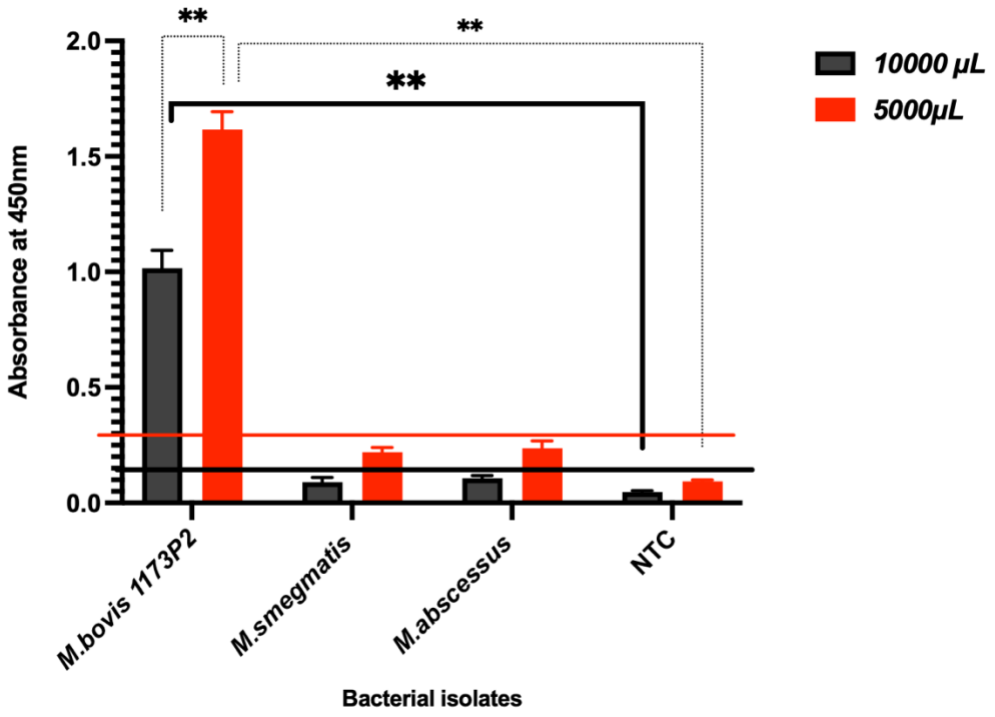

Figure 5.14 The effect of sample volume upon the ability of the ELOSHA assay to detect target DNA. A10 ng of ssDNA extracted from *M. bovis* 1173P2 using the Qiagen method was suspended in 5,000 µL or 10,000 µL of water.

ssDNA from *M. abscessus* ATCC 19977 and *M. smegmatis* Mc2155 S2 was also suspended in separate 5,000 µL or 10,000ul of water. The ELOSHA assay was performed as previously described using *IS1081* DNA Probe-Functionalised C1 MPs. The ability to distinguish between *M. bovis* and non-bovis isolates relied on the magnitude of the HRP-generated colour change, which was determined by measuring the mean absorbance. The cut-off concentrations for a negative sample (*abscessus* ATCC 19977) for both probes were calculated as 0.13 and 0.35, respectively. These values are depicted as black (10,000 µL) and red (5000 µL) lines. An NTC was included. Data represent mean of triplicate experiment ± standard deviation.**Represents a significant value (p value < 0.001).

5.7 Discussion

The first goal of this chapter was to maximise the isolation of ssDNA from *M. bovis* 1173P2 using a combination of microwaves and a large sample cartridge (10,000 µL) designed specifically for this purpose. The levels of ssDNA released from three test bacteria—*M. bovis* 1173P2, *M. abscessus* ATCC 19977, and *M. smegmatis* Mc2155(S2)—suspended in water and simulated sputum were compared. Significantly higher levels of ssDNA were released from *M. bovis* 1173P2 suspended in water than from the other two strains.

Electron microscopy images of these microwaved bacteria revealed marked changes in the cell wall ultrastructure of *M. bovis*, which were not seen in the images of the other two organisms (Wilson-Garner et al., 2024). These images, which highlight the structural alterations in *M. bovis*, are included in Appendix 1 for reference.

Although mycobacteria's fundamental cell wall structure is consistent across species, known differences in the chemical composition of cell wall constituents might explain variations in DNA release (Butler & Guthertz, 2001). Mycolic acids, exclusive to this genus, are a significant element of the mycobacterial cell wall, providing an additional hydrophobic barrier through which DNA must traverse. The mycolic acid content of *M. bovis* differs from that of the other test mycobacteria, and it is tempting to speculate that this difference may contribute to the greater DNA release from this species (Truyts et al., 2024).

Several factors—such as viscosity and chemical composition—could account for the variability observed in ssDNA results regarding bacteria suspended in simulated sputum. While water is known for its high polarity, simulated sputum contains nitrocellulose, which is less polar. This is relevant because microwave radiation requires interaction with polar molecules (Tanaka and Sato, 2007). Therefore, nitrocellulose in simulated sputum may limit the interaction with microwaves, potentially hindering the radiation penetration necessary for

optimal DNA isolation (Gupta & Prasad, 2016). Additionally, the operation of the NanoDrop spectrophotometer is adversely affected by viscous samples. Thus, any variations in ssDNA results could partly stem from the limitations of the measurement method rather than actual biological variability.

It is important to note that these challenges may not apply when working with real-world sputum samples. In clinical settings, compounds such as mucolytic agents can be employed to reduce sputum viscosity, potentially improving the efficacy of DNA extraction methods. Future studies could explore the impact of using such compounds to optimise DNA extraction from actual sputum samples and whether they mitigate the effects of viscosity on analytical outcomes.

Regarding the sensitivity of the large sample volume cartridge compared to the small-volume Microcentrifuge tube approach, both methods exhibited a lower detection limit of approximately 1,000 bacteria. Although these values were similar, it is important to note that they represent the total number of bacteria recovered from the samples, which differed by a factor of 10 in volume. When expressed as CFU/mL, the lower limit of detection for the Microcentrifuge tube method (200 µL) was approximately 5,000 bacteria/mL, whereas for the large cartridge (10,000 µL), it corresponded to approximately 100 bacteria/mL

Our results suggest that enhancing the sensitivity of the large cartridge approach should be possible. By reducing the sample volume to 5,000 µL but maintaining the other parameters, the assay generated an approximately double signal observed when the sample volume was 10,000 µL. This may be attributed to an increased local concentration of DNA molecules in smaller volumes, which enhances their likelihood of binding to the magnetic beads. The reduced diffusion distance in smaller sample volumes can also facilitate more efficient hybridisation.

These findings highlight the critical role of bead-to-target ratio and probe concentration in determining assay sensitivity. Modifications to the number of magnetic beads, the agitation parameters, the concentration of detector probes, and signal reporter chemistry should be considered to enhance the assay's efficacy.

As previously noted, the use of HRP as a reporter system has its drawbacks. The enzyme's biological activity is adversely affected by microwaves, meaning that it must be added after microwave exposure. Also, its mode of action requires that processed samples be repeatedly washed to remove contaminating organic material, which can lead to increased processing time and lower throughput.

Chapter 7 General Discussion

6.1 General discussion

This project aimed to advance the development of a point-of-care (POC) assay capable of detecting the presence of *M. tuberculosis* in clinical samples. This builds on previous research between the Cardiff Schools of Engineering and Pharmacy, which sought to develop a microwave-based POC assay to detect pathogenic microorganisms in clinical samples. The current project employed the BCG strain of *M. bovis*, a harmless relative of *M. tuberculosis* that shares considerable genetic homology with the latter. The following objectives were established:

1. To evaluate and compare different DNA extraction methods from bacteria suspended in water and simulated sputum, focusing on yield, extraction time, and quality.
2. To develop high sensitivity and specificity gene targets for *M. bovis* as a surrogate model for *M. tuberculosis*.
3. To optimise DNA capture methods for small sample volumes (200 μL) of bacteria suspended in water and simulated sputum.
4. To increase the sample volume (10,000 μL) to more closely model real-world clinical samples.

The rapid release of target DNA from a pathogen at a scale and purity compatible with the downstream assay system is a fundamental requirement of any DNA-based detection system. In Chapter 3, the ability of different approaches to release DNA from *M. bovis* suspended in water and simulated sputum was evaluated and compared. Releasing DNA from this species of microorganism is challenging due to the complex nature of the cell wall. In a previous study, microwaves were used to release DNA from *M. abscessus*, a fast-growing relative of *M. bovis* (Ahortor, 2019). As expected, exposure to microwaves resulted in DNA release

from bacteria suspended in either water or simulated sputum in less than a minute—considerably faster than any of the other methods evaluated.

Somewhat surprisingly, the level of DNA purity, as determined by optical density measurements, was comparable to that seen for DNA isolated using the commercial Qiagen method. In a previous study, it was shown that exposure of *M. smegmatis* to microwaves under similar conditions resulted in temporary disruption of the cell wall, allowing latex particles to enter the cell while leaving the body of the bacteria intact (Ahortor et al., 2020). It is intriguing to speculate that temporary microwave-mediated disruption may have resulted in the release of intracellular DNA while retaining the bulk of the cellular material within the bacterium's structure.

It was also observed that the concentration of single-stranded DNA (ssDNA) released following microwave treatment consistently exceeded that of double-stranded DNA (dsDNA), which is likely attributable to microwave-induced denaturation or strand separation, as previously described (Ranjha et al., 2018). This phenomenon may be particularly pronounced in small-volume formats (e.g. 200 µL Eppendorf tubes), where constrained geometry and reduced thermal mass can promote the formation of localised hotspots, resulting in non-uniform temperature distributions and enhanced strand disruption. Whether this disproportionate ssDNA yield is maintained under large-volume conditions (e.g. 10 mL cartridge format) remains to be fully elucidated; however, the larger thermal mass and lower surface-area-to-volume ratio are expected to mitigate localised overheating effects. From an assay design perspective, this preferential release of ssDNA is advantageous, as the hybridisation probes employed are specific to single-stranded target sequences.

Chapter 4 describes the development of specific probes for *M. bovis* / *M. tuberculosis* based on proven diagnostic PCR primers. Individual nucleotide sequences were modified to meet

the requirements of our assay format while maintaining target specificity. Due to the genetic variation of the global *M. tuberculosis* population, detection rates have been reported to increase from 77.1% to 89.2% when multiple gene targets are employed (Kulkarni et al., 2012).

A literature review identified three potential gene targets: *IS6110*, *mpb64*, and *IS1081*. While the presence of *IS6110* and *IS1081* was confirmed in the two *M. bovis* isolates used in this study, an *mpb64*-specific signal could not be generated. A subsequent literature review revealed that this was uncommon (Liu et al., 1993). Given our reliance on these isolates to drive the development of the assay, this gene target was omitted from our subsequent work.

In Chapter 5, the ability of our *IS6110* and *IS1081*-specific probes to detect microwaved *M. bovis* suspended in 200 µL of water or simulated sputum, when attached to magnetic nanoparticles, was confirmed. Preliminary specificity studies confirmed that our probes could distinguish *M. bovis* from *M. smegmatis* and *M. abscessus*. Further studies against a larger and more diverse panel of bacterial isolates will be required to confirm specificity.

Regarding sensitivity, the assay detected 0.6 pg/µL of chemically purified DNA target and 10^3 microwaved *M. bovis* bacilli suspended in either water or simulated sputum. This makes the current version of the assay more sensitive than smear microscopy (LOD 10^5), which is the current paradigm for tuberculosis diagnosis. However, it is less sensitive than PCR, which typically reaches 10^1 to 10^2 bacilli (Wakode et al., 2022). Further work is needed to optimise the sensitivity of the assay system.

Different optimisation protocols were tested to improve the assay's sensitivity, specificity, and efficiency for bacteria suspended in water and simulated sputum. In its current configuration, the assay required approximately 90 minutes to generate a result. While this

timeframe is faster than PCR-based detection assays, such as GeneXpert (which requires two hours to generate a result), further reduction would be beneficial (Wakode et al., 2022).

Results suggest the potential to enhance sensitivity and reduce the time required to generate a result. A major time-saving could be made by replacing the HRP enzyme reporter with a fluorescence probe, a strategy previously reported by Aslan et al. (2008) and Joshi et al. (2014). This approach eliminates the need for the time-consuming washing steps required by ELOSHA.

To enhance the assay's sensitivity, a sample cartridge of increased size, capable of handling samples up to 10,000 µL, was designed and manufactured. This cartridge could be incorporated into a portable handheld diagnostic device. In Chapter 6, the optimisation of the release and subsequent detection of ssDNA from microwaved *M. bovis* suspended in either water or simulated sputum within this new cartridge is described. Using this approach, the lower detection limit was reduced to 100 bacteria/mL, a ten-fold increase in sensitivity compared to the previous method. Interestingly, a greater level of DNA release was observed from *M. bovis* compared to the other mycobacterial species following microwave irradiation, a phenomenon not observed at the 200 µL level. This could reflect differences in the chemical composition of the cell wall of *M. bovis* and the fact that at the 200 µL level, the microwave power levels were optimised using *M. abscessus*, not *M. bovis*. This underscores the importance of optimising the system using the ultimate target organism and real-world samples.

6.2 Conclusions

In this study, the development of an assay for the rapid detection of *M. bovis* (used as a surrogate for *M. tuberculosis*) in water and simulated sputum samples was advanced. It was

demonstrated that microwaves can rapidly release DNA from mycobacteria, with *M. bovis* exhibiting a different response to microwave energy than other mycobacterial species. The sample volume that could be processed was increased from 200 µL to 10,000 µL through a combination of microwaves and magnetic nanoparticles. As a result, the detection limit was decreased from 5,000 to 100 bacteria/mL using this approach. The results suggest that there is potential to enhance the assay's sensitivity while simultaneously reducing the time required to generate a result.

6.3 Future Work

To further advance the development of a rapid point-of-care assay for mycobacteria, the following research challenges need to be addressed:

1. **Confirming the assay's specificity for clinical isolates:** Work has focused on a small number of laboratory strains, which may only approximate global genetic diversity. In the future, the specificity of the assay will be confirmed using a diverse collection of real-world clinical isolates.
2. **Improving the model for clinical samples:** While synthetic sputum can model some of the physical properties of sputum, it lacks host-derived cellular material, making it an approximation of clinical samples. Future studies will employ a macrophage infection model, previously developed in this laboratory, to confirm the assay's ability to detect intracellular organisms. Additionally, the efficacy of the approach will be validated using clinical samples.
3. **Developing probes for rifampicin resistance:** Studies have shown that the inclusion of multiple detection targets increases an assay's predictive power. In future work, DNA probes capable of detecting rifampicin resistance will be developed, and the potential for multiplexing these probes with the diagnostic probes developed in this study will be explored.

4. **Enhancing assay sensitivity:** This study's results identified several areas in which sensitivity could be enhanced, including optimising nanoparticle size, DNA probe loading, and contact with target DNA, aiming to achieve sensitivity levels comparable to PCR.
5. **Reducing assay time:** To reduce the time required to generate results, the HRP enzyme reporter will be replaced with a fluorophore, such as Alexa 495. Previous studies undertaken in the Baillie laboratory have shown that this approach significantly reduces the time needed to generate results.
6. **Developing an integrated system:** Future work will focus on developing an integrated system that combines all assay elements into a single device. This system will minimise operator interaction, reduce the risk of exposure to the agent, and generate simple-to-interpret results.

Reference

Abebe, G., Aragaw, D. and Tadesse, M. 2020. Fluorescence microscopy for the diagnosis of smear-negative pulmonary tuberculosis in Ethiopia. *African Journal of Laboratory Medicine* 9(1). doi: 10.4102/ajlm.v9i1.810.

Abi El Hessen, T., Saleem, S., Hani, R.H., Chadli, F.Z. and Makarem, J.A. 2022. Peritoneal Tuberculosis Mimicking Peritoneal Carcinomatosis in an Immunocompetent Patient. *Cureus*. doi: 10.7759/cureus.31464.

Abuzerr, S. and Zinszer, K. 2023. Computer-aided diagnostic accuracy of pulmonary tuberculosis on chest radiography among lower respiratory tract symptoms patients. *Frontiers in Public Health* 11. doi: 10.3389/fpubh.2023.1254658.

AĞEL, E., SAĞCAN, H., CEYHAN, İ. and DURMAZ, R. 2020. Optimization of isothermal amplification method for *Mycobacterium tuberculosis* detection and visualization method for fieldwork. *TURKISH JOURNAL OF MEDICAL SCIENCES* 50(4), pp. 1069–1075. doi: 10.3906/sag-1910-6.

Ahortor, E.K., Malyshev, D., Williams, C.F., Choi, H., Lees, J., Porch, A. and Baillie, L. 2020. The biological effect of 2.45 GHz microwaves on the viability and permeability of bacterial and yeast cells. *Journal of Applied Physics* 127(20), p. 204902. Available at: https://doi.org/10.1063/1.5145009.

Allwood, B.W. et al. 2020. Transition from restrictive to obstructive lung function impairment during treatment and follow-up of active tuberculosis. *International Journal of Chronic Obstructive Pulmonary Disease* 15, pp. 1039–1047. doi: 10.2147/COPD.S219731.

Alsayed, S.S.R. and Gunosewoyo, H. 2023. Tuberculosis: Pathogenesis, Current Treatment Regimens and New Drug Targets. *International Journal of Molecular Sciences* 24(6), p. 5202. doi: 10.3390/ijms24065202.

Andama, A. et al. 2022. Accuracy of Tongue Swab Testing Using Xpert MTB-RIF Ultra for Tuberculosis Diagnosis. *Journal of Clinical Microbiology* 60(7). doi: 10.1128/jcm.00421-22.

Arbués, M.D. and Rossetti, M.L.R. 2024. Evaluation of the GeneXpert MTB/RIF to diagnose tuberculosis in a public health laboratory. *Revista de Saúde Pública* 58(1), p. 3. doi: 10.11606/s1518-8787.2024058005306.

Arias-Carrasco, R., Vásquez-Morán, Y., Nakaya, H.I. and Maracaja-Coutinho, V. 2018. StructRNAfinder: an automated pipeline and web server for RNA families prediction. *BMC Bioinformatics* 19(1), p. 55. doi: 10.1186/s12859-018-2052-2.

Armstrong, D.T., Eisemann, E. and Parrish, N. 2023. A Brief Update on Mycobacterial Taxonomy, 2020 to 2022. *Journal of Clinical Microbiology* 61(4). doi: 10.1128/jcm.00331-22.

Asai, Y., Nakatsui, M. and Matsuno, H. 2024. Editorial: Systems bioinformatics for medicine. *BioSystems* 239, p. 105211. doi: 10.1016/j.biosystems.2024.105211.

Aslan, K., Previte, M.J.R., Zhang, Y., Gallagher, T., Baillie, L. and Geddes, C.D. 2008. Extraction and Detection of DNA from *Bacillus anthracis* Spores and the Vegetative Cells within 1 min. *Analytical Chemistry* 80(11), pp. 4125–4132. doi: 10.1021/ac800519r.

Athanasopoulou, K., Boti, M.A., Adamopoulos, P.G., Skourou, P.C. and Scorilas, A. 2021. Third-Generation Sequencing: The Spearhead towards the Radical Transformation of Modern Genomics. *Life* 12(1), p. 30. doi: 10.3390/life12010030.

Ayan, E. et al. 2022. Cooperative allostery and structural dynamics of streptavidin at cryogenic- and ambient-temperature. *Communications Biology* 5(1), p. 73. doi: 10.1038/s42003-021-02903-7.

Ayele, B.A. and Amogne, W. 2021. Central Nervous System Tuberculosis (CNS-TB) in treated HIV-infected adults in Tikur Anbessa Specialized Hospital, Ethiopia: A cross-sectional study. *Journal of Clinical Tuberculosis and Other Mycobacterial Diseases* 24, p. 100252. doi: 10.1016/j.jctube.2021.100252.

Azcárate, J.C., Corthey, G., Pensa, E., Vericat, C., Fonticelli, M.H., Salvarezza, R.C. and Carro, P. 2013. Understanding the Surface Chemistry of Thiolate-Protected Metallic Nanoparticles. *The Journal of Physical Chemistry Letters* 4(18), pp. 3127–3138. doi: 10.1021/jz401526y.

Baghdasaryan, Z., Babajanyan, A., Parsamyan, H., Friedman, B., Kim, S., Lee, J.-H. and Lee, K. 2022. 3D visualization of microwave electric and magnetic fields by using a metasurface-based indicator. *Scientific Reports* 12(1), p. 6150. doi: 10.1038/s41598-022-10073-7.

Bahadır, E.B. and Sezgintürk, M.K. 2016. Lateral flow assays: Principles, designs and labels. *TrAC Trends in Analytical Chemistry* 82, pp. 286–306. doi: 10.1016/j.trac.2016.06.006.

Banerjee, U., Baloni, P., Singh, A. and Chandra, N. 2021. Immune Subtyping in Latent Tuberculosis. *Frontiers in Immunology* 12. doi: 10.3389/fimmu.2021.595746.

Barchanski, A., Hashimoto, N., Petersen, S., Sajti, C.L. and Barcikowski, S. 2012. Impact of Spacer and Strand Length on Oligonucleotide Conjugation to the Surface of Ligand-Free Laser-Generated Gold Nanoparticles. *Bioconjugate Chemistry*23(5), pp. 908–915. doi: 10.1021/bc200462b.

Barker, E. et al. 2023. A cost-effectiveness evaluation of latent tuberculosis infection screening of a migrant population in Malaysia. *Scientific Reports* 13(1), p. 2390. doi: 10.1038/s41598-023-29648-z.

Bayot, M.L., Mirza, T.M. and Sharma, S. 2024. Acid Fast Bacteria.
Bellaousov, S., Reuter, J.S., Seetin, M.G. and Mathews, D.H. 2013. RNAstructure: web servers for RNA secondary structure prediction and analysis. *Nucleic Acids Research* 41(W1), pp. W471–W474. doi: 10.1093/nar/gkt290.

Bello, G.L. et al. 2020. Improvement of *Mycobacterium tuberculosis* detection in sputum using DNA extracted by sonication. *The Brazilian Journal of Infectious Diseases* 24(5), pp. 398–404. Available at: https://linkinghub.elsevier.com/retrieve/pii/S1413867020301215 [Accessed: 16 September 2024].
BI, K. et al. 2022. The past, present and future of tuberculosis treatment. *Journal of Zhejiang University (Medical Sciences)* 51(6), pp. 657–668. doi: 10.3724/zdxbyxb-2022-0454.

Bohn, M.K. et al. 2020. Molecular, serological, and biochemical diagnosis and monitoring of COVID-19: IFCC taskforce evaluation of the latest evidence. *Clinical Chemistry and Laboratory Medicine (CCLM)* 58(7), pp. 1037–1052. doi: 10.1515/cclm-2020-0722.

Boom, W.H., Schaible, U.E. and Achkar, J.M. 2021. The knowns and unknowns of latent *Mycobacterium tuberculosis*infection. *Journal of Clinical Investigation* 131(3). doi: 10.1172/JCI136222.

Borham, M., Oreiby, A., El-Gedawy, A., Hegazy, Y., Khalifa, H.O., Al-Gaabary, M. and Matsumoto, T. 2022. Review on Bovine Tuberculosis: An Emerging Disease Associated with Multidrug-Resistant *Mycobacterium* Species. *Pathogens*11(7), p. 715. doi: 10.3390/pathogens11070715.

Borzova, V.A. et al. 2016. Kinetics of Thermal Denaturation and Aggregation of Bovine Serum Albumin. *PLOS ONE*11(4), p. e0153495. doi: 10.1371/journal.pone.0153495.

Bovo, D., Rugge, M. and Shiao, Y.H. 1999. Origin of spurious multiple bands in the amplification of microsatellite sequences. *Molecular Pathology* 52(1), pp. 50–51. doi: 10.1136/mp.52.1.50.

Brandenburg, J. et al. 2022. Tuberculostearic Acid-Containing Phosphatidylinositols as Markers of Bacterial Burden in Tuberculosis. *ACS Infectious Diseases* 8(7), pp. 1303–1315. doi: 10.1021/acsinfecdis.2c00075.

Brlek, P. et al. 2024. Implementing Whole Genome Sequencing (WGS) in Clinical Practice: Advantages, Challenges, and Future Perspectives. *Cells* 13(6), p. 504. doi: 10.3390/cells13060504.

Broger, T. et al. 2023. Diagnostic yield of urine lipoarabinomannan and sputum tuberculosis tests in people living with HIV: a systematic review and meta-analysis of individual participant data. *The Lancet Global Health* 11(6), pp. e903–e916. doi: 10.1016/S2214-109X(23)00135-3.

Brown, L., Wolf, J.M., Prados-Rosales, R. and Casadevall, A. 2015. Through the wall: extracellular vesicles in Gram-positive bacteria, mycobacteria and fungi. *Nature Reviews Microbiology* 13(10), pp. 620–630. doi: 10.1038/nrmicro3480.

Bruijns, B., Hoekema, T., Oomens, L., Tiggelaar, R. and Gardeniers, H. 2022. Performance of Spectrophotometric and Fluorometric DNA Quantification Methods. *Analytica* 3(3), pp. 371–384. doi: 10.3390/analytica3030025.

de Bruin, O.M., Chiefari, A., Wroblewski, D., Egan, C. and Kelly-Cirino, C.D. 2019. A novel chemical lysis method for maximum release of DNA from difficult-to-lyse bacteria. *Microbial Pathogenesis* 126, pp. 292–297. doi: 10.1016/j.micpath.2018.11.008.

Bwalya, P. et al. 2022. Characterization of embB mutations involved in ethambutol resistance in multi-drug resistant *Mycobacterium tuberculosis* isolates in Zambia. *Tuberculosis* 133, p. 102184. doi: 10.1016/j.tube.2022.102184.

Campelo, T.A., Cardoso de Sousa, P.R., Nogueira, L. de L., Frota, C.C. and Antas, P.R. 2022. Corrigendum: Revisiting the methods for detecting *Mycobacterium tuberculosis*: What has the new millennium brought thus far? *Access Microbiology* 4(1). doi: 10.1099/acmi.0.000294.

Canady, T.D., Berlyoung, A.S., Martinez, J.A., Emanuelson, C., Telmer, C.A., Bruchez, M.P. and Armitage, B.A. 2020. Enhanced hybridization selectivity using structured GammaPNA probes. *Molecules* 25(4), p. 970. doi: 10.3390/molecules25040970.

Carranza, C. and Chavez-Galan, L. 2019. Several routes to the same destination: Inhibition of phagosome-lysosome fusion by *Mycobacterium tuberculosis*. *The American Journal of the Medical Sciences* 357(3), pp. 184–194. doi: 10.1016/j.amjms.2018.12.003.

Chakravorty, S. et al. 2017. The new Xpert MTB/RIF ultra: Improving detection of *Mycobacterium tuberculosis* and resistance to Rifampin in an assay suitable for point-of-care testing. *mBio*. doi: 10.1128/mBio.00812-17.

Chang, A. et al. 2022. Metagenomic DNA sequencing to quantify *Mycobacterium tuberculosis* DNA and diagnose tuberculosis. *Scientific Reports* 12(1), p. 16972. doi: 10.1038/s41598-022-21244-x.
Chen, G. 2021. The nature of the sulfur-metallic bonds (metal = Ni, Pd, and Pt) in doped gold nanoclusters: A density functional approach. *Computational and Theoretical Chemistry* 1195, p. 113094. doi: 10.1016/j.comptc.2020.113094.

Chen, J. et al. 2022. Transmission of multidrug-resistant tuberculosis within family households by DTM-PCR and MIRU-VNTR genotyping. *BMC Infectious Diseases* 22(1), p. 192. doi: 10.1186/s12879-022-07188-7.

Chen, N. and Yuan, X. 2023. A quick DNA extraction method for high throughput screening in Gram-positive bacteria. *BIO-PROTOCOL* 13(8). doi: 10.21769/BioProtoc.4653.

Cheng, P. et al. 2020. The prevalence and mechanism of fluoroquinolone resistance in *Escherichia coli* isolated from swine farms in China. *BMC Veterinary Research* 16(1), p. 258. doi: 10.1186/s12917-020-02483-4.

Chew, Y.-L., Khor, M.-A. and Lim, Y.-Y. 2021. Choices of chromatographic methods as stability indicating assays for pharmaceutical products: A review. *Heliyon* 7(3), p. e06553. doi: 10.1016/j.heliyon.2021.e06553.

Chiang, C.-H., Tang, P.-U., Lee, G.H., Chiang, T.-H., Chiang, C.-H., Ma, K.S.-K. and Fang, C.-T. 2021. Prevalence of nontuberculous *Mycobacterium* infections versus tuberculosis among autopsied HIV patients in sub-Saharan Africa: A systematic review and meta-analysis. *The American Journal of Tropical Medicine and Hygiene* 104(2), pp. 628–633. doi: 10.4269/ajtmh.20-0973.

Chin, K.L., Sarmiento, M.E., Alvarez-Cabrera, N., Norazmi, M.N. and Acosta, A. 2020. Pulmonary non-tuberculous mycobacterial infections: Current state and future management. *European Journal of Clinical Microbiology & Infectious Diseases* 39(5), pp. 799–826. doi: 10.1007/s10096-019-03771-0.

Coleman, M., Martinez, L., Theron, G., Wood, R. and Marais, B. 2022. *Mycobacterium tuberculosis* transmission in high-incidence settings—new paradigms and insights. *Pathogens* 11(11), p. 1228. doi: 10.3390/pathogens11111228.

Collins, Á.B., Floyd, S., Gordon, S.V. and More, S.J. 2022. Prevalence of *Mycobacterium bovis* in milk on dairy cattle farms: An international systematic literature review and meta-analysis. *Tuberculosis* 132, p. 102166. doi: 10.1016/j.tube.2022.102166.

Collins, J.A. and Osheroff, N. 2024. Gyrase and topoisomerase IV: Recycling old targets for new antibacterials to combat fluoroquinolone resistance. *ACS Infectious Diseases* 10(4), pp. 1097–1115. doi: 10.1021/acsinfecdis.4c00128.

Correia-Neves, M. et al. 2019. Biomarkers for tuberculosis: The case for lipoarabinomannan. *ERJ Open Research* 5(1), pp. 00115–02018. doi: 10.1183/23120541.00115-2018.

Correia-Neves, M., Nigou, J., Mousavian, Z., Sundling, C. and Källenius, G. 2022. Immunological hyporesponsiveness in tuberculosis: The role of mycobacterial glycolipids. *Frontiers in Immunology* 13. doi: 10.3389/fimmu.2022.1035122.

Court, R. et al. 2021. Neuropsychiatric toxicity and cycloserine concentrations during treatment for multidrug-resistant tuberculosis. *International Journal of Infectious Diseases* 105, pp. 688–694. doi: 10.1016/j.ijid.2021.03.001.

Cronan, M.R. 2022. In the thick of it: Formation of the tuberculous granuloma and its effects on host and therapeutic responses. *Frontiers in Immunology* 13. doi: 10.3389/fimmu.2022.820134.

Curk, T. et al. 2020. Computational design of probes to detect bacterial genomes by multivalent binding. *Proceedings of the National Academy of Sciences* 117(16), pp. 8719–8726. doi: 10.1073/pnas.1918274117.

Dash, S., Rahman, S.R., Hines, H.M. and Feng, W. 2021. iBLAST: Incremental BLAST of new sequences via automated e-value correction. *PLOS ONE* 16(4), p. e0249410. doi: 10.1371/journal.pone.0249410.

Day, P.J., Flora, P.S., Fox, J.E. and Walker, M.R. 1991. Immobilization of polynucleotides on magnetic particles: Factors influencing hybridization efficiency. *Biochemical Journal* 278(3), pp. 735–740. doi: 10.1042/bj2780735.

Delahaye, C. and Nicolas, J. 2021. Sequencing DNA with nanopores: Troubles and biases. *PLOS ONE* 16(10), p. e0257521. doi: 10.1371/journal.pone.0257521.

Demers, A.-M., Boulle, A., Warren, R., Verver, S., van Helden, P., Behr, M.A. and Coetzee, D. 2010. Use of simulated sputum specimens to estimate the specificity of laboratory-diagnosed tuberculosis. *The International Journal of Tuberculosis and Lung Disease* 14(8), pp. 1016–1023.

Dian, S., Ganiem, A.R. and van Laarhoven, A. 2021. Central nervous system tuberculosis. *Current Opinion in Neurology*34(3), pp. 396–402. doi: 10.1097/WCO.0000000000000920.

Dinkele, R., Khan, P.Y. and Warner, D.F. 2024. *Mycobacterium tuberculosis* transmission: The importance of precision. *The Lancet Infectious Diseases* 24(7), pp. 679–681. doi: 10.1016/S1473-3099(24)00154-3.

Doğan, H.O. 2024. Metabolomics: A review of liquid chromatography mass spectrometry-based methods and clinical applications. *Turkish Journal of Biochemistry* 49(1), pp. 1–14. doi: 10.1515/tjb-2023-0095.

Dörr, T., Moynihan, P.J. and Mayer, C. 2019. Editorial: Bacterial cell wall structure and dynamics. *Frontiers in Microbiology* 10. doi: 10.3389/fmicb.2019.02051.

Egan, A.J.F., Errington, J. and Vollmer, W. 2020. Regulation of peptidoglycan synthesis and remodelling. *Nature Reviews Microbiology* 18(8), pp. 446–460. doi: 10.1038/s41579-020-0366-3.
Elrobaa, I.H., Khan, K. and Mohamed, E. 2024. The role of point-of-care testing to improve acute care and health care services. *Cureus*. doi: 10.7759/cureus.55315.

Falcao, B., Dsouza, N. and Gokarn, K. 2022. Effect of mutations on the structure of *Mycobacterium tuberculosis* KatG protein and interactions with Isoniazid – An in-silico study. *Research Journal of Biotechnology* 17(9), pp. 66–73. doi: 10.25303/1709rjbt66073.

Farinha, P., Coelho, J.M.P., Reis, C.P. and Gaspar, M.M. 2021. A comprehensive updated review on magnetic nanoparticles in diagnostics. *Nanomaterials* 11(12), p. 3432. doi: 10.3390/nano11123432.

Feng, J.-Y., Chen, W.-C., Chen, Y.-Y. and Su, W.-J. 2020. Clinical relevance and diagnosis of nontuberculous mycobacterial pulmonary disease in populations at risk. *Journal of the Formosan Medical Association* 119, pp. S23–S31. doi: 10.1016/j.jfma.2020.05.012.

Flores, J., Cancino, J.C. and Chavez-Galan, L. 2021. Lipoarabinomannan as a point-of-care assay for diagnosis of tuberculosis: How far are we to use it? *Frontiers in Microbiology* 12. doi: 10.3389/fmicb.2021.638047.

Frankena, K., White, P.W., O'Keeffe, J., Costello, E., Martin, S.W., Van Grevenhof, I. and More, S.J. 2007. Quantification of the relative efficiency of factory surveillance in the disclosure of tuberculosis lesions in attested Irish cattle. *Veterinary Record*. doi: 10.1136/vr.161.20.679.

Gao, M., Wu, Q., Wang, X., Sun, X., Li, M. and Bai, G. 2024. Advancements in LAM-based diagnostic kit for tuberculosis detection: Enhancing TB diagnosis in HIV-negative individuals. *Frontiers in Microbiology* 15. doi: 10.3389/fmicb.2024.1367092.

García-Díez, J., Saraiva, S., Moura, D., Grispoldi, L., Cenci-Goga, B.T. and Saraiva, C. 2023. The importance of the slaughterhouse in surveilling animal and public health: A systematic review. *Veterinary Sciences* 10(2), p. 167. doi: 10.3390/vetsci10020167.

Gcebe, N., Hlokwe, T.M., Bouw, A., Michel, A. and Rutten, V.P.M.G. 2024. The presence of esat-6 and cfp10 and other gene orthologs of the RD1 region in non-tuberculous mycobacteria, mycolicibacteria, mycobacteroides and mycolicibacter as possible impediments for the diagnosis of (animal) tuberculosis. *Microorganisms* 12(6), p. 1151. doi: 10.3390/microorganisms12061151.

Gloria, L. de L., Bastos, M.L., Santos Júnior, B. dos and Trajman, A. 2021. A simple protocol for tuberculin skin test reading certification. *Cadernos de Saúde Pública* 37(8). doi: 10.1590/0102-311x00027321.

Gong, W. and Wu, X. 2021. Differential diagnosis of latent tuberculosis infection and active tuberculosis: A key to a successful tuberculosis control strategy. *Frontiers in Microbiology* 12. doi: 10.3389/fmicb.2021.745592.

Gopal, P. et al. 2020. Pyrazinamide triggers degradation of its target aspartate decarboxylase. *Nature Communications*11(1), p. 1661. doi: 10.1038/s41467-020-15516-1.

Gu, Q., Josephs, E.A. and Ye, T. 2022. Hybridization and self-assembly behaviors of surface-immobilized DNA in close proximity: A single-molecule perspective. *Aggregate* 3(4). doi: 10.1002/agt2.186.

Guallar-Garrido, S., Campo-Pérez, V., Sánchez-Chardi, A., Luquin, M. and Julián, E. 2020. Each *Mycobacterium* requires a specific culture medium composition for triggering an optimized immunomodulatory and antitumoral effect. *Microorganisms* 8(5), p. 734. doi: 10.3390/microorganisms8050734.

Guerrero, D., Bautista, R., Villalobos, D.P., Cantón, F.R. and Claros, M.G. 2010. AlignMiner: A web-based tool for detection of divergent regions in multiple sequence alignments of conserved sequences. *Algorithms for Molecular Biology*5(1), p. 24. doi: 10.1186/1748-7188-5-24.

Gupta, E. et al. 2023. Fast track diagnostic tools for clinical management of sepsis: Paradigm shift from conventional to advanced methods. *Diagnostics* 13(2), p. 277. doi: 10.3390/diagnostics13020277.

Gupta, N. 2019. DNA extraction and polymerase chain reaction. *Journal of Cytology* 36(2), p. 116. doi: 10.4103/JOC.JOC_110_18.

Ha, D.T., Ghosh, S., Ahn, C.H., Segal, D.J. and Kim, M.-S. 2018. Pathogen-specific DNA sensing with engineered zinc finger proteins immobilized on a polymer chip. *The Analyst* 143(17), pp. 4009–4016. doi: 10.1039/C8AN00395E.

Hameed, H.A. et al. 2020. Detection of novel gene mutations associated with pyrazinamide resistance in multidrug-resistant *Mycobacterium tuberculosis* clinical isolates in southern China. *Infection and Drug Resistance* 13, pp. 217–227. doi: 10.2147/IDR.S230774.

Le Hang, N.T. et al. 2021. Phenotypic and genotypic features of the *Mycobacterium tuberculosis* lineage 1 subgroup in central Vietnam. *Scientific Reports* 11(1), p. 13609. doi: 10.1038/s41598-021-92984-5.

Harpaz, D., Eltzov, E., Ng, T.S.E., Marks, R.S. and Tok, A.I.Y. 2020. Enhanced colorimetric signal for accurate signal detection in paper-based biosensors. *Diagnostics* 10(1), p. 28. doi: 10.3390/diagnostics10010028.

Hedin, W. et al. 2023. A rough colony morphology of *Mycobacterium abscessus* is associated with cavitary pulmonary disease and poor clinical outcome. *The Journal of Infectious Diseases* 227(6), pp. 820–827. doi: 10.1093/infdis/jiad007.

Heidary, M., Shirani, M., Moradi, M., Goudarzi, M., Pouriran, R., Rezaeian, T. and Khoshnood, S. 2022. Tuberculosis challenges: Resistance, co-infection, diagnosis, and treatment. *European Journal of Microbiology and Immunology* 12(1), pp. 1–17. doi: 10.1556/1886.2021.00021.

Hertel, S., Spinney, R.E., Xu, S.Y., Ouldridge, T.E., Morris, R.G. and Lee, L.K. 2022. The stability and number of nucleating interactions determine DNA hybridization rates in the absence of secondary structure. *Nucleic Acids Research*50(14), pp. 7829–7841. doi: 10.1093/nar/gkac590.

Heyckendorf, J., Gillespie, S.H. and Ruhwald, M. 2020. Culture-free proof of *Mycobacterium tuberculosis*: A new assay for viable bacteria. *eBioMedicine* 62, p. 103117. doi: 10.1016/j.ebiom.2020.103117.

Ho, J., Marks, G.B. and Fox, G.J. 2015. The impact of sputum quality on tuberculosis diagnosis: A systematic review. *The International Journal of Tuberculosis and Lung Disease* 19(5), pp. 537–544. doi: 10.5588/ijtld.14.0798.

Holzheimer, M., Buter, J. and Minnaard, A.J. 2021. Chemical synthesis of cell wall constituents of *Mycobacterium tuberculosis*. *Chemical Reviews* 121(15), pp. 9554–9643. doi: 10.1021/acs.chemrev.1c00043.

Hong, J.M., Lee, H., Menon, N.V., Lim, C.T., Lee, L.P. and Ong, C.W.M. 2022. Point-of-care diagnostic tests for tuberculosis disease. *Science Translational Medicine* 14(639). doi: 10.1126/scitranslmed.abj4124.

Howard, S.T., Oughton, M.T., Haddad, A. and Johnson, W.M. 1998. Absence of the genetic marker IS 6110 from a strain of *Mycobacterium tuberculosis* isolated in Ontario. *Canadian Journal of Infectious Diseases* 9(1), pp. 48–53. doi: 10.1155/1998/292491.

Huang, J. et al. 2021. Two target genes based multiple cross displacement amplification combined with a lateral flow biosensor for the detection of *Mycobacterium tuberculosis* complex. *BMC Microbiology* 21(1), p. 267. doi: 10.1186/s12866-021-02328-6.

Huang, M. et al. 2022. Fast microwave heating-based one-step synthesis of DNA and RNA modified gold nanoparticles. *Nature Communications* 13(1), p. 968. doi: 10.1038/s41467-022-28627-8.

Huyen, M.N.T. et al. 2013. Characterisation of *Mycobacterium tuberculosis* isolates lacking IS 6110 in Viet Nam. *The International Journal of Tuberculosis and Lung Disease* 17(11), pp. 1479–1485. doi: 10.5588/ijtld.13.0149.

Ivanov, A.V., Safenkova, I.V., Biketov, S.F., Zherdev, A.V. and Dzantiev, B.B. 2023. Engineering of DNA structures attached to magnetic particles for effective trans- and cis-cleavage in Cas12-based biosensors. *International Journal of Molecular Sciences* 24(5), p. 4484. doi: 10.3390/ijms24054484.

Ivanova, O., Hoffmann, V.S., Lange, C., Hoelscher, M. and Rachow, A. 2023. Post-tuberculosis lung impairment: Systematic review and meta-analysis of spirometry data from 14,621 people. *European Respiratory Review* 32(168), p. 220221. doi: 10.1183/16000617.0221-2022.

Jacobo-Delgado, Y.M., Rodríguez-Carlos, A., Serrano, C.J. and Rivas-Santiago, B. 2023. *Mycobacterium tuberculosis*cell-wall and antimicrobial peptides: A mission impossible? *Frontiers in Immunology* 14. doi: 10.3389/fimmu.2023.1194923.

Jaganath, D. et al. 2020. Evaluation of multi-antigen serological screening for active tuberculosis among people living with HIV. *PLOS ONE* 15(6), p. e0234130. doi: 10.1371/journal.pone.0234130.
Jansson, L. et al. 2024. Assessment of DNA quality for whole genome library preparation. *Analytical Biochemistry* 695, p. 115636. doi: 10.1016/j.ab.2024.115636.

Johnson, T.M., Byrd, T.F., Drummond, W.K., Childs-Kean, L.M., Mahoney, M.V., Pearson, J.C. and Rivera, C.G. 2023. Contemporary pharmacotherapies for nontuberculosis mycobacterial infections: A narrative review. *Infectious Diseases and Therapy* 12(2), pp. 343–365. doi: 10.1007/s40121-022-00750-5.

Joshi, L.T., Mali, B.L., Geddes, C.D. and Baillie, L. 2014. Extraction and sensitive detection of toxins A and B from the human pathogen *Clostridium difficile* in 40 seconds using microwave-accelerated metal-enhanced fluorescence. *PLOS ONE* 9(8), p. e104334. doi: 10.1371/journal.pone.0104334.

Joudeh, N. and Linke, D. 2022. Nanoparticle classification, physicochemical properties, characterization, and applications: A comprehensive review for biologists. *Journal of Nanobiotechnology* 20(1), p. 262. doi: 10.1186/s12951-022-01477-8.

Justus, W., Valle, S., Barton, O., Gresham, A. and Shannon, G. 2024. A review of bovine tuberculosis transmission risk in European wildlife communities. *Mammal Review*. doi: 10.1111/mam.12347.

Kabir, S. et al. 2018. Role of PCR method using IS6110 primer in detecting *Mycobacterium tuberculosis* among the clinically diagnosed childhood tuberculosis patients at an urban hospital in Dhaka, Bangladesh. *International Journal of Infectious Diseases* 68, pp. 108–114. doi: 10.1016/j.ijid.2018.01.015.

Kanabalan, R.D., Lee, L.J., Lee, T.Y., Chong, P.P., Hassan, L., Ismail, R. and Chin, V.K. 2021. Human tuberculosis and *Mycobacterium tuberculosis* complex: A review on genetic diversity, pathogenesis, and omics approaches in host biomarkers discovery. *Microbiological Research* 246, p. 126674. doi: 10.1016/j.micres.2020.126674.

Kang, L. et al. 2023. Microbial keratitis isolates at a Midwestern tertiary eye care center. *Cornea* 42(12), pp. 1488–1496. doi: 10.1097/ICO.0000000000003198.

Kaso, A.W. and Hailu, A. 2021. Costs and cost-effectiveness of Gene Xpert compared to smear microscopy for the diagnosis of pulmonary tuberculosis using real-world data from Arsi zone, Ethiopia. *PLOS ONE* 16(10), p. e0259056. doi: 10.1371/journal.pone.0259056.

Katrak, S.M. 2021. Central nervous system tuberculosis. *Journal of the Neurological Sciences* 421, p. 117278. doi: 10.1016/j.jns.2020.117278.

Kaur, N. and Toley, B.J. 2023. Tuberculosis diagnosis using isothermal nucleic acid amplification in a paper-and-plastic device, pp. 295–306. doi: 10.1007/978-1-0716-2950-5_17.

Kay, A.W. et al. 2022. Xpert MTB/RIF Ultra assay for tuberculosis disease and rifampicin resistance in children. *Cochrane Database of Systematic Reviews* 2022(9). doi: 10.1002/14651858.CD013359.pub3.

Ketema, W., Woubishet, K., Tesfaye, S., Gutema, S., Taye, K., Shibeshi, M.S. and Tagesse, N. 2022. A breakthrough in the challenges of tuberculosis diagnosis: Lateral flow urine lipoarabinomannan (LAM) assay for the diagnosis of active tuberculosis in a subset of human immunodeficiency virus (HIV) patients at Hawassa University Comprehensive Specialized Hospital, Hawassa, Ethiopia. *International Medical Case Reports Journal* Volume 15, pp. 393–397. doi: 10.2147/IMCRJ.S373197.

Khan, A.R., Hussain, W.L., Shum, H.C. and Hassan, S.U. 2024. Point-of-care testing: A critical analysis of the market and future trends. *Frontiers in Lab on a Chip Technologies* 3. doi: 10.3389/frlct.2024.1394752.

Khandelwal, G. and Bhyravabhotla, J. 2010. A phenomenological model for predicting melting temperatures of DNA sequences. *PLOS ONE* 5(8), p. e12433. doi: 10.1371/journal.pone.0012433.

Kim, S., Thal, R. and Szkwarko, D. 2023. Management of latent tuberculosis infection. *JAMA* 329(5), p. 421. doi: 10.1001/jama.2022.24362.

Kim, S.-E., Tieu, M. Van, Hwang, S.Y. and Lee, M.-H. 2020a. Magnetic particles: Their applications from sample preparations to biosensing platforms. *Micromachines* 11(3), p. 302. doi: 10.3390/mi11030302.
Klumpp-Thomas, C. et al. 2021. Standardization of ELISA protocols for serosurveys of the SARS-CoV-2 pandemic using clinical and at-home blood sampling. *Nature Communications* 12(1), p. 113. doi: 10.1038/s41467-020-20383-x.

Krishnakumariamma, K., Ellappan, K., Muthuraj, M., Tamilarasu, K., Kumar, S.V. and Joseph, N.M. 2023. Diagnostic performance of real-time PCR for the detection of *Mycobacterium tuberculosis* in cerebrospinal fluid samples. *Indian Journal of Medical Microbiology* 42, pp. 7–11. doi: 10.1016/j.ijmmb.2022.12.012.

Krishnan, R. et al. 2022. Influence of dew point temperature on the occurrence of *Mycobacterium tuberculosis* disease in Chennai, India. *Scientific Reports* 12(1), p. 6147. doi: 10.1038/s41598-022-10111-4.

Kulkarni, S., Singh, P., Memon, A., Nataraj, G., Kanade, S., Kelkar, R. and Rajan, M.G.R. 2012. An in-house multiplex PCR test for the detection of *Mycobacterium tuberculosis*, its validation & comparison with a single target TB-PCR kit. *The Indian Journal of Medical Research* 135(5), pp. 788–94.

Lagune, M., Kremer, L. and Herrmann, J.-L. 2023. *Mycobacterium abscessus*, a complex of three fast-growing subspecies sharing virulence traits with slow-growing mycobacteria. *Clinical Microbiology and Infection*. doi: 10.1016/j.cmi.2023.08.036.

Lamont, E.A., Dillon, N.A. and Baughn, A.D. 2020. The bewildering antitubercular action of pyrazinamide. *Microbiology and Molecular Biology Reviews* 84(2). doi: 10.1128/MMBR.00070-19.

Lasch, P., Schneider, A., Blumenscheit, C. and Doellinger, J. 2020. Identification of microorganisms by liquid chromatography-mass spectrometry (LC-MS1) and in silico peptide mass libraries. *Molecular & Cellular Proteomics*19(12), pp. 2125–2139. doi: 10.1074/mcp.TIR120.002061.

Lee, H. and Kim, S. Il. 2022. Review of liquid chromatography-mass spectrometry-based proteomic analyses of body fluids to diagnose infectious diseases. *International Journal of Molecular Sciences* 23(4), p. 2187. doi: 10.3390/ijms23042187.

Lemmon, G.H. and Gardner, S.N. 2008. Predicting the sensitivity and specificity of published real-time PCR assays. *Annals of Clinical Microbiology and Antimicrobials* 7(1), p. 18. doi: 10.1186/1476-0711-7-18.

Li, X., Bosch-Tijhof, C.J., Wei, X., de Soet, J.J., Crielaard, W., Loveren, C. van and Deng, D.M. 2020. Efficiency of chemical versus mechanical disruption methods of DNA extraction for the identification of oral Gram-positive and Gram-negative bacteria. *Journal of International Medical Research* 48(5), p. 030006052092559. doi: 10.1177/0300060520925594.

Li, Z. 2002. Multiple thiol-anchor capped DNA-gold nanoparticle conjugates. *Nucleic Acids Research* 30(7), pp. 1558–1562. doi: 10.1093/nar/30.7.1558.

Li, Z. et al. 2024. The incremental value of *Mycobacterium tuberculosis* trace nucleic acid detection in CT-guided percutaneous biopsy needle rinse solutions for the diagnosis of tuberculosis. *Frontiers in Microbiology* 15. doi: 10.3389/fmicb.2024.1335526.

Liebenberg, D., Gordhan, B.G. and Kana, B.D. 2022. Drug resistant tuberculosis: Implications for transmission, diagnosis, and disease management. *Frontiers in Cellular and Infection Microbiology* 12. doi: 10.3389/fcimb.2022.943545.

Lim, M.Y., Song, E.-J., Kim, S.H., Lee, J. and Nam, Y.-D. 2018. Comparison of DNA extraction methods for human gut microbial community profiling. *Systematic and Applied Microbiology* 41(2), pp. 151–157. doi: 10.1016/j.syapm.2017.11.008.

Lin, C.-R., Wang, H.-Y., Lin, T.-W., Lu, J.-J., Hsieh, J.C.-H. and Wu, M.-H. 2021. Development of a two-step nucleic acid amplification test for accurate diagnosis of the *Mycobacterium tuberculosis* complex. *Scientific Reports* 11(1), p. 5750. doi: 10.1038/s41598-021-85160-2.

Liu, H.Y., Hopping, G.C., Vaidyanathan, U., Ronquillo, Y.C., Hoopes, P.C. and Moshirfar, M. 2019. Polymerase chain reaction and its application in the diagnosis of infectious keratitis. *Medical Hypothesis, Discovery & Innovation Ophthalmology Journal* 8(3), pp. 152–155.

Lodha, L., Mudliar, S.R., Singh, J., Maurya, A., Khurana, A.K., Khadanga, S. and Singh, S. 2022. Diagnostic performance of multiplex PCR for detection of *Mycobacterium tuberculosis* complex in presumptive pulmonary tuberculosis patients and its utility in smear negative specimens. *Journal of Laboratory Physicians* 14(04), pp. 403–411. doi: 10.1055/s-0042-1757231.

Lorenson, M.Y., Chen, K.-H.E. and Walker, A.M. 2019a. Enzyme-linked oligonucleotide hybridization assay for direct oligo measurement in blood. *Biology Methods and Protocols* 4(1). doi: 10.1093/biomethods/bpy014.

Lu, X.-Y., Wu, D.-C., Li, Z.-J. and Chen, G.-Q. 2011. Polymer nanoparticles. pp. 299–323. doi: 10.1016/B978-0-12-416020-0.00007-3.

Ludi, Z. et al. 2023. Diagnosis and biomarkers for ocular tuberculosis: From the present into the future. *Theranostics*13(7), pp. 2088–2113. doi: 10.7150/thno.81488.

Luong, J.H.T. and Vashist, S.K. 2020. Chemistry of biotin–streptavidin and the growing concern of an emerging biotin interference in clinical immunoassays. *ACS Omega* 5(1), pp. 10–18. doi: 10.1021/acsomega.9b03013.

Ma, X., Li, X., Luo, G. and Jiao, J. 2022. DNA-functionalized gold nanoparticles: Modification, characterization, and biomedical applications. *Frontiers in Chemistry* 10. doi: 10.3389/fchem.2022.1095488.

Ma, Y. et al. 2020. Comparison of Lowenstein-Jensen medium and MGIT culture system for recovery of *Mycobacterium tuberculosis* from abscess samples. *Diagnostic Microbiology and Infectious Disease* 96(4), p. 114969. doi: 10.1016/j.diagmicrobio.2019.114969.

Ma, Y. et al. 2024. One-pot assembly of mannose-capped lipoarabinomannan motifs up to 101-mer from the *Mycobacterium tuberculosis* cell wall. *Journal of the American Chemical Society* 146(6), pp. 4112–4122. doi: 10.1021/jacs.3c12815.

Mahardika, I.H., Naorungroj, S., Khamcharoen, W., Kin, S., Rodthongkum, N., Chailapakul, O. and Shin, K. 2023a. Point-of-care testing (POCT) devices for DNA detection: A comprehensive review. *Advanced NanoBiomed Research*3(11). doi: 10.1002/anbr.202300058.

Maitra, A., Munshi, T., Healy, J., Martin, L.T., Vollmer, W., Keep, N.H. and Bhakta, S. 2019. Cell wall peptidoglycan in *Mycobacterium tuberculosis*: An Achilles' heel for the TB-causing pathogen. *FEMS Microbiology Reviews* 43(5), pp. 548–575. doi: 10.1093/femsre/fuz016.

Maladan, Y., Krismawati, H., Wahyuni, T., Tanjung, R., Awaludin, K., Audah, K.A. and Parikesit, A.A. 2021. The whole-genome sequencing in predicting *Mycobacterium tuberculosis* drug susceptibility and resistance in Papua, Indonesia. *BMC Genomics* 22(1), p. 844. doi: 10.1186/s12864-021-08139-3.

Malenfant, J.H. and Brewer, T.F. 2021. Rifampicin mono-resistant tuberculosis—A review of an uncommon but growing challenge for global tuberculosis control. *Open Forum Infectious Diseases* 8(2). doi: 10.1093/ofid/ofab018.

Man, M.A., NiŢu, M.F., Strâmbu, L., Florescu, C., Streba, C.T. and Trofor, A.C. 2016. Tuberculous constrictive pericarditis complicated with tuberculous mediastinitis - case report. *Romanian Journal of Morphology and Embryology*57(1), pp. 237–242.

Mantefardo, B. and Sisay, G. 2021. Case report: Kanamycin ototoxicity and MDR-TB treatment regimen. *International Medical Case Reports Journal* Volume 14, pp. 815–817. doi: 10.2147/IMCRJ.S336259.

Marco, L. and Roberta, F. 2003. Isolation of total DNA from bacteria and yeast. *African Journal of Biotechnology* 2(8), pp. 251–253. doi: 10.5897/AJB2003.000-1052.

Martusevich, A.K., Nazarov, V. V., Surovegina, A. V. and Novikov, A.V. 2022. Near-field microwave tomography of biological tissues: Future perspectives. *Critical Reviews in Biomedical Engineering* 50(4), pp. 1–12. doi: 10.1615/CritRevBiomedEng.2022042194.

Meehan, C.J., Barco, R.A., Loh, Y.-H.E., Cogneau, S. and Rigouts, L. 2021. Reconstituting the genus *Mycobacterium*. *International Journal of Systematic and Evolutionary Microbiology* 71(9). doi: 10.1099/ijsem.0.004922.

Mehta, A.A., Belagundi, P., Oommen, M.S., Paul, T., Haridas, N. and Kumar, A. 2022. Performance of Xpert MTB/RIF assay on thoracoscopic pleural biopsy in undiagnosed exudative pleural effusion. *Indian Journal of Tuberculosis* 69(4), pp. 635–640. doi: 10.1016/j.ijtb.2021.09.010.

Mendelsohn, S.C. et al. 2022. Clinical predictors of pulmonary tuberculosis among South African adults with HIV. *eClinicalMedicine* 45, p. 101328. doi: 10.1016/j.eclinm.2022.101328.

Meyer, A.N.D., Giardina, T.D., Khawaja, L. and Singh, H. 2021. Patient and clinician experiences of uncertainty in the diagnostic process: Current understanding and future directions. *Patient Education and Counseling* 104(11), pp. 2606–2615. doi: 10.1016/j.pec.2021.07.028.

Minhas, N., Gurav, Y.K., Sambhare, S., Potdar, V., Choudhary, M.L., Bhardwaj, S.D. and Abraham, P. 2023. Cost-analysis of real time RT-PCR test performed for COVID-19 diagnosis at India's national reference laboratory during the early stages of pandemic mitigation. *PLOS ONE* 18(1), p. e0277867. doi: 10.1371/journal.pone.0277867.

Mohorič, T. and Bren, U. 2020. How does microwave irradiation affect the mechanism of water reorientation? *Journal of Molecular Liquids* 302, p. 112522. doi: 10.1016/j.molliq.2020.112522.

Morel, F., Jaffré, J., Sougakoff, W., Aubry, A. and Véziris, N. 2020. Place de la biologie moléculaire dans le diagnostic de la tuberculose. *Revue des Maladies Respiratoires* 37(5), pp. 412–416. doi: 10.1016/j.rmr.2019.09.004.

Moyo, M., Lebina, L., Milovanovic, M., MacPherson, P., Michel, A. and Martinson, N. 2021. Tuberculosis patients at the human-animal interface: Potential zooanthroponotic and zoonotic transmission. *One Health* 13, p. 100319. doi: 10.1016/j.onehlt.2021.100319.

Muteeb, G., Rehman, M.T., Shahwan, M. and Aatif, M. 2023. Origin of antibiotics and antibiotic resistance, and their impacts on drug development: A narrative review. *Pharmaceuticals* 16(11), p. 1615. doi: 10.3390/ph16111615.

Mvelase, N.R. and Mlisana, K.P. 2022. Xpert MTB/XDR for rapid detection of drug-resistant tuberculosis beyond rifampicin. *The Lancet Infectious Diseases* 22(2), pp. 156–157. doi: 10.1016/S1473-3099(21)00481-3.

Mvubu, N.E. and Jacoby, K. 2023. *Mycobacterium tuberculosis* complex molecular networks and their regulation: Implications of strain heterogeneity on epigenetic diversity and transcriptome regulation. *Heliyon* 9(12), p. e22611. doi: 10.1016/j.heliyon.2023.e22611.

Nalunjogi, J. et al. 2021. Accuracy and incremental yield of the chest X-ray in screening for tuberculosis in Uganda: A cross-sectional study. *Tuberculosis Research and Treatment* 2021, pp. 1–6. doi: 10.1155/2021/6622809.

Navarro, C.E. and Betancur, J.E. 2024. Cost-effectiveness analysis comparing QuantiFERON-TB Gold Plus test and tuberculin skin test for the diagnosis of latent tuberculosis infection in immunocompetent subjects in Colombia. *Value in Health Regional Issues* 41, pp. 54–62. doi: 10.1016/j.vhri.2023.11.010.

Navickaite, D., Ruzgys, P., Novickij, V., Jakutaviciute, M., Maciulevicius, M., Sinceviciute, R. and Satkauskas, S. 2020. Extracellular-Ca2+-induced decrease in small molecule electrotransfer efficiency: Comparison between

microsecond and nanosecond electric pulses. *Pharmaceutics* 12(5), p. 422. doi: 10.3390/pharmaceutics12050422.

Nehra, M., Kumar, V., Kumar, R., Dilbaghi, N. and Kumar, S. 2022. Current scenario of pathogen detection techniques in agro-food sector. *Biosensors* 12(7), p. 489. doi: 10.3390/bios12070489.

Nel, M., Franckling-Smith, Z., Pillay, T., Andronikou, S. and Zar, H.J. 2022. Chest imaging for pulmonary TB—An update. *Pathogens* 11(2), p. 161. doi: 10.3390/pathogens11020161.

Neshani, A., Zare, H., Sadeghian, H., Safdari, H., Riahi-Zanjani, B. and Aryan, E. 2023. A comparative study on visual detection of *Mycobacterium tuberculosis* by closed tube loop-mediated isothermal amplification: Shedding light on the use of Eriochrome Black T. *Diagnostics* 13(1), p. 155. doi: 10.3390/diagnostics13010155.

Nghiem, M.N., Van Nguyen, B., Nguyen, S.T., Vo, T.T.B. and Van Nong, H. 2015a. A simple, single triplex PCR of IS6110, IS1081, and 23S ribosomal DNA targets, developed for rapid detection and discrimination of *Mycobacterium*from clinical samples. *Journal of Microbiology and Biotechnology*. doi: 10.4014/jmb.1409.09089.

Nguyen, J.A. and Yates, R.M. 2021. Better together: Current insights into phagosome-lysosome fusion. *Frontiers in Immunology* 12. doi: 10.3389/fimmu.2021.636078.

Nimmo, C., Millard, J., Faulkner, V., Monteserin, J., Pugh, H. and Johnson, E.O. 2022. Evolution of *Mycobacterium tuberculosis* drug resistance in the genomic era. *Frontiers in Cellular and Infection Microbiology* 12. doi: 10.3389/fcimb.2022.954074.

Ofori-Anyinam, N. et al. 2023. KatG catalase deficiency confers bedaquiline hyper-susceptibility to isoniazid resistant *Mycobacterium tuberculosis*. *bioRxiv* : the preprint server for biology. doi: 10.1101/2023.10.17.562707.

Otoo, J.A. and Schlappi, T.S. 2022. REASSURED multiplex diagnostics: A critical review and forecast. *Biosensors* 12(2), p. 124. doi: 10.3390/bios12020124.

Owusu, W. et al. 2023. A multiplex PCR assay for the differentiation of *Mycobacterium tuberculosis* complex reveals high rates of mixed-lineage tuberculosis infections among patients in Ghana. *Frontiers in Cellular and Infection Microbiology* 13. doi: 10.3389/fcimb.2023.1125079.

Pal, R., Bisht, M.K. and Mukhopadhyay, S. 2022. Secretory proteins of *Mycobacterium tuberculosis* and their roles in modulation of host immune responses: Focus on therapeutic targets. *The FEBS Journal* 289(14), pp. 4146–4171. doi: 10.1111/febs.16369.

Parham, N.J. et al. 2007. Specific magnetic bead-based capture of genomic DNA from clinical samples: Application to the detection of group B streptococci in vaginal/anal swabs. *Clinical Chemistry*. doi: 10.1373/clinchem.2007.091389.

Park, H.-E., Kim, S., Shim, S., Park, H.-T., Park, W. Bin, Im, Y. Bin and Yoo, H.S. 2020. 16S and 23S rRNA gene mutation independent multidrug resistance of non-tuberculous mycobacteria isolated from South Korean soil. *Microorganisms* 8(8), p. 1114. doi: 10.3390/microorganisms8081114.

Patel, M., Gonzalez, R., Halford, C., Lewinski, M.A., Landaw, E.M., Churchill, B.M. and Haake, D.A. 2011. Target-specific capture enhances sensitivity of electrochemical detection of bacterial pathogens. *Journal of Clinical Microbiology*. doi: 10.1128/JCM.01261-11.

Paul, R., Ostermann, E. and Wei, Q. 2020. Advances in point-of-care nucleic acid extraction technologies for rapid diagnosis of human and plant diseases. *Biosensors and Bioelectronics* 169, p. 112592. doi: 10.1016/j.bios.2020.112592.

Pereira, A.C., Ramos, B., Reis, A.C. and Cunha, M. V. 2020. Non-tuberculous mycobacteria: Molecular and physiological bases of virulence and adaptation to ecological niches. *Microorganisms* 8(9), p. 1380. doi: 10.3390/microorganisms8091380.

Peterson, A.W. 2001. The effect of surface probe density on DNA hybridization. *Nucleic Acids Research* 29(24), pp. 5163–5168. doi: 10.1093/nar/29.24.5163.

Phan, T.T.M., Phan, T.M. and Schmit, J.D. 2023. Beneficial and detrimental effects of non-specific binding during DNA hybridization. *Biophysical Journal* 122(5), pp. 835–848. doi: 10.1016/j.bpj.2023.01.034.

Pilo, P., Tiley, A.M.M., Lawless, C., Karki, S.J., Burke, J. and Feechan, A. 2022. A rapid fungal DNA extraction method suitable for PCR screening fungal mutants, infected plant tissue and spore trap samples. *Physiological and Molecular Plant Pathology* 117, p. 101758. doi: 10.1016/j.pmpp.2021.101758.

Prajwal, P. et al. 2023. Optimizing mycobacteria molecular diagnostics: No decontamination! Human DNA depletion? Greener storage at 4 °C! *Frontiers in Microbiology* 14. doi: 10.3389/fmicb.2023.1104752.

Prakash Babu, S. et al. 2023. Comparison of IGRA and TST in the diagnosis of latent tuberculosis among women of reproductive age in South India. *Indian Journal of Tuberculosis* 70(1), pp. 12–16. doi: 10.1016/j.ijtb.2022.03.011.

Prakoeswa, F.R.S., Rumondor, B.B. and Prakoeswa, C.R.S. 2022. Acid-Fast Staining Revisited, a Dated but Versatile Means of Diagnosis. *The Open Microbiology Journal* 16(1). doi: 10.2174/18742858-v16-e2206081.

Qi, C.-C. et al. 2023. Prevalence and risk factors of tuberculosis among people living with HIV/AIDS in China: a systematic review and meta-analysis. *BMC Infectious Diseases* 23(1), p. 584. doi: 10.1186/s12879-023-08575-4.

Qutob, M., Rafatullah, M., Muhammad, S.A., Alosaimi, A.M., Alorfi, H.S. and Hussein, M.A. 2022. A Review of Pyrene Bioremediation Using *Mycobacterium* Strains in a Different Matrix. *Fermentation* 8(6), p. 260. doi: 10.3390/fermentation8060260.

Rahlwes, K.C., Dias, B.R.S., Campos, P.C., Alvarez-Arguedas, S. and Shiloh, M.U. 2023. Pathogenicity and virulence of *Mycobacterium tuberculosis*. *Virulence* 14(1). doi: 10.1080/21505594.2022.2150449.

Raj, A. et al. 2016. Comparative evaluation of several gene targets for designing a Multiplex-PCR for an early diagnosis of extrapulmonary tuberculosis. *Yonsei Medical Journal*. doi: 10.3349/ymj.2016.57.1.88.

Ranjha, L., Howard, S.M. and Cejka, P. 2018. Main steps in DNA double-strand break repair: an introduction to homologous recombination and related processes. *Chromosoma* 127(2), pp. 187–214. doi: 10.1007/s00412-017-0658-1.

van der Reis, A.L., Beckley, L.E., Olivar, M.P. and Jeffs, A.G. 2023. Nanopore short-read sequencing: A quick, cost-effective and accurate method for DNA metabarcoding. *Environmental DNA* 5(2), pp. 282–296. doi: 10.1002/edn3.374.

Rekha, B., Dushyant Singh, G., Aarti, K. and Anuradha, K. 2021. Comparison of Ziehl-Neelsen (ZN) Staining and Fluorescent (FL) Staining in Suspected Cases of Tuberculosis. *International Journal of Pathology and Clinical Research*7(1). doi: 10.23937/2469-5807/1510122.

Remm, S., Earp, J.C., Dick, T., Dartois, V. and Seeger, M.A. 2022. Critical discussion on drug efflux in *Mycobacterium tuberculosis*. *FEMS Microbiology Reviews* 46(1). doi: 10.1093/femsre/fuab050.

Rentschler, S., Kaiser, L. and Deigner, H.-P. 2021. Emerging Options for the Diagnosis of Bacterial Infections and the Characterization of Antimicrobial Resistance. *International Journal of Molecular Sciences* 22(1), p. 456. doi: 10.3390/ijms22010456.

Rusu, A., Munteanu, A.-C., Arbănași, E.-M. and Uivarosi, V. 2023. Overview of Side-Effects of Antibacterial Fluoroquinolones: New Drugs versus Old Drugs, a Step Forward in the Safety Profile? *Pharmaceutics* 15(3), p. 804. doi: 10.3390/pharmaceutics15030804.

S., G. and E.R., V. 2023. Protein Secondary Structure Prediction Using Cascaded Feature Learning Model. *Applied Soft Computing* 140, p. 110242. doi: 10.1016/j.asoc.2023.110242.

Sakiyama, M. et al. 2021. Specificity of tuberculin skin test improved by BCG immunization schedule change in Japan. *Journal of Infection and Chemotherapy* 27(9), pp. 1306–1310. doi: 10.1016/j.jiac.2021.04.016.

Salazar, M.P., da Costa Lima Suassuna Monteiro, J.F., Veloso Carvalho-Silva, W.H., Nunes Diniz, G.T., Werkhauser, R.P., Lapa Montenegro, L.M. and Schindler, H.C. 2024. Development and evaluation of a single-tube nested PCR with colorimetric assay for *Mycobacterium tuberculosis* detection. *BioTechniques* 76(6), pp. 235–244. doi: 10.2144/btn-2023-0080.

Sandmann, G. 2022. HPLC analysis of carotenoids from bacteria. pp. 139–153. doi: 10.1016/bs.mie.2021.10.006.

Satish, N., Kamble, R. and Kajal, V. 2023. In vitro mucolytic activity determination of N-acetyl cysteine effervescent tablet using suspended level viscometer. International Journal of Applied Pharmaceutics, pp. 141–144. doi: 10.22159/ijap.2023v15i5.48069.

Sayers, E.W. et al. 2023. Database resources of the National Center for Biotechnology Information in 2023. *Nucleic Acids Research* 51(D1), pp. D29–D38. doi: 10.1093/nar/gkac1032.

Schami, A., Islam, M.N., Belisle, J.T. and Torrelles, J.B. 2023. Drug-resistant strains of *Mycobacterium tuberculosis*: cell envelope profiles and interactions with the host. *Frontiers in Cellular and Infection Microbiology* 13. doi: 10.3389/fcimb.2023.1274175.

Scharf, S., Bartels, A., Kondakci, M., Pfeffer, K., Henrich, B. and Haas, R. 2020. Introduction of a bead beating step improves fungal DNA extraction from selected patient specimens. *International Journal of Medical Microbiology* 310(6), p. 151443. doi: 10.1016/j.ijmm.2020.151443.

Shaheen, A., Tariq, A., Iqbal, M., Mirza, O., Haque, A., Walz, T. and Rahman, M. 2021. Mutational Diversity in the Quinolone Resistance-Determining Regions of Type-II Topoisomerases of *Salmonella* Serovars. *Antibiotics* 10(12), p. 1455. doi: 10.3390/antibiotics10121455.

Sharma, M., Singh, R., Sharma, A., Gupta, V. and Sharma, K. 2022. IS1081-based Multi-targeted LAMP: An Opportunity to Detect Tubercular Uveitis. *Ocular Immunology and Inflammation* 30(1), pp. 168–173. doi: 10.1080/09273948.2020.1787462.

Shea, J. et al. 2021. Low-level rifampin resistance and rpoB mutations in *Mycobacterium tuberculosis*: An analysis of whole-genome sequencing and drug susceptibility test data in New York. Journal of Clinical Microbiology 59(4). doi: 10.1128/JCM.01885-20.

Shin, S.K., Lee, Y., Kwon, H., Rhee, J. and Kim, J.K. 2021. Validation of direct boiling method for simple and efficient genomic DNA extraction and PCR-based macroalgal species determination. Journal of Phycology 57(4), pp. 1368–1372. doi: 10.1111/jpy.13175.

Shivakumar, P. and Shettigar, K.S. 2023. Tuberculosis diagnosis: Updates and challenges. doi: 10.5772/intechopen.107168.

da Silva, R.M., Bazzo, M.L. and Chagas, M. 2010. Quality of sputum in the performance of polymerase chain reaction for diagnosis of pulmonary tuberculosis. The Brazilian Journal of Infectious Diseases 14(1), pp. 116–120. doi: 10.1016/S1413-8670(10)70022-2.

Singh, K., Kumari, R., Tripathi, R., Gupta, S. and Anupurba, S. 2020a. Detection of clinically important non-tuberculous mycobacteria (NTM) from pulmonary samples through one-step multiplex PCR assay. BMC Microbiology 20(1), p. 267. doi: 10.1186/s12866-020-01952-y.

Singh, R., Dwivedi, S.P., Gaharwar, U.S., Meena, R., Rajamani, P. and Prasad, T. 2020b. Recent updates on drug resistance in *Mycobacterium tuberculosis*. Journal of Applied Microbiology 128(6), pp. 1547–1567. doi: 10.1111/jam.14478.

Song, J., Liu, S., Xie, Y., Zhang, C. and Xu, C. 2024. Diagnostic value of DNA or RNA-based metagenomic next-generation sequencing in lower respiratory tract infections. Heliyon 10(9), p. e30712. doi: 10.1016/j.heliyon.2024.e30712.

Song, Y. and Gyarmati, P. 2022. Rapid DNA visual detection of polymicrobial bloodstream infection using filter paper. Scientific Reports 12(1), p. 4515. doi: 10.1038/s41598-022-08487-4.

Souche, E. et al. 2022. Recommendations for whole genome sequencing in diagnostics for rare diseases. European Journal of Human Genetics 30(9), pp. 1017–1021. doi: 10.1038/s41431-022-01113-x.

Sun, L., Liu, Y., Lehnert, T., Gijs, M.A.M. and Li, S. 2022. The enhancement of DNA fragmentation in a benchtop ultrasonic water bath with needle-induced air bubbles: Simulation and experimental investigation. Biomicrofluidics 16(4). doi: 10.1063/5.0101740.

Taglia, F., Wang, L., Setser, C.H., Fernández-Tejero, N., McCord, B.R. and Lee, S.B. 2022a. Development of a microwave-based extraction for forensic biological samples. Forensic Science International: Synergy 5, p. 100291. doi: 10.1016/j.fsisyn.2022.100291.

Thomas, S.N., French, D., Jannetto, P.J., Rappold, B.A. and Clarke, W.A. 2022. Liquid chromatography–tandem mass spectrometry for clinical diagnostics. Nature Reviews Methods Primers 2(1), p. 96. doi: 10.1038/s43586-022-00175-x.

Tieng, F.Y.F., Abdullah-Zawawi, M.-R., Md Shahri, N.A.A., Mohamed-Hussein, Z.-A., Lee, L.-H. and Mutalib, N.-S.A. 2023. A hitchhiker's guide to RNA–RNA structure and interaction prediction tools. Briefings in Bioinformatics 25(1). doi: 10.1093/bib/bbad421.

Tsurusawa, N. et al. 2021. Modified ELISA for ultrasensitive diagnosis. *Journal of Clinical Medicine* 10(21), p. 5197. doi: 10.3390/jcm10215197.

Tunstall, T., Phelan, J., Eccleston, C., Clark, T.G. and Furnham, N. 2021. Structural and genomic insights into pyrazinamide resistance in *Mycobacterium tuberculosis* underlie differences between ancient and modern lineages. *Frontiers in Molecular Biosciences* 8. doi: 10.3389/fmolb.2021.619403.

Vanino, E. et al. 2023. Update of drug-resistant tuberculosis treatment guidelines: A turning point. *International Journal of Infectious Diseases* 130, pp. S12–S15. doi: 10.1016/j.ijid.2023.03.013.

Viswanathan, V.K. 2023. Latent TB infection in children and adolescents: Scientific rationale and programmatic management. *Indian Journal of Tuberculosis* 70, pp. S35–S38. doi: 10.1016/j.ijtb.2023.09.001.

Wang, N., Zou, W., Li, X., Liang, Y. and Wang, P. 2022. Study and application status of the nonthermal effects of microwaves in chemistry and materials science – a brief review. *RSC Advances* 12(27), pp. 17158–17181. doi: 10.1039/D2RA00381C.
Wang, X.F. et al. 2021a. A fast, visual, and instrument-free platform involving rapid DNA extraction, chemical heating, and recombinase aided amplification for on-site nucleic acid detection. *Frontiers in Bioengineering and Biotechnology* 9. doi: 10.3389/fbioe.2021.764306.

Wang, Y., Zhao, Y., Bollas, A., Wang, Y. and Au, K.F. 2021b. Nanopore sequencing technology, bioinformatics, and applications. *Nature Biotechnology* 39(11), pp. 1348–1365. doi: 10.1038/s41587-021-01108-x.

Wieszczycka, K., Staszak, K., Woźniak-Budych, M.J., Litowczenko, J., Maciejewska, B.M. and Jurga, S. 2021. Surface functionalization – The way for advanced applications of smart materials. *Coordination Chemistry Reviews* 436, p. 213846. doi: 10.1016/j.ccr.2021.213846.

Wilson-Garner, S., Alzeer, S., Baillie, L. and Porch, A. 2024. High-volume biological sample processing using microwaves. *Journal of Applied Physics* 135(4). doi: 10.1063/5.0178755.

Wu, Z. et al. 2022. mbtD and celA1 association with ethambutol resistance in *Mycobacterium tuberculosis*: A multiomics analysis. *Frontiers in Cellular and Infection Microbiology* 12. doi: 10.3389/fcimb.2022.959911.

Xia, J., Liu, Y., Ma, Y., Yang, F., Ruan, Y., Xu, J.-F. and Pi, J. 2023. Advances of long non-coding RNAs as potential biomarkers for tuberculosis: New hope for diagnosis? *Pharmaceutics* 15(8), p. 2096. doi: 10.3390/pharmaceutics15082096.

Yadav, S. 2022. A case of cutaneous tuberculosis presenting as lupus vulgaris in an immunocompetent Indian child during the pandemic of COVID-19. *Cureus*. doi: 10.7759/cureus.27996.

Yang, K.B. et al. 2023. High-resolution landscape of an antibiotic binding site. *Nature* 622(7981), pp. 180–187. doi: 10.1038/s41586-023-06495-6.

Yang, X. et al. 2021a. Rapid and visual differentiation of *Mycobacterium tuberculosis* from the *Mycobacterium tuberculosis* complex using multiplex loop-mediated isothermal amplification coupled with a nanoparticle-based lateral flow biosensor. *Frontiers in Microbiology* 12. doi: 10.3389/fmicb.2021.708658.

Yang, X. et al. 2021b. Rapid and visual differentiation of *Mycobacterium tuberculosis* from the *Mycobacterium tuberculosis* complex using multiplex loop-mediated isothermal amplification coupled with a nanoparticle-based lateral flow biosensor. *Frontiers in Microbiology* 12. doi: 10.3389/fmicb.2021.708658.

Yoon, S.H., Lee, N.K. and Yim, J.J. 2012. Impact of sputum gross appearance and volume on smear positivity of pulmonary tuberculosis: A prospective cohort study. *BMC Infectious Diseases* 12, p. 172. doi: 10.1186/1471-2334-12-172.

Zeineldin, M.M., Lehman, K., Camp, P., Farrell, D. and Thacker, T.C. 2023. Diagnostic evaluation of the IS1081-targeted real-time PCR for detection of *Mycobacterium bovis* DNA in bovine milk samples. *Pathogens* 12(8), p. 972. doi: 10.3390/pathogens12080972.

Zhang, H., Liu, M., Fan, W., Sun, S. and Fan, X. 2022. The impact of *Mycobacterium tuberculosis* complex in the environment on one health approach. *Frontiers in Public Health* 10. doi: 10.3389/fpubh.2022.994745.

Zhang, L. et al. 2020. Structures of cell wall arabinosyltransferases with the anti-tuberculosis drug ethambutol. *Science*368(6496), pp. 1211–1219. doi: 10.1126/science.aba9102.

Zhang, Y., Zhan, B., Hao, X., Wang, W., Zhang, X., Fang, C. and Wang, M. 2023. Factors associated with diagnostic delay of pulmonary tuberculosis among children and adolescents in Quzhou, China: Results from the surveillance data 2011–2021. *BMC Infectious Diseases* 23(1), p. 541. doi: 10.1186/s12879-023-08516-1.

Zhao, X., Dong, G. and Wang, C. 2021. The non-thermal biological effects and mechanisms of microwave exposure. *International Journal of Radiation Research* 19(3), pp. 483–494. doi: 10.52547/ijrr.19.3.483.

Zhu, H. et al. 2021. Strong histamine torsion Raman spectrum enables direct, rapid, and ultrasensitive detection of allergic diseases. *iScience* 24(11), p. 103384. doi: 10.1016/j.isci.2021.103384.

Zimba, O. et al. 2019. The effect of sputum quality and volume on the yield of bacteriologically-confirmed TB by Xpert MTB/RIF and smear. *The Pan African Medical Journal* 33, p. 110. doi: 10.11604/pamj.2019.33.110.15319.

A: Appendix 1

A1: Streaking and Microscopic Examination of *M. bovis* 1173P2

For purity determination of *M. bovis* 1173P2, the streaking method was performed, as shown in Figure A1.1. Examination of the *M. bovis* 1173P2 colonies under the microscope was carried out using two different staining techniques: Ziehl-Neelsen (ZN) staining (Figure A1.2) and Gram staining (Figure A1.3).

Figure A1.1: A photograph demonstrating the streaking of *M. bovis* 1173P2 colonies on LB agar.

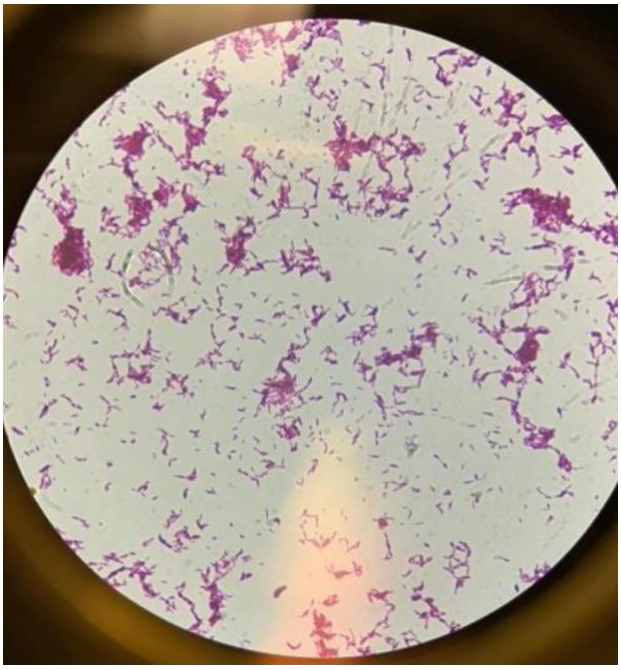

Figure A1.2: *M. bovis* 1173P2 under light microscope, stained with ZN stain.

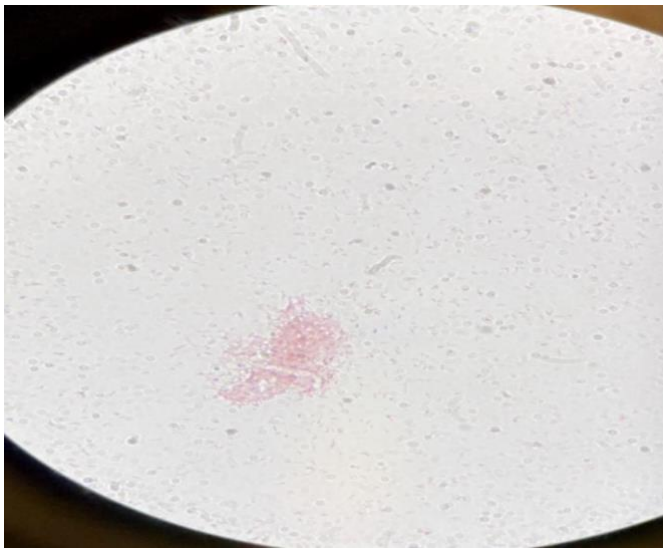

Figure A1.3 :*M. bovis* 1173P2 under light microscope, stained with gram stain .

A2: Standardisation of bacterial cell concentration using the Miles and Misra method

The drop count method was employed to construct a standard curve for determining the OD600 of bacterial suspensions, corresponding to a concentration of 1.0×10^8 CFU/mL (Thacker et al., 2015). The bacterial strains used in this process included *M. tuberculosis* H37Ra, *M. bovis* 1173P2, *M. bovis* NCTC 5692, *M. smegmatis* Mc2155 S2, *M. abscessus* ATCC 19977, and *E. coli* NCTC 1093. The probit value derived from the standard

curve (*M. bovis* 1173P2) was 0.99, and the OD600 value for a concentration of 1.0×10^8 CFU/mL was 0.1 (Figure A2). This concentration, expressed in CFU/mL, directly represents the total bacterial quantity used in the experiment. An exact bacterial quantity of 10^8 total bacteria was utilised consistently across all methods. All bacterial isolates exhibited the same OD600 value of 0.1, except for *E. coli*NCTC 1093, which gave an OD600 value of 0.15.

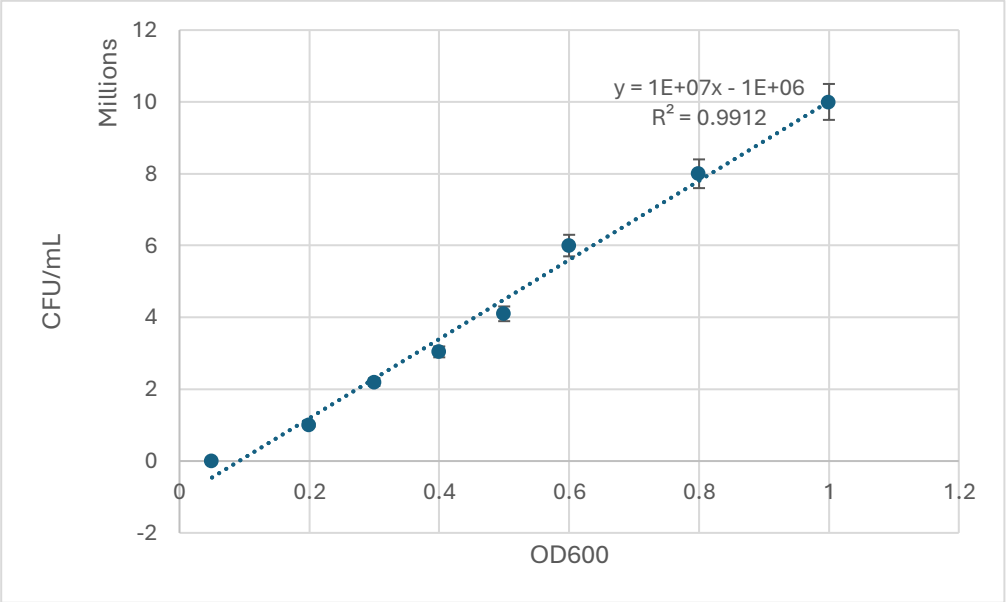

Figure A2: Standard curve showing the relationship between Optical Density (OD600) and bacterial concentration (CFU/mL) of *M. bovis* 1173P2. Each data point represents the mean of three independent experiments (n=3), with error bars indicating the standard deviation (SD) of the measurements.

A 3: Screening of probe combinations for secondary structures

The secondary structure of each anchor and detection probe was examined using a web-based program. The following example focuses on two groups of probes targeting the *IS1081* gene. Figure A3.1 illustrates an undesirable interaction between the anchor and detection probes, where ineffective binding could result in diminished probe efficacy. Figure A3.2, however, demonstrates no binding between the detection and anchor probes, which is the optimal result as it ensures proper probe performance without interference. However, some

minor binding between the bases of the detection probe was observed, and further testing will be conducted to evaluate its impact.

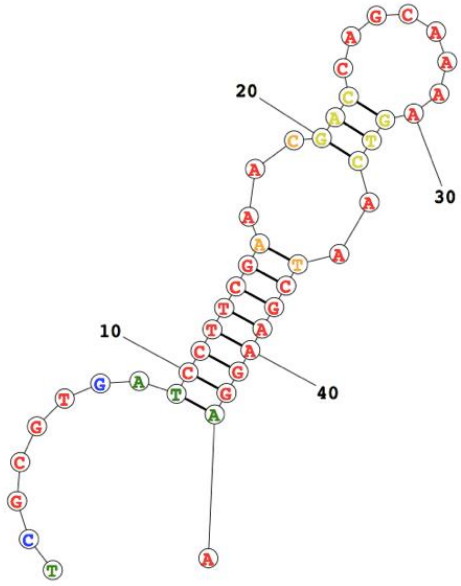

Figure A3.1: Analysis of the secondary structure of selected anchor and detection probes targeting the *IS1081* gene. The analysis revealed an undesirable interaction between the anchor and detection probes, where ineffective binding could lead to reduced probe efficacy.

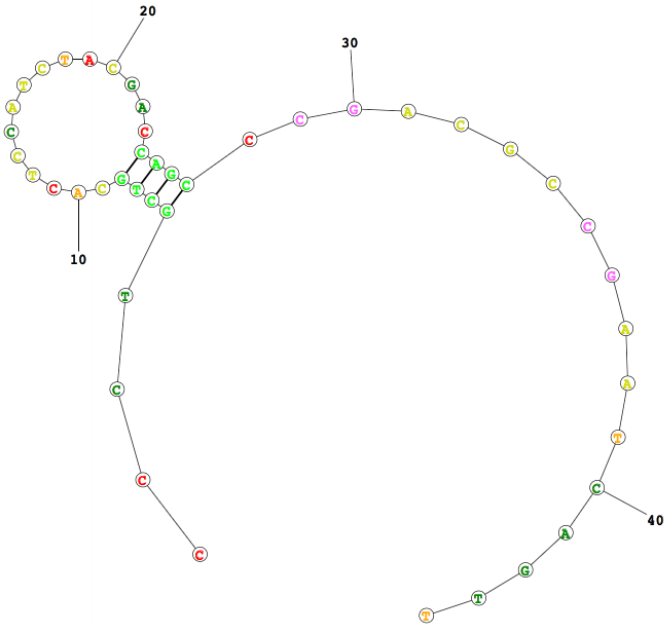

Figure A3.2: Secondary structure analysis of the anchor and detection probes targeting the *IS1081* gene. This analysis demonstrated the absence of binding between the probes, indicating optimal configuration for reliable probe performance.

A4: Scanning electron microscope imaging of mycobacteria

To characterise the ultrastructure of different strains of mycobacteria before and after microwave exposure, samples of *M. smegmatis*, *M. bovis*, and *M. abscessus* were sputter-coated with approximately 20 nm of AuPd to ensure conductivity, using a BIORAD SC500 coater. The samples were imaged with the In-Lens secondary electron detector on a Zeiss Sigma HD FEG-SEM at the School of Earth and Environmental Sciences, Cardiff University, under high vacuum conditions (Figure A 4.1).

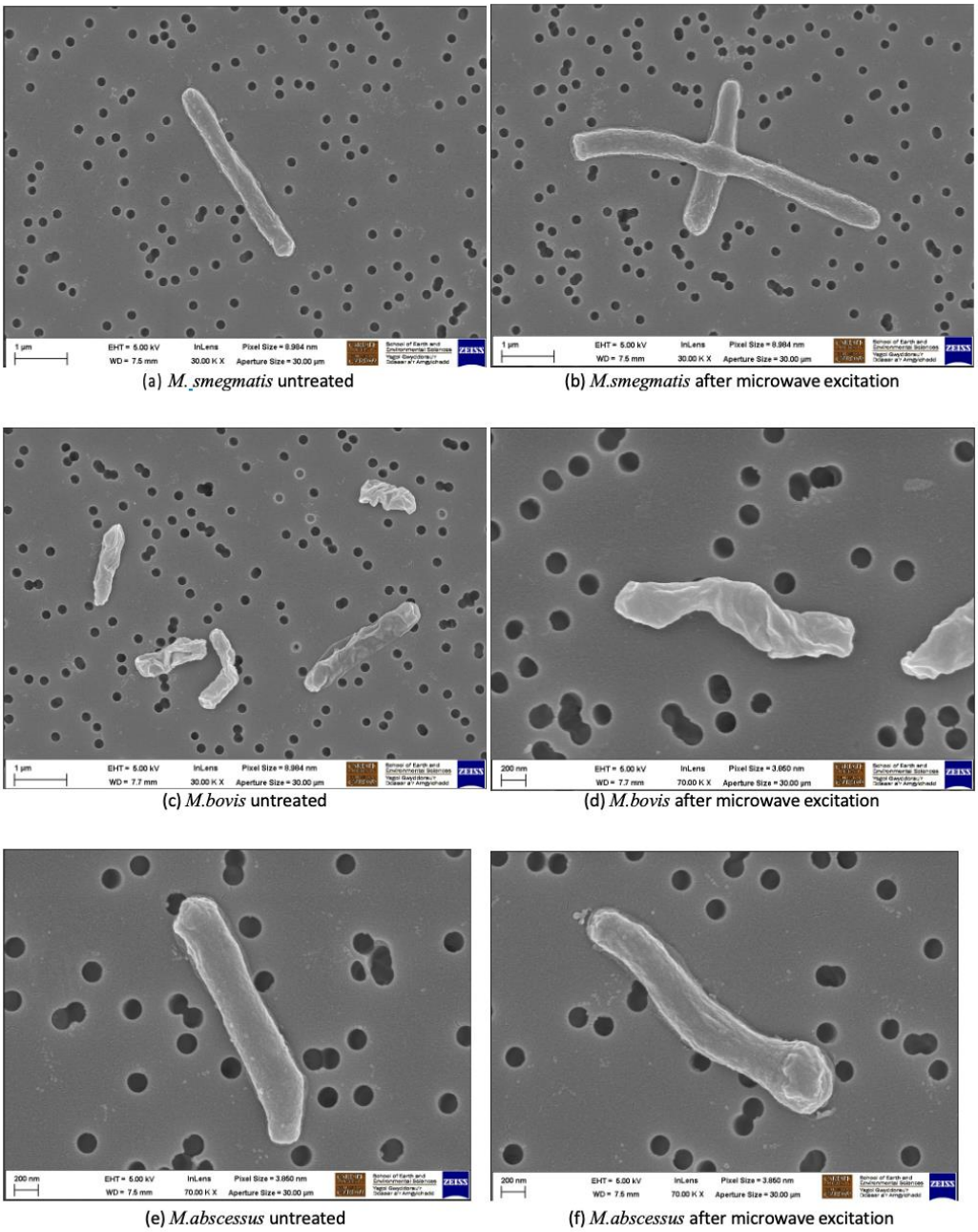

Figure A4.1: Images of *M. smegmatis*, *M. bovis*, and *M. abscessus* were captured using a Zeiss Sigma HD FEG-SEM with an In-Lens secondary electron detector.

A beam energy of 5 kV was used with a 30 µm diameter final aperture and a working distance of 7.5 mm. The magnification of images (a), (b), and (c) is ×30K, and the magnification of images (d), (e), and (f) is ×70K. (Wilson-Garner et al. 2024).